# Stabilization of Natural Clay Riverbanks with Rockfill Columns:
# A Full-Scale Field Test and Numerical Verification

by

Kendall Thiessen

A Thesis submitted to the Faculty of Graduate Studies of
The University of Manitoba

in partial fulfillment of the requirements of the degree of
DOCTOR OF PHILOSOPHY

Department of Civil Engineering
University of Manitoba
Winnipeg

## Abstract

Rockfill columns have been used to stabilize the clay riverbanks in the Winnipeg area for over two decades. The construction methods used in Manitoba are uniquely adapted to the local soil conditions. The performance of rockfill columns in Manitoba has generally been satisfactory, except that in some cases significant deformations have occurred during and after construction (Yarechewski and Tallin 2003). This thesis will discuss the full-scale test loading of a riverbank that was stabilized with rockfill columns. The purpose of the test was to measure the load-deformation characteristics of a reinforced slope in order to further the understanding of rockfill column behaviour. Rockfill column technology has evolved from granular shear key methods for stabilizing slopes. The relatively weak and soft lacustrine clay is reinforced with compacted columns of stronger and stiffer limestone rockfill.

The research test site is located along the natural banks of the Red River in The City of Winnipeg. The project involved an extensive site investigation, and soils characterization program in preparation for the field test. Eleven columns, 2.1 m in diameter were tested by surcharging the slope with 1920 tonnes of fill. The deformations were measured with standard and in-place inclinometers while the porewater pressure response of the in-situ soils was continuously monitored with vibrating wire piezometers.

The research further investigated the mobilization of resistance along the length of the rockfill columns with finite element models. The analysis of the model results illustrated the mobilization of shear resistance within the rockfill and the

development of stresses across the column cross section. The important engineering characteristics of rockfill are discussed in the context of rockfill column design and the importance of effective compaction is highlighted. The results of this research are used to develop recommendations for rockfill column design, analysis and construction.

## Acknowledgements

I am grateful for the opportunity to have been involved in this project, but the credit for the success of the project is due to many people and organizations

I would like to thank my academic co-advisors Dr. Marolo Alfaro and Dr. James Blatz for their valuable guidance, encouragement and support. I must also acknowledge Dr. Jim Graham for his help, especially for his patient editing of this document. I have benefited greatly from the friendships, technical discussions and help from fellow graduate students at the University of Manitoba including Michael Van Helden, Neil Privat, Ray Offman, Alena James, Nazri Mohadin, Hamid Batenipour and David Kurz. The help from Carly Delavau and David Kurz during the summers of 2006 and 2007 was greatly appreciated.

The technical, financial, labour, and logistical contributions of the project sponsors were vital to the implementation and success of the project. The project sponsors and primary contributors were:

- Subterranean (Manitoba) Ltd. and Peter Mignacca.
- The City of Winnipeg and Don Kingerski.
- National Science and Engineering Research Council (NSERC).
- UMA|AECOM (now AECOM) and Ken Skaftfeld.
- KGS Group Ltd. and Rob Kenyon.
- AMEC Earth and Environmental and Harley Pankratz.
- Manitoba Water Stewardship Fund.

This project could not have happened without the very generous donations of materials and equipment and labour from Subterranean (Manitoba) Ltd. I would specifically like to thank Peter Mignacca for enabling this project by providing people and equipment of the highest calibre. The expertise, patience and understanding provided by Subterranean's site supervisors, Don White and Rob Tachus was invaluable. UMA|AECOM, KGS Group Ltd. and AMEC also graciously provided all the needed field support during the construction and test loading.

Finally, I would like to thank my family and my God. My wife Debbie has been extremely loving and supportive. She has done much more than her share, especially with the birth of our son Joel, in June 2009. Thank You.

## Table of Contents


1. Introduction ..... 1

1.1 Slope stability in the Winnipeg area ..... 2

1.1.1 Stabilization methods ..... 4

1.2 Rockfill columns ..... 6

1.2.1 Current practice ..... 6

1.3 Performance of Rockfill Columns ..... 9

1.4 Full-Scale Field Test ..... 12

1.5 Objectives and Hypothesis ..... 14

1.5.1 Hypotheses ..... 14

1.5.2 Objectives ..... 14

1.6 Organization and scope of thesis ..... 15

2. Literature Review ..... 21

2.1 Introduction ..... 21

2.2 Properties of soil in the Winnipeg region ..... 21

2.3 The stability of slopes in the Winnipeg region ..... 25

2.4 Testing of Materials ..... 27

2.4.1 Measured Properties of Rockfill ..... 27

2.4.2 Properties of rockfill-clay composites ..... 35

2.4.3 Increase in density from compaction ..... 37
2.5 Rockfill Columns ..... 38
2.5.1 Design methods ..... 40
2.5.2 Rockfill columns for slope stabilization ..... 45
2.5.3 Numerical Modeling ..... 46
2.6 Related technologies ..... 47
2.6.1 Stabilization by Piles ..... 47
2.6.2 Other ground improvement techniques ..... 49
2.6.3 Shear and bending in columns ..... 50
2.7 Full-scale field tests ..... 51
3. Site investigation and soils testing ..... 65
3.1 Introduction ..... 65
3.2 Location, topography and natural environment ..... 67
3.3 Site investigation ..... 69
3.3.1 Stratigraphy ..... 72
3.4 Laboratory Testing ..... 75
3.4.1 Grain size distribution ..... 75
3.4.2 Natural water contents ..... 75
3.4.3 Atterberg limits ..... 76
3.4.4 Testing for constitutive properties ..... 77

3.4.4.1 Triaxial tests ..... 78
3.4.4.2 Direct shear tests ..... 82
3.4.5 One-dimensional consolidation ..... 85
3.4.6 Hydraulic conductivity ..... 87
3.4.7 Rockfill Testing ..... 87
3.4.7.1 Grain size distribution ..... 88
3.4.7.2 Water content ..... 88
3.5 Conclusion ..... 89
4. Instrumentation ..... 114
4.1 Introduction ..... 114
4.2 Plan and layout ..... 116
4.2.1 Slope inclinometer locations ..... 117
4.2.2 Piezometer locations ..... 118
4.3 Slope inclinometers ..... 118
4.3.1 Installation ..... 119
4.3.2 In-place inclinometers ..... 121
4.3.3 Monitoring ..... 122
4.3.4 Baseline observations ..... 126
4.4 Piezometers ..... 127
4.4.1 Installation ..... 127

4.4.2 Monitoring ..... 128
4.4.3 Baseline observations ..... 129
4.5 Real-time monitoring ..... 129
4.6 Additional instrumentation and monitoring ..... 132
4.7 Ongoing monitoring ..... 133
5. Field Testing Program ..... 152
5.1 Design ..... 152
5.1.1 Rockfill material ..... 154
5.1.2 Column layout ..... 155
5.1.3 Void columns ..... 155
5.2 Logistics ..... 157
5.3 Scheduling ..... 159
5.4 Construction ..... 160
5.4.1 Installation of rockfill columns ..... 160
5.4.2 Compaction ..... 163
5.4.3 Post-construction monitoring ..... 165
5.5 Test Loading ..... 165
5.5.1 Schedule ..... 166
5.5.2 Load placement ..... 168
5.5.3 Termination of the test ..... 170

5.5.4 Load removal and site re-grading ..... 170

5.6 Restoration ..... 171

6. Observations, results and commentary ..... 192

6.1 Introduction ..... 192

6.2 Survey results ..... 193

6.3 Inclinometer monitoring results ..... 194

6.3.1 Zone 1: SI-1 and SI-2 ..... 198

6.3.2 Zone 2 Centerline: SI-4, SI-6, SI-7, SI-8 and SI-9 ..... 199

6.3.3 Zone 2 Edges: SI-11 and SI-12 ..... 201

6.3.4 Zone 3: SI-10 ..... 203

6.3.5 SI-5 ..... 204

6.4 Piezometer monitoring results ..... 204

6.5 Ongoing monitoring ..... 208

6.6 Other observations ..... 210

6.7 Additional Interpretation ..... 211

6.7.1 Load – deformation ..... 211

6.7.2 Elastic rebound ..... 212

6.7.3 Bending behaviour ..... 213

6.7.4 Till anchor ..... 217

6.7.5 Impacts of frozen ground ..... 218

6.8 Summary and conclusions ..... 218

7. Analysis and Numerical Modeling ..... 245

7.1 Introduction ..... 245

7.2 Model development ..... 248

7.2.1 Cross sections ..... 248

7.2.2 Clay ..... 249

7.2.2.1 Modified Cam Clay ..... 251

7.2.3 Rockfill ..... 253

7.2.3.1 Failure envelopes for rockfill ..... 253

7.2.3.2 Poisson's ratio ..... 256

7.2.3.3 Hyperbolic model ..... 256

7.2.4 Till ..... 258

7.2.5 Loading fill ..... 259

7.3 Porewater pressure modelling ..... 259

7.3.1 In-Situ porewater pressure development ..... 260

7.4 Stress deformation modeling ..... 262

7.4.1 Model development ..... 262

7.4.1.1 Coefficient of earth pressure at rest ($K_0$) ..... 263

7.4.1.2 Creating the valley ..... 265

7.4.1.3 Column stresses ..... 265

7.4.1.4 Modeling of test loading ..... 268

7.5 Stress-deformation analysis: Results and commentary ..... 269

7.5.1 Case 1: Linear-elastic analysis ..... 270

7.5.1.1 Sensitivity analysis ..... 272

7.5.2 Case 2: Analysis using the elastic-perfectly plastic model for clay and the hyperbolic model for rockfill ..... 273

7.5.3 Case 3: Analysis using the modified Cam-Clay model for clay and the hyperbolic model for rockfill ..... 275

7.5.4 Case 4: Case 2 with interface ..... 276

7.5.5 Shear in columns ..... 277

7.5.6 Bending behaviour in columns ..... 279

7.5.6.1 Equivalent stiffness and second moment of area ..... 282

7.5.6.2 Rockfill columns as a structural element ..... 283

7.5.7 Elastic rebound ..... 284

7.5.8 Other Comments ..... 285

7.6 Post-construction deformations ..... 286

7.6.1 Test loading with surcharge compared to piezometric loading ..... 289

7.7 Slope stability analysis ..... 291

7.7.1 Comments on slope stability ..... 292

7.8 Summary and conclusions from numerical analysis ..... 293

8. Summary, Conclusions and Recommendations ..... 323

8.1 Summary ..... 323

8.2 Major Conclusions ..... 324

8.2.1 Minor Conclusions ..... 327

8.3 Design and construction considerations ..... 328

8.3.1 Rockfill Properties ..... 329

8.3.2 Compaction ..... 329

8.3.3 Overall stability ..... 330

8.3.4 Limiting shallow deformations ..... 330

8.4 Recommendations for future research ..... 332

## Appendices

Appendix A: Test-hole logs

Appendix B: Raw monitoring data from test loading – on DVD

Appendix C: Modeling files – on DVD

## List of Tables

Table 2.1. Geotechnical properties. Modified from Baracos et al. (1983). ..... 54

Table 3.1. Grain size distributions for select samples (samples from TH-3). ..... 90

Table 3.2. Summary of properties measured from triaxial tests. ..... 91

Table 3.3. Summary of properties measured from direct shear tests. ..... 92

Table 3.4. Summary of assorted properties properties (averaged). ..... 93

Table 3.5. Results from one dimensional consolidation testing on clay specimens. ..... 94

Table 3.6. Summary of results from hydraulic conductivity tests. ..... 94

Table 4.1. Instrumentation types ..... 135

Table 4.2. Piezometer installations. ..... 136

Table 4.3. Slope inclinometer installations. ..... 137

Table 5.1. Calculated factors of safety for slope at research site (without loading) ..... 173

Table 5.2. Summary of weights and volumes of delivered fill ..... 174

Table 6.1. Summary of total pressure head (m) measured by vibrating wire piezometers. ..... 220

Table 7.1. Summary of analysis cases presented. ..... 296

Table 7.2. Summary of parameters used for modified elastic-perfectly plastic clay materials. ..... 297

Table 7.3. Summary of parameters used for modified Cam-Clay materials. .... 297

Table 7.4 Summary of parameters used for the numerical modeling of rockfill using the Duncan and Chang (1970) constitutive model for nonlinear analysis. ..... 298

Table 7.5 Summary of parameters used for the slope stability analysis ..... 298

Table 7.6. Summary of stability analysis. ..... 299

## List of Figures

Figure 1.1. a) and b) Examples of failed riverbanks in The City of Winnipeg. ... 16

Figure 1.2. Post-construction displacements measured over an 4.5 year period at the Seine River Siphon stabilization project a) near crest, up-slope of columns b) between rows of columns (updated from Yarechewski and Tallin 2003) ..... 17

Figure 1.3. Deformations measured at research site, between columns. 20 months after construction. ..... 18

Figure 1.4. Project timeline. ..... 19

Figure 1.5. Research site during test loading ..... 20

Figure 2.1 Three-part peak strength envelope (after Baracos and Graham 1981) ..... 55

Figure 2.2 Shear strength envelopes for loose and dense rockfill samples.After Abdul Razaq (2007). Reproduced with permission from Abdul Razaq, April 2010. ..... 55

Figure 2.3. Shear mobilizations of a) dense rockfill and b) loose rockfill materials. After Abdul Razaq (2007). Reproduced with permission from Abdul Razaq, April 2010. ..... 56

Figure 2.4. Dilation of a) dense and b) loose rockfill samples. After Abdul Razaq (2007). Reproduced with permission from Abdul Razaq, April 2010. ..... 57

Figure 2.5. Friction angle plotted vs. normal pressure for a variety of gravels, rockfills and sands. After Leps (1970). Reproduced with permission from ASCE, January 2010. ..... 58

Figure 2.6. Development of strength envelope. After Maksimovic (1996). Reproduced with permission from Electronic Journal of Geotechnical Engineering, March 2010. ..... 59

Figure 2.7 Dilation measured across top of dense rockfill sample during direct shearing. Modified from Alfaro et al. (2009)..... 60

Figure 2.8. Normalized stress deformation plots for large-scale direct shear tests on crushed Manitoba limestone..... 61

Figure 2.9. Normalized stress strain from direct shear tests of composite rockfill-clay samples. After Abdul Razaq (2007). Reproduced with permission. ..... 61

Figure 2.10. Test apparatus used by Murugesan and Rajagopal (2009) Reprinted, with permission, from the *Geotechnical Testing Journal*, Vol. 32, No. 1, copyright ASTM International, 100 Barr Harbor Drive, West Conshohocken, PA 19428..... 62

Figure 2.11. Rockfill columns modeled as equivalent strips. After Abdul Razaq (2007). Reproduced with permission from Abdul Razaq, March 2010..... 63

Figure 2.12. Failure mechanisms for non-rigid columns. After Navin and Filz (2005). Reproduced with permission from ASCE, June 2010. ..... 63

Figure 2.13.Behavior characteristics for piles subjected to lateral soil movement. After Poulos (1995). © 2008 NRC Canada or its licensors. Reproduced with permission, March 2010. ..... 64

Figure 3.1. Map showing research site along Red River in WInnipeg. (Modified from City of Winnipeg 2000). ..... 95

Figure 3.2 Aerial photo of the area surrounding the research test site. ..... 96

Figure 3.3. Research site after instrumentation installation. October 2007 ..... 97

Figure 3.4. Research site viewed from across the Red River. July 2007..... 97

Figure 3.5. East bank of Red River a) downstream of research test site b) upstream of research test site, October 10, 2007..... 98

Figure 3.6. Research site in June 2004. Looking downstream. ..... 99

Figure 3.7. Failed slope immediately downstream of test section. Photo taken April 2007 with high water levels. ..... 99

Figure 3.8. Cross section of research showing locations of Phase 1 instrumentation, prior to major site work. ..... 100

Figure 3.9. Plan view of research site showing elevation contours before the test loading. Some grading was done to accommodate the construction of the rockfill columns and void columns. ..... 101

Figure 3.10. RM-30 drill rig during installation of SI-12. December 2008. ..... 102

Figure 3.11. Tension crack formed along lower bank during fall drawdown. October 2007 ..... 103

Figure 3.12. Summary of stratigraphy and select laboratory results ..... 104

Figure 3.13. Silt layer exposed on riverbank. October 2007. ..... 105

Figure 3.14. Triaxial specimen of brown clay showing vertical fissure with rootlets. Sample T6 from TH-1 at elevation 228.6 m. ..... 105

Figure 3.15. Lower bank of test section, showing exposed rip-rap. Looking upstream from south edge of test section. November 2007. ..... 106

Figure 3.16. Grain size distribution for two samples from test site ..... 106

Figure 3.17. Principal stresses along a slip surface ..... 107

Figure 3.18. q-p' plots for triaxial tests for a) specimens of brown clay and b) specimens of grey clay ..... 108

Figure 3.19. For sample T8 tested at 300 kPa confining pressure a) q vs. strain and b) excess porewater pressure vs. strain ..... 109

Figure 3.20. Peak and post peak strengths for grey and brown specimens with interpreted failure envelopes. ..... 109

Figure 3.21. Mohr-Coulomb failure envelope for post-peak strength of clay. ... 110

Figure 3.22. Direct shear results for sample T6 tested with a 50 kPa normal stress with multiple reversals. ..... 110

Figure 3.23. Summary of direct shear testing results, plotting shear stress against normal stress. ..... 111

Figure 3.24. Results from oedometer specimens from elevations of a) 228.7 m and b) 223.3 m. ..... 112

Figure 3.25. Grain size distribution of crushed limestone used for backfilling rockfill columns. ..... 113

Figure 4.1. Instrumentation layout at the research test site. See Figure 3.9 for a more detailed site layout. ..... 138

Figure 4.2 Instrumentation cross section with slope inclinometer installations. 139

Figure 4.3. Instrumentation cross section with piezometer installations. ..... 140

Figure 4.4. Required water:cement ratio to achieve a desired unconfined compresseive strength for cement-bentonie grout. After Contreras et al. (2008). ..... 141

Figure 4.5. Compacting around SI-9, installed directly into a rockfill column .... 142

Figure 4.6. Installing a string of in-place inclinometers in SI-9. ..... 143

Figure 4.7. Late night monitoring of slope inclinometers. ..... 144

Figure 4.8. Measured Phase I slope deformations in the A-direction prior to column installation. August 2006-November 2007. ..... 145

Figure 4.9. Time vs. displacement for SI-4, from the time of installation to the beginning of the test loading. ..... 146

Figure 4.10. Recommended water:cement ratios for grout used for backfillling piezometers. After Contreras et al. (2008). Reproduced with permission from Contreras, January 2010. ..... 147

Figure 4.11 River levels and total heads measured at test site prior to field test (Aug 2006 to February 2008)..... 148

Figure 4.12. Data logger and peripherals in protective box ..... 149

Figure 4.13. Protecting instrumentation cables prior to test loading a) PZ-E and F facing the river b) beneath the fill footprint. ..... 150

Figure 4.14. Tethered aerostat at research site. ..... 151

Figure 5.1. Rockfill column layout detail. ..... 175

Figure 5.2. Cross-section used for stability analysis, with winter water level. ... 176

Figure 5.3. Cross section showing void columns and fill pile. ..... 177

Figure 5.4. B-direction displacements measured in SI-11 and SI-12 over the test loading period to look at the effect of the void columns. ..... 178

Figure 5.5 Drilling rockfill columns. ..... 179

Figure 5.6 a) and b) Compacting rockfill with vibrolance ..... 180

Figure 5.7. Sample printout of compaction effort from vibrolance control module. Hydraulic pressure and depth are plotted versus time..... 181

Figure 5.8. Deformations measured in SI-1, 2 and 4 from October 2007 to February 2008. The columns were installed in November 2007..... 182

Figure 5.9. Displacement vs. time for SI's 4,7,8 and10 following construction (Dec 14, 2007 to Feb 20, 2008)..... 183

Figure 5.10. Plot of fill load vs time during test loading..... 183

Figure 5.11. Test site one day prior to start of test loading..... 184

Figure 5.12.Test site on Day 1 of loading. ..... 184

Figure 5.13. a) and b)Day 2 of test loading. ..... 185

Figure 5.14. a) and b) Day 5 of test loading. ..... 186

Figure 5.15. a) and b) Day 7 of test loading. ..... 187

Figure 5.16. a) and b) Day 8 of test loading. ..... 188

Figure 5.17. a) and b)Test site with final load in place on Day 9. Photos taken from river. ..... 189

Figure 5.18. Test site on day 9 at end of loading. Photos taken along crest a) from downstream and b) from upstream..... 190

Figure 5.19. Research test section a) during re-grading and b) after the final site remediation work. ..... 191

Figure 6.1. Illustration of relationship between baseline readings and incremental and cumulative displacements from slope inclinometer monitoring. ..... 221

Figure 6.2. Relationship between horizontal displacement and shear strain along sloped shear zones. Modified from Gould and Dunnicliff (1971). ..... 222

Figure 6.3. Select instrumentation and instrumentation zones at the research test site. ..... 223

Figure 6.4. SI-1 deflections during the field test. Back from crest of slope. ..... 224

Figure 6.5. SI-2 deflections during field test. Downslope from crest. ..... 225

Figure 6.6. SI-4 deflections during field test. Installed between rockfill columns in upper row. ..... 226

Figure 6.7. SI-6 deflections during field test. Installed in a column in upper row. ..... 227

Figure 6.8. SI-7 deflections during field test. Installed directly in a rockfill column in the upper row. ..... 228

Figure 6.9. SI-8 deflections during the field test. Installed between rows of rockfill columns ..... 229

Figure 6.10. SI-9 deflections during the field test. Installed in column in lower row. Readings are erroneous due to shifting of casing during removal of in-place inclinometers. ..... 230

Figure 6.11. SI-10 deflections during the field test. Installed downslope of columns. ..... 231

Figure 6.12. SI-11 deflections during the field test. Installed near downstream edge of test site, between rows of columns. ..... 232

Figure 6.13. SI-12 deflections during the field test. Installed near upstream edge of test section, upslope of columns..... 233

Figure 6.14. Cumulative displacement vs. time at specified elevations for a) SI-4 and b) SI-7 and c) SI-10 ..... 234

Figure 6.15. Incremental displacement measured by in-place inclinometers in a) SI-8 (note: IPI 218.5-219.5 inoperable before day 2.5) and b) SI-9. ..... 235

Figure 6.16. Cumulative displacements and normalized incremental displacements for a)SI-4, b)SI-6, c) SI-7, d) SI-8. ..... 236

Figure 6.17. Contours of horizontal stress $\sigma_x$ beneath an embankment. After Poulos and Davis (1991). Reproduced with permission from Poulos, April 2010. ..... 237

Figure 6.18. Contours of maximum shear $\tau_{max}$ beneath and embankment. After Poulos and Davis (1991). Reproduced with permission from Poulos, April 2010. ..... 237

Figure 6.19. Porewater pressure response to loading and unloading..... 238

Figure 6.20. Displacements measured after test loading a) SI-4, b) SI-6, c) SI-7 ..... 239

Figure 6.21. Displacements measured after test loading a) SI-8, b) SI-11 ..... 240

Figure 6.22. Dispacement plotted against time at select elevations for a) SI-4, b) SI-7, and c) SI-8. ..... 241

Figure 6.23. a) Locations of cracking at test site on day 10 of testing b) crack at crest near centerline of test section ..... 242

Figure 6.24. Percentage of total fill placed versus cumulative displacement, including unload..... 243

Figure 6.25. Normalized average ground pressure due to fill plotted against displacement ..... 243

Figure 6.27. Dry sand sample under vacuum pressure, subjected to approximately 20 N cantilever load..... 244

Figure 7.1. Typical section of test loading used in numerical analysis..... 300

Figure 7.2. Interpreted failure envelopes for rockfill using method presented in Maksimovic (Maksimovic 1996). ..... 300

Figure 7.3. Friction angle corresponding to the estimated ultimate strength (asymptote to a fitted hyperbolic stress-strain curve) versus void ratio for crushed rockfill. ..... 301

Figure 7.4. Stress-strain curves for direct shear tests of dense limestone rockfill fitted with the hyperbolic model. ..... 301

Figure 7.5. Modulus of elasticity of rockfill (initial) versus confining pressure at various densities. ..... 302

Figure 7.6. Modulus of elasticity of rockfill (initial) and modulus number plotted versus initial void ratio. ..... 302

Figure 7.7. Mobilized shear strength and friction angle for dense specimen at 100 kPa confining pressure. Based on hyperbolic constitutive model fit to large scale direct shear test results. ..... 303

Figure 7.8. Hydraulic conductivity and volumetric water content curves for clay, used in the numerical modeling. ..... 304

Figure 7.9. Initial porewater pressure distribution, after simulating unloading during construction. ..... 304

Figure 7.10. Vertical and horizontal effective stresses and Ko distribution for Case 3. ..... 305

Figure 7.11 Illustration of plausible in-situ vertical stress profiles in a compacted rockfill column. ..... 305

Figure 7.12. In-situ stresses used for day 0 for MCC stress-deformation modeling (Case 3). a) Vertical effective stress and b) horizontal effective stress. ..... 306

Figure 7.13. Measured displacements compared to modeled displacements from the four modeling cases. ..... 307

Figure 7.14. Modeled versus measured porewater pressures for a) VW-A, b) VW-B, c) VW-D and d) VW-E. ..... 308

Figure 7.15. Linear-elastic analysis (Case 1) of test loading showing a) Y-effective stress increase and b) X-direction displacement due to loading. ..... 309

Figure 7.16. Linear-elastic analysis (Case 1) of test loading showing a) maximum shear stress and b) maximum shear strains at day 11 of the test loading. ..... 310

Figure 7.17. Sensitivity of displacement to normalized parameters. Maximum and minimum values (normalized to 0 and 1 respectively) are typical or reasonable bounds for the specific parameter. Displacements were recorded at elevation 223.5 (Point '4' in Figure 7.16) ..... 311

Figure 7.18. Case 2 stress-deformation analysis of test loading showing a) Z-effective stresses and b) X-direction displacement at day 11 of the test loading. ..... 312

Figure 7.19.Case 2: Stress-deformation analysis of test loading showing a) maximum shear stress and b) maximum shear strains, at day 11 of the test loading ..... 313

Figure 7.20. Case 2 q/p'. ..... 314

Figure 7.21. Stress-paths in q-p' space for select points. Rockfill points are taken at the clay-till interface, ~0.1m from the upslope and downslope edges of the upper equivalent strip. ..... 314

Figure 7.22. Case 3: a) Contours of Z-effective stress, and b) maximum shear strain. ..... 315

Figure 7.23. Horizontal stress change distributed along vertical edges of the upslope row of columns (equivalent strips) and in-between rows. Max shear stress along centerline of upper row column. ..... 316

Figure 7.24. Incremental shear stresses (day 11 –day 0) in modeled equivalent strip, and between equivalent strips, also showing cumulative (integrated from surface downward) incremental stress increase across equivalent strip. ..... 316

Figure 7.25. Vertical effective stress distribution across the equivalent strips at elevation 219 m. Section (A-A) shown in Figure 7.12 a). ..... 317

Figure 7.26. Deviatoric stress (q) and mean effective stress (p') near the edges of the upslope equivalent strip. ..... 317

Figure 7.27. Elastic rebound, measured and modeled for SI-8, in-between rows of columns. ..... 318

Figure 7.28. Total head boundary condition for simulated flood event. ..... 318

Figure 7.29. Boundary conditions for flood event analysis. ..... 319

Figure 7.30 Porewater pressure, vertical effective and vertical total stress distributions in clay for a) initial condition b) day 35 of flood stage c) immediately after drawdown. ..... 319

Figure 7.31 Post-test displacements from the research site, both measured and modeled. ..... 320

Figure 7.32.Cross section from stability analysis, showing slip surface 1719... 321

Figure 7.33. Summary of stability analysis results for test loading. The base cases have a zone of soil at residual strength at the toe. ..... 321

Figure 7.34. Mobilized shear strength and shear resistance along slip surface 1719 (day 9) ..... 322

Figure 7.35. Distribution of normal, porewater and suction pressures along slip surface 1719 (day 9)..... 322

## List of Copyrighted Material

Figure 2.1 Three-part peak strength envelope..... 55

Baracos, A. and Graham, J. 1981. Landslide problems in Winnipeg, Canadian Geotechnical Journal, 18: 390-401.

Figure 2.2 Shear strength envelopes for loose and dense rockfill samples..... 55

Abdul Razaq, W.F. 2007. Evaluation of riverbank stabilization using rockfill and soil-cement columns. Ph.D. University of Manitoba, Winnipeg, Manitoba.

Figure 2.3. Shear mobilizations of a) dense rockfill and b) loose rockfill materials. ..... 56

Abdul Razaq, W.F. 2007. Evaluation of riverbank stabilization using rockfill and soil-cement columns. Ph.D. University of Manitoba, Winnipeg, Manitoba.

Figure 2.4. Dilation of a) dense and b) loose rockfill samples.. ..... 57

Abdul Razaq, W.F. 2007. Evaluation of riverbank stabilization using rockfill and soil-cement columns. Ph.D. University of Manitoba, Winnipeg, Manitoba.

Figure 2.5. Friction angle plotted vs. normal pressure for a variety of gravels, rockills and sands ..... 58

Leps, T.M. 1970. Review of shearing strength of rockfill, Journal of the Soil Mechanics and Foundations Division, 96: 1159-1170.

Figure 2.6. Development of strength envelope ..... 59

Maksimovic, M. 1996. A family of nonlinear failure envelopes for non-cemented soils and rock discontinuities, Electronic Journal of Geotechnical Engineering.

Figure 2.7 Dilation measured across top of dense rockfill sample during direct shearing ..... 60

Alfaro, M.C., Blatz, J.A., Abdulrazaq, W.F., and Kim, C. 2009. Evaluating shear mobilization in rockfill columns used for riverbank stabilization, Canadian Geotechnical Journal, 46(8): 976-986.

Figure 2.9. Normalized stress strain from direct shear tests of composite rockfill-clay samples. ..... 61

Abdul Razaq, W.F. 2007. Evaluation of riverbank stabilization using rockfill and soil-cement columns. Ph.D. University of Manitoba, Winnipeg, Manitoba.

Figure 2.10. Test apparatus used by Murugesan and Rajagopal (2009) ..... 62

Murugesan, S. and Rajagopal, K. 2009. Shear load tests on stone columns with and without geosynthetic encasement, Geotechnical Testing Journal, 32(1): 76-85.

Figure 2.11. Rockfill columns modeled as equivalent strips ..... 63

Abdul Razaq, W.F. 2007. Evaluation of riverbank stabilization using rockfill and soil-cement columns. Ph.D. University of Manitoba, Winnipeg, Manitoba.

Figure 2.12. Failure mechanisms for non-rigid columns ..... 63

Navin, M.P. and Filz, G.M. 2006. Numerical stability analyses of embankments supported on deep mixed columns. In Ground Modification and Seismic Mitigation - GeoShanghai Conference, Shanghai, China: 1-8.

Figure 2.13.Behavior characteristics for piles subjected to lateral soil movement. ..... 64

Poulos, H. G. 1995. Design of reinforcing piles to increase slope stability, Canadian Geotechnical Journal, 32: 808-818.

Figure 3.1. Map showing research site along Red River in WInnipeg. ..... 95

City of Winnipeg. 2000. Riverbank stability characterization study for city owned riverbanks. City of Winnipeg Planning, Property & Development Department: Waterways Section, Winnipeg, Manitoba.

Figure 4.4. Required water:cement ratio to achieve a desired unconfined compressive strength. ..... 141

Contreras, I.A., Grosser, A.,T., and Ver Strate, R.H. 2008. The use of the fully-grouted method for piezometer installation: Part 2. Geotechnical News: 33-37.

Figure 4.10. Recommended water:cement ratios for grout used for backfillling piezometers. ..... 147

Contreras, I.A., Grosser, A.,T., and Ver Strate, R.H. 2008. The use of the fully-grouted method for piezometer installation: Part 2. Geotechnical News: 33-37.

Figure 6.2. Relationship between horizontal displacement and shear strain along sloped shear zones. Modified from Gould and Dunnicliff (1971). ..... 222

Gould, J. and Dunnicliff, J. 1971. Accuracy of field deformation measurements. *In* 4th PanAmerican Conference on Soil Mechanics: 313-366.

Figure 6.17. Contours of horizontal stress $\sigma_x$ beneath an embankment. ..... 237

Poulos, H. and Davis, E. 1991. Elastic solutions for soil and rock mechanics. Centre for Geotechnical Research, University of Sydney, Sydney.

Figure 6.18. Contours of maximum shear $\tau_{max}$ beneath and embankment.. ..... 237

Poulos, H. and Davis, E. 1991. Elastic solutions for soil and rock mechanics. Centre for Geotechnical Research, University of Sydney, Sydney.

# 1. INTRODUCTION

The City of Winnipeg was established at the meeting point of two major regional rivers, the Assiniboine and Red River. The Assiniboine River flows into the city from the West, and the Red River from the South. These rivers were historically important transportation routes, with Winnipeg being a major trading outpost, and transportation hub connecting the prairies in the South and West with the Great Lakes to the East and Hudson Bay to the North. As Winnipeg grew, development began along the riverbanks and then continued outward. The rivers remain a major source of identity for the people of Winnipeg, although they are no longer the economic and transportation backbones of the community. “The Forks,” located in Winnipeg’s downtown, is still considered to be the cultural and public center of the city.

The rivers were essential to the early development of Winnipeg as a city, but they also presented the community with some great challenges. The floods of 1950 and 1997 immediately come to mind. Much more common, and also devastating to those affected, are riverbank slope instabilities which plague parklands, infrastructure and homes. In an urban environment, where land is precious, especially along the river, the value of a property affected by slope instability usually warrants an investment in remediation.

Rockfill columns have been found to be a suitable stabilization method for many problem sites in Winnipeg soil conditions. Rockfill columns are constructed by boring a shaft through the unstable soil mass into a stable soil layer below. The

shaft is backfilled with crushed rockfill which is then often compacted. Rockfill columns work on a basic theory. At the location of the columns, the weak clay is replaced with stronger and stiffer rockfill, thereby stabilizing the slide mass and reducing ongoing deformations.

Slope stabilization works that utilize rockfill columns have been successful by most measures; however deformations after construction have in some cases been greater than expected. Current standard analysis and design methods neither predict nor explain these deformations.

This thesis will discuss a full-scale field test of rockfill columns, provide results, present analysis and give recommendations on their use and performance. The research was conducted at the University of Manitoba by the author, with guidance from academic advisors and the project steering committee.

## 1.1 Slope stability in the Winnipeg area

Winnipeg has approximately 240 km of riverfront within the city's limits, with 108 km being owned by The City. Much of the publicly owned riverfront is parkland, while the majority of the privately owned riverfront property has been developed for single or multi-family residential use. With much of the City's most valuable property located along the rivers, it is always a concern when this property is lost or disturbed by slope instabilities.

Riverbank failures in Winnipeg are often triggered by elevated porewater pressure conditions and/or a drawdown of the river level. Flooding or long wet

periods saturate the banks. When the river level drops following the event, high porewater pressures can remain in the clay banks after the buttressing effect of the floodwater is gone. The high porewater pressures reduce the effective stresses, and therefore the strength of the in-situ soils, potentially leading to slope failure. Figure 1.1 shows two failed sections of bank in the City of Winnipeg.

Artificially controlled water level changes may also be a factor in triggering slope movements. The water level of the Red River in the City of Winnipeg is partially controlled by the St. Andrews Locks and Dam to the north of The City. In summer, the water level is maintained at a relatively constant level for navigation and aesthetic reasons. In fall, the river level is lowered by approximately 2 m to minimize ice formation (Baracos and Graham 1981).

Other triggers of slope instability include surcharge loading along the crest, or the removal of soil near the toe by natural processes or human activity. Flowing water will naturally erode the soil along the submerged portion, eventually leading to a slope failure. With time, formerly safe upland property can become threatened with instability.

Development often contributes to the problem through the removal of established vegetation and the placement of structures near the crest. Established vegetation contributes to stability by mechanical reinforcing provided by the root mass, by limiting erosion and by reducing pore water pressures through water uptake via the roots. Poor drainage, overwatering, surcharging the crest and

other factors may also contribute to slope instabilities (Turner and Schuster 1996).

The economic consequences of localized riverbank instabilities have risen as riverfront development has increased. The cost of stabilizing and restoring an unstable riverbank is a relatively large expense, even without considering collateral damages. For example, the City of Winnipeg recently estimated the cost of restoring the 12 highest priority riverbank sections to be $23 million (Wiebe 2009).

### 1.1.1 Stabilization methods

Several other techniques, besides rockfill columns, have been used to address slope instabilities around Winnipeg. One of the most basic methods is to reduce driving forces by unloading the top of the slope, and/or increasing resisting forces by building a toe berm. Armouring the slope along the waterline is a simple but effective way of slowing the erosion of the toe. Unless the armouring is designed to act as a toe-berm, it will not increase the stability of the slope (Turner and Schuster 1996).

Granular shear keys are the most similar to rockfill column methods. A shear key is excavated, and backfilled with a coarse-grained aggregate. The fill material is then compacted with a vibratory hoe-pack or roller packer if conditions permit. The construction method of shear keys often leads to large displacements during construction because a significant area of the lower slope must be excavated to

the till layer before backfilling and compaction can begin (Tallin and Thiessen 2009).

Granular ribs which typically extend to the till, and trench drains which are generally shallower, are aligned perpendicular to the river bank and provide additional stability by replacing weak clay with stronger granular materials. These methods also provide a drainage path for excess porewater pressures (Lew and Graham 1988). Soil nailing may be suitable for over-steepened slopes where shallow wedge failures are the concern (Turner and Schuster 1996).

More rigid methods including concrete or sheet-pile retaining walls with anchoring can be effective, but are generally an expensive option. Retaining walls are often the technology of choice when protecting important structures situated near the crest of the slope when space is limited (Abramson et al. 1996). In other cases the best alternative is to relocate any threatened structures, and allow the river to run its natural course (Baracos and Graham 1981).

The thesis does not suggest that rockfill columns are always superior to any other method for stabilizing a riverbank. Each situation is unique, and the benefits, disadvantages, risks and costs of the range of alternatives should be considered before choosing the best option. The responsibility remains with the engineer to determine the most appropriate design.

## 1.2 Rockfill columns

The most common use of rockfill columns in Manitoba is to stabilize slopes with existing deep seated rotational or translational failures in the clay. These failures typically develop in glaciolacustrine clay deposits, although it is common for the failure to pass through fill material or an alluvial stratum.

In other cases rockfill columns can be used to protect property proactively where future environmental conditions or land use might otherwise cause the slope to become unstable. Generally, precautionary applications of rockfill columns are limited to sites with commercial developments or infrastructure installations, where the cost-benefit-risk analysis favours preventative measures.

### 1.2.1 Current practice

A general standard practice for the design and construction of rockfill columns has evolved in the Winnipeg area as the technology has become more common; however, design and construction practices still vary somewhat within the industry. Rockfill column installations typically consist of 2 or more rows of columns spaced in a triangular or rectangular pattern along the middle to lower slope. The columns usually have diameters between 1.2 and 3 m. Specifications generally call for the columns to penetrate into the underlying till layer by at least 0.3 m to anchor the base of the column, but a specified minimum till penetration of 1 m into competent till is becoming more common. There have been cases where the rockfill columns have been terminated in the clay layer, when the depth to till is too large to reach practically, and the critical slip surfaces

are within the clay. Spacing between column edges varies, but is commonly between 0.3 and 1 m. Contractors have found that closer spacings carry more risk of having the clay between columns blow-out at depth during construction (Personal communication with Jeffrey Tallin November 2009 and personal communication with Don White November 2007).

A crushed limestone rockfill is the standard backfill material. The specified gradation is typically a 150 mm minus, but other maximum sizes have also been used. The benefit of compacting rockfill columns has been debated within the industry, but compaction is becoming the standard as designers seek to take advantage of the increased stiffness and strength of denser rockfill. A hydraulically actuated vibrolance has been shown to provide effective compaction of rockfill (UMA Engineering Ltd. 2001, KGS Group Ltd. 2002). Previously, columns were compacted with an I-beam actuated by a vibratory pile driver or not at all, before a vibrolance became available locally.

The lack of construction guidelines or standard practice is due in part to the differences in the methods used in Winnipeg, from those used elsewhere. The construction methods and applications of rockfill column methods will be discussed in the following chapters.

Locally, the typical engineering process involves:

- Site visit and characterization noting scarps, tension cracks, toe bulging, and conditions affecting stability (such as erosion, loading, sources of excess ground moisture, and so forth.)

- Detailed site survey.
- Test hole drilling using solid or hollow stem augers to collect samples, characterize the soil, install instrumentation and possibly look for slickensided surfaces.
- Installation and monitoring of slope inclinometers to identify depth of active failure surface(s) and rates of movement.
- Installation and monitoring of piezometers.
- Laboratory testing and advanced strength testing as necessary.
- Back analysis of slope stability to determine appropriate shear strength properties of in-situ soils. Inclinometer monitoring results are used to choose an appropriate “critical” slip surface. The back analysis method is only applicable to slopes that have failed already.
- Analysis of slope with the inclusion of rockfill columns to determine appropriate design using slope stability software.
- Preparation of design, recommendations and specifications.
- Construction monitoring.
- Post-construction monitoring.

Some steps may be omitted or additional engineering components added on a project by project basis, considering experience, existing information, design criteria and risk.

This research was initiated without preconceived ideas that the industry standard design and construction methods were wrong; rather, the goal has been to further the understanding of the technology, allowing it to be utilized more effectively and with greater confidence.

## 1.3 Performance of Rockfill Columns

According to limit states design methods, engineering designs must meet a serviceability criterion, which defines acceptable deformations, and an ultimate strength criterion which is meant to ensure that catastrophic failure will not occur. Load and resistance factors are applied to account for the variability in materials, construction and end use (CFEM 2006).

Current design practices for engineering stabilization works using rockfill columns, and the field of geotechnical engineering in general, are based on working stress methods which do not address deformations in a direct way. The working stress design method ensures that the estimated available resisting forces exceed the driving forces by some prescribed factor of safety. There is no rational method for determining an appropriate factor of safety; instead, factors of safety are generally based on observations of past performance and

consequence of failure (CFEM 2006).[1] An appropriately chosen and applied factor of safety should ensure the deformations are acceptable, and that stresses remain within the allowable range. In some cases, such as for shallow footing design, deformations must be considered separately.

To the author's knowledge, there has not been a broad investigation into rockfill column performance from which appropriate design factors of safety were determined. Without a wealth of experience and previous successes, there is little assurance that commonly used factors of safety are adequate for all site conditions and design criteria.

The measure of rockfill column performance is deformation but the standard for acceptable rockfill column performance will vary from project to project. Post-construction slope deformations in the order of decimetres may be acceptable in a naturally vegetated park area. If repairs become necessary, they may involve little more than some landscaping. In comparison, acceptable deformations around basements, building foundations, bridge support structures or buried infrastructure are an order of magnitude lower (centimetres), while the cost of repairs may be many orders of magnitude higher.

Using current design methods, the only difference in the design of stabilization for a slope in a wooded parkland versus a slope at the base of a multi-story apartment building is the chosen design factor of safety (1.3 versus 1.5, for

[1] There is an ongoing movement towards limit states design in geotechnical engineering, but it is not yet the standard in practice. The Canadian Foundation Engineering Manual, 4th Edition (2006) contains a concise description and comparison of the methods from the geotechnical engineering perspective.

example). The one major design criterion that differs between the aforementioned projects (that is, the limit of acceptable deformations) is not explicitly addressed in the design process.

There is a wide range of experience with respect to post construction deformations of banks stabilized with rockfill columns. For example, Figure 1.2 shows the post construction deformation profile measured by a slope indicator at the Seine River Siphon, and Figure 1.3 shows cumulative deformations measured at the Author's research site. The Seine River site had a history of slope movements. Movements had been concentrated between 219 and 220 m at the monitoring point before the stabilization with rockfill columns. The subsurface conditions at the research site are discussed in more detail in Chapter 3 and 4.

From an end-user's perspective, it is somewhat irrelevant whether post-construction movements are due to elastic shear mobilization, plastic yielding, bending of the column or creep. From a design practitioner's perspective, knowing the cause and nature of these observed slope movements is of the utmost importance. Without an understanding whether deformations are due to shear mobilization, yielding, bending or creep, the design engineer cannot properly address either the serviceability criterion or the ultimate strength of slope reinforced with rockfill columns.

A useful logical step would be to incorporate some method of addressing potential deformations in rockfill column design. This thesis will not provide a

rigorous method to accomplish this, but will discuss the characteristics of the deformations observed in slopes reinforced with rockfill columns. This document will present concepts and supporting evidence for possible mechanisms that can explain the observed deformations.

## 1.4 Full-Scale Field Test

The large amount of stabilization work required in Winnipeg, and the significant associated costs led the sponsors of this project to initiate and fund this research. The City of Winnipeg realized that there was a potential opportunity to improve design and construction methods, leading to economic efficiencies. Geotechnical consultants saw value in further investigating rockfill column behaviour because it could lead to an improved design method and increased reliability. For contractors, the field test afforded an opportunity to demonstrate a technology that had not yet been fully accepted locally or elsewhere.

The project steering committee, consisting of representatives from the University of Manitoba, The City of Winnipeg, Subterranean (Manitoba) Ltd. UMA|AECOM, KGS Group Ltd. and AMEC Earth and Environmental, proposed that a full-scale field test was warranted to study the performance of full-scale rockfill columns installed in a natural riverbank. The limitations of laboratory scale testing, and numerical models do not always allow us to predict or understand the natural behaviour of engineering works. Full-scale tests are useful because they can provide an additional point of reference by stressing the technology beyond normal service conditions. The test results can then be used for calibrating

models and design methods. Analysis of the test results may even lead to a new or improved understanding of how fundamental engineering and scientific principles are at work in the system.

This research project seeks to further the understanding of the behaviour of rockfill columns by way of a full-scale field test. Chapter 5 will discuss how the test design balanced the need for controlled experimental conditions while still testing the columns in a prototype environment.

As illustrated in Figure 1.4, the site works began in May 2006. The columns were installed in November and December 2007 and the test loading began in February 2008. The field test consisted of reinforcing the bank with eleven 2.1 m diameter rockfill columns over a 19 m reach of riverbank. The slope was then loaded with fill to induce displacements in the clay slope and rockfill columns. The picture in Figure 1.5 was taken during the test loading. The instrumentation and monitoring captured the response to the loading. The field test will be discussed in detail in the following chapters.

This research focuses on applications in Winnipeg soil conditions, but the results will be of interest to all those considering rockfill columns for slope stabilization in weak, fine-grained soils.

## 1.5 Objectives and Hypothesis

### 1.5.1 Hypotheses

From research, theory and observations during the full-scale field test of the rockfill columns, the author has developed the following hypotheses:

- Rockfill columns undergo shear strains and bending deformations in the process of resisting slope movements.
- Deformations can be predicted with finite element modeling using material properties determined from laboratory and field testing.

### 1.5.2 Objectives

The objectives of this research are to:

- Use observations of a full-scale field test to demonstrate the effectiveness of rockfill columns for riverbank stabilization.
- Identify mechanisms that govern the behaviour of individual rockfill columns when stressed by unstable slope conditions.
- Identify mechanisms that govern the behaviour of rockfill columns as a group when loaded by an unstable slope.
- Strengthen numerical modeling practice and present improvements to methods for analysis of rockfill columns.

## 1.6 Organization and scope of thesis

This thesis will begin with a literature review of theories related to the performance and analysis of rockfill columns in stabilizing natural slopes. Chapter 3 discusses the characterization of the site, and presents the results of the laboratory testing program. The instrumentation and monitoring program will be presented in Chapter 4. Chapters 5 and 6 discuss the implementation of the full-scale field test and the monitoring results, respectively. Chapter 7 reviews the analysis and numerical modeling results and implications. This leads into the final chapter which presents recommendations and conclusions stemming from the research. Chapters 7 and 8 also include some analysis of monitoring results from other commercial rockfill column projects around Winnipeg, for the purpose of verification.

Background information will be included in the appendixes at the end of this document. Complete monitoring results are included in the attached digitized appendix.

The research by the author has focused on the full-scale field test. Research by Abdul Razaq (2007) and Kim (2007) at the University of Manitoba included materials testing and numerical modeling of rockfill, and soil-cement columns. The present work is intended to expand on the work done previously, and the work done by others will only be mentioned where it is necessary for continuity or reference.

Figure 1.1. a) and b)  Examples of failed riverbanks in The City of Winnipeg.

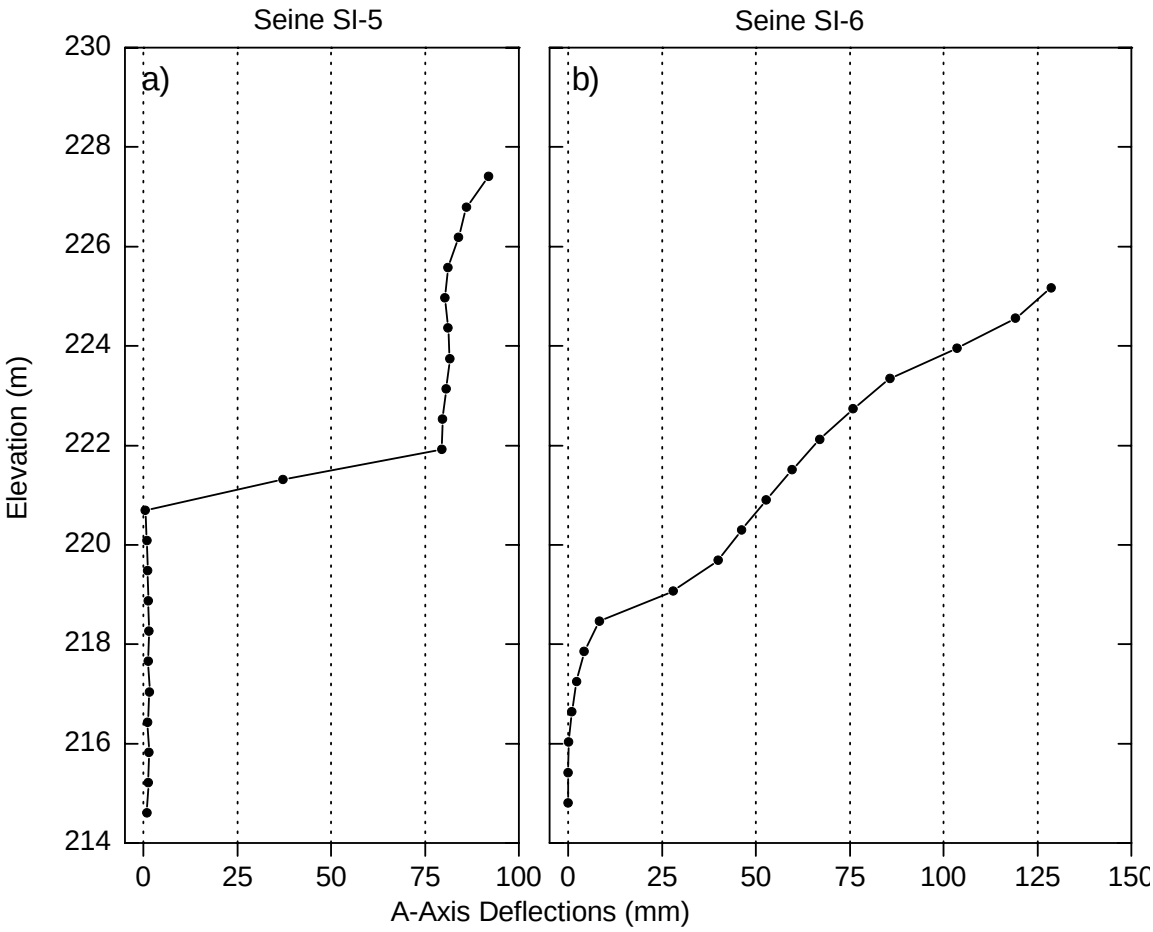


Figure 1.2. Post-construction displacements measured over an 4.5 year period at the Seine River Siphon stabilization project a) near crest, up-slope of columns b) between rows of columns (updated from Yarechewski and Tallin 2003)

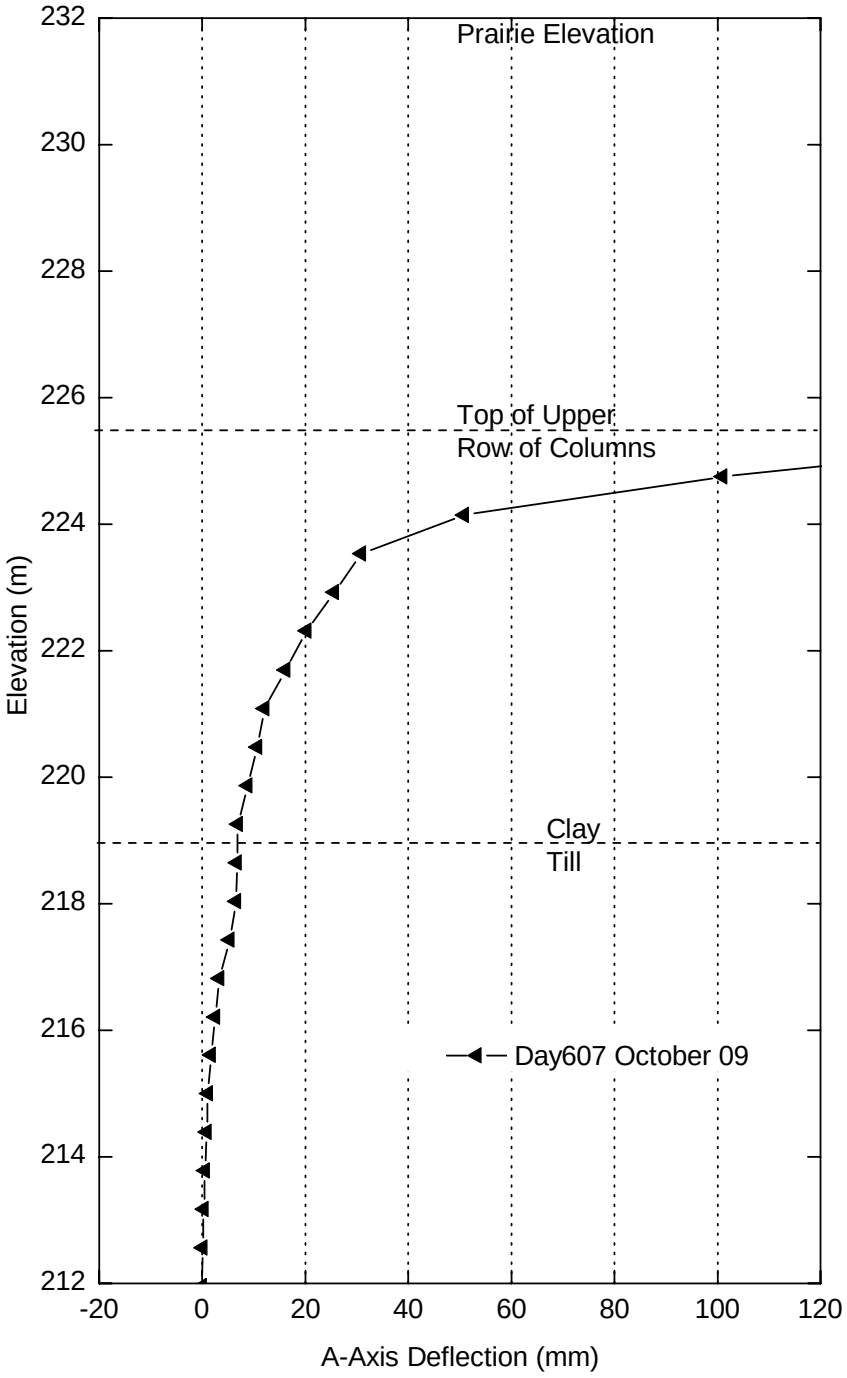


Figure 1.3. Deformations measured at research site, between columns. 20 months after construction.

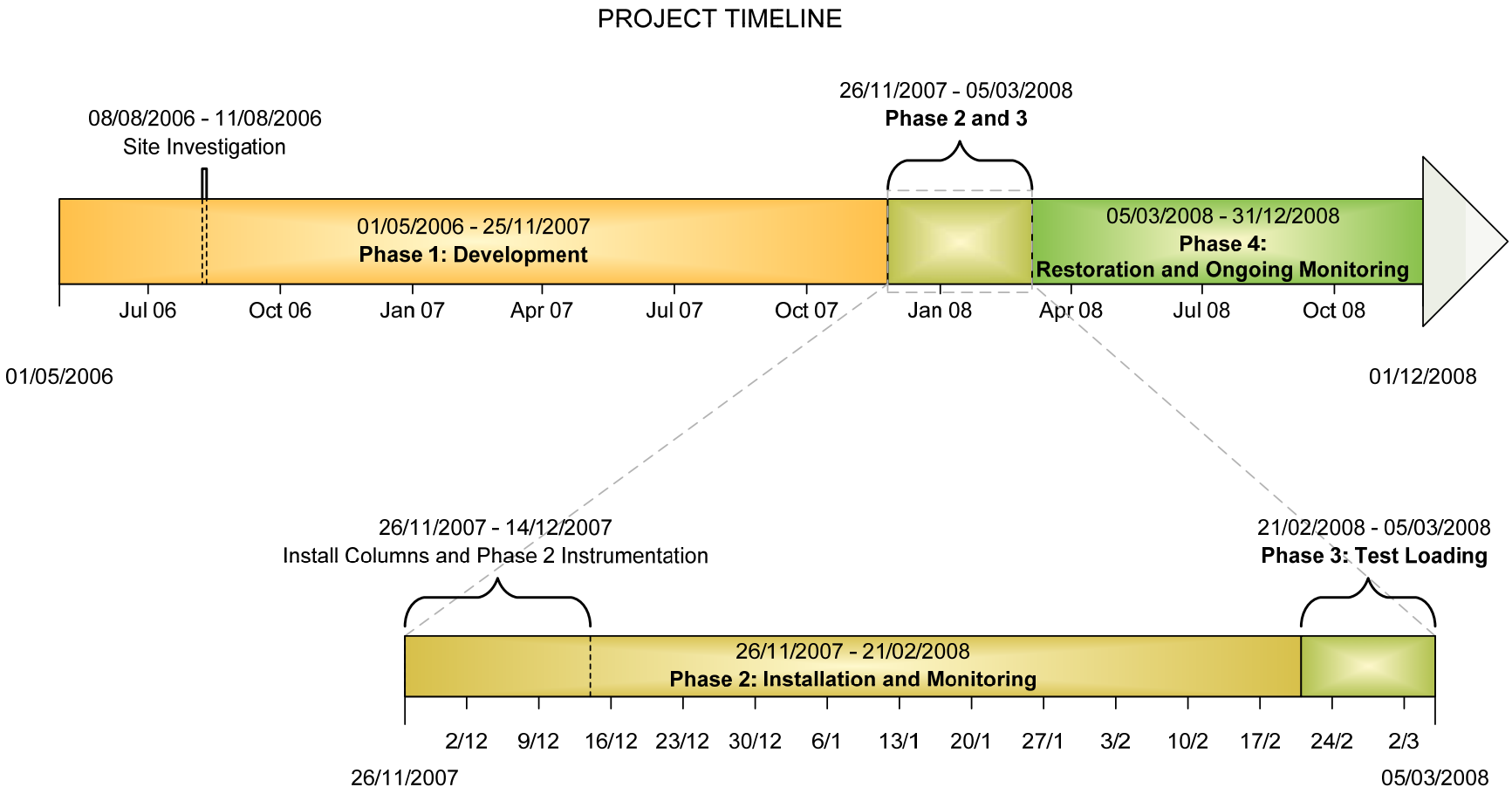


Figure 1.4. Project timeline.

Figure 1.5. Research site during test loading

# 2. LITERATURE REVIEW

## 2.1 Introduction

The effectiveness of using rockfill columns as a stabilization method for a riverbank depends on the site conditions, the materials, the design, and the construction technique. This chapter begins with an overview of the geotechnical conditions specifically relevant to rockfill column applications in the Winnipeg area. This is followed by a discussion of the important aspects of rockfill behaviour, including a summary of some test results. The final sections of this chapter will discuss the design, use and testing of rockfill columns, and comment on some related technologies.

The field test of rockfill columns discussed in this thesis is the third phase of a research project undertaken by researchers at the University of Manitoba. Prior research at the University of Manitoba was completed by Kim (2007) and Abdul Razaq (2007) with further discussion in Alfaro et al. (2009). The work of Abdul Razaq and Kim involved advanced laboratory testing and numerical modeling. It is highlighted here because it applies to the present research.

## 2.2 Properties of soil in the Winnipeg region

An overview shows that the soil conditions in the Winnipeg area are relatively simple. There are only three distinct soil units: an upper complex zone, glaciolacustrine clay and till. The soils are underlain by limestone bedrock

(Baracos et al. 1983a). Despite the apparent simplicity, the soil conditions can present some major challenges for engineers related to shear strength, bearing capacity, consolidation and slope stability.

Baracos (1977) and Baracos et al. (1983a) provided an extensive summary of the geological conditions and soil properties around Winnipeg. The typical upper and lower bounds for a variety of measurable properties for Winnipeg's clay and till are shown in Table 2.1. Baracos et al. (1983b) included a map set of the geology in the Winnipeg region.

The upper complex zone is typically less than 3 m thick, and consists of a variable stratigraphy of organic soil, fill, clay and silt layers. The local till is generally composed of a silt matrix with a heterogeneous blend of clay, sand, gravel, cobbles and boulders. The till is commonly low-plastic or non-plastic with a natural water content below 15%. The tills were placed during the Wisconsin Glaciation, between 24,000 and 12,000 BP. (Baracos et al. 1983a).

The glaciolacustrine clay was deposited by glacial Lake Agassiz. The clay unit varies gradually in thickness and character over a region that is many thousands of square kilometres in size. Winnipeg is located near the former center of this glacial lake, and thus the glaciolacustrine deposits are deeper and finer-grained than to the east or west (Teller 1976), though they are deeper to the south. In the Winnipeg area, the clay deposits range from 0 to 20 m in thickness. The clay is generally silty, with trace silt and gypsum inclusions. It is highly plastic and appears overconsolidated due to cementation. Its consistency varies from very

soft to very stiff. The clay is brown due to weathering near the surface, and becomes grey with depth (Baracos et al. 1983a). The natural water content typically ranges from 30 to 70%. The depositional process resulted in anisotropy due to horizontal laminations and preferentially oriented particles (Baracos 1977). Freeman (1970) (as cited by Baracos (1977)) demonstrated that the anisotropy results in increased hydraulic conductivity and lower strength parallel to bedding planes. The anisotropy also affects the elastic behaviour (Graham and Houlsby 1983) and the stability (Graham 1979) of the in-situ clay soils.

Winnipeg clays are often differentiated by the upper brown layer overlying a grey coloured clay layer. Baracos (1977) concluded that the mineralogical composition of these two layers is similar; Smectite, illite and kaolinite are the primary clay minerals while quartz, dolomite and calcite are the most prevalent non-clay minerals. Oxidation is the reason for the colour change from grey to brown.

Two projects, the Transcona Grain Elevator, and the Red River Floodway, have led to extensive research into the engineering properties of local soils. The failure of the Transcona Grain Elevator in north-east Winnipeg, contributed to the early development of bearing capacity theories (Baracos 1957) and it is still a significant case study many years later, for example (Morley 1996, Skaftfeld 1998, Blatz and Skaftfeld 2003).

The Red River Floodway was the world's second largest excavation project at the time of construction, which began in 1962 (Manitoba Floodway Authority

2010). The results of a test pit excavation and other geotechnical testing for the floodway design (Prairie Farm Rehabilitation Administration 1962) have contributed greatly to the understanding of local soil conditions and slope stability issues with publications by Mishtak (1964), Freeman and Sutherland(1973), Render (1970) and Anderson et al. (2004) among others.

In addition to the research work associated with the aforementioned projects, researchers at the University of Manitoba have done extensive testing on Winnipeg clays. Some areas of study include shear strength, plastic yielding, anisotropy, and permeability. Baracos et al. (1980) determined that a three-part shear strength envelope was appropriate for describing the peak strength of undisturbed clay samples from Winnipeg. Figure 2.1 shows this failure envelope. Graham et al. (1983) concluded that cementation contributed to the peak strength of undisturbed clay samples. Graham et al.(2009) identified a number of natural processes which degrade soil strength, including wetting-drying, freezing-thawing, heating-cooling, desiccation and chemistry changes. They explained that these processes can cause previously stable slopes to become unstable with time.

Yuen (1998) reported that the measured hydraulic conductivity for local clays is $10^{-10}$ to $10^{-13}$ m/s. The horizontal conductivity is generally two times greater than the vertical conductivity. Fissures and other discontinuities further increase the averaged large scale hydraulic conductivity (Render 1970).

Case studies by Anderson et al. (2004) and Van Helden et al. (2008) have demonstrated the application of the Modified Cam Clay constitutive model to clays in Winnipeg. The specifics of the relevant site and soil conditions are discussed in more detail in Chapter 3.

## 2.3 The stability of slopes in the Winnipeg region

Problems with slope stability in the Winnipeg area have been the focus of a number of research efforts. The literature addresses analysis methods, material properties, triggering conditions, failure mechanisms, and stabilization techniques. Baracos et al. (1989) show how the understanding of slope behaviour in Winnipeg has improved with time, as experience has increased and analysis methods have improved.

In 1961, Casagrande, as reported by Sutherland (1966), established the long standing rule of thumb for slopes in Winnipeg; Casagrande stated that a slope should not be greater than 6H:1V to be considered safe, or greater than 9H:1V if there is evidence of past failure. Research has since established a more rigorous theoretical understanding of the stability of riverbank slopes in Winnipeg.

By 1964 it was realized that total stress analysis of natural riverbank slopes in Winnipeg was insufficient, as total stress methods grossly overestimated the stability of banks (Mishtak 1964). Despite the research demonstrating otherwise, total stress analysis remained popular until the middle of the 1970's when the use of effective stress analysis began to increase (Baracos et al. 1989). As

effective stress analysis methods were adopted, Sutherland (1966) noted that new research was required to determine appropriate effective strength parameters for Winnipeg clay.

When considering the stability of a slope in overconsolidated clay, the engineer faces a dilemma as to whether peak, post-peak or residual strength definitions should be used for the analysis. Skempton (1985) discussed how shearing of clay soils reduces the interparticle bonds. Shear strains beyond the peak state break the interparticle cementation bonds to reduce the strength to a fully softened state. Further shearing reorients the clay particles to decrease the strength to a residual value. Freeman and Sutherland (1973), Baracos and Graham (1981) and Graham (1986) stated that use of the measured residual strength is appropriate when analyzing previously failed slopes in Winnipeg clay.

Baracos and Graham (1981) recommended using fully softened strengths for analysis and design of slopes in clay that had not been subject to large movements (failure). Tavenas and Leroueil (1981) suggested that the limit state approaches the critical state line with time, reinforcing the use of critical state properties for soils that are previously unfailed. Rivard and Lu (1978) made similar recommendations, and concluded that the normally consolidated strength is the most appropriate for analysis when designing slopes in fissured clays, even though the intact peak strength is higher. Peck (1967) demonstrated that the average strength along a potential rupture surface of a slope is greater than the residual strength but less than the peak strength of the clay. This is because of progressive mobilization of shear resistance along the failure surface, and the

non-uniform constitutive relationships along the slip surface. Potts et al. (1997) came to a similar conclusion in their research on the progressive failure of slopes.

The emergent use of effective stress methods in the 1970's increased the interest in groundwater conditions and their influence on slope stability. Early work in this area was done by Baracos (1978) and more recently by Tutkaluk (2000). Throughout much of the Red River valley, there is an upward groundwater gradient from the upper carbonate aquifer through the till and into the overlying clay, with seasonal exceptions (Render 1970). The base elevation of the Red River is controlled by intermittent contact with the local high points of the till layer. Lefebvre (1986) suggests that once the river bottom has eroded the clay so that the porewater pressures in the till can dissipate into the river, the porewater pressure will decrease in the clay banks, thereby increasing stability. At that point, the gradient becomes oriented more perpendicular to the riverbank as flows are influenced by river levels.

## 2.4 Testing of Materials

### 2.4.1 Measured Properties of Rockfill

The body of research on the properties of rockfill is largely focussed on applications in gravity dams, but this work is still generally applicable to rockfill used in columns. Only limited testing has specifically considered rockfill column

applications, with a focus on the shear strength and the mobilization of shear stresses within the rockfill.

Testing rockfill by direct shear is considered to be suitable for determining material properties used in the design of laterally loaded stone columns (Bachus and Barksdale 1989). Direct shear tests were done for a number of rockfill column projects using an in-situ apparatus (Munfakh et al. 1984) or large scale shear boxes (Bachus and Barksdale 1984, Goughnour et al. 1991, Yarechewski and Tallin 2003). Wisam Abdul Razaq (2007) working with Chang Seuk Kim (2007) completed an extensive program of tests on limestone rockfill materials, undisturbed clay, re-molded clay, rockfill-clay composites, cemented rockfill and soil-cement samples. Abdul Razaq and Kim used the large-scale direct shear box at the University of Manitoba, which accommodated specimens up 600 mm square and 400 mm deep.

Test results in Alfaro et al. (2009) demonstrated that the peak strength of the rockfill material is greatly affected by its density (Figure 2.2 and Figure 2.3). The void ratio (e) of the dense samples was 0.39 and 0.754 for the loose samples. Note that although the “loose” samples were not compacted, they showed dilatant behaviour while shearing (Figure 2.4). Negussey et al. (1988) suggests that this behaviour is expected with granular materials except for very loose samples at high confining pressures. The rockfill that was used for the current project was of similar origin to the rockfill tested by Abdul Razaq and Kim. The rockfill is crushed dolomitic carbonate bedrock (limestone). The rockfill is quarried at pits to the North and East of Winnipeg. The transition friction angle,

as described by Negussey et al. (1988) approximates the critical state friction angle.

The peak strength envelope of dense rockfill, like other granular materials, cannot be described by a single friction angle (Φ). The range of peak strengths is more reasonably described with an expression of secant Φ that depends on both stress and density (Bolton 1986). For rockfill column analysis, one should not use a single linear strength envelope for all cases without ensuring that it is appropriate for the confining pressures (Goughnour et al. 1991).

Abdul Razaq (2007) used a 'best fit' curve to produce the peak strength envelope in Figure 2.2 but there are other ways of interpreting this data. There are several empirical relationships and semi-empirical methods for developing non-linear peak strength envelopes. Leps (1970) compiled the shear strength characteristics of over 100 samples of rockfill and gravel from 15 different sources (Figure 2.5). The friction angles were measured with large scale triaxial apparatuses. The samples were tested at a variety of densities, which contributed to the scatter, but this also demonstrates the benefits of densification.

Leps (1970) commented that his research did not adequately consider the shear strength at low stresses, that is, below 70 kPa. Work by Maksimovic (1989, 1996) and Fannin et al. (2005) have addressed the low stress strength more directly. Maksimovic (1996) developed the following equation for a nonlinear failure envelope:

$$\tau = c' + \sigma_n \tan\left(\phi'_B + \frac{\Delta\phi'}{1 + \frac{\sigma'_n}{p_n}}\right) \qquad 2.1$$

where:

$\Phi_B$ = the basic angle of friction, which approximates the critical state friction angle.

$\Delta\Phi$ = the maximum angle difference (that is the difference between the secant friction angle as the confining pressure approaches zero, and the critical state friction angle).

$p_n$ = median angle normal stress (the normal stress at the median friction angle as shown on Figure 2.6)

Maksimovic's equation addresses the effects of dilatancy without relying on a direct measurement of it. Figure 2.6 shows the essential elements of the Maksimovic model.

The large scale direct shear test results of rockfill material led Abdul Razaq (2007) to conclude that the mobilization of shear resistance occurs from the up-slope edge of a rockfill column and proceeds towards the down-slope edge. The leading edge of the specimen (analogous to the upslope side of a rockfill column) began to dilate at a low strain, whereas the trailing edge of the sample contracted more, and began dilation at a higher shear strain as shown in Figure 2.7. Kim

(2007) was able to reasonably replicate the progressive mobilization with a numerical finite difference model.

The shear modulus (G) for direct shear tests is estimated by (Davis and Selvadurai 1996):

$$G=\frac{\Delta\tau}{\Delta s}h \qquad 2.2$$

and the shear strain is calculated as:

$$\gamma = \frac{\Delta s}{h} \qquad 2.3$$

where:

$\Delta\tau$ = change in shear stress

$\Delta s$ = horizontal displacement

h = height of specimen

$\gamma$ = shear strain

Abdul Razaq (2007) calculated an elastic modulus (E) of 22,000 kPa from the direct shear test results. This is slightly lower than the elastic modulus predicted by empirical relationships. A commonly used estimate of the initial tangent modulus ($E_i$) was developed by Janbu (as reported in Duncan and Chang (1970)):

$$E_i = k p_a \left(\frac{\sigma_3}{p_a}\right)^{n'} \quad 2.4$$

where:

k = modulus number, based on material type

$p_a$ = atmospheric pressure

n' = exponent for curve fitting

Barksdale and Bachus (1983) report modulus values varying between 30,000 and 60,000 kPa for rockfill columns loaded vertically. Rough estimates of the elastic modulus (below 1% strain) based on triaxial tests by Marsal (1967) range between 30,000 and 50,000 kPa. Research by Kokusho (1980) demonstrated that by 0.1% strain, the tangent shear modulus (for sands) had decreased by 50% from the initial maximum value, under a confining pressure of 100 kPa. Graham et al. (2004) showed similar results. The large scale shear test equipment used by Abdul Razaq and Kim was not able to identify the small strain modulus of the rockfill.

Test results from Abdul Razaq (2007) demonstrated that the initial shear modulus of dense rockfill was up to four times greater than that of loose rockfill. Figure 2.3 plots the measured stress-strain behaviour of loose and dense rockfill samples. Abdul Razaq (2007) and Kim (2007) also tested the rockfill in a medium density condition (e=0.531) but did not publish the results. Figure 2.8 shows the normalized stress-strain relationships from Figure 2.3 (a),

complemented by test results from UMA Engineering Ltd. (1992). The UMA tests used a less sophisticated apparatus, but the material was of similar origin (that is, crushed local limestone) to the material used in the present full-scale field test, and the tests done by Abdul Razaq and Kim.[1]

Most laboratory testing on rockfill, including (Bachus and Barksdale 1984, Alfaro et al. 2009) used a scaled down grain size distribution. Varadarajan et al. (2006) observed that the friction angle ($\phi$) and elastic modulus (E) decrease with increased maximum particle size for quarried rockfill, based on testing of samples up to a maximum grain size of 100 mm. Varadarajan found no correlation between the maximum grain size and Poisson's ratio.

#### 2.4.1.1 Constitutive models

There are several constitutive models available that attempt to describe the stress-strain characteristics of granular materials, for example Gajo and Wood (1999), Duncan and Chang (1970), Bauer and Zhu (2004), and Varadarajan et al. (2006). Some of these formulations, such as Duncan and Chang (1970) have

---

[1] The tests by UMA Engineering Ltd. (1992) were conducted with a large scale direct shear box, 600 x 600 mm by 350 mm high on crushed limestone with a 100 mm maximum grain size. The normal load was applied to the compacted specimens via a plate and a rigid hydraulic jack. The pressure (and thus the applied normal load) of the hydraulic jack was monitored, but the sample was not allowed to freely dilate. The normal pressure increased significantly as the load was applied. As expected (based on dilitant behavior of granular materials), the vertical stress increased more dramatically for the samples with the lower confining pressures. The results presented in Figure 2.8 have been normalized at each datum point.

been developed for sands, but may be reasonably extended to a large range of grain sizes.

Duncan and Chang (1970) present a method using hyperbolas to describe the stress-deformation characteristics of a soil. The method does not take into account stress history, density, volume change, or strain softening. A hyperbolic model, based on Duncan and Chang (1970), is supported by the Geo-Studio[2] software package. The large scale direct shear test results from Abdul Razaq (2007) were used to develop the parameters for the Duncan and Chang model, specific to limestone rockfill. This will be discussed further in Chapter 7.

The Duncan and Chang (1970) model defines the tangent modulus ($E_t$) as:

$$E_t = \left[1 - Rf\frac{(\sigma_1-\sigma_3)}{(\sigma_1-\sigma_3)_{failure}}\right]^2 E_i \qquad 2.5$$

where:

Rf = relates the asymptote strength to the failure strength

$E_i$=initial modulus as defined in Equation 2.4.

The initial modulus $E_i$ is also used as the elastic modulus for unload-reload stress conditions.

[2] Geo-Studio 2007. Geo-Slope International Ltd., Calgary Alberta.

Deluzarche and Cambou (2006) suggest that the continuum assumptions of finite element models may not be valid for rockfill because of the large size of the particles. Discrete element theoretical models such as those developed by Emeriault and Chang (1997), Sitharam and Nimbkar (2000), Deluzarche and Cambou (2006) or Froiio et al. (2006) eliminate the issues related to the relative size of individual particles because they model each particle as an individual element. A discrete element model would require a large amount of computing power to solve a simulation of rockfill column behaviour. It would also be difficult to model the interface between the discrete rockfill elements and the continuum clay. Exploring discrete element modeling of rockfill was not considered to be practical for the current project.

### 2.4.2 Properties of rockfill-clay composites

Abdul Razaq (2007) and Kim (2007) tested composite rockfill-clay samples to determine the effect of the area replacement ratio (the area of the rockfill columns in plan divided by the area of the improved zone). Small diameter (270 mm) rockfill columns were constructed within a re-molded clay specimen (600 mm diameter). The direct shear tests investigated area replacement ratios between 14% and 30%, with the column diameters ranging from 220 to 320 mm respectively (Figure 2.9). Abdul Razaq concluded that the shear resistance increased with increased area replacement ratio, but the net shear stiffness of the composite sample was not affected by the area replacement ratio or column diameter. (Abdul Razaq 2007)

Figure 2.9 taken from Alfaro et al. (2009) shows an unusual stress-strain relationship with an initial plastic yield point, followed by a second stage of increasing shear resistance. This result may be further evidence to support the suggestion of Barksdale and Bachus (1983) and Enoki et al. (1991) that the in-situ clay will yield before the resistance of the rockfill is fully mobilized. Following from this conclusion, one must be aware of the strength state throughout a soil mass, before predicting how the rockfill columns contribute their resistance to sliding.

Bachus and Barksdale (1984) tested model stone columns under lateral loading, and produced some unexpected results. They found that for low area replacement ratios (0.14), the composite sample was actually weaker than clay alone, which they attribute to flow of clay around the column. Bachus and Barksdale acknowledge that the soil-column interaction is very complex, and that full-scale verification tests are necessary to further understand the interactions.

Murugesan and Rajagopal (2009) also conducted rockfill-clay composite direct shear tests. They used much weaker clay and a smaller test apparatus than was used at the University of Manitoba. Murugesan and Rajagopal concluded that because of the poor confinement provided by the weak clay, the contribution of the rockfill columns was less than what is theoretically calculated. Murugesan and Rajagopal also performed a laboratory scale test of stone columns subjected to lateral loads with the apparatus detailed in Figure 2.10. They found that the columns did reduce lateral deformations, over an unreinforced sample, but a rotational failure developed through the columns. The laboratory scale columns

were 75 mm in diameter, and 600 mm long and spaced at 150 mm center to center.

### 2.4.3 Increase in density from compaction

UMA Engineering Ltd. (UMA Engineering Ltd. 2001a) conducted a field test to measure the effectiveness of compacting rockfill columns with a vibrolance. The rockfill was compacted with the same vibrolance used for the current research project (PTC 400HL Vibrolance with a V400 Powerpack).

The field test involved drilling a series of holes and backfilling them with a known mass of crushed limestone. Two columns were installed to a nominal depth of 10 m and a third was installed to 4 m. The 4 m column and one of the 10 m columns was sleeved with a steel casing. The second 10 m shaft was left un-sleeved. The average initial loose (uncompacted) density for the three columns was 17.0 kN/m$^3$. Final compacted densities of 21.5 kN/m$^3$ (for the unsleeved column assuming no increase in volume) and 21.8 kN/m$^3$ (sleeved) were achieved for the 10 m columns. The compacted density of the rockfill in the 4 m column was 20.5 kN/m$^3$. These results generally confirm the assumption that there is negligible volume change of the drilled shaft due to compaction. Water and air were jetted through the tip of the vibrolance during compaction, but the test columns were not filled with water before compaction.

A similar test by the KGS Group Ltd. (2002) involved compaction tests on two columns 3.05 m in diameter and 2.93 m in depth. The final measured densities were 17.9 kN/m$^3$ and 18.7 kN/m$^3$ for dry and submerged conditions respectively.

These tests were also done with the same PTC 400HL vibrolance. The conclusion is that adding water to the rockfill will increase the compacted density.

The results of UMA Engineering Ltd. (2001a) and the KGS Group Ltd. (2002) also show that compaction produces higher final densities in deeper and narrower columns. The limited data precludes the calculation of more precise relationships.

Chen and Bailey (2004) used SPT and CPT test results to conclude that vibro-compacted stone columns do not significantly improve the strength or density of cohesive soils. Goughnour et al. (1991), Priebe (1995), and Barksdale and Takefumi (1991) also suggest that there is marginal improvement to the in-situ clay due to vibro-compaction. In contrast, Guetif et al. (2007) reported an increase in the stiffness and strength of the in-situ clay as a result of installing stone columns using vibro techniques. It should be noted that the test methods and column installations were not equivalent in the above contrasting results. Vibro-compaction is more effective at improving in-situ sand and silt than improving in-situ clay (Chen and Bailey 2004).

## 2.5 Rockfill Columns

The realm of rockfill or stone column technology includes a number of applications and construction methods. An overview of the available literature suggests that most rockfill column applications employ either the vibro-displacement, vibro-replacement or rammed-aggregate methods of rockfill

column construction, (Barksdale and Bachus 1983, Diyaljee and Pariti 1990, Goughnour et al. 1991, Slocombe and Moseley 1991, Stark and Yacyshyn 1991).

The vibro-replacement method uses a vibratory lance to create a columnar void by advancing the lance downward while jetting water through the tip. The water then carries the loosened material to the surface. The hole is backfilled as the lance is retracted. The vibro-displacement method uses jetted air to help advance the probe, and the in-situ soil is displaced laterally to accommodate the probe and rockfill material (Bachus and Barksdale 1989). The Japanese “sand compaction pile” technique also produces a similar column of sand using a different construction method (Barksdale and Takefumi 1991).

The vibro-displacement and replacement methods are practical in soft clays, but in soils with undrained shear strengths greater than 50-100 kPa it becomes difficult to advance the probe to depth without pre-boring (Barksdale and Bachus 1983). The local (Manitoba) practice described in Chapter 1 involves pre-boring the columns with an auger. Variations of drilled shaft methods have been described by Datye and Nagaraju (1981), Barksdale and Bachus (1983), Diyaljee and Pariti (1990) and Tweedie et al. (2004).

Rockfill columns are often used to increase bearing capacity or reduce settlements beneath structures or embankments (Broms and Anttikoski 1984, Barksdale 1987, Guetif et al. 2007). The use of rockfill columns specifically for improving slope stability is less common. Some of the design objectives, such as increasing shear strength and resisting lateral deformations, are common to both

bearing capacity and slope stability applications (Goughnour et al. 1991). Some articles that discuss the use of rockfill columns specifically for slope stability applications include: Barksdale and Bachus (1983), Diyaljee and Pariti(1990), Goughnour et al. (1991), Abramson et al. (1996), Yarechewski and Tallin (2003), Thiessen et al.(2008) and Alfaro et al. (2009).

### 2.5.1 Design methods

Methods for analysing rockfill columns for the stabilization of a riverbank are similar to methods for laterally loaded piles and ground improvement technologies. It is generally assumed that the slope is failing (or will potentially fail) along a slip surface that can be identified by slope stability software. By replacing weak clay with stronger rockfill along an existing or potential failure surface, the factor of safety against sliding is increased. The rockfill derives its strength from interparticle friction as a function of density and pressure. As explained in Chapter 1, there are no current design procedures to explicitly address deformations of slopes stabilized by rockfill columns.

Numerical modeling of rock columns as a two-dimensional plane-strain problem is accomplished by using either equivalent strips or averaged strength parameters (Barksdale and Bachus 1983). Both of these methods use the area replacement ratio ($A_r$), which is the area of the rockfill columns divided by the improved area. The area replacement ratio for a triangular array is calculated as (Goughnour et al. 1991):

$$A_r = \frac{\pi d^2}{4S^2 \cos 30^\circ} \qquad 2.6$$

where:

S = center to center column spacing

d = column diameter.

For a 2.13 m diameter column and 3.1 m spacing (as was used at the site of the current full-scale field test), the area replacement ratio is 0.43 (43%).

The equivalent strip method converts the 3-dimensional columns into a continuous strip that has the same volume per unit length. The equivalent strip is then suitable for two-dimensional plane-strain stability analysis. Figure 2.11 demonstrates how a multiple rows of rockfill columns can be modeled as equivalent strips. The width of an equivalent strip for one continuous row of rockfill columns is:

$$W = \frac{A_s}{S} \qquad 2.7$$

where:

$A_s$ = area of a single column

The equivalent strip method is especially useful for numerical modeling, and was used for stability analysis by numerous authors, including Barksdale and Bachus

(1983), Bergado (1996), Christoulas et al. (1997), Stewart et al. (2004) and Ghazavi and Shahmandi (2008).

The average shear strength method models the improved soil as a homogenous material by averaging the strength parameters of the rockfill and clay. Equations 2.8 and 2.9 show how the average Φ and c values can be calculated (Barksdale and Bachus 1983):

$$\tan\phi_{avg} = \frac{\gamma_s A_r \tan\phi_s + \gamma_c (1-A_r)\tan\phi_c}{\gamma_s A_r + \gamma_c (1-A_r)} \qquad 2.8$$

and

$$c_{avg} = c_c (1-A_r) \qquad 2.9$$

where:

$\gamma_s$, $\gamma_c$ = wet unit weights of rockfill and clay respectively

$\phi_s$, $\phi_c$ = friction angles of the rockfill and clay respectively

$c_c$ = cohesion of the clay

Navin and Filz (2006) and Christoulas et al.(1997) obtained similar results using the averaged parameters and equivalent strip methods for analysing the stability of an embankment founded on columns.

A third method of calculating shear strength in the improved zone is the Japanese method (Aboshi et al. 1979). The average shear strength is calculated by:

$$\tau_{ave}=(1-A_r)\tau_c+A_r\tau_s\cos\alpha \qquad 2.10$$

where:

$\tau_{ave}, \tau_c, \tau_s$ = average, clay and rockfill shear strengths

$\alpha$ = angle of inclination of the failure surface

The Japanese method is less appropriate for computer analysis because the average shear strength must be calculated at each point along a potential slip surface.

Enoki et al. (1991) proposed that the conventional method for considering the composite nature of ground reinforced with rock or sand columns is not complete. The conventional method sums the shear resistance of the clay and rockfill proportionally along a common slip surface. The implicit assumption is that the coarse grained column material and the surrounding fine grained material fail simultaneously at the point where they are providing the full shear resistance defined by their respective failure criteria.

Direct shear and triaxial test results for composite samples reported by Enoki et al. (1991) and Abdul Razaq (2007) showed that the clay fails before the rockfill inclusion. Therefore, the shear resistance predicted by the conventional method

will overestimate the mobilized shear resistance of the composite material under certain conditions. Because the method proposed by Enoki et al (1991) is intended for assessing bearing capacity beneath embankments, it does not consider pre-existing mobilized shear stresses in the ground. A slope, by nature, will have in-situ shear stresses mobilized at depth (Chowdhury 1976, Silvestri and Tabib 1983).

The analysis proposed by Enoki et al. (1991) sought to account for the anisotropy of the composite soil. The method considers the resistances in the active zone of a slide (analogous to axial compression), and in the passive zone (analogous to axial extension), separately.

#### 2.5.1.1 Failure modes

Kivelo (1998) and Kivelo and Broms (1999) discussed the eight potential modes of failure illustrated in Figure 2.12. The subject of their research is lime/cement columns but the same failure modes have been applied to piles (Broms 1972 as reported in Navin and Filz 2006) and are generally applicable to rockfill columns. Modes a-c show failure due to bending, mode d is flow of clay around the columns and mode e is rotation of the columns. Modes f and g are horizontal translation and shear failure respectively.

Test results show that the critical failure mode depends on the shear strength and geometry; therefore all failure modes should be considered (Kivelo and Broms 1999, Kitazume and Maruyama 2007). Stability analysis considers only Mode g, which is shearing through the column. It follows that if the other failure

modes are possible, and are critical under certain conditions, then limit equilibrium analysis overestimates the stability of the composite slope in those cases (Filz and Navin 2006).

Priebe and Grundbau (1995) stated that ground improved with vibro-replacement columns does not fail catastrophically until the shear strength of all of the columns is mobilized. Stone columns deform with relatively little loss in shear strength capacity, until the neighbouring columns are also loaded to capacity. With piles or cemented columns, individual elements may fail before the theoretical capacity of the system is achieved.

### 2.5.2 Rockfill columns for slope stabilization

Poulos (1995) recommended that stabilizing piles should be installed at the deepest point of the slip surface to prevent development of a truncated failure upslope or downslope of the piles. Enoki et al. (1991) recommended that granular columns be located slightly upslope of the deepest point of the slip surface in order to derive some resistance to sliding by partially mobilizing the compressive strength of the rockfill, and incidentally increasing the vertical effective stresses. Installing the column at the deepest point of the slip surface is the most efficient use of the rockfill by maximizing the weight of rockfill above the critical zone while minimizing the volume of rockfill beneath the critical zone (per. com. Tallin 2009[3])

[3] Personal communication with Jeffrey Tallin, November 2009. AECOM, Winnipeg MB.

### 2.5.3 Numerical Modeling

Computing capacity has progressed along a roughly similar timeline to modern geotechnical engineering. The use of numerical modeling methods has become entrenched in geotechnical research and practice and there is a selection of software packages that are commercially available. Providing a general review of numerical analysis methods is beyond the scope of this document; relevant aspects of the theory and methodology of numerical modeling are discussed as necessary in Chapter 7.

Improvements to the stability of a slope can be estimated by incorporating rockfill columns into a limit-equilibrium slope stability analysis, using the methods described in Section 2.5.1 (Christoulas et al. 1997). Stability analyses can use stresses calculated by finite element (FE) models for calculating the factor of safety (Krahn 2003). Finite Element models can be used to calculate a factor of safety by the strength reduction or gravity increase methods. Navin and Filz (2006) recommend the strength reduction method for the analysis of deep-mixed columns because it allows the designer to identify the critical failure mechanism (as described in Section 2.5.1.1.)

Three-dimensional (3-D) models are the best way to account for geometry when conducting stability, seepage or stress deformation modeling; however, the use of 3-D models is relatively infrequent because of modeling complexity, limited software availability and insufficient computing power. Navin (2006) reports that 2-D and 3-D models produced very similar deformation results when modeling an

embankment stabilized with deep mixed columns. Duncan (1996) reported that the results of 2-D and 3-D analyses were similar for a large sampling of projects.

Turner and Shuster (1996) pointed out that FE modeling of natural slope deformations is difficult. On the other hand, FE modeling has been used successfully in many cases to model deformations associated with loading of ground that was improved with rockfill or deep mixing method (DMM) columns (Stewart et al. 2004, Deng et al. 2006, Navin and Filz 2006).

## 2.6 Related technologies

### 2.6.1 Stabilization by Piles

Traditional piles (such as cast in place, sheet or soldier piles) have been successfully used for many slope stabilization projects (Brandshaug et al. 2001, Martin and Chen 2005, Poulos 1995, Turner and Shuster 1996, Viggiani 1981). The differences in engineering behaviour between piles and rockfill columns are significant, but the similarities warrant a brief discussion. The difference in stiffness and strength between rockfill and concrete or steel is many orders of magnitude. Furthermore, rockfill is not able to resist negative stress, and this limits its ability to resist bending stresses.

Analyses of piles subjected to lateral soil movements vary somewhat from the methods used to analyse piles subjected to horizontal loads applied by the superstructure at the ground surface. Poulos (1973) developed an analysis for a single pile in moving soil using the soil flexibility factor $K_R$:

$$K_R = \frac{E_p I_p}{E_s L^4} \qquad 2.11$$

Where $E_p$, $E_s$ = the elastic moduli of the the pile and soil respectively

$I_p$ = moment of inertia of the pile

L = length of the pile above the anchored depth

The study demonstrated that with a $K_R$ less than $10^{-3}$, the deformation profile of a pile is very similar to that of the surrounding soil. The formulation presented by Poulos (1973) also shows that stiffer piles develop higher internal moments.

Viggiani (1981) proposed a method to calculate the ultimate shear force in a vertical pile that is loaded by slope movements. The study also identified six modes of failure, similar to those of Kivelo (1998), and the respective failure conditions. Poulos (1995) described three modes that characterized the behaviour of laterally loaded piles. These modes are shown in Figure 2.13. Poulos (1995) emphasized that piles used for stabilizing a slope must be of relatively large diameter and stiffness to generate a large stabilizing force without failing the pile. A drawback of piles for slope stabilization is their inability to withstand deformations (Turner and Schuster 1996).

Chen and Poulos (1994) and Reese et al. (1992) used P-Y curves to calculate deflection profiles of piles subjected to soil movement. Chen and Poulos (1997) include design charts for determining loads and deflections of piles and pile groups subjected to lateral soil movement.

The interaction between a pile and the in-situ soil is an important consideration. The limiting contact pressure for an individual pile in clay is commonly taken as $9 \bullet s_u$, where $s_u$ is the undrained shear strength (Chen and Poulos 1997). Brandshaug et al. (2001) presented a method for estimating the horizontal bearing capacity of a pile using a 2-D FEM numerical model. The model incorporates the discrete piles into a 2-D stability model by distributing the columns into an equivalent wall. Martin and Chen (2005) used 3-D models to assess the behaviour of piles passing though a sliding soil mass, considering shear forces as well as bending moments. The 3-D model was able to predict the development of flow around the piles as the stiffness of the piles was increased.

### 2.6.2 Other ground improvement techniques

Rockfill columns are used for similar applications to lime/cement columns or deep mixing method (DMM) improved ground. The cementation gives DMM or lime/cement columns increased stiffness and cohesive strength compared to rockfill. Failures of cemented soil tend to be brittle (Kivelo and Broms 1999). Centrifuge tests of DMM improved ground (Kitazume et al. 2000, Kitazume and Maruyama 2007) have identified many of the conditions that lead to the failure modes discussed in Section 2.5.1.1.

Ground improvement methods which involve cementing agents are analyzed to account for high apparent cohesion of the materials. The undrained shear strength envelope is defined by a composite failure surface (Kivelo and Broms

1999). The stress-strain characteristics of these improved soils are different as well; they exhibit a higher modulus of elasticity than untreated ground or rockfill (Abdul Razaq 2007). Rockfill/sand columns improved with geogrid reinforcement (Sharma et al. 2004), or geosynthetic encasement (Murugesan and Rajagopal 2009) have been shown to be stiffer and stronger than unimproved columns.

### 2.6.3 Shear and bending in columns

The following discussion on the apparent bending behaviour of rockfill columns borrows from the theories of structural engineering. To the Author's knowledge, there is no specific research on the subject of bending of rockfill columns. Byrum (2008) mentioned bending of rockfill members, but did not present any tests or theories. Navin (2005) and Kivelo (1998) discussed bending of lime/cement deep mixed soil columns as a potential failure mode.

Shear deformations are usually ignored in structural engineering applications with concrete or steel members because shear deformations are much smaller than the bending deformations. This is especially true for sections with a large span-to-depth ratio (MacLeod 2005). The relationship between shear and bending deformations is approximately estimated according to (MacLeod 2005):

$$\frac{\Delta_b}{\Delta_s} = \frac{0.04AL^2}{I} \qquad 2.12$$

It is assumed that the shear and bending deformations are superimposed so that:

$$\Delta=\Delta_b+\Delta_s \quad (2.13)$$

where

A = cross sectional area of member

L = length of member

$\Delta_b$,$\Delta_s$ = bending deformation and shear deformation

I = 2nd moment of inertia of cross section

Shear and bending deformations may both need to be considered when the span to depth ratio of a beam is less than 10:1 (MacLeod 2005). Resources such as Young and Budynas (2002) provide formulas for assessing shear and bending deformations under a variety of loading conditions.

## 2.7 Full-scale field tests

There have been no published full-scale field tests that used rockfill columns for stabilizing a natural slope. The installation methods used for the current project are also unique among full-scale field tests for other applications.

Munfakh et al. (1984) tested the performance of a full-scale embankment founded on stone columns in New Orleans. The stone columns were installed using the vibro-replacement technique into a soft clay soil. The test was monitored with slope inclinometers, pneumatic piezometers, settlement gauges and pressure plates. The columns were installed by the vibro-replacement

method. The researchers brought the embankment to failure through a combination of surcharge loading and excavating at the toe. The test was terminated when a rotational failure developed through the embankment and stone columns.

Munfakh et al. also conducted in-place direct shear tests on columns, reporting a peak friction angle of 54˚. A friction angle of 42˚ was used as the final design friction angle. As part of Munfakh's project, an un-reinforced control section was also tested. The researchers reported that the stone columns reduced settlements, improved pore-pressure dissipation, decreased lateral displacements and provided cost savings.

Bergado (1996) discussed a test embankment built on soft clay ground improved by compacted sand columns. The compacted sand columns were 0.3 m in diameter and arranged with triangular spacing with 1.5 m centre to centre spacing. Greenwood (1991) summarized the results from test loading a number of embankments built on stone column foundations, but the results focus on settlement and stress concentrations, and not horizontal displacement. Greenwood (1991) fittingly concluded that:

> *It is apparent from the above experiences that anything other than full scale load testing is potentially misleading when assessing a foundation on soft clays strengthened by stone columns. The stiffness of the composite system is dependent to a very large degree on the interaction between the columns and clay: mobilised strengths in each are continually*

*changing with applied load as each deforms to accommodate and equate stresses.*

A study of material properties, related applications and similar technologies provides valuable insight into the expected behaviour or rockfill columns used for riverbank stabilization; however, the ground conditions, installation methods and applications make rockfill column applications in Manitoba unique. The observed past performance of stabilized slopes and the long term need for an economic and practical solution warrant a full-scale field test to help engineers understand the complexities of riverbanks stabilized with rockfill columns.

Table 2.1. Geotechnical properties. Modified from Baracos et al. (1983).

| Geotechnical Property | Typical Lower | Typical Upper |
|---|---|---|
| Glaciolacustrine Clay | | |
| Unit weight – moist (kN/m$^3$) | 15.7 | 18.1 |
| Unit weight – dry (kN/m$^3$) | 10.2 | 13.4 |
| Liquid limit (%) | 65 | 110 |
| Plastic limit (%) | 20 | 35 |
| Plasticity index (%) | 40 | 75 |
| Clay size fraction (%) | 70 | 85 |
| Sensitivity | 2 | 4 |
| Compression index – $C_c$ | 0.5 | 1 |
| Overconsolidation ratio | 1 | 5 |
| Unconfined compressive strength (kPa) | 50 | 120 |
| Normally consolidated friction angle (°) | 17 | 23 |
| Normally consolidated residual friction angle (°) | 8 | 12 |
| Deformation modulus (kPa) | 3500 | 20500 |
| Till | | |
| Unit weight – saturated (kN/m$^3$) | | 23.5 |
| Unit weight – dry (kN/m$^3$) | | 22 |
| Clay size fraction (%) | 10 | 20 |
| Silt size fraction (%) | 30 | 40 |
| Sand size fraction (%) | 25 | 35 |
| Pressuremeter modulus (kPa) | | 240000 |

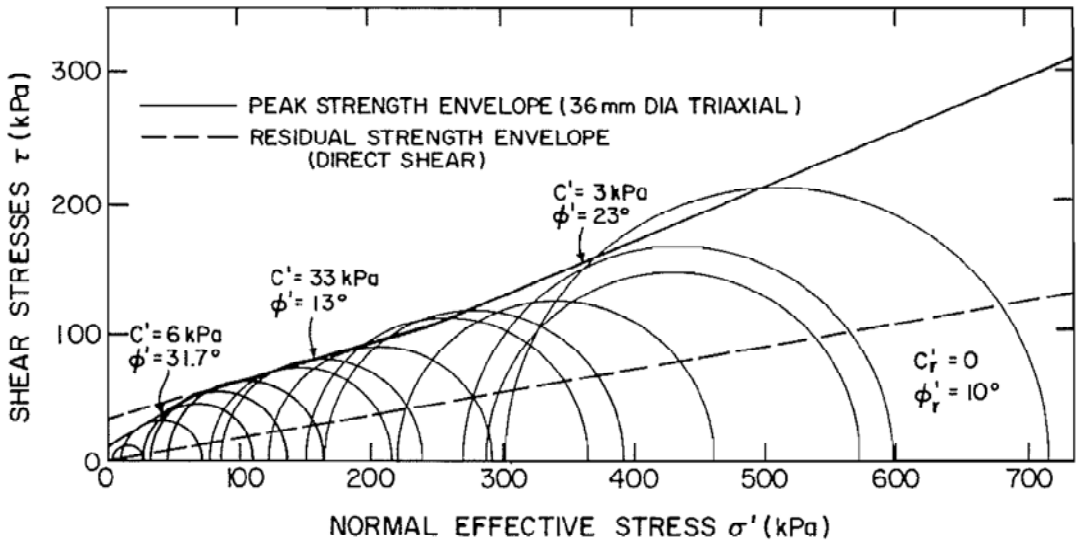


Figure 2.1 Three-part peak strength envelope (after Baracos and Graham 1981)



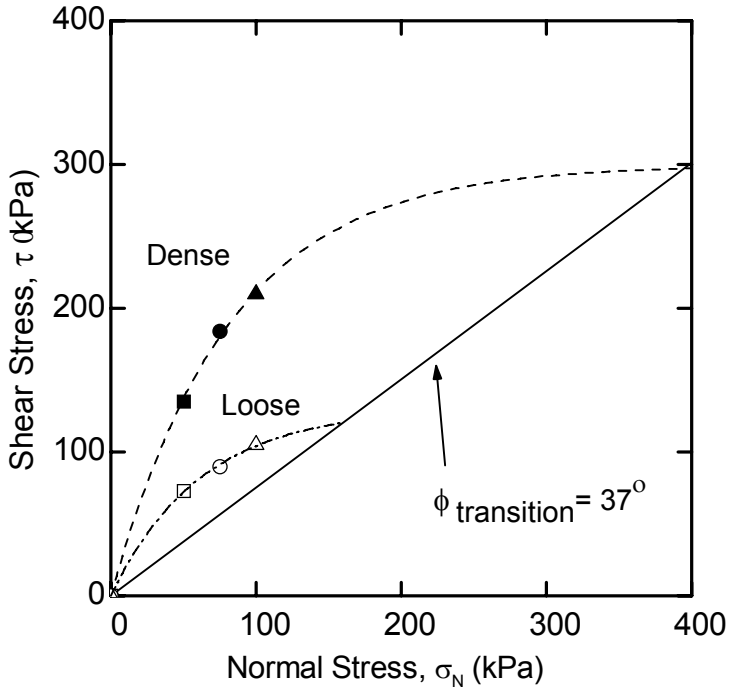


Figure 2.2 Shear strength envelopes for loose and dense rockfill samples.After Abdul Razaq (2007). Reproduced with permission from Abdul Razaq, April 2010.

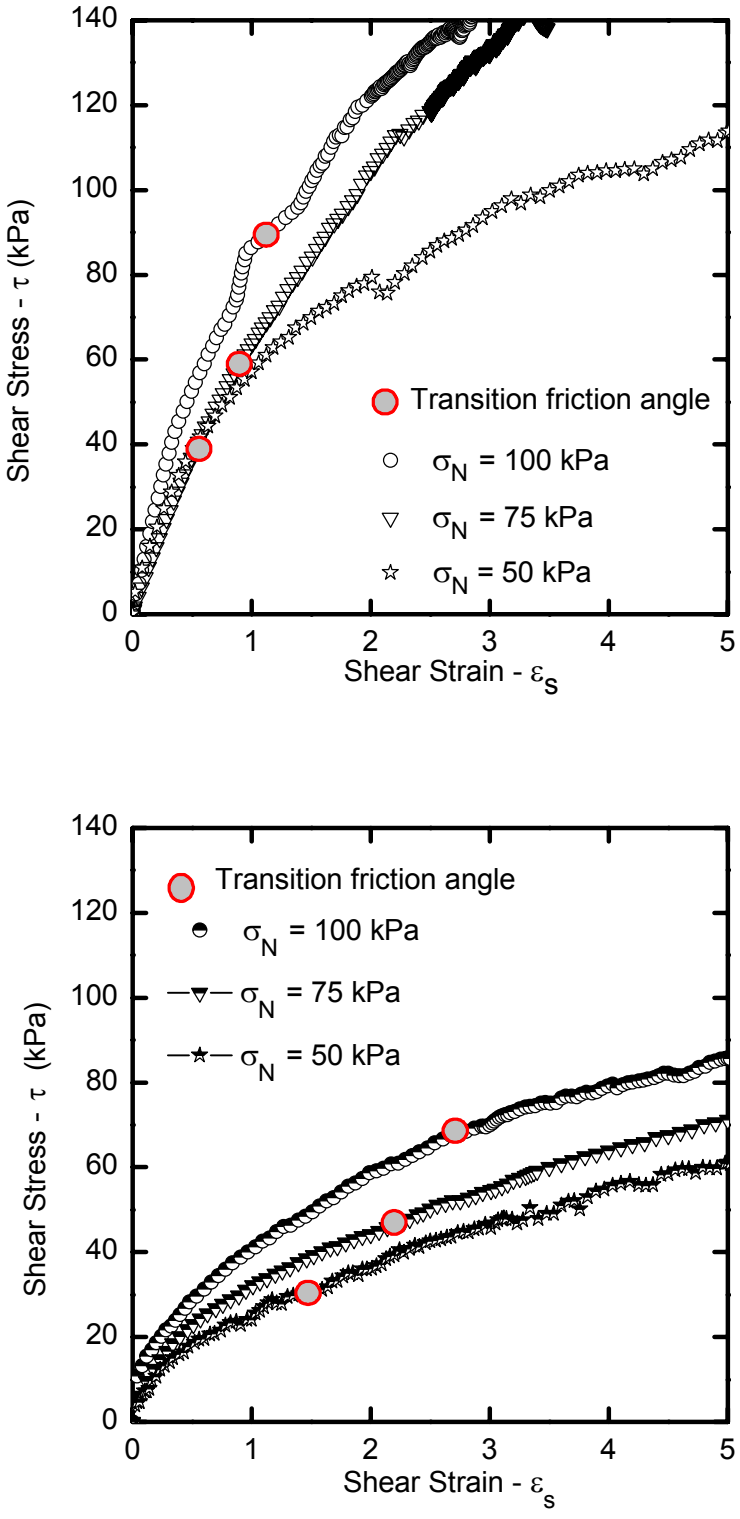


Figure 2.3. Shear mobilizations of a) dense rockfill and b) loose rockfill materials. After Abdul Razaq (2007). Reproduced with permission from Abdul Razaq, April 2010.

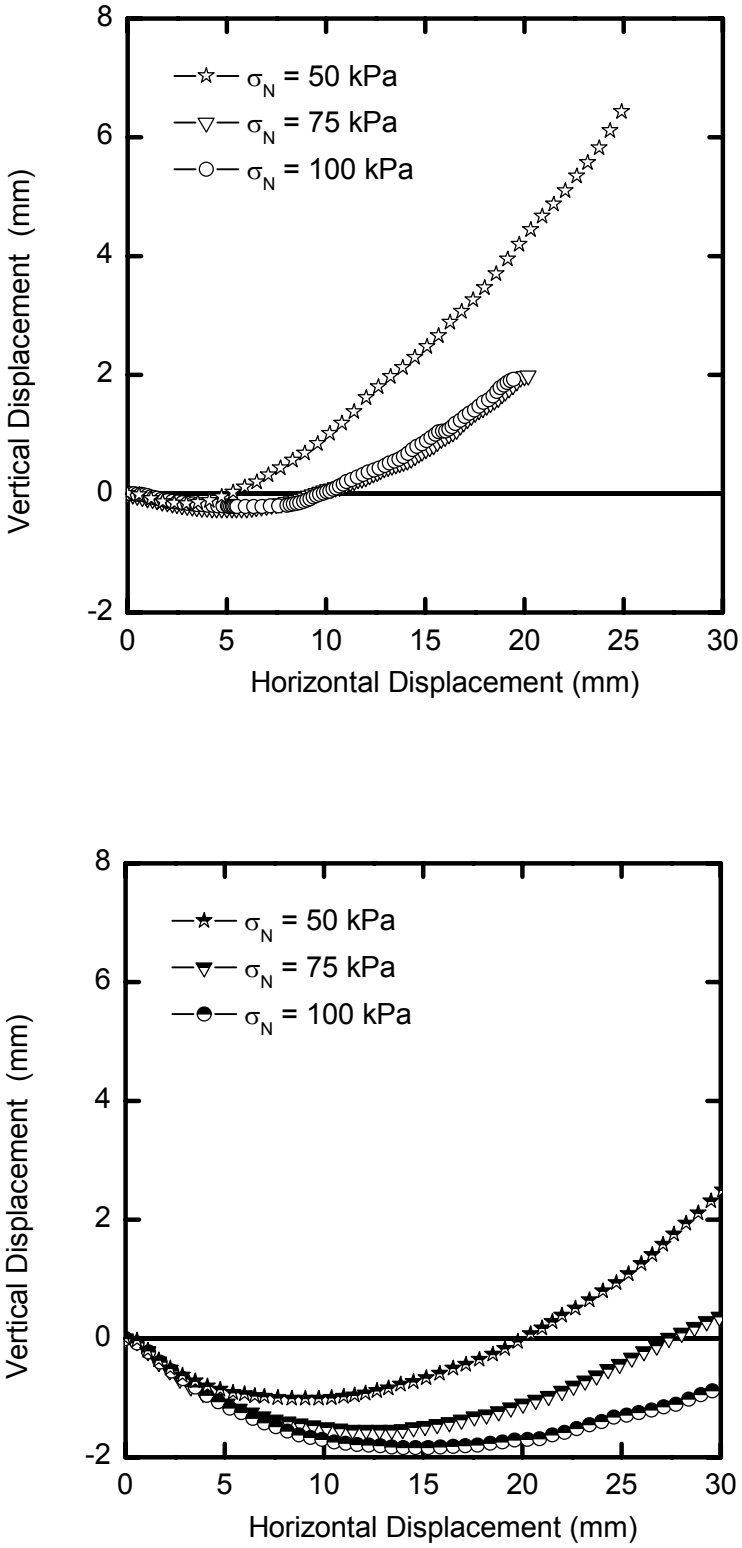


Figure 2.4. Dilation of a) dense and b) loose rockfill samples. After Abdul Razaq (2007). Reproduced with permission from Abdul Razaq, April 2010.

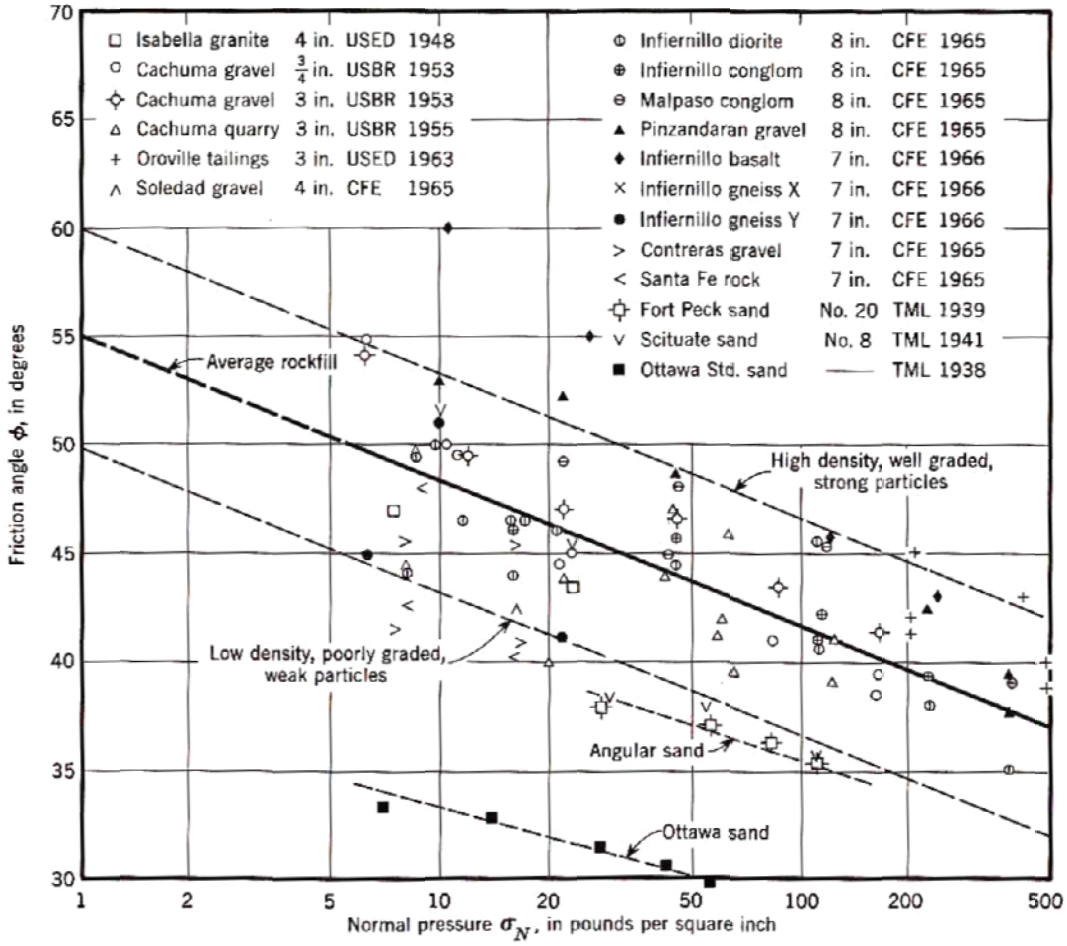


Figure 2.5. Friction angle plotted vs. normal pressure for a variety of gravels, rockfills and sands. After Leps (1970). Reproduced with permission from ASCE, January 2010.

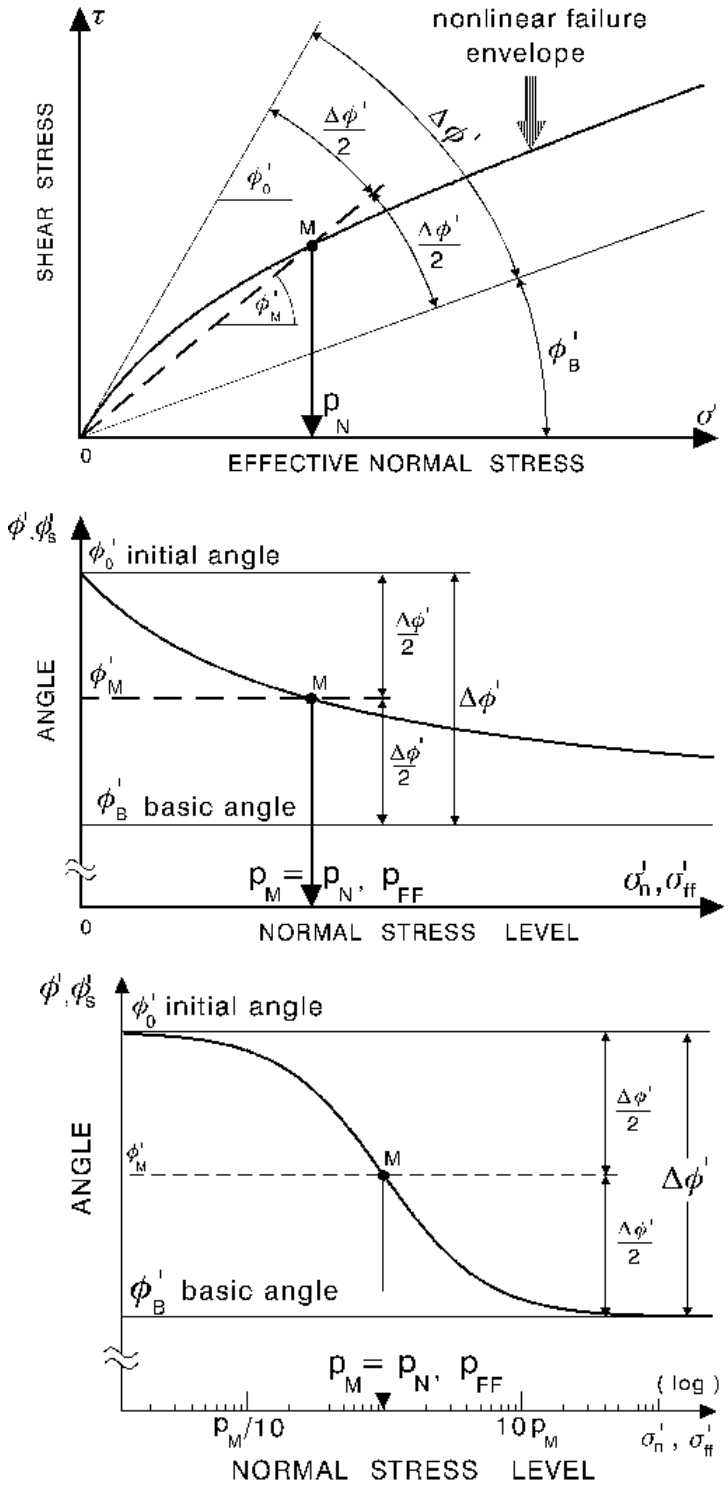


Figure 2.6. Development of strength envelope. After Maksimovic (1996). Reproduced with permission from Electronic Journal of Geotechnical Engineering, March 2010.

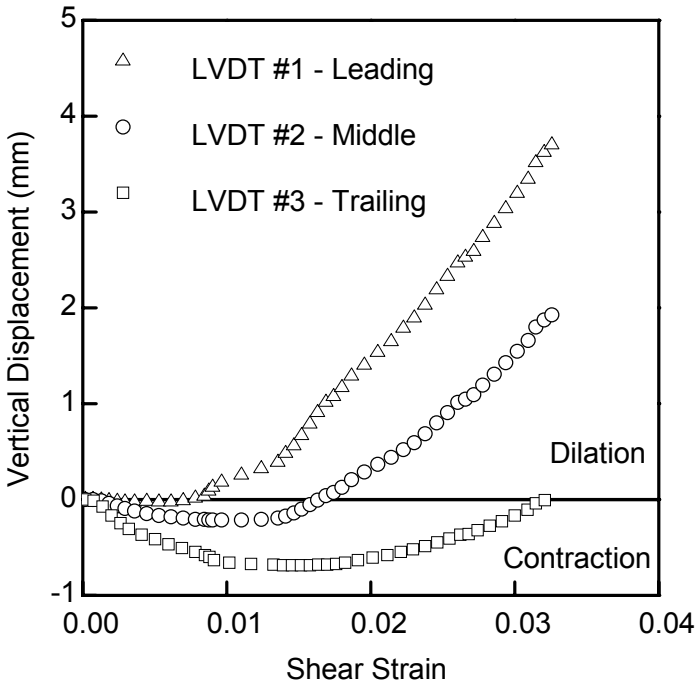


Figure 2.7 Dilation measured across top of dense rockfill sample during direct shearing. Modified from Alfaro et al. (2009)

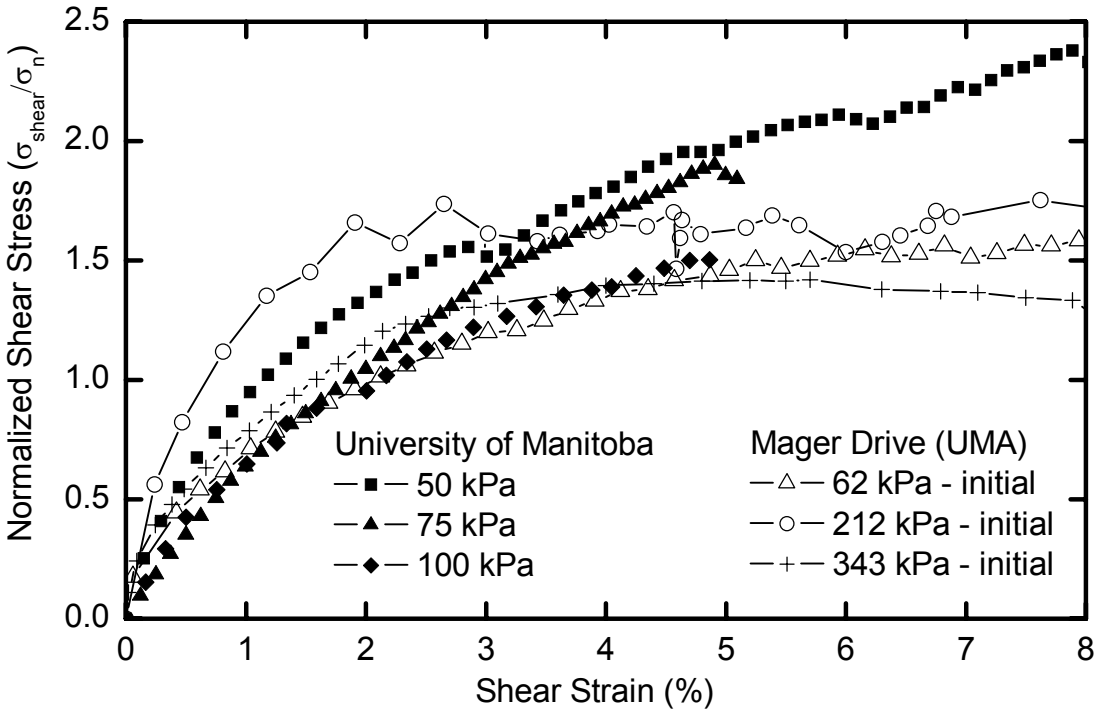


Figure 2.8. Normalized stress deformation plots for large-scale direct shear tests on crushed Manitoba limestone.

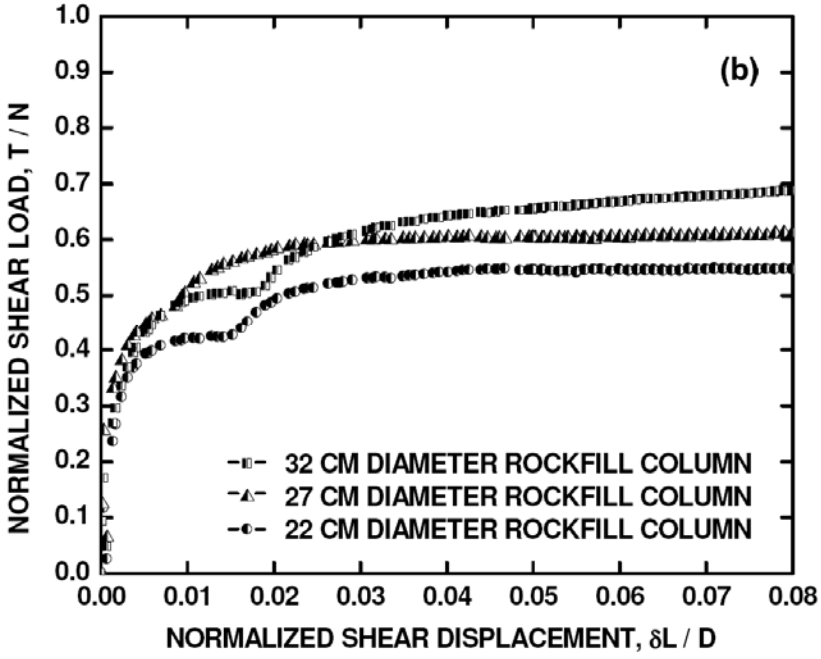


Figure 2.9. Normalized stress strain from direct shear tests of composite rockfill-clay samples. After Abdul Razaq (2007). Reproduced with permission.

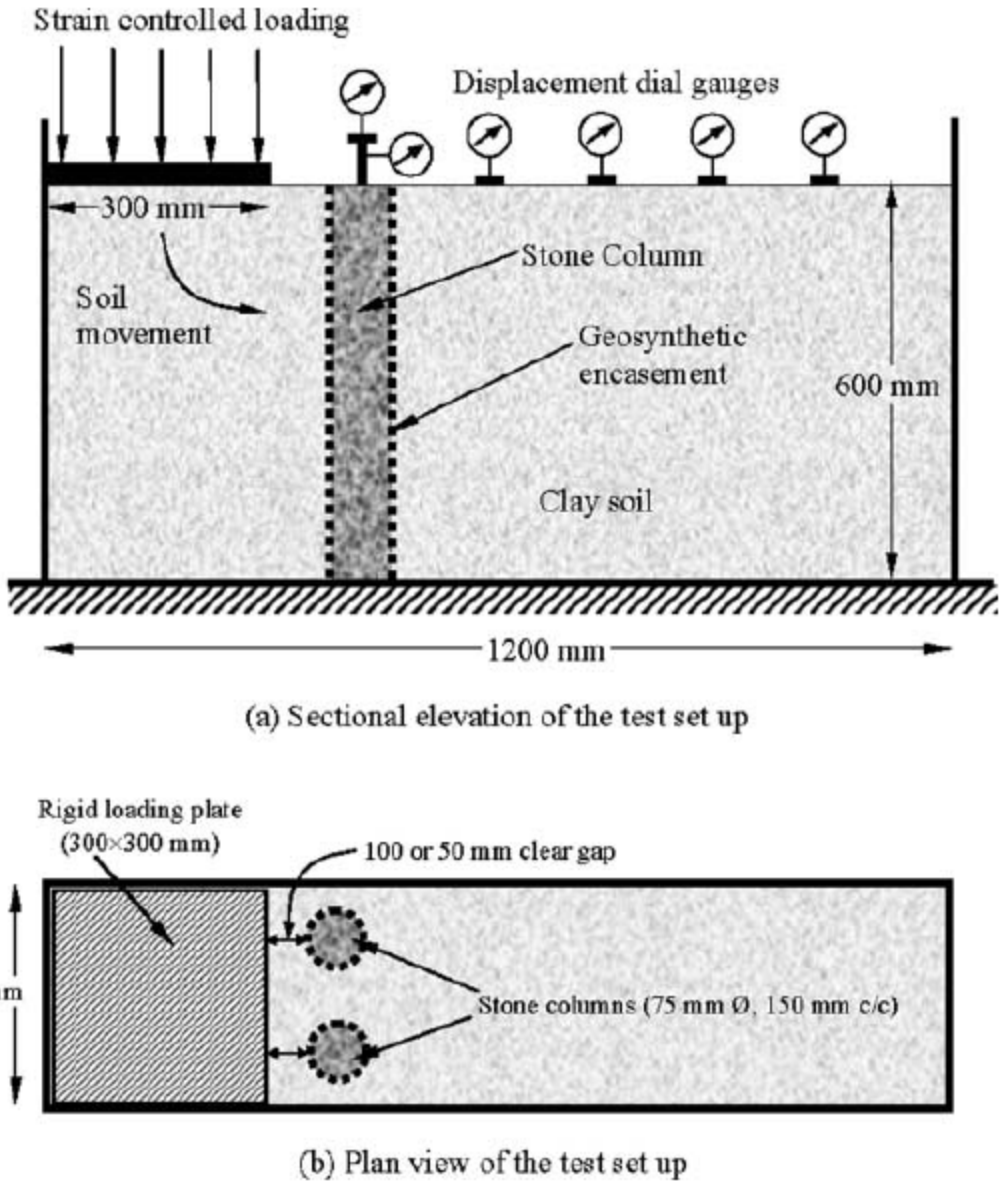


Figure 2.10. Test apparatus used by Murugesan and Rajagopal (2009) Reprinted, with permission, from the *Geotechnical Testing Journal*, Vol. 32, No. 1, copyright ASTM International, 100 Barr Harbor Drive, West Conshohocken, PA 19428

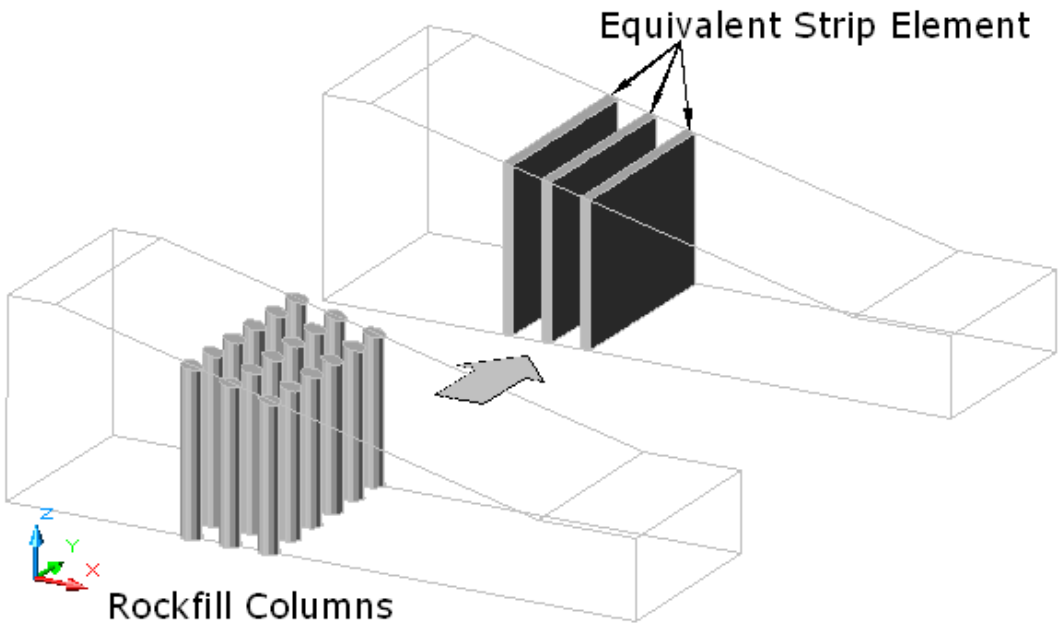


Figure 2.11. Rockfill columns modeled as equivalent strips. After Abdul Razaq (2007). Reproduced with permission from Abdul Razaq, March 2010.

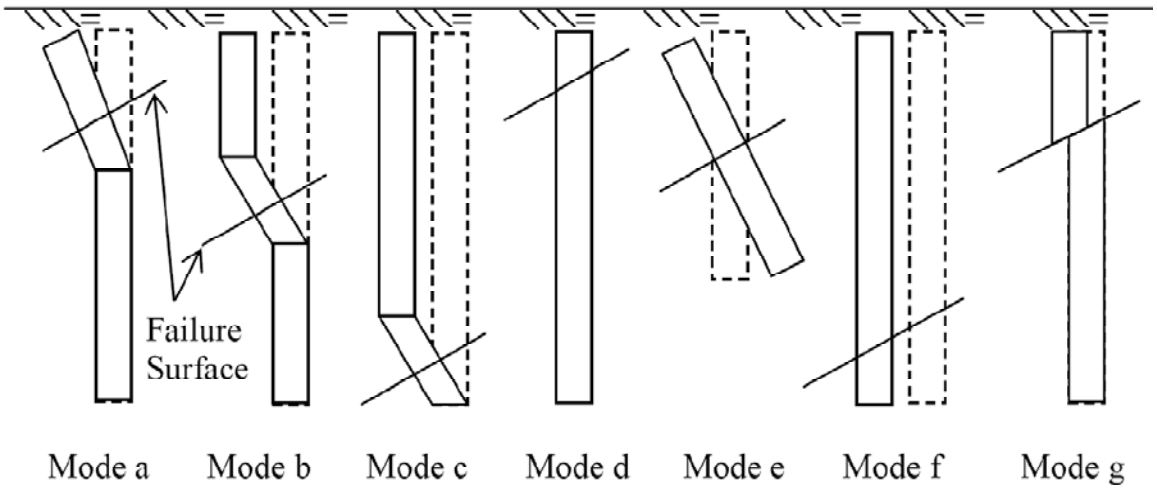


Figure 2.12. Failure mechanisms for non-rigid columns. After Navin and Filz (2005). Reproduced with permission from ASCE, June 2010.

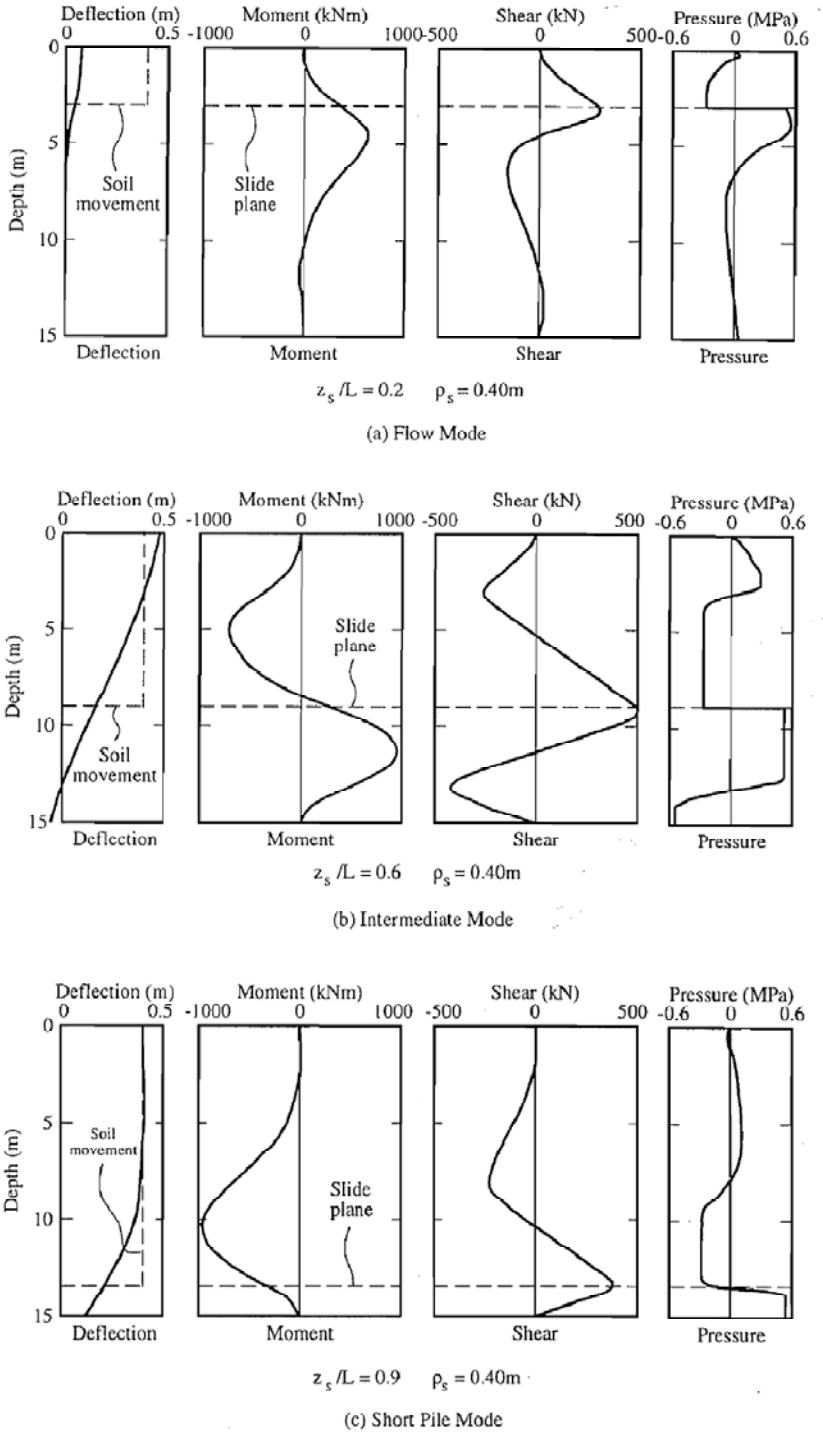


.

Figure 2.13.Behavior characteristics for piles subjected to lateral soil movement. After Poulos (1995). © 2008 NRC Canada or its licensors. Reproduced with permission, March 2010.

# 3. SITE INVESTIGATION AND SOILS TESTING

## 3.1 Introduction

The characterization of the ground conditions at the research site is an important aspect of this project. When conducting a field test, experimental control is dictated by the variability of the ground conditions identified in the site investigation. It is reasonable to assume that there is a positive correlation between the accuracy of the site characterization and the accurate interpretation of the response of the test subject (in this project, the rockfill columns). While the results of a full-scale field test are enriched by the "real-life" application, the researcher does not have control over many of the test conditions. In a typical laboratory based test, it is the controlled environment that allows for accurate and reproducible measurements of performance.

The careful characterization of the in-situ clay is especially important for this field test of rockfill columns. The columns are relatively small inclusions, considering the size of the test section, and the volume of clay influenced by the loading. Though the material properties of the rockfill are significantly different from those of the in-situ clay, the net influence of the columns can be largely masked by natural variations of the clay properties within the typical ranges characteristic of the local glaciolacustrine deposit (such as those reported by Baracos et al. 1983).

It is not possible to determine the effectiveness of the rockfill columns without a way of filtering the contributions of the rockfill columns from that of the in-situ clay. It is therefore important that the site investigation be thorough in order to improve the reliability of the test results by reducing the unknowns and identifying the probable scope of natural variability.

Ideally, a full-scale field test would have a parallel control section that has not been reinforced, which would be loaded at the same time as the reinforced section to provide a baseline for performance. The size of the research site and the project budget did not allow for a control section. The natural variability in ground conditions would limit the scientific reliability of a control section, even if it had been located immediately adjacent to the test section. As discussed further in the following section, the riverbank can change between stable and unstable conditions over short intervals.

This chapter describes the site conditions, discusses the site characterization and presents results from the laboratory characterization of the in-situ soils. The site investigation addressed relevant site conditions and identified the extents, character and variations of the in-situ soil units. The laboratory testing program focussed on the measurable parameters that had the most influence on the interpretation of the experiment results.

## 3.2 Location, topography and natural environment

Chapter 2 presented an overview of the regional topography and general site stratigraphy. The following discussion focuses on the characteristics of the research site and immediate surroundings.

The City of Winnipeg provided a research test site in River Road Park, which is located in the St. Vital district of The City of Winnipeg and encompasses approximately 400 m of riverbank. The general location of the site is shown in Figure 3.1 and Figure 3.2. The research site is located on the north riverbank of a westward flowing meander of the Red River. The Red River generally flows northward towards Lake Winnipeg. The test section is located on an outside bend of the river. The river begins a 190° direction change before the test section, with the bend having a radius of approximately 420 m. The research site is located approximately 160° through the bend. The Red River is about 125 m wide at this point during the summer months.

This section of riverbank has been considered as a priority site for stabilization works by The City of Winnipeg (The City of Winnipeg 2000, The City of Winnipeg 2004, James 2009) Figure 3.3 to Figure 3.5 are photographs of the test site taken during Phase I (as defined in Figure 1.4) after the installation of the instrumentation. River Road Park has a history of slope movements. Figure 3.6 was taken soon after the most recent instabilities developed at the test section, in 2004. Visual and measured (Independent Test-Lab Ltd. 1993) observations of adjacent portions of the bank suggest that slope movements were deep seated in nature, making it a suitable candidate for remediation by rockfill columns. A 120

m reach of riverbank was remediated to the south-east (up-stream) of the chosen test site,with a combination of a shear key, sand drains, rip rap, rockfill columns and re-grading in the 1980's (I. D. Engineering Company 1984) and 1990's (Independent Test-Lab Ltd. 1993). The riverbank also shows signs of active deep-seated movement (Figure 3.7) to the west (down-stream) of the test section.

The chosen test site is typical of many other unstable riverbank sections in the Winnipeg region. The test section is located on an outside bend in the river with over-steepened lacustrine clay banks. Most of the natural vegetation has been removed, and replaced with grass. The test section is also located near the University of Manitoba, and a safe distance from buildings or infrastructure, further adding to its suitability. The unstable section shown in Figure 3.7 was not used for the test loading because of its close proximity to private property. Figure 3.8 shows a cross section of the test area prior to the start of the site work. The elevation of the riverbank crest at the test section is approximately 232.0 m above sea level, and this will be considered 'prairie elevation.' Beyond the crest of the riverbank, the research site has very little relief, with the exception of an abandoned shallow drainage ditch running diagonally away from the river from south-east to north-west. The invert of the ditch is approximately 0.6 m below prairie elevation.

The riverbank at this location had an average slope of 3H:1V, when measured from the regulated summer river level to the base of the head scarp. The slope

varied from 2.6H:1V to 3.3H:1V in the test area. The head scarp varied from 1-2 m in height.

The natural riverbank in River Road Park demonstrates the reinforcing effects of trees and other vegetation. Both upstream and downstream of the test section the riverbank appears to be stable at the present time, possibly as a result of the trees and shrubs growing on the upper slope and crest (Figure 3.5 ).

The level of the Red River inside the City of Winnipeg is influenced by the operation of the Red River Floodway upstream of The City, and the St. Andrews Locks and Dam, downstream of The City. The Floodway is used to divert water around Winnipeg during peak flood events. The St. Andrews Dam is used to maintain a fairly constant river level in Winnipeg during the summer months for aesthetic and recreation purposes. The St. Andrews dam is also used to lower the river level in October of each year, to reduce the volume of ice formed during winter, and increase capacity for the spring freshet. The “Regulated Summer River Level” at the research site is roughly 224.2 m above sea level. The winter ice level at the research site was 222.1 m when it was measured during the test loading. The groundwater conditions are discussed in more detail in Chapters 4 and 6.

## 3.3 Site investigation

The investigation of the geotechnical conditions at the research site involved drilling testholes, sampling soil, a site survey, and a desktop review of

geotechnical reports from nearby projects. This work was done at the beginning of the project before the design and implementation of the experiment.

The testhole locations for the Phase I site investigation were chosen both for the immediate purposes of sample collection and ground proofing, but also for installing instrumentation for monitoring. The instrumentation at the research site is discussed in detail in Chapter 4. Figure 3.9 shows the layout of the five testhole locations from Phase I.

Additional testholes were drilled in December 2007 for the purpose of instrumentation installation, as part of Phase II. The stratigraphy was logged, but no samples were collected, and no in-situ tests were conducted.

Paddock Drilling Ltd. was contracted to provide drilling services. Figure 3.10 shows the RM-30 drill rig, mounted on a tracked Bombardier M7 carrier that was used for the testhole drilling.

The five testholes drilled in Phase I were advanced into the till layer until practical auger refusal in the till (between 1 and 4.3 m into the till layer). Proofing the bedrock was not deemed necessary because the local (Independent Test-Lab Ltd. 1993) and regional stratigraphy (Baracos et al. 1983) was generally well known. It was determined that sufficient anchoring for the inclinometer casings was achieved at the depths reached with the augers. The full testhole logs are included in Appendix A. Specific sample locations and some testing results are shown on the logs.

Testholes TH-1,2,4 and 5 were drilled with continuous flight, solid stem augers, 125 mm in diameter. The borings remained open during drilling, without significant sloughing or squeezing, and thus sampling could be done through the auger holes without compromising the quality of the samples. TH-3 was drilled with hollow stem augers to accommodate continuous wire-line sampling. The wire-line samples were inspected for slickensided surfaces or other anomalies that might be missed in Shelby tube samples or disturbed by augering. No smooth slickensided surfaces were found. Existing shear surfaces are difficult to find during a site investigation, even when using continuous sampling (Graham 1986).

Instabilities were seen on the lower bank during the fall drawdown of 2006 and 2007. The upper edge of these instabilities developed near the normal summer water level. Figure 3.11 shows a tension crack that formed in the lower bank after the river drawdown in fall of 2006. The drawdown can result in excess porewater pressures in the weak clay at the toe of the slopes, while removing the stabilizing effect of the external water pressure. The fall drawdown event can larger slope movements along Winnipeg's riverbanks (Baracos and Graham 1981).

The slope above 225 m was generally intact and was not considered to have experienced shear failure at depth. When the clay unit was modeled with residual strengths, the slope stability analysis computed a factor of safety of less than unity for the unreinforced slope, which has no practical meaning. Therefore

using residual soil strengths for analysis of the field test is not appropriate. Chapters 5 and 7 discuss the slope stability analysis in more detail.

A pocket penetrometer and torvane were used to help characterize the consistency of the clay, but these results have not been reported. Field vane tests were also done at selected depths in TH-1. The results of the field vane, pocket penetrometer and torvane were of limited use in the analysis because they only measure total stress parameters under undrained conditions. Standard penetration tests (SPT) were performed in the till with the results shown on the testhole logs.

### 3.3.1 Stratigraphy

As discussed in Chapter 2, the general stratigraphy of the Red River valley consists of an upper complex zone, overlying a glaciolacustrine clay deposit, a silt matrix till and limestone bedrock. Figure 3.12 is a summary of the stratigraphy and test results from testholes TH-1 to TH-5.

At the research site, a layer of light brown silt varying in thickness from 0.3 to 0.6 m was encountered near the ground surface in testholes TH-1 and TH-5. The silt layer was also exposed along the head scarp near the crest, and can clearly be seen in Figure 3.13. The silt was loose and dry at the time of drilling. After a rainy period, water was observed seeping from the exposed silt on the vertical scarp.

The glaciolacustrine clay deposit extends from the base of the silt layer to the top of the till, with the bottom of the clay at an average elevation of 219.0 m. The clay was stiff near the surface, becoming firm to soft with depth[1]. As discussed in Chapter 2, the brown and grey clay are believed to be of the same origin, with the difference in colour being a result of historic groundwater changes leading to oxidation in the upper clay exposed to oxidizing conditions. The transition from brown to grey occurred at about 224 m in testholes TH-1, 2, 3 and 5. In TH-4, which is closer to the river, the colour transition occurred near 222 m, presumably because the seasonal fluctuations of the river allowed for oxidation to reach a lower elevation. Alternatively, the brown clay around SI-4 may have been displaced downward by historic slope movements. Trace silt and gypsum inclusions were found in the clay. The measurable properties of the clay are discussed in more detail in Section 3.5.

Planar discontinuities were found in clay samples from TH-1 and similar features were observed in the clay removed while drilling some of the columns located near the downstream edge of the test section. The discontinuities were oriented almost vertically. Figure 3.14 shows one of these discontinuities found in a Shelby tube sample. The surfaces were light grey, with rootlets growing along the planes. These discontinuities were observed at depths greater than 3 m and may be relics of past slope movements at the site, or in-filled fissures.

[1] Descriptive terms for soil classification are used in accordance with the soil classification system described in the Canadian Foundation Engineering Manual (2007).

The top of the till was encountered between 218.6 and 219.1 m. The till is sandy, with a silt matrix and trace to some gravel, trace cobbles and trace boulders. Thin water bearing sand layers were encountered in testholes TH-1, 2 and 4 around 215 m elevation. The upper 1.5 to 3 m of till was loose, but the till became dense to very dense with depth. Samples of the loose upper till were taken with Shelby tubes for analysis. The loose till was possibly water laid (ablation till) and therefore not subjected to the weight of an overlying glacier. Drilling through the loose till required little effort with either the geotechnical drill rig or the large rig used for column installation, except where cobbles and boulders were encountered.

There is evidence of rip-rap placement along the summer river level over the length of the test site. Figure 3.15 shows the rip-rap as it was on October 26, 2007[2]. The rip-rap was probably placed in 1993 (Collins and Myska 1993) as part of the stabilization project completed upstream of the test site. The rip-rap layer had a specified thickness of 0.5 m. It is unclear from the design report how far down-slope from the summer river level the rip-rap blanket extends.

[2] In the fall/winter of 2006, the rip-rap was not noted because it was mostly covered by alluvial sediment.

## 3.4 Laboratory Testing

### 3.4.1 Grain size distribution

Grain size distributions were done for both clay and till samples, using sieve analysis for the coarse-grained fraction, and hydrometer analysis for the fine-grained fraction in accordance with ASTM 422 (2002). Table 3.1 summarizes the results of the tests. The grain size distributions for a single clay and till specimen are plotted in Figure 3.16. These distributions are representative of other test results from the respective soil types. All of the “clay” samples were more than 27% silt by weight.

There was not a significant difference in the grain size distributions between dense and loose till. The till was generally silt with over 27% sand, and less than 10% clay, except along seams of sand where the silt content was lower. The grain size distributions were used to confirm or modify the characterization of the soils shown on the testhole logs in Appendix A.

### 3.4.2 Natural water contents

The natural gravimetric water contents were determined for all grab samples from testholes TH-1,2, 4 and 5 and well as select continuous samples from TH-3. Each Shelby tube sample was also tested for water content at the time the sample was extracted from the tube.

The results from the natural water content tests are included in Figure 3.12 which shows all the results from testholes TH-1 to 5 combined, with the water content

plotted versus elevation. The water contents in the clay ranged from 29 to 55 % with an average of 43%. The lowest measured till water content was 7% while it reached 20% along the clay-till transition. The average water content in the till was 13.5%.

### 3.4.3 Atterberg limits

Measurements of the Atterberg limits (liquid and plastic limits) were done in general accordance with ASTM D4318 (2005). The liquid and plastic limits are useful for characterizing soil composition and predicting soil behaviour from a wealth of empirical relationships based on these indices.

The Atterberg limits are shown in Figure 3.12 as range bars surrounding selected water content data points. The average plastic limit ($w_P$) was 29% and the average liquid limit ($w_L$) was 91%, and therefore the average plasticity index ($I_p$) was 62%. For tests on clay samples, the maximum and minimum measured plastic limits were 36% and 11% respectively while the maximum and minimum liquid limits were 107% and 75%. The plasticity indices in the clay ranged from 48% to 74%.

One sample in the clay deposit (at 225.15 m in TH-5) had a plasticity index of 48% and was not highly plastic. The average liquidity index from all clay tests was 0.26, with a range from 0.16 to 0.4. There was not a consistently identifiable difference in the plastic or liquid limits and indices between the grey and the brown clays.

The Atterberg limits were determined for only one till sample. The liquid limit and plastic limit of a sample from 217 m in TH-2 were 21% and 11% respectively.

### 3.4.4 Testing for constitutive properties

Testing of soil samples was needed for determining the strengths and constitutive relationships of the in-situ soils. These would be used in stability and stress deformation models. The strength of the clay was determined through direct shear and triaxial tests and the till was tested in direct shear. The results of the triaxial testing are interpreted to provide peak, post-peak, and large-strain strengths. The direct shear tests provided peak and residual strengths. The triaxial test method is considered to be superior to direct shear testing in many ways, but it generally cannot be used to estimate the residual strength of clays. The shortcomings of direct shear testing have been well documented by Saada (2000) and others. The main shortcomings are:

- severe stress concentrations
- the thickness of the shear zone is unknown
- no parameter is measured directly
- the sample is not realistically confined
- most soils do not deform and fail along a plane (with the noted exception of overconsolidated clays)
- Porewater pressures cannot be measured with undrained tests

The residual strength has been shown to correlate well with the back analysed shear strengths of failing slopes (Baracos et al. 1980). Figure 3.17 illustrates that the stress conditions along the base of a mobilized slide mass are best replicated by a direct shear test, while the triaxial compression test is more appropriate for soils in the upslope, active zone of a slide mass. No triaxial extension tests were done.

All testing was done in the geotechnical laboratory at the University of Manitoba, except as noted.

#### 3.4.4.1 Triaxial tests

Triaxial testing was done using the consolidated undrained compression test method (CIŪ) for measuring the strength of undisturbed clay. The tests generally followed ASTM D-4767 (2004). The specimens were trimmed to a diameter of 50 mm and a length of 100 mm from 75 mm diameter Shelby tube samples. Undrained consolidated test procedures were used because they most closely reflect the expected stress conditions in the ground during the test loading. The field test was conducted over a relatively short period which did not allow complete excess porewater pressure dissipation between applications of successive loads. The specimens were saturated using a back pressure of 200 kPa, and then consolidated to effective confining pressures ranging from 50 to 300 kPa. To ensure (nearly) saturated conditions, a B-value of 98 percent was obtained before shearing the specimens. The specimens were typically sheared at 0.005 mm/m to between 15 and 20 percent axial strain.

Results from the triaxial testing were plotted in q-p' space where:

$$q = \sigma'_1 - \sigma'_3 = \sigma_1 - \sigma_3 \quad (3.1)$$

and

$$p' = (\sigma'_1 + 2\sigma'_3)/3 \quad (3.2)$$

Figure 3.18 shows the results of the shearing phase for thirteen triaxial specimens, plotted in q-p' space. When comparing the results from the brown and grey clay specimens, the peak strength envelope of the brown clay is notably higher, but the post-peak strengths are very similar. Most samples, including all the "brown" clay specimens, failed along shear planes, while other specimens yielded plastically, showing visible bulging. It is evident from the test results that the clay is anisotropic as evidenced by the sloping initial portion of the curves in Figure 3.18. The negative slope of the q – p' stress path indicates that the soil is stiffer in the horizontal direction than in the vertical direction (Graham and Houlsby 1983)

Table 3.2 summarizes the results of the triaxial testing. The strength envelope used for most of the analyses in the following chapters is the post-peak strength envelope which is defined by a friction angle of 18° and cohesion intercept of 5 kPa. The results are shown for grey and brown clay separately and combined,

even though it has been shown that the colour difference does not signify a difference in material (as discussed in Chapter 2).

Figure 3.19 is an example of the deviator stress and excess porewater pressure plotted against axial strain for a test specimen. The point at which the post peak strength was calculated is highlighted. The terms “post-peak,” “fully-softened,” “critical state” and “normally consolidated” refer to a similar strength condition and the terms can be used somewhat interchangeably as noted by Graham (2006).

The post-peak strength was determined for each specimen at the point where the deviator stress and porewater pressure approached a steady-state with respect to axial strain (that is $dq/d\varepsilon=0$ and $du/d\varepsilon=0$). As illustrated in Figure 3.19, these parameters remain in a state of flux and some judgement was required in determining the reported values. When the post-peak strength is determined in this way, it is a reasonable approximation of the critical state strength for fine grained soils (Graham and Au 1985). The peak and post-peak deviator stresses are plotted against the mean effective stress in Figure 3.20 for the 13 triaxial tests. Peak strength envelopes have been fit to the data, as shown in Figure 3.20, but these values have not been used in analysis for the reasons discussed in Chapter 2. There is some scatter in the peak strength measurements, but this is typical of the material. A higher peak strength envelope for the brown clay compared to the grey clay is reasonable, considering the over consolidation of the upper clay caused by weathering.

The shear and normal stresses at failure were calculated by determining a specimen specific phi angle ($\phi$) according to the following equations for each specimen:

$$\phi = \sin^{-1}\left[\frac{\left((\sigma'_1-\sigma'_3)/2\right)}{\left((\sigma'_1+\sigma'_3)/2\right)}\right] \quad 3.3$$

$$\tau = \sin(90-\phi)\cdot\frac{(\sigma'_1-\sigma'_3)}{2} \quad 3.4$$

$$\sigma_n = \frac{\tau}{\tan\phi} \quad 3.5$$

The resultant shear strength was plotted against the normal stress for each specimen to determine a representative friction angle ($\phi$) and cohesion (c) for the soil unit (Figure 3.21). The best fit line shown in Figure 3.21 is forced through the point $\tau$ = 5 at $\sigma_n$ = 0, essentially assigning the material a small amount of cohesive strength. This is a common interpretation of the slightly curved shear strength envelope of Winnipeg clays (for example Baracos 1981 or Graham 1986). In the analysis, where post-peak strengths are used, a friction angle ($\phi$) of 18° along with 5 kPa of cohesion will be assigned to clay. The peak-strength will not be used, in the analysis, for the reasons explained in Section 2.3 (for example Rivard and Lu, 1978).

Both the tangent (initial) and secant (to peak) modulus values were calculated for all triaxial tests on clay specimens. The modulus is calculated as:

$$E=\frac{q}{\varepsilon} \quad 3.6$$

The average calculated modulus values are included in Table 3.2.

Poisson's ratio, $\nu'$, can be estimated by calculating K' from the consolidation phase and E' from the shearing phase, and using the relationship:

$$K'=\frac{E'}{3(1-2\nu')} \quad 3.7$$

The calculated $\nu'$ varied greatly (from 0.1 to 0.4). Poissons ratio ($\nu'$) was assumed to be 0.33, but it was varied as part of the sensitivity analysis. A Poisson's ratio of 0.4 falls at the low end of the range reported by Baracos et al. (1983) and Bowles (1997), although it is not clear whether they are reporting a value for drained or undrained conditions. Budhu (2000) suggests that $\nu'$ should be between 0.3 and 0.35 for a medium stiffness clay.

#### 3.4.4.2 Direct shear tests

Six clay and three till specimens were tested in direct shear. The tests were done general accordance with ASTM Standard D 3080 (2004). The specimens were cylindrical and nominally 70 mm in diameter and 28 mm in height.

Direct shear testing is used to calculate the shear strength ($\tau$) of soil by:

$$\tau=\frac{P_x}{A} \quad 3.8$$

where

A = corrected cross sectional area of the sample

$P_x$ = horizontal force

All specimens were tested using multiple reversals of the direction of shearing to reduce the shearing resistance to residual strength along a slickensided surface. After completing an initial pass to determine the peak strength, the direction of shearing was reversed. This process was repeated until a consistent residual strength was obtained. Figure 3.22 shows the shear stress versus displacement plot for one specimen.

The chosen samples were tested at three consolidation pressures, nominally 50, 175 and 300 kPa, similar to the range of confining pressures chosen for the triaxial testing. The clay and till samples were tested at the same effective stresses to provide easy comparison of the testing results. Figure 3.23 is a plot of the measured peak and residual strengths for all direct shear tests. The average residual friction angle for the tested clay specimens is 8.3°, with zero cohesion. The residual strength measured by direct shear is significantly lower than the post-peak strengths reported in Table 3.2 from triaxial compression tests. Table 3.3 provides a summary of parameters calculated from the direct shear results.

The shear modulus, G, was calculated for the direct specimens according to (Davis and Selvadurai 1996):

$$G=\frac{\Delta\tau}{\Delta s}\cdot h \qquad 3.9$$

where

- s = horizontal displacement of the shear box and
- h = height of the specimen.

The shear modulus is related to the elastic modulus E:

$$E=2G(1+v) \qquad 3.10$$

The modulus values calculated from the direct shear tests are somewhat lower than those calculated from the triaxial testing. Generally the values measured by the triaxial compression tests are used in analysis, but sensitivity analysis was used to explore the influence of the material stiffness.

The only strength testing done on the till was a set of three direct shear tests. It is difficult to collect an undisturbed sample from the till. A number of Shelby tube samples were retrieved, but there was difficulty in preparing the sandy silt samples for testing without disturbing the sensitive specimen. It would not have been possible to trim an undisturbed sample for triaxial testing. Some SPT tests were performed in the compact till at depth, but unfortunately no SPT's were done (successfully) in the looser till. It was noted that the consistency of the till after completing the direct shear test was stiffer than it was in its in-situ condition (as observed on the augers or collected samples). The water content at the end

of the test was lower (8.3% at 175 kPa normal pressure) than the initial water content (11.9%).

Table 3.4 lists some other material properties calculated in the process of preparing triaxial, direct shear and oedometer samples.

### 3.4.5 One-dimensional consolidation

Two clay specimens were tested for properties in one-dimensional consolidation using incremental loading with a mechanical oedometer, following ASTM D2435 (2004). The specimens were chosen from different elevations to provide a representation of the profile. The tests were conducted to determine the preconsolidation pressure, $p'_c$, the coefficient of consolidation, $c_V$, and the compression and re-compression indices, $C_{c,}$ and $C_r$ respectively. Hydraulic conductivities were also confirmed from the oedeometer test results.

The loading plots are shown in Figure 3.24 and the results are summarized in Table 3.5. The clay is highly overconsolidated near the surface, with the preconsolidation pressure and overconsolidation ratio decreasing with depth. The preconsolidation pressure was evaluated using the Casagrande procedure. The preconsolidation pressures in Figure 3.24 are not sharply defined; this is partially due to sample disturbance, but may also be a result of the samples in-situ location along an unstable riverbank which has been subjected to a wide range of stress conditions. Overconsolidation of Lake Agassiz clay is not caused by historic overburden pressures, but is rather the result of weathering

processes. This explains the decrease in the apparent preconsolidation pressure with depth (Baracos et al. 1980).

The value of the constrained Young's modulus of elasticity, $E_c$ , was determined from the consolidation results. It is calculated as:

$$E_c = \frac{1}{m_{vr}} = \frac{\Delta\sigma}{\Delta\varepsilon} \qquad 3.11$$

where

- $m_{vr}$ = modulus of volume recompressibility
- $\Delta\sigma$ = change in the vertical stress
- $\Delta\varepsilon$ = strain associated with the vertical stress change

The constrained Young's modulus must be calculated along the unload-reload line where deformations are primarily recoverable. This is important because the modulus increases with increased confining pressure. The constrained modulus ($E_c$) provides another measure of the elastic stiffness, and is related to the modulus of elasticity (E) according to (Davis and Selvadurai 1996):

$$E = E_c \left[ \frac{(1+v)(1-2v)}{1-v} \right] \qquad 3.12$$

The values of E calculated from recompression curve of the consolidation tests fall in between the initial tangent and secant (to peak) modulus values calculated from the triaxial compression results shown in Table 3.2.

### 3.4.6 Hydraulic conductivity

The hydraulic conductivity of the clay was measured by flexible walled permeameter tests. The tests were done in general accordance with ASTM 5084 (2003). Two of the specimens tested were taken from the upper brown clay layer, and one specimen from the grey clay. The results of the testing are summarized in Table 3.6.

The samples were tested at confining pressures between 80 and 120 kPa. The effective confining pressures were chosen to be similar to the calculated in-situ vertical effective stress. The samples were saturated before testing at back pressures of 200 kPa.

The silt content of sample T68 was higher than the average based on visual observation and it also had a significantly greater hydraulic conductivity than the other two tested samples. The plasticity index of sample T68 was 48%, compared to the average of 62%, suggesting that it was somewhat of an outlier. This is an important observation though, as seams or inclusions of more permeable soil can significantly increase the overall hydraulic conductivity of the soil mass.

### 3.4.7 Rockfill Testing

Extensive laboratory testing of rockfill properties was performed at the University of Manitoba and published by Abdul Razaq (2007) and Kim (2007). Some important components of their testing have been discussed in Chapter 2. The limestone rockfill used in the current field test is assumed to be very similar to

that which was tested by Abdul Razaq and Kim, and therefore the testing on the crushed limestone used for the columns was limited to grain size analysis, water contents and density estimations. The estimated density of the compacted rockfill is discussed in Chapter 5.

#### 3.4.7.1 Grain size distribution

The grain size distribution for the rockfill was measured by UMA|AECOM in their geotechnical laboratory. The sample was taken from the same source as the rockfill used to construct the columns. Figure 3.25 shows the cumulative grain size distribution. The tested sample had a fines content of 3.1%, based on the total percent passing the 0.08 mm sieve. The coefficient of uniformity was calculated to be 20 and the coefficient of curvature is 1.84, indicating that the rockfill is well graded.

Marsal (1973) noted that the “ideal” rockfill is a well graded gravel with a coefficient of uniformity of 15 or more, with less than 10% of the particles (by weight) smaller than 0.2 mm. The grain size distribution of the rockfill used at the research test site satisfied these recommendations.

#### 3.4.7.2 Water content

Three water content samples were taken randomly from the rockfill material as it was delivered to site. The gravimetric water content was found to be 4.3%, averaged over the three samples. The water content samples did not contain

particles over 25 mm in diameter, and as such, the calculated values represent the moisture content of the component below this grain size. It was not practical to test a large representative sample and the moisture content of a full sample is presumed to be lower than 4.3%. The in-situ moisture content was not measured, but the columns were charged with water prior to compaction, and therefore it can be assumed that the pore space was filled with water below the water table.

## 3.5 Conclusion

The previous sections have described the site characterization and soils testing. The application of these results in analysis will be discussed in more detail in Chapter 7.

The scope and quantity of the testing done for this project exceeds the laboratory testing programs implemented for the design of a typical riverbank stabilization project; as demonstrated by the results and comments, it is still difficult to confidently report a representative value of any parameter. This is the nature of geotechnical engineering, and working with natural materials. The testing has nonetheless been useful in narrowing the scope of probable performance. Sensitivity analysis will be used to evaluate the influence of the remaining variability.

Table 3.1. Grain size distributions for select samples (samples from TH-3).

| | | | Grain Size Distribution | | | | | |
|---|---|---|---|---|---|---|---|---|
| Sample | Elevation (m) | Description | Gravel | Coarse Sand | Medium Sand | Fine Sand | Silt | Clay |
| C30 | 226.4 | brown clay | - | - | - | - | 30% | 70% |
| C37 | 222.9 | grey clay | - | - | - | - | 43% | 57% |
| C42 | 220.3 | grey clay | - | - | - | - | 27% | 73% |
| C46 | 218.3 | till | 8% | 9% | 34% | 29% | 17% | 4% |
| C48 | 217.3 | till | - | - | - | 61% | 30% | 9% |
| C50 | 216.3 | till | 30% | 5% | 9% | 13% | 35% | 7% |
| C52 | 215.2 | till | 26% | 5% | 10% | 12% | 41% | 6% |
| C53 | 214.7 | till | 3% | 5% | 28% | 62% | 3% | - |

Table 3.2. Summary of properties measured from triaxial tests.

| | Units | Brown Clay | Grey Clay | Combined Brown and Grey Clay |
|---|---|---|---|---|
| $\Phi'_{post\ peak}$ – c' = 5 kPa | deg. | 17.3 | 19.1 | 18.0 |
| $\Phi'_{post\ peak}$ (c') - best fit | deg. (kPa) | 14.3 (17) | 13.7 (21) | 13.8 (20) |
| Post Peak $\sigma'_1/\sigma'_3$ [1] | | 2.26 | 2.41 | 2.33 |
| E- initial tangent [1] | kPa | 24100 | 16500 | 20900 |
| E - secant [1] | kPa | 8100 | 5900 | 7100 |
| $\varepsilon_{peak}$ [1] | | 2.26 | 2.9 | 2.58 |

[1] Averaged from all tests

Table 3.3. Summary of properties measured from direct shear tests.

| | Units | Brown Clay | Grey Clay | Combined Brown and Grey Clay | Till |
|---|---|---|---|---|---|
| $\Phi'_{peak}$ (c) | deg. (kPa) | 14.1 (34) | 15.4 (22) | 14.7(28) | 42 (3) |
| $\Phi'_{resid}$ (c) | deg. (kPa) | 5.6 (7) | 7.8 (6) | 6.7(6) | - |
| $\Phi'_{resid}$ - c=0 | deg. | 7.3 | 9.3 | 8.3 | - |
| $G_{initial}$ [1] | kPa | 4400 | 5800 | 5100 | 7900 [2] |
| $G_{secant\ to\ peak}$ [1] | kPa | 1800 | 1600 | 1700 | 2200 |

[1]averaged from all tests

[2]measured at 175 kPa confining pressure

Table 3.4. Summary of assorted properties properties (averaged).

| | Units | Brown | Grey | Brown and Grey | Till |
|---|---|---|---|---|---|
| $e_0$ | | 1.33 | 1.39 | 1.36 | Varies |
| $\gamma_{bulk}$ | $kN/m^3$ | 17.3 | 16.8 | 17.1 | 23.0 |
| $\gamma_{dry}$ | $kN/m^3$ | 11.7 | 11.2 | 11.6 | 20.9 |
| Gs | | 2.79 | 2.77 | 2.78 | 2.78 |

Table 3.5. Results from one dimensional consolidation testing on clay specimens.

| Parameter | Sample T6 | Sample T80 |
|---|---|---|
| $p_c$ (kPa) | 700 | 490 |
| OCR | 13 | 3 |
| $C_c$ | 0.61 | 0.67 |
| $C_r$ | 0.20 | 0.14 |
| $m_v$ ($kPa^{-1}$) | $2.2 \cdot 10^{-4}$ | $2.8 \cdot 10^{-4}$ |
| $m_{vr}$ ($kPa^{-1}$) | $4.6 \cdot 10^{-5}$ | $6.2 \cdot 10^{-5}$ |
| $C_v$ ($m^2/s$) | $4.1 \cdot 10^{-7}$ | $1.4 \cdot 10^{-8}$ |

Table 3.6. Summary of results from hydraulic conductivity tests.

| Testhole (sample #) | Soil description | Elevation (m) | Hydraulic Conductivity (m/s) |
|---|---|---|---|
| TH-5 (T68) | Brown clay | 225.5 | $4.0 \cdot 10^{-8}$ |
| TH-3 (T57) | Brown clay | 224.7 | $1.3 \cdot 10^{-10}$ |
| TH-5 (T73) | Grey clay | 219.4 | $8.6 \cdot 10^{-11}$ |

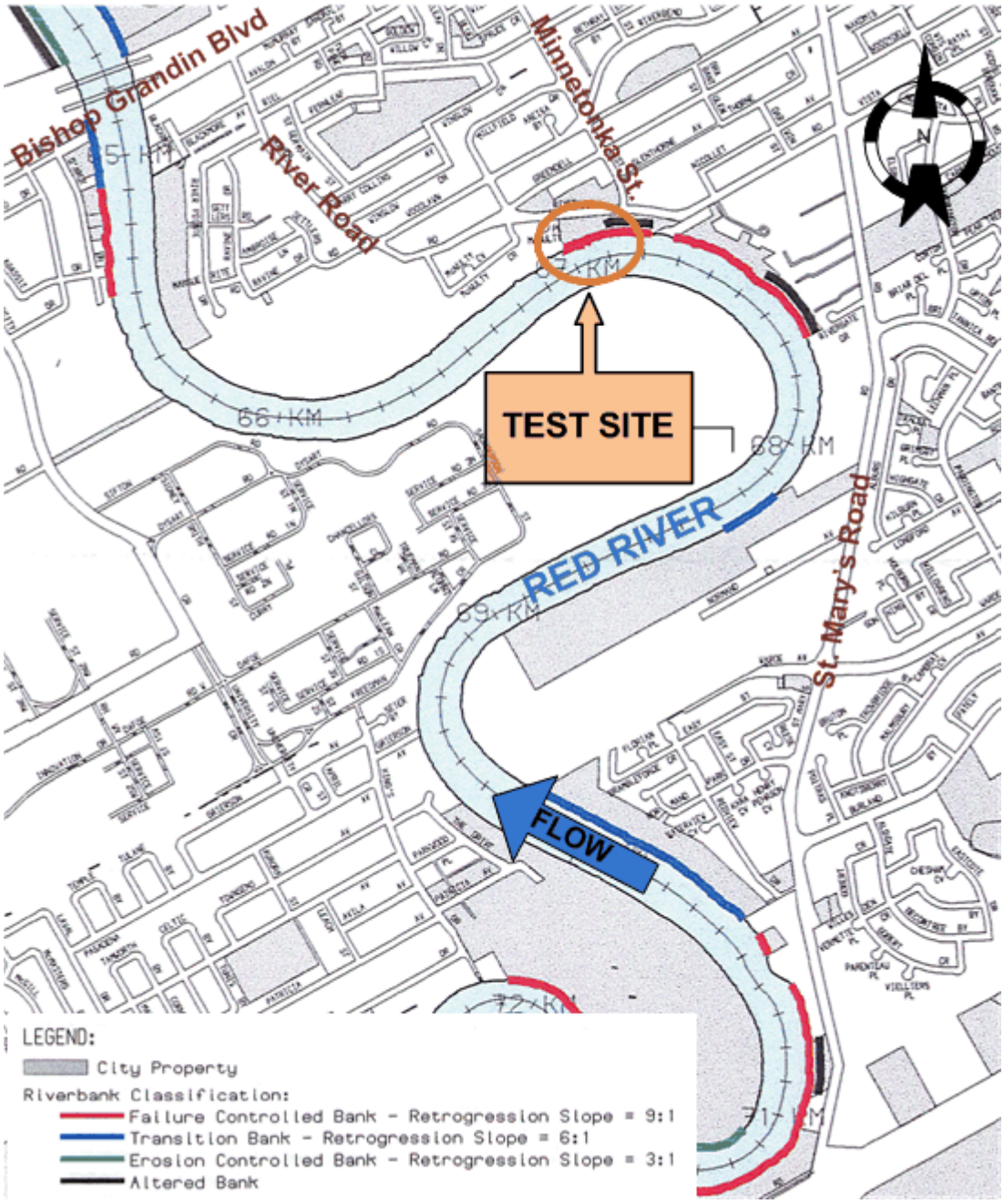


Figure 3.1. Map showing research site along Red River in WInnipeg. (Modified from City of Winnipeg 2000).

Reproduced with permission from The City of Winnipeg, January 2010.

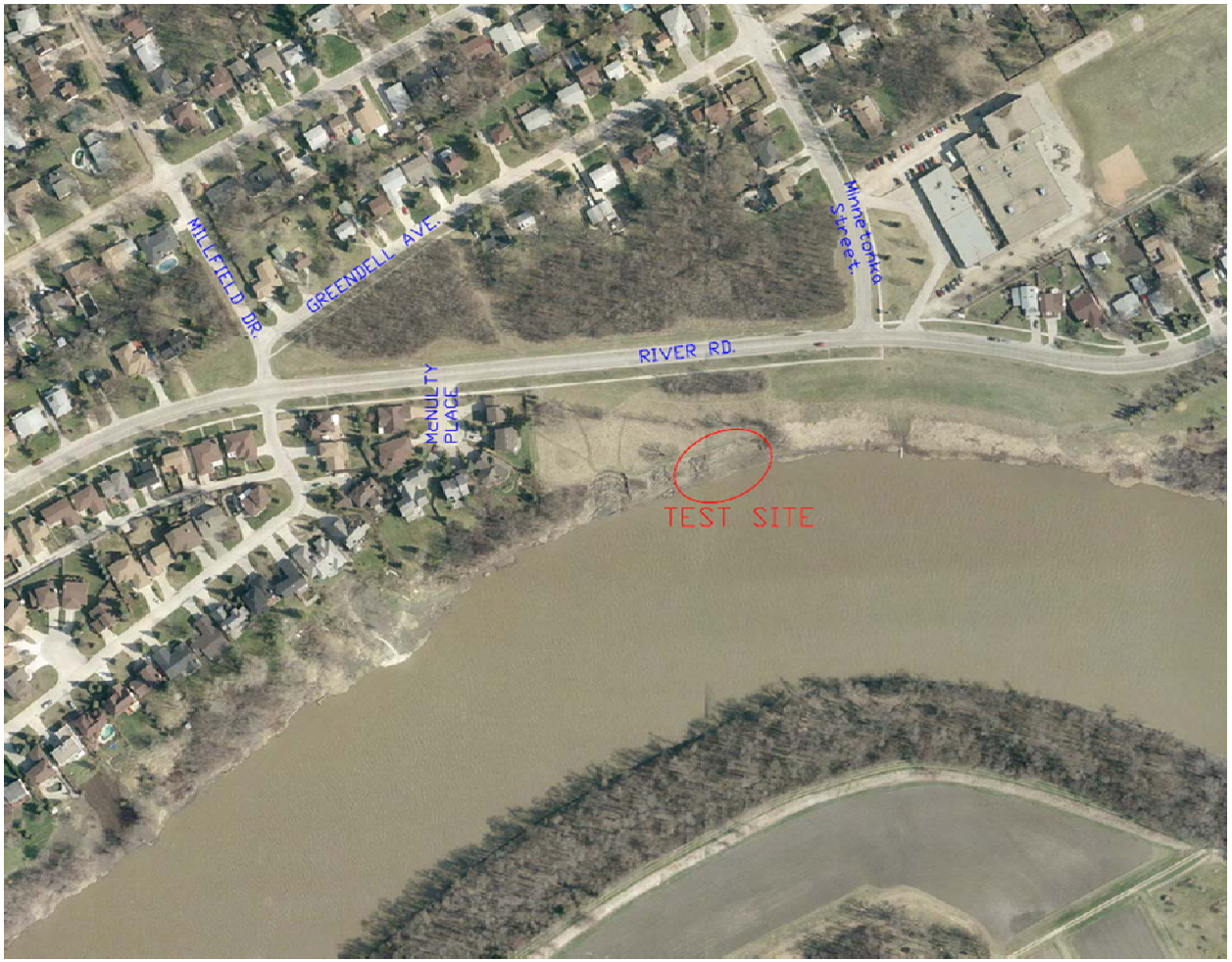


Figure 3.2 Aerial photo of the area surrounding the research test site.

Figure 3.3. Research site after instrumentation installation.  October 2007

Figure 3.4. Research site viewed from across the Red River. July 2007.



Figure 3.5. East bank of Red River a) downstream of research test site b) upstream of research test site, October 10, 2007.


Figure 3.6. Research site in June 2004. Looking downstream.

Photo reproduced with permission from The CIty of Winnipeg, January 2010.

Figure 3.7. Failed slope immediately downstream of test section. Photo taken April 2007 with high water levels.

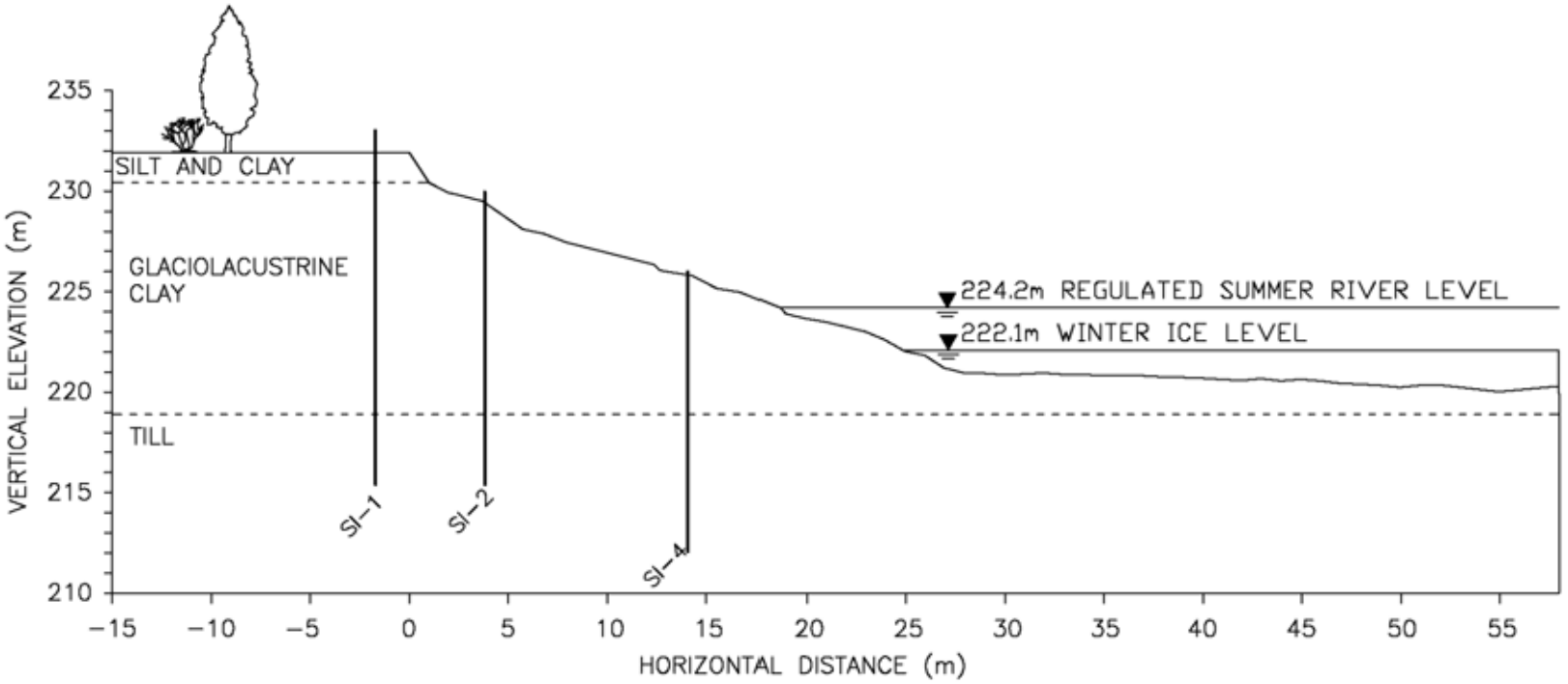


Figure 3.8. Cross section of research showing locations of Phase 1 instrumentation, prior to major site work.

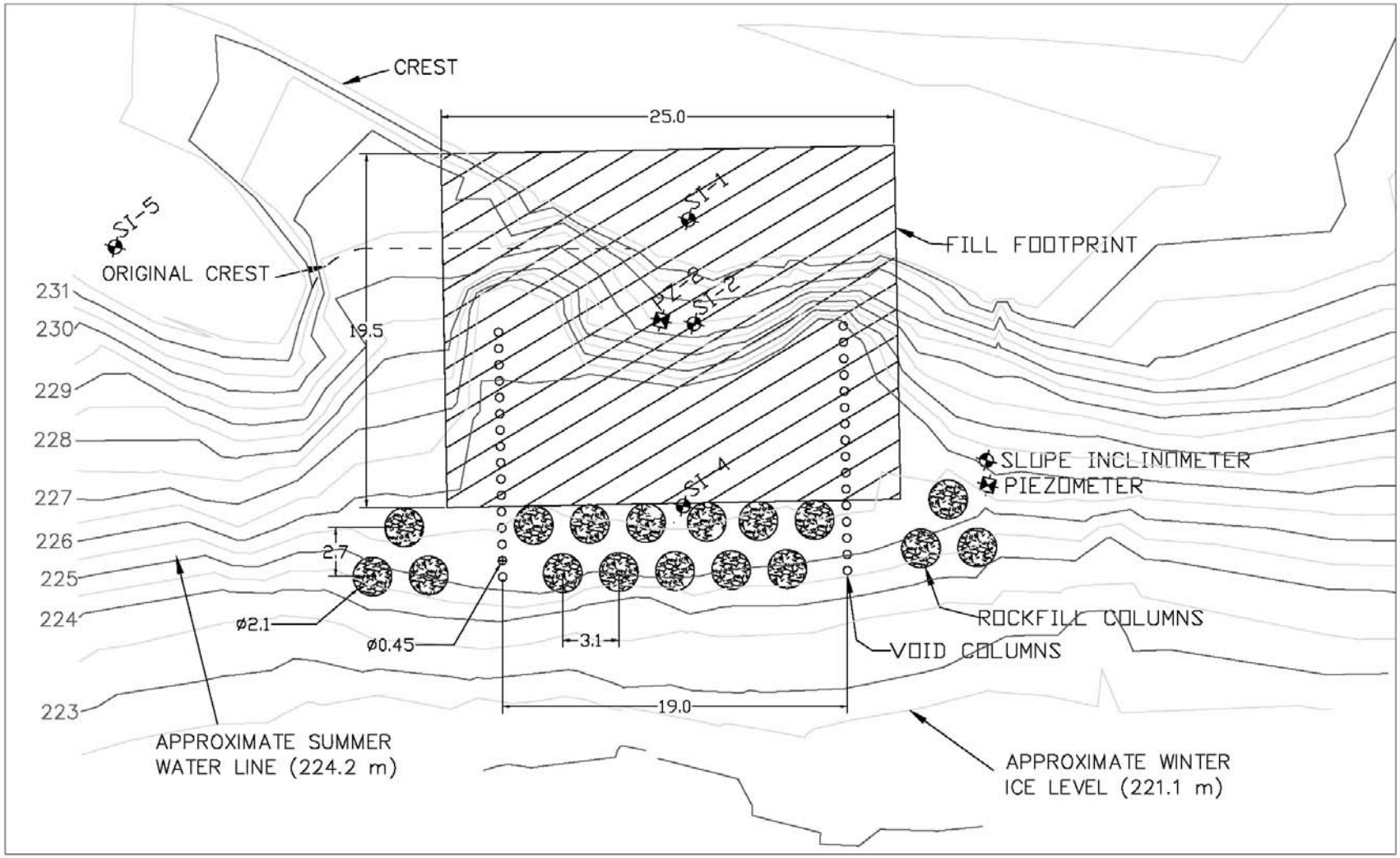


Figure 3.9. Plan view of research site showing elevation contours before the test loading. Some grading was done to accommodate the construction of the rockfill columns and void columns.

Figure 3.10. RM-30 drill rig during installation of SI-12.  December 2008.

Figure 3.11. Tension crack formed along lower bank during fall drawdown.

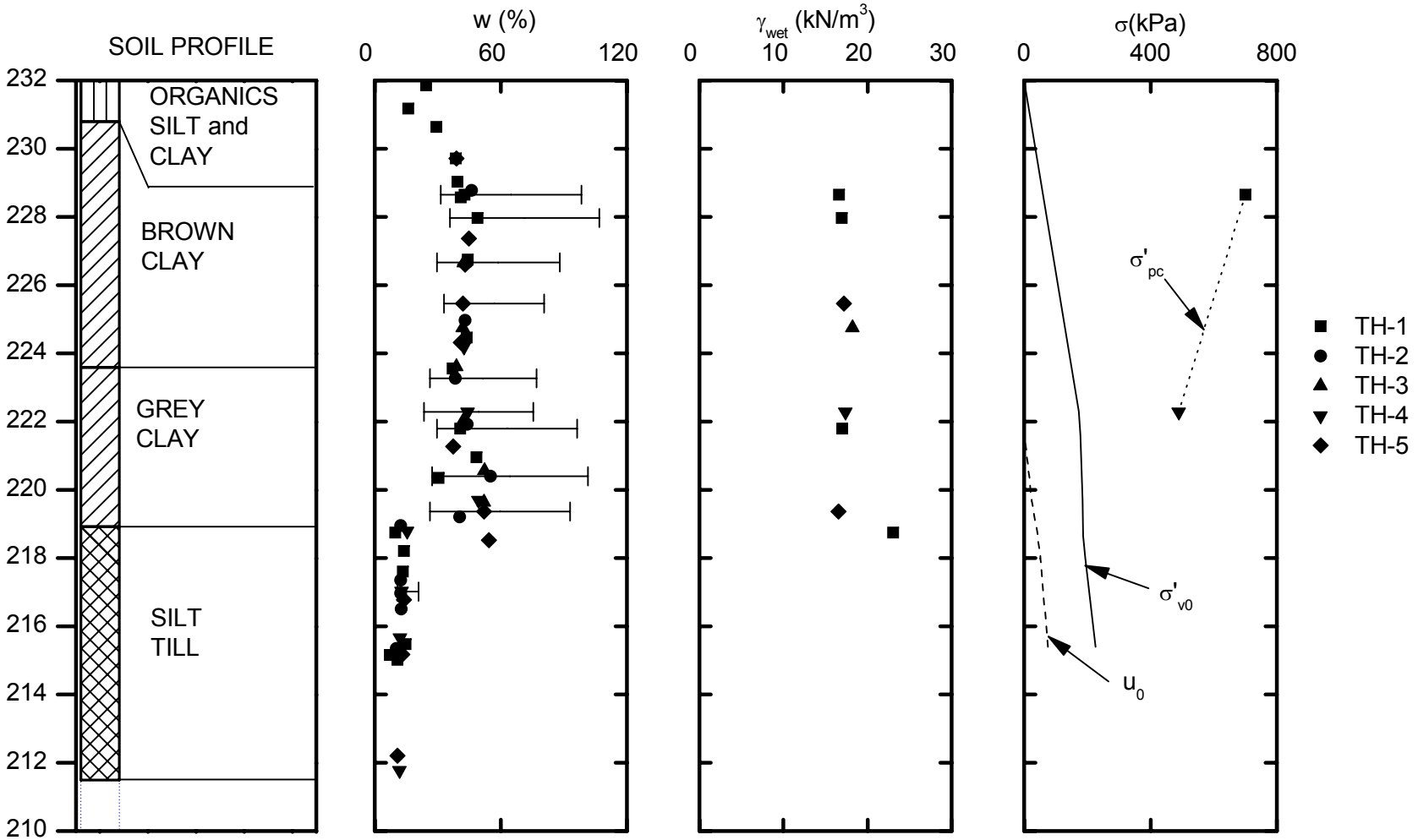


Figure 3.12. Summary of stratigraphy and select laboratory results


Figure 3.13. Silt layer exposed on riverbank. October 2007.


Figure 3.14. Triaxial specimen of brown clay showing vertical fissure with rootlets. Sample T6 from TH-1 at elevation 228.6 m.

Figure 3.15. Lower bank of test section, showing exposed rip-rap. Looking upstream from south edge of test section. November 2007.

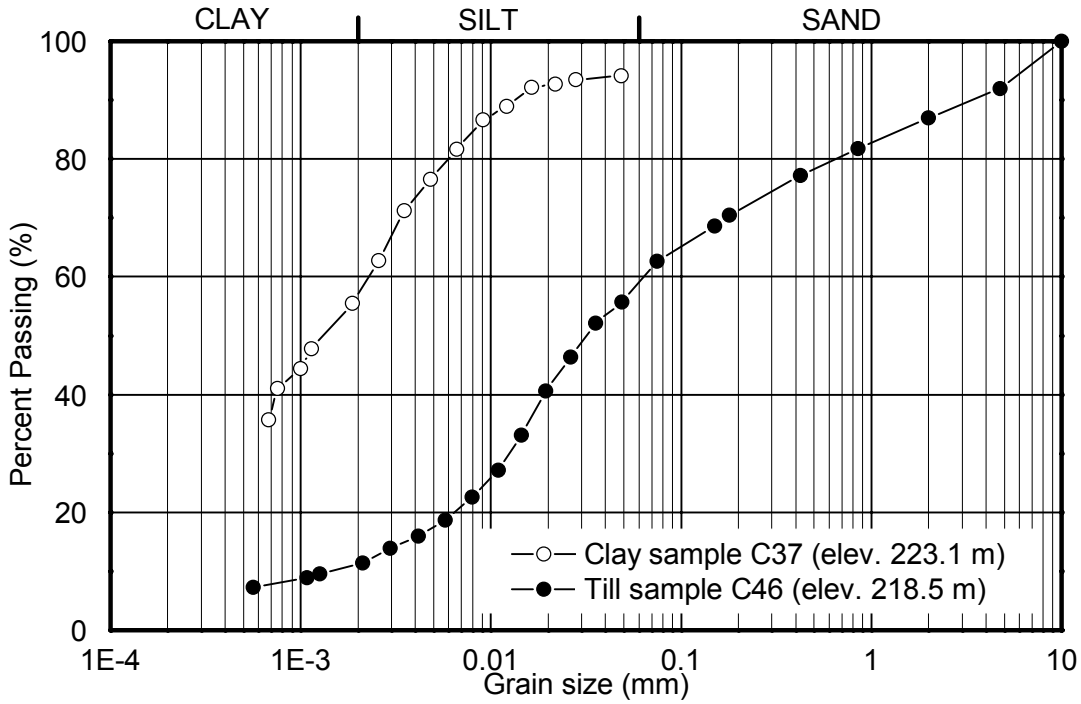


Figure 3.16. Grain size distribution for two samples from test site.

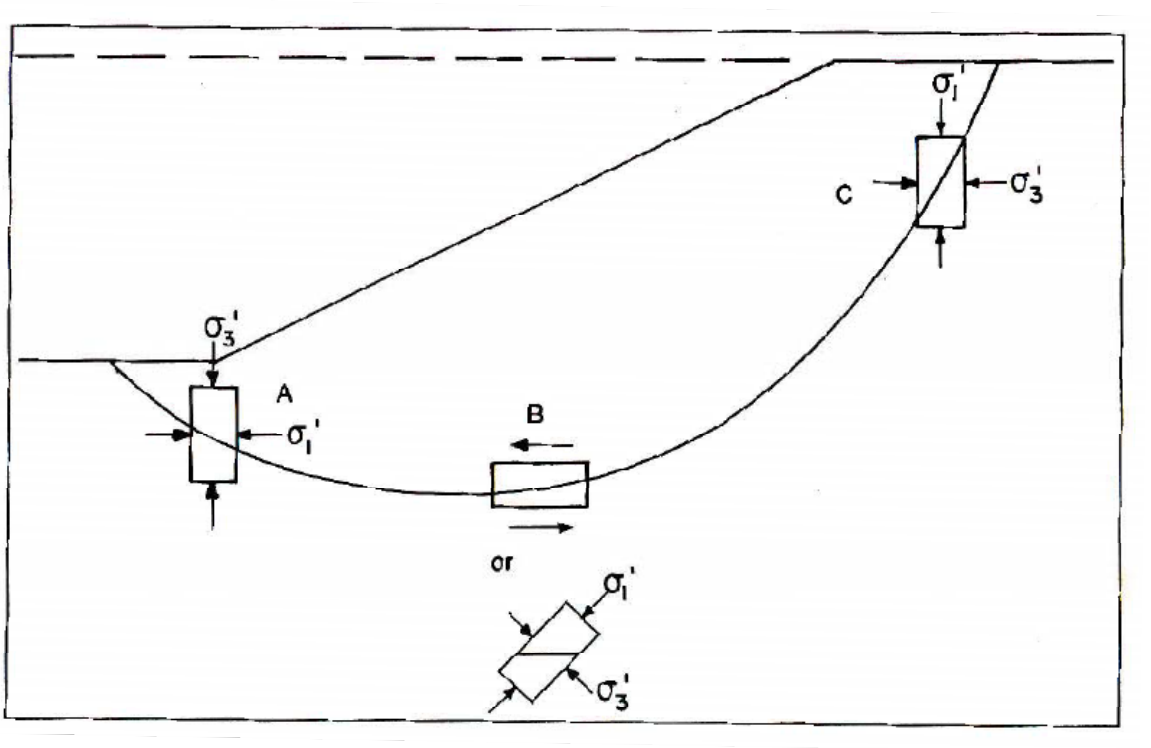


Figure 3.17. Principal stresses along a slip surface.

From Special Report 247: Landslides: Investigation and Mitigation. Figure 12-2, p. 321. Copyright, National Academy of Sciences, Washington, D.C., 2008. Reproduced with permission of the Transportation Research Board.

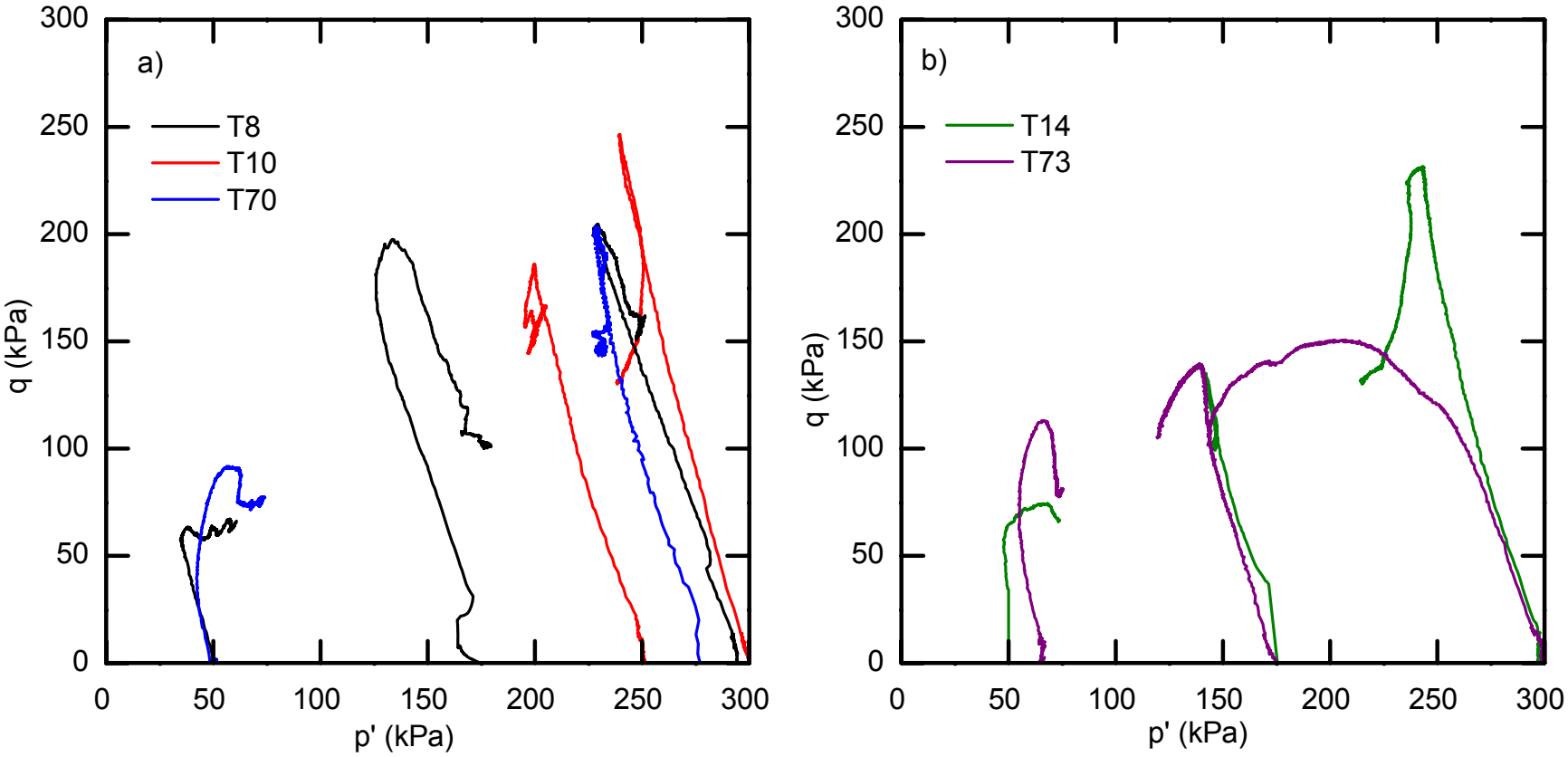


Figure 3.18. q-p' plots for triaxial tests for a) specimens of brown clay and b) specimens of grey clay

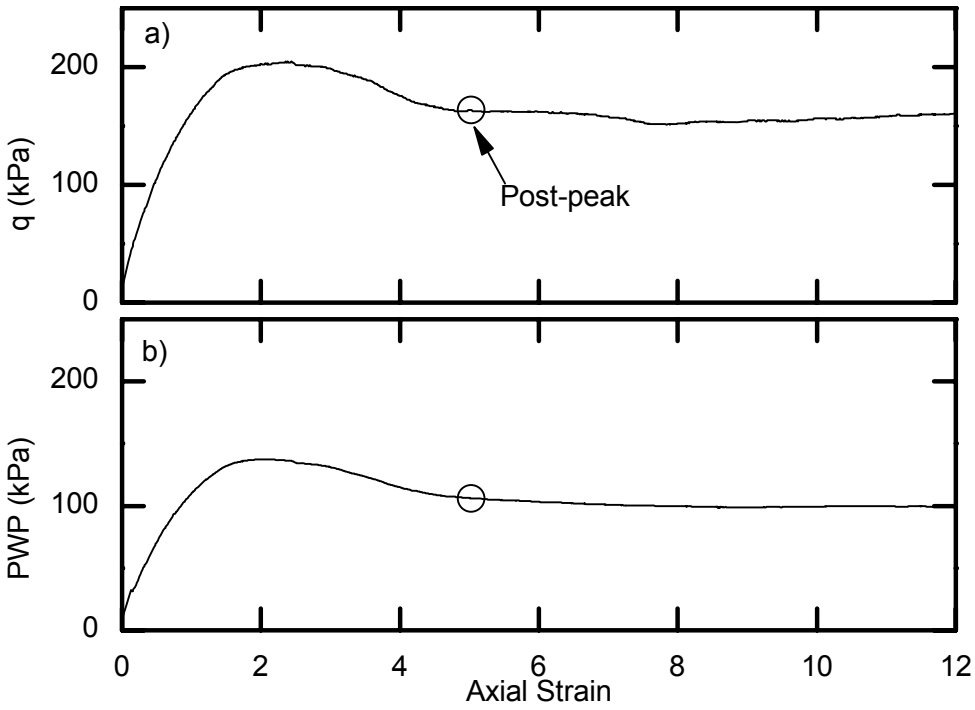


Figure 3.19. For sample T8 tested at 300 kPa confining pressure a) q vs. strain

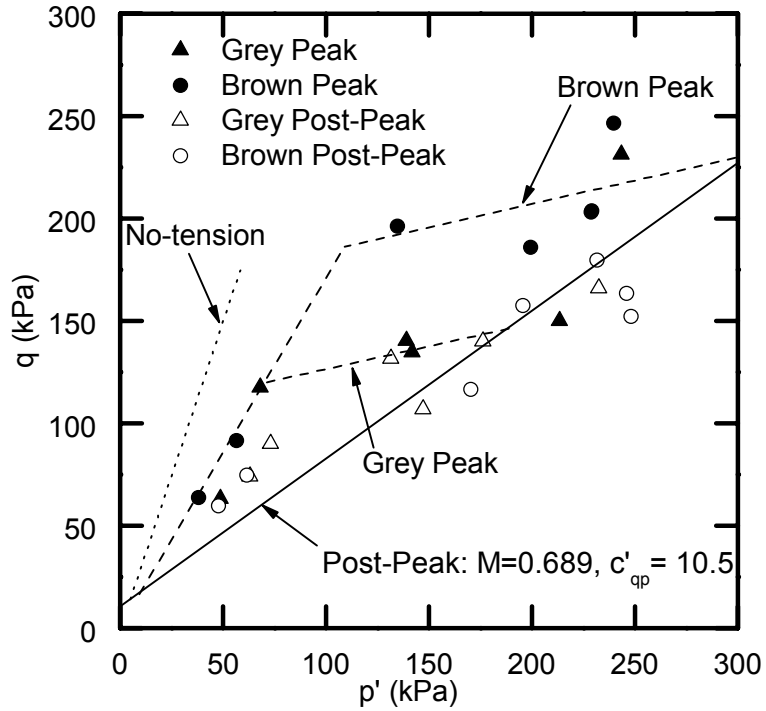


Figure 3.20. Peak and post peak strengths for grey and brown specimens with interpreted failure envelopes.

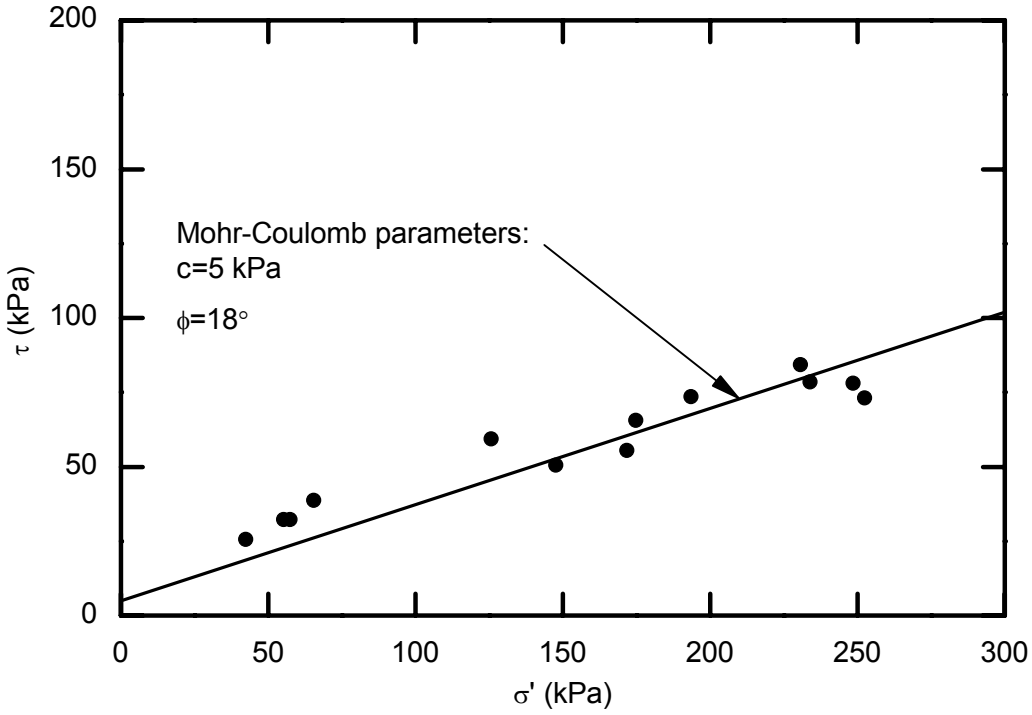


Figure 3.21. Mohr-Coulomb failure envelope for post-peak strength of clay.

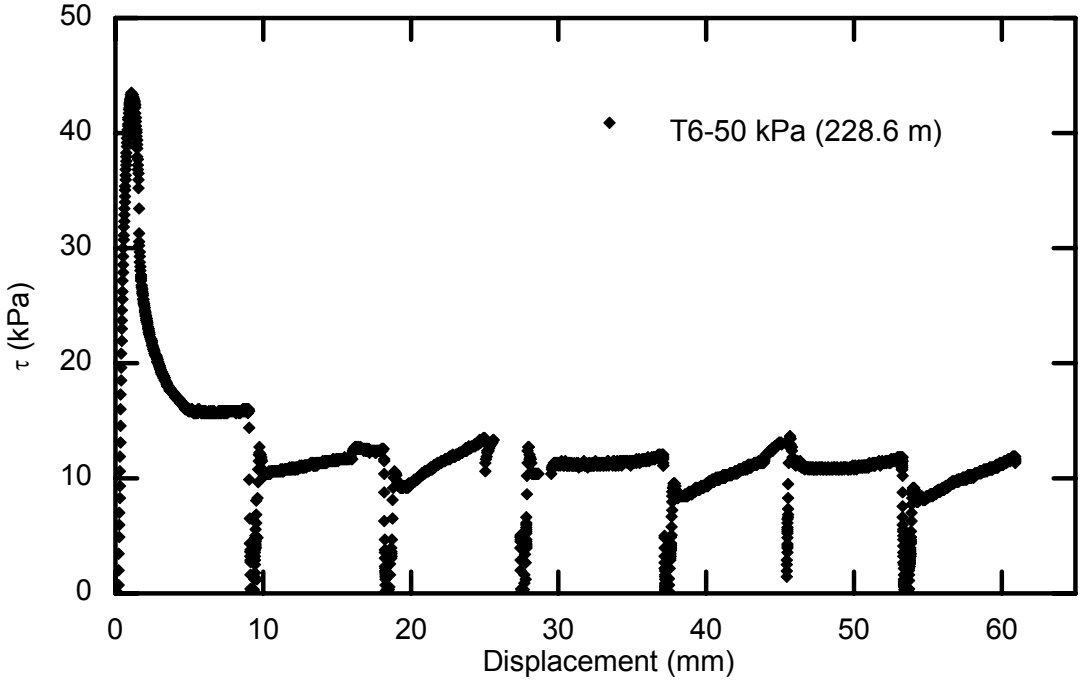


Figure 3.22. Direct shear results for sample T6 tested with a 50 kPa normal stress with multiple reversals.

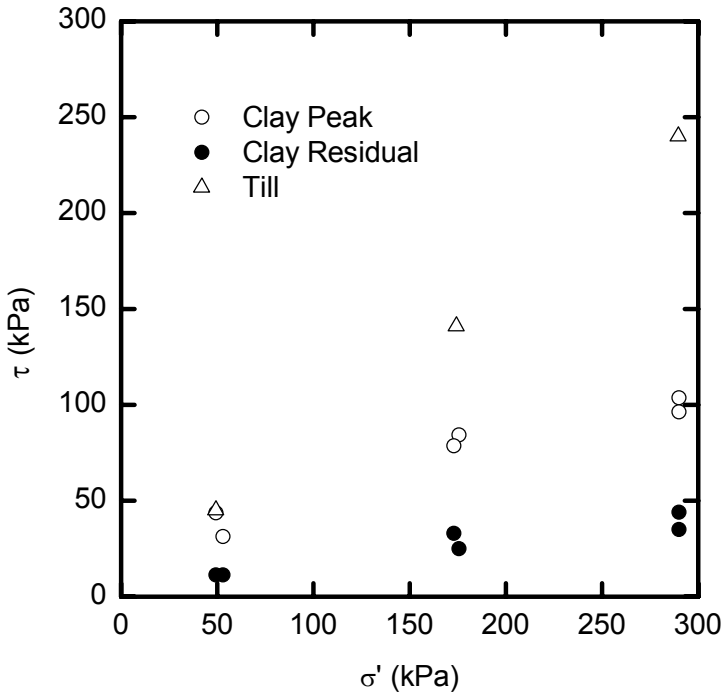


Figure 3.23. Summary of direct shear testing results, plotting shear stress against normal stress.

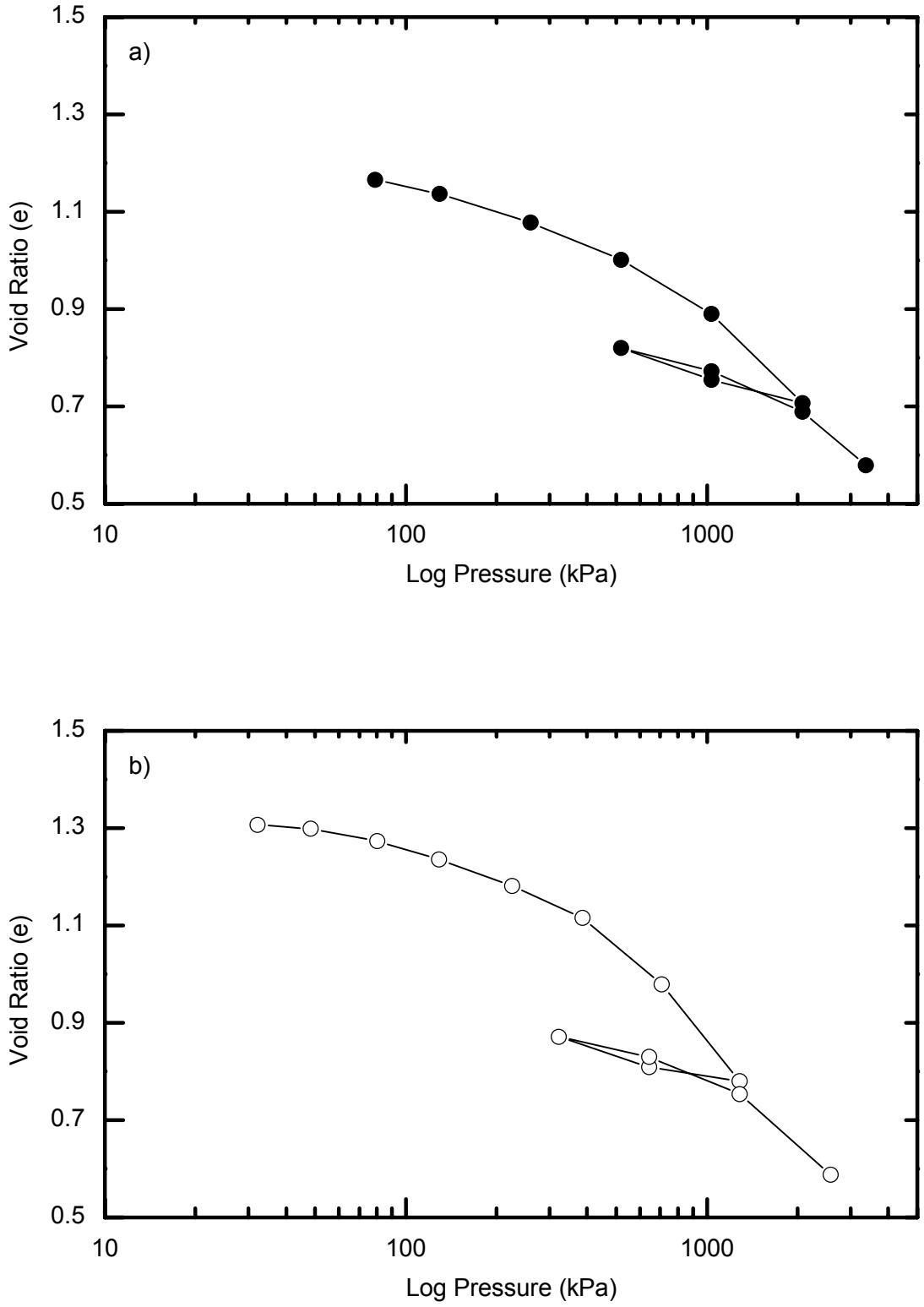


Figure 3.24. Results from oedometer specimens from elevations of a) 228.7 m and b) 223.3 m.

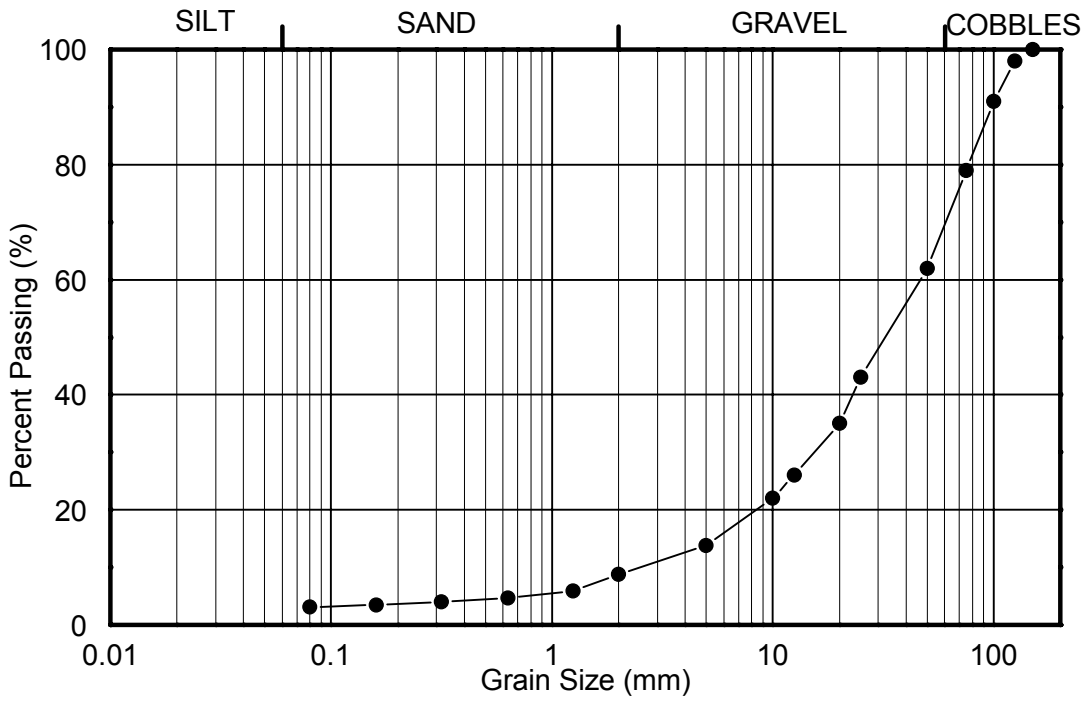


Figure 3.25. Grain size distribution of crushed limestone used for backfilling rockfill columns.

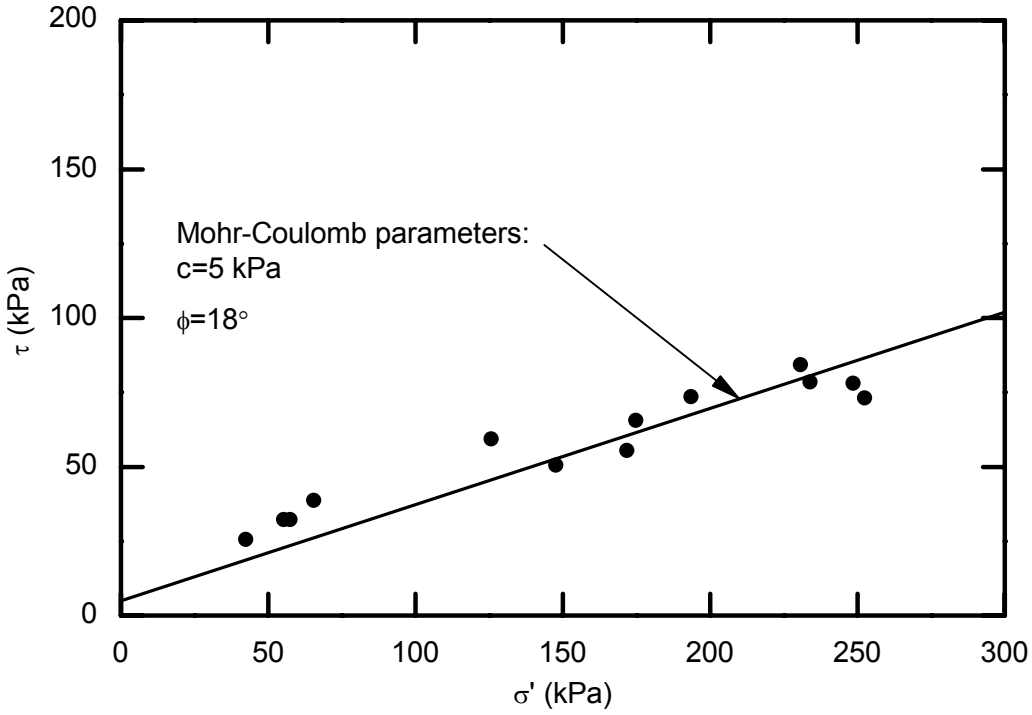


Figure 3.21. Mohr-Coulomb failure envelope for post-peak strength of clay.

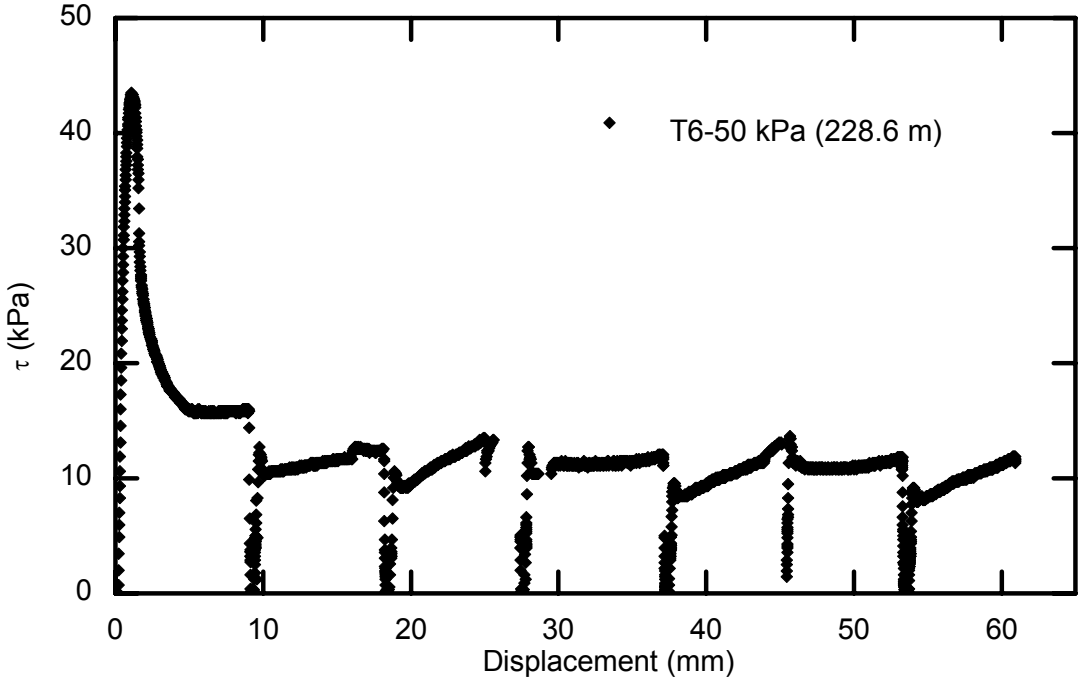


Figure 3.22. Direct shear results for sample T6 tested with a 50 kPa normal stress with multiple reversals.

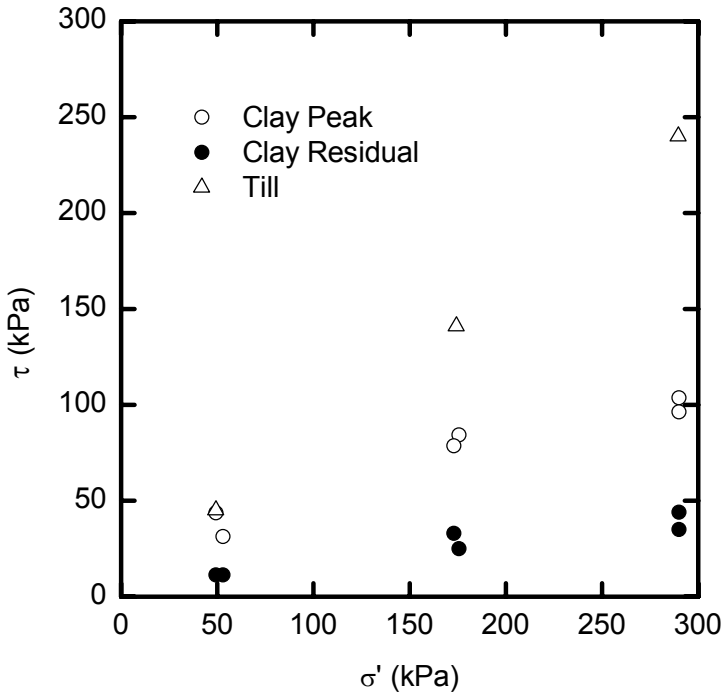


Figure 3.23. Summary of direct shear testing results, plotting shear stress against normal stress.

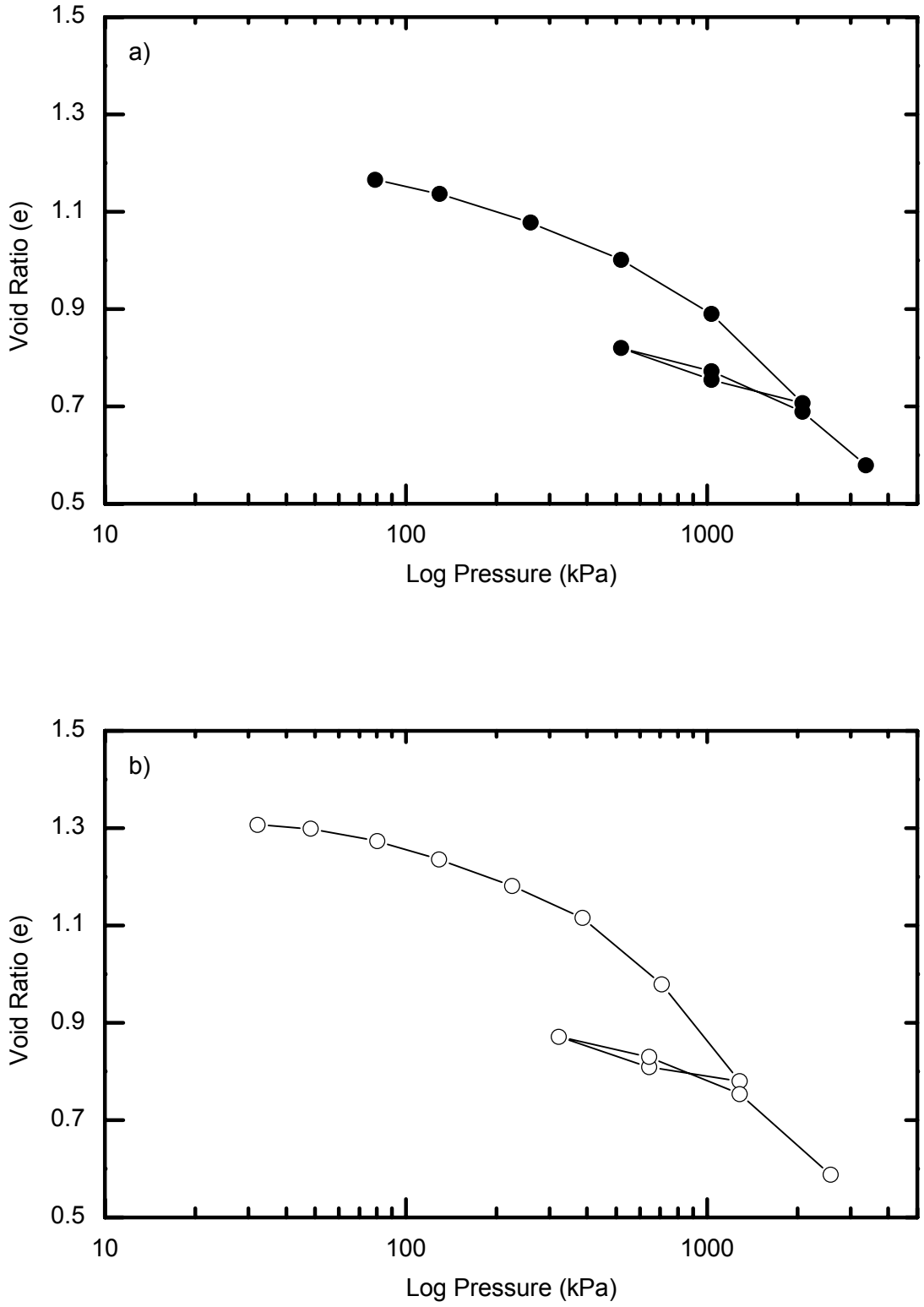


Figure 3.24. Results from oedometer specimens from elevations of a) 228.7 m and b) 223.3 m.

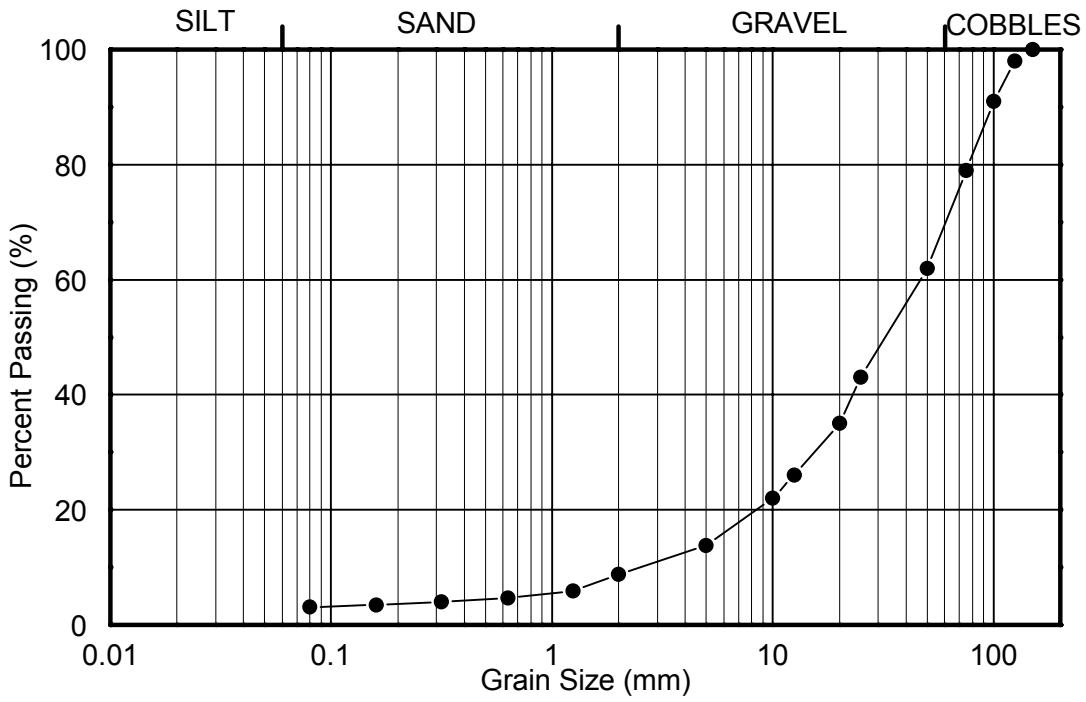


Figure 3.25. Grain size distribution of crushed limestone used for backfilling rockfill columns.

# 4. INSTRUMENTATION

## 4.1 Introduction

The site monitoring plan was developed to establish instrumentation requirements at the test site for gathering measurements of the surface and subsurface soil behaviour critical to understanding the performance of rockfill columns under the applied loading. Measurement is a critical element of the scientific method and the quality of the measurements can have implications on the interpretation of results for the research. In selecting instrumentation, there are limitations that have to be balanced against the benefits of more or better measurements. In this research project, some of the limitations included space, time, monitoring ability and cost.

Decisions on the measurement plan follow from the hypothesis that initiated the project. The instrumentation should contribute to either proving or disproving the hypothesis. The steps outlined by Dunnicliff (1988) for developing a geotechnical instrumentation plan, were used as a general guide for making decisions about instrumentation. The test-loading of the bank was a stress-deformation experiment where a load was applied, and the response of the reinforced ground was the primary interest. The main questions that the instrumentation needed to answer for this project were:

- What are the stress conditions in the ground, measured in both time and space domains?

- What are the magnitudes and directions of displacements with respect to both time and space?

These main questions also require an answer to the question:

- What is the distribution of porewater pressures in time and space?

The field test was conducted in February 2008, when the in-situ porewater pressures and stresses existed in a relatively steady-state. The addition of the loading altered the stress regime. The stress state was in flux for the remainder of the field test. Porewater pressures increased in response to loading, and then began to dissipate, thus affecting the in-situ effective stress state. There are corresponding normal, shear and volumetric strains with every change in stress. The net horizontal displacement components of these element-level strains can then be measured indirectly by slope-inclinometers. With some knowledge of the initial stress state, we can calibrate a stress-deformation finite element model with the measured porewater pressure response. The modeled deformations can then be compared with the measured displacements, which in turn speak to the accuracy of the model as a whole. The following chapters provide an in-depth discussion of the results, interpretation, and implications of the field measurements, and numerical modeling.

After consultations with members of the steering committee of the research project, it was determined that slope inclinometers and piezometers would best be able to answer the above questions. There are many other types of instruments that could potentially also have been beneficial, such as settlement gauges, pressure cells and extensometers. The costs would have been large,

and the observations may have had little technical benefit. The inclinometers and piezometers were complimented by logistical records, surveys, and ground and aerial photos to record the test progress and capture data. Table 4.1 shows the convention for naming the instruments used in this project.

Geotechnical instrumentation is practical and generally sufficient for monitoring site conditions on typical engineering projects. It does not, however, generally perform to the levels of precision and accuracy expected in a research environment. Redundancy was built into the instrumentation plan to account for some of the shortcomings of individual instruments and readings. Even though every instrument served to improve the quality and breadth of the results, no single instrument or monitoring point was absolutely critical to the success of the test. The vibrating wire piezometers and in-place inclinometer sensors were chosen based on quality, performance and price, but were otherwise industry standard “off-the-shelf” products.

## 4.2 Plan and layout

Table 4.2 and Table 4.3 list the instrumentation installations. The individual instruments will be addressed by the installation identifications (ie. VW-A, SI-7 or IPI-9). Figure 4.1 shows instrumentation locations in plan view, and Figure 4.2 and Figure 4.3 show the locations of select inclinometers and piezometers in cross section.

Installation of the instruments in Phase I took place from August 8-10, 2006. Slope inclinometers SI-1,2 4,5 and piezeomters VW-A, B and C were installed at

that time. The second phase of instrumentation installation took place during or immediately after the rockfill column construction, between November 30 and December 13, 2007. The installations in Phase II included inclinometers SI-6 to 12 and vibrating wire piezometers VW-D through F.

### 4.2.1 Slope inclinometer locations

The test-hole locations for the Phase I site investigation were chosen both for the immediate purposes of sample collection and ground proofing, but also for installing equipment for long term monitoring. Test-hole locations were chosen along the guidelines put forth by Turner and Shuster (1996). In Phase I, slope inclinometers were installed behind the crest, downslope from the scarp, and near the estimated center of the slide mass. SI-5 was located nearby, but outside the immediate test section.

Phase II installations included SI-11 and SI-12 added near the edges of the test section, and SI-6, 7, 8 and 9 amongst the columns. As illustrated in Figure 4.1 there was a concentration of inclinometers near the centerline of the test site, in the area of the columns. These installations sought to capture the deformation behaviour of the columns and the clay between the columns. SI-10 was installed as far downslope (toward the river) as was reasonable considering the terrain. There was some redundancy built into the layout in case inclinometers were damaged during the site activities.

### 4.2.2 Piezometer locations

The piezometer locations were chosen to measure a representative distribution of the porewater pressure response within the cross section. It was assumed that the porewater pressure response would be relatively consistent in the dimension parallel to the riverbank. The greatest porewater pressure response to loading was expected to occur directly beneath the fill. VW piezometers A, B, C, E and F were installed beneath the fill footprint. VW-D was installed in the clay in the same borehole as SI-8, in-between the rows of rockfill columns. Piezometers were installed in "strings" (ie. VW-A,B and C or VW-E and F) to measure vertical porewater pressure gradients, and determine the variations in porewater pressure response vertically through the clay.

Slope inclinometer casings, SI-2 and SI-7 were also used as standpipe piezometers. PZ-2 measured the total head in the till while PZ-7 monitored the water level in a rockfill column. The installation methods will be discussed in the following sections.

## 4.3 Slope inclinometers

The plan for the slope inclinometers was designed to record the development of strains and displacements throughout the test area, but especially in the rockfill columns and surrounding clay. All slope inclinometer casings were purchased from Slope Indicator (Mukilteo WA). SI casings 7 and 9 were 85 mm in diameter, while the others were 70 mm in diameter. The larger diameter casings were chosen for these installations because the casings are more robust and they were thought to be more suitable for installing directly into the rockfill columns.

Positive “A” direction displacements are in the downslope direction. Positive “B” direction displacements are oriented 90° clockwise from the A direction. Displacements with both A and B components can be calculated using trigonometry.

### 4.3.1 Installation

All inclinometer casings except SI-6,7 and 9 were installed in 125 mm diameter boreholes drilled through the clay into the till. Any space between the inclinometer casings and the drilled soils were backfilled with a cement-bentonite grout. The mix design generally followed the recommendations of Mikkelson (2002). Figure 4.4 shows the relationship between the water:cement ratio and the undrained shear strength. A water:cement ratio of approximately 5.5:1 by weight was used to match the strength of the grout backfill with the strength of the in-situ soil. Powdered bentonite was added to the mixed cement and water to achieve a thick, but workable consistency. The grout was tremied to the base of the inclinometer casing, and was pumped until all the water in the borehole was displaced and the gap was filled with the grout.

Three of the slope inclinometer casings, SI-6, SI-7 and SI-9 were installed directly into rockfill columns. To the knowledge of the author, there has been no previous inclinometer casing installations directly in rockfill columns. The SI-6 casing was placed into the column boring before backfilling the column with rockfill. The backfilling and subsequent compacting of the rockfill deformed the

casing, but it remained operational. This installation method allowed for direct observation of the column's response to compaction.

Temporary steel pipes, shown in Figure 4.5, were placed in the open drilled shafts and the rockfill was backfilled and compacted around the pipes to install SI-7 and SI-9. The continuous steel pipe had an outer diameter of approximately 280 mm. The ABS inclinometer casing was placed inside the larger diameter steel pipe after the rockfill was compacted. The gap between the rockfill and inclinometer casing was backfilled with silica sand to anchor the casing as the outer steel pipe was removed. The silica sand backfill is not as reliable as a cement-bentonite grout because of the potential for bridging during backfill or migration of sand particles into voids in the surrounding material. Arching of the backfill sand occurred during installation of SI-7, but it collapsed as the steel casing was pulled up past the arched sand location. Arching did not occur in the backfilling of casing SI-9 because the water level remained low. A granular backfill was preferred over a grout backfill for installations into a rockfill column. A grout backfill would also fill the voids in the rockfill, thus changing the physical characteristics of the compacted material. A pea-gravel backfill would have been equal, if not more suitable than sand. The installation methods used for SI-6 and SI-8 and SI-9 both worked sufficiently well, and have since provided valuable deformation data.

Most of the inclinometer casings were partially filled with water during installation to offset the effects of buoyancy. The water in the casings also helped to stabilize the probe temperatures more rapidly, which results in more consistent

readings. The water also created challenges because much of the work was done in sub-zero temperatures. The casings were susceptible to complete freezing if the water level was too high, or build-up of frost and ice along the frozen length occurred. On a number of occasions during the field test, inclinometer surveys were delayed or skipped while ice was thawed with the aid of a steamer.

### 4.3.2 In-place inclinometers

Strings of three in-place inclinometers (IPI's) were installed in SI-8 between 217.5 and 220.5 m and in SI-9 between 218 and 221 m elevation. Each IPI sensor spanned 1m. The sensors in SI-8 were biaxial, so they measured displacements in both the A and B directions, while the IPI's installed in SI-9 were uniaxial. Biaxial measurements were thought to be more critical in SI-8, which was installed in the clay between rockfill columns, where there was a potential for "flow" of clay around the columns.

In-place inclinometers were chosen for this test site because tracking deformations and changes in the rate of deformation were important. Figure 4.6 shows an in-place inclinometer sensor being installed in February 2008. The in-place inclinometers were kept in place for the duration of the test, but were removed after the unloading of the slope, prior to site restoration.

In-place inclinometer technologies are not new, but because they are relatively expensive and less practical for small or short term projects, they have not seen widespread use. In-place inclinometers are best suited for applications where

long term monitoring is required, and where immediate notification of movement is critical (Bailey, 1979). The in-place inclinometers use electro-level sensors to measure verticality.

The monitoring system was not set up to send real-time observations to a remote computer because of the cost and complexity. The data could be downloaded and viewed within minutes by the person on site. The site was monitored in person for 15 hours per day, with approximately 8 hours of monitoring after the final daily lift was placed so the chance of "missing" something was considered to be small.

### 4.3.3 Monitoring

Two slope inclinometer probes were used during the loading portion of the field test. Both instruments were Digitilt Inclinometer Probes, manufactured by Slope Indicator with a 2'(0.305 m) wheelbase. Baseline readings were done with each probe, cable and read-out box setup. The newer of the two inclinometer probes with a 200' (60.9 m) cable and a Digitilt Datamate auto-logger was used for most of the inclinometer surveys.

Monitoring slope inclinometers is a time consuming activity, taking 15-40 minutes per survey. A monitoring schedule was established for the duration of the loading and unloading so that all inclinometers would be read at least twice per day. Priority installations, including SI's 4,6,7 and 10 were read at least three times per day on days when loading was taking place, and one or two times per

day on days when no additional load was placed. Figure 4.7 is a picture of a volunteer monitoring a slope inclinometer at night.

SI-8 and 9 could not be regularly monitored over the full length because of the in-place inclinometers. After the final fill load was placed, the IPI's were temporarily removed to allow for a complete manual inclinometer survey of the casing. The data collected after the re-installation of the in-place sensors is somewhat poor as the inclinometers took time to "settle down" after re-installation, resulting in excess noise in some of the data.

The monitoring program for this project was made possible by volunteers from the University of Manitoba and the other project partners. Those helping all had technical skills in the area of geotechnical site work, but the human factor still remained. The accuracy and reliability of slope inclinometer surveys are very dependent on the methods and care of the operator (Slope Indicator 2001). A brief training and information session was held for those helping with monitoring; however it is believed that there are likely still some errors that could have been eliminated if it there was more consistency amongst those doing the inclinometer surveys.

The monitoring of the in-place inclinometers will be discussed in Section 4.5 below.

#### 4.3.3.1 Accuracy and error correction

It is important to understand the limitations of instrumentation, both to establish trust in the results, but also to identify errors and other problems. With

inclinometer data, there are installation corrections and error corrections. The installation corrections can account for casing orientation, casing spiral or changes in the casing height. Error corrections account for bias, or erroneous readings. Many errors cannot be reliably corrected without comparing a survey with the surveys taken before and after the one in question. If an error is identified in the field, it is usually best to re-do the survey. Corrections to the reduced data have been done using DigiPro for Windows[1].

When readings have been judged to be erroneous, the data may have been discarded, left as is, or modified based on the author's engineering judgment. It should be noted that the large majority of the datasets have been left untouched, and that uncorrected errors and inaccuracies are still evident in the reported data. Correcting all "errors" would be onerous, unnecessary and scientifically unsound.

All inclinometer data have been corrected for orientation, with the A+ direction being parallel to the dip direction of the natural slope, and thus perpendicular to the rows of rockfill columns. The azimuth of the column rows is 75˚ from grid North. The orientation corrections are listed in Table 4.3

The "double pass" method of reading inclinometers eliminates most systematic and instrument error by averaging the data readings of consecutive survey passes with the probe facing opposite directions. The remaining sources of error are caused by changes in the instrument during the process of surveying a

[1] Digi-Pro for 32-Bit Windows Systems (Version 1.34.1) 2006. DGE Slope Indicator.

casing (Gould and Dunnicliff 1971). Care was taken to ensure that the probe temperature had stabilized and that the probe was treated gently to prevent bias shift (Slope Indicator 2001) to minimize these forms of error. The large number of datasets for each inclinometer installation and the consistency of the observed trends provide confidence that when corrections have been made, they are not introducing another source of error.

The accuracy of a slope inclinometer monitoring system is ±0.3”/100’ (1mm/4.01m) including both random and systematic errors. The systematic errors can be corrected if properly identified and dealt with (Mikkelsen 2003). The precision of a single reading, without systematic error, is ±0.007” (0.178mm) while the systematic error has been found to be 0.005”(0.125mm). As an example, for a 56’ traverse (equal to the length SI-1, which is the longest in the test section), the total error is:

$$\text{Total error} = \text{Random Error} + \text{Systematic Error} \qquad 4.1$$

$$\text{Total error} = 0.007 \times \sqrt{n} + 0.005n = 0.007 \times \sqrt{28} + 0.005 \times 28 = 0.177"$$

With systematic errors removed, the limit of accuracy is 0.037” (0.94mm).

SI-4 and SI-6 showed the most random error during the field test. This is attributed to the large and irregular deformations that these casings underwent during the construction of the rockfill columns.

### 4.3.4 Baseline observations

Four slope inclinometers, SI-1, 2, 4 and 5 were installed in Phase I. They were monitored for 15 months from August 2006 to November 2007, before the installation of the rockfill columns. Monitoring was conducted every four to six weeks during the summer and winter months, with increased monitoring in spring and fall when changes in the river levels and groundwater conditions combine to theoretically reduce the factor of safety. These four inclinometers were monitored closely during and immediately following the installation of the columns in November and December 2007.

The purpose of the 15 month monitoring period was to identify any ongoing slope movements in the existing slope. Relatively little deformation at depth was observed over this period, as illustrated by Figure 4.8 and Figure 4.9. This led to the conclusion that the upper portion this slope, above the summer water level, was not unstable in the months leading up to the test loading. That is, the factor of safety was greater than unity. Slight movements observed during the fall drawdown and spring flood (Figure 4.9) suggested that zones of yielding were developing, and that the right combination of conditions could possibly lead to the development of a large deep-seated failure surface.

As discussed in Section 3.3, significant instabilities were observed along the lower slope (downslope of SI-4) during the fall drawdown of the Red River in the 2006 and 2007. Fresh scarps and tension cracks of up to 450 mm in width were observed across the width of the test section at an elevation between 224 and 225 m (Figure 3.11).

## 4.4 Piezometers

Vibrating wire piezometers were chosen over pneumatic and standpipe piezometers to read pore water pressures in the clay because: they respond rapidly to porewater pressure changes, they can easily be monitored with a data-logger, and they are unaffected by the cold. Accurate and rapid measurements of the porewater pressure response to loading were important for calibrating the numerical models. Table 4.2 shows the installation depths of the individual piezometers. All but one of the vibrating wire piezometers were manufactured by Slope Indicator. The exception, VW-D, was manufactured by RST Instruments Ltd.

### 4.4.1 Installation

A string of three vibrating wire sensors, VW-A, B and C, was installed in a single borehole at the depths listed in Table 4.2. The piezometers were strapped to a 25mm diameter PVC pipe, which was also used as a tremie line for grouting. The sensors were installed with the porous stone facing upward so that the tip could be filled with water to maintain saturation of the stone during the installation process. The piezometer installation was backfilled with a cement-bentonite grout. This method has been proven and is recommended because installation is easier than installing piezometers in sand pockets, and the response time is improved (McKenna 1995, Mikkelsen 2002, Mikkelsen and Green 2003). The grout mix was designed to approximately match the permeability of the in-situ clay soils. A water:cement ratio of approximately 2:1

was used. Figure 4.10 shows suggested water:cement ratios for various consolidation pressures and permeabilities (Contreras et al. 2008).

Vibrating wire piezometers VW-E and F were installed using the push in method. A borehole was drilled to a depth 0.6 m above the desired depth of the piezometer tip. The piezometer was then pushed through the in-situ clay for the remaining 0.6m to the desired elevation depth. The holes were backfilled with bentonite grout to the surface.

The inclinometer casing for SI-2 was also used as a standpipe piezometer and SI-7 served as a monitoring well. The high permeability of the till provides an adequately rapid response, despite the larger diameter of the casing. The bottom 0.3 m of the casings were slotted and wrapped in filter cloth to allow flow of water in and out of the casing. The bottom 1.5 m of SI-2 was backfilled with sand. The rest of the annulus was backfilled with a cement-bentonite grout like the other slope inclinometers. Appendix A shows the details of the instrumentation installations for TH-1 to 5 in the testhole logs.

### 4.4.2 Monitoring

Regular monitoring of the vibrating wire piezometers was done with a readout box that measured the frequency response (Hz) of the “vibrating wire.” The frequency was then converted to a pressure using calibration records provided by the manufacturer. The calibration curves were confirmed prior to installation at the University of Manitoba. An atmospheric correction was not applied to the buried vibrating wire piezometers because they directly measure the actual pore

water pressures experienced at the time of the reading (Slope Indicator 2007). The monitoring of the vibrating wire piezometers during the field test will be discussed in Section 4.5.

The standpipe piezometers were manually monitored with an electronic reel-mounted water level meter. During the test loading there was negligible change in the till water pressure.

### 4.4.3 Baseline observations

Figure 4.11 shows the results of monitoring the porewater pressures prior to the full-scale field test. The high porewater pressure events are generally connected to flood events, with a slight time lag. The lowest porewater pressures are measured in late winter. There is generally an upward gradient from the till into the clay during times with normal or low river levels.

VW-C was unintentionally installed above the water table, because the water table was unknown at the time of installation. As a result, VW-C did not provide reasonable or useful results during the project.

## 4.5 Real-time monitoring

Real-time monitoring of slope movements and pore-water pressure responses was accomplished with a data logger during the test loading and unloading. A Campbell-Scientific CR-23X data logger was used for this purpose. The six vibrating wire piezometers were connected via a Campbell Scientific AM16/32 multiplexer and an AVW1 vibrating wire interface. The same data logger was

used to monitor the six in-place inclinometers via a Campbell Scientific AM416 multiplexer and an EL-relay board. Figure 4.12 shows the datalogger and peripherals as setup in the field. The cables from the vibrating wire piezometers and the in-place inclinometers were routed through HDPE piping for protection as pictured in Figure 4.13.

The data-logger recorded the raw measurements from the instruments plus the time, ambient temperature (in the data logger enclosure), and instrument temperatures. The piezometers and IPI's have built in thermistors to allow for temperature corrections of the raw data although temperatures at depth varied by less than $1^{o}$C. The vibrating wire piezometer and inclinometer sensors were read at 10 minute intervals throughout the field test. The programming for the data logger was initially prepared by Slope Indicator, but was modified further to suit the purposes of the project.

The data-logger setup and IPI's were tested in the laboratory before installation in the field. A spreadsheet was developed to quickly provide a summary of observations after downloading the data. Hardware and software capable of uploading, processing, presenting and communicating the data in real-time are available from instrument suppliers. The benefits of real-time communications did not justify the additional expense because the site access was convenient, there were no labour cost savings, and the site was to be manned for most of the testing period.

It was recommended by the manufacturer that the IPI's should receive five minutes of excitation for readings to stabilize, prior to every reading. This power

requirement was too great to depend only on battery and/or solar power. For the field test, power was supplied by a generator and an uninterrupted power supply and a surge protector were placed in series to provide backup power and prevent surges from damaging the equipment.

The in-place inclinometers were installed on February 16, 2008. The data-logger was used intermittently between February 16th and February 20th when a portable battery power source was used to power the data logger. On the morning of February 21st a generator was made available, and the instrumentation was monitored continuously until March 6th.

Vibrating wire piezometer D was connected to the data logger on February 16. VW piezometers A-C and E-F were connected to the data-logger on the morning that the test loading began. These piezometers could not have been connected earlier because the lead wires needed to cross an area which had equipment traffic prior to that time.

There were a number of technical complications with both the data-logger and instrumentation that resulted in the loss of some data. Upon installation, it was observed that one of the IPI sensors was malfunctioning. A replacement was rushed out from the manufacturer, but only arrived in time to be installed on Day 3 of the test loading (February 23, 2007). It is suspected that water got past the seals in the malfunctioning instrument and into the electronic components. Another sensor performed well most of the time, but had periods when large amounts of noise covered the actual observations. A third sensor also performed poorly for the entire duration of the test, showing a cyclic response

which did not correspond with other observations. These problems resulted in the loss of some data, but the built in redundancy minimized the effect on the final results.

The data-logger also malfunctioned on two occasions (possibly related to the above issues). No data were collected between 11:40 and 13:10 on February 26. The data-logger automatically shut-off as a precautionary measure after the low voltage threshold of the battery was breached. A suspected short-circuit interrupted all automatic data collection between 18:50 on February 29$^{th}$ and 16:47 on March 2$^{nd}$. The data-logger continued to run, but all data-values were null.

## 4.6 Additional instrumentation and monitoring

Survey work during the field test was done with a Real-Time Kinetic (RTK) GPS system. The equipment can produce sub-centimeter accuracy, although to achieve these accuracies each point needs to be surveyed for an extended period. There are a number of other factors which also affected accuracy. The base station was set up and taken down each day, and was located in relatively close proximity to working heavy equipment, resulting in less than ideal conditions to maximize accuracy. The RTK-GPS system was chosen over a total station because its accuracy is similar but it is not affected by adverse weather conditions or changing sight-lines

A grid of survey pins was established prior to the test loading, and they were monitored daily for the duration of the field test. The deformations observed

during the field test were not much greater than the accuracy of the survey equipment, and therefore the results have little value, and may, in some cases be misleading. The results of monitoring the survey pins have not been reported in this document.

The survey equipment was also used to do daily surveys of the placed fill. The equipment was more than adequate for this task, allowing for quick, accurate topographic surveys of the site. These surveys were used to determine volumes, develop cross sections, and locate instrumentation and other details for the drawings.

A 6.4m long tethered aerostat (commonly called a blimp) pictured in Figure 4.14 was used to suspend a remotely operated high resolution digital camera over the site. The aerostat was used on days when wind conditions permitted. The aerostat was helium filled, and flown at 30m or less above the site. The pictures provide a valuable and unique documentation of the project's progress.

## 4.7 Ongoing monitoring

The instrumentation and monitoring program was developed with a focus on the field test, and although long term monitoring of the site was not a primary objective of the project, periodic monitoring since the completion of the test loading has provided some valuable observations. The unloading, bank restoration and ice flows have damaged or destroyed some instruments:

- SI-9 and 12 were destroyed by ice flows in the spring of 2008.

- SI-2 was abandoned during the restoration of the site because it was situated in the middle of the work area.
- SI-1 was destroyed by vandals. Piezometers A, B, C, E, and F were damaged when the excavator snagged the cables while removing the fill following the field test.
- SI-10 was decommissioned in accordance with the University of Manitoba's restoration plan submitted to The Department of Fisheries and Oceans. The casing was cut off below the ground level, and was backfilled with bentonite.

SI casings 4,6,7,8, and 11 and VW-D are still operational. The remaining SI casings have been cut-off so that they are near the ground surface and less susceptible to damage by ice or vandals.

The data-logger was removed from the site at the end of the field test to be re-used on other projects at the University of Manitoba.

Table 4.1. Instrumentation types

| Label | Installation | Measurement | Monitoring |
|---|---|---|---|
| SI | Slope inclinometer | Horizontal deformation | Slope inclinometer probe, manual |
| IPI | In-place inclinometer | Horizontal deformation | In-place inclinometer sensor, data logger |
| VW | Vibrating wire piezometer | Porewater pressure | Vibrating wire readout, manual or data logger |
| PZ | Standpipe piezometer | Standing head | Water level meter, manual |

Table 4.2. Piezometer installations.

| Testhole | Installation | Method | Location | Piezometer Elevation (m) | Ground Elevation (m) |
|---|---|---|---|---|---|
| 2 | PZ-2 | Solid stem | Upper slope | 215.40 | 229.46 |
| 3 | VW-A | Hollow stem | Upper slope | 218.65 | 229.62 |
| 3 | VW-B | Hollow stem | Upper slope | 222.29 | 229.62 |
| 3 | VW-C | Hollow stem | Upper slope | 226.56 | 229.62 |
| 7 | PZ-7 | Cased | Upper row | well | 225.52 |
| 8 | VW-D | Solid stem | Between rows | 219.61 | 225.40 |
| 13 | VW-E | Push-in | Beneath fill | 219.70 | 225.79 |
| 14 | VW-F | Push-in | Beneath fill | 222.16 | 225.81 |

Table 4.3. Slope inclinometer installations.

| Testhole | Installation | Method | Location | Ground (m) | Bottom Reading (m) | Orientation Correction (°) |
|---|---|---|---|---|---|---|
| 1 | SI-1 | Solid stem | Crest | 232.01 | 215.30 | 6.80 |
| 2 | SI-2 | Solid stem | Upper slope | 229.46 | 215.27 | 10.80 |
| 4 | SI-4 | Solid stem | Mid-slope | 225.65 | 211.95 | 28.80 |
| 5 | SI-5 | Solid stem | Outside test | 231.86 | 212.16 | 18.80 |
| 6 | SI-6 | Direct | Upper row | - | 218.30 | -4.20 |
| 7 | SI-7 | Cased | Upper row | 225.52 | 216.69 | 5.80 |
| 8 | SI-8, IPI-8 | Solid stem | Between rows | 225.40 | 214.28 | 4.80 |
| 9 | SI-9, IPI-9 | Cased | Lower row | - | 217.61 | -1.20 |
| 10 | SI-10 | Solid stem | Lower slope | 223.47 | 213.87 | -1.20 |
| 11 | SI-11 | Solid stem | Downstream mid-slope | 225.38 | 215.32 | -30.20 |
| 12 | SI-12 | Solid stem | Upstream mid-slope | 225.57 | 212.86 | -32.20 |

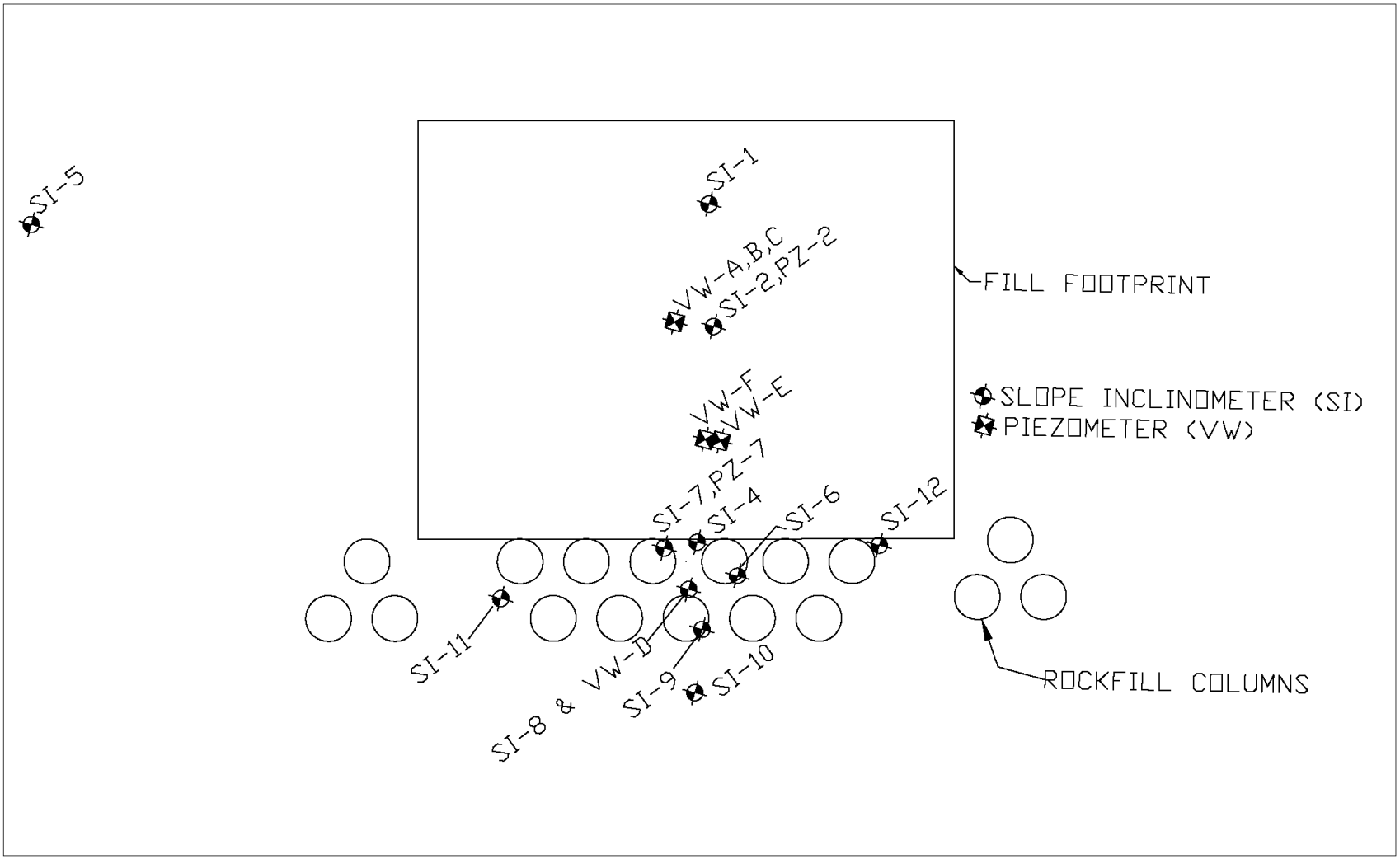


Figure 4.1. Instrumentation layout at the research test site. See Figure 3.9 for a more detailed site layout.

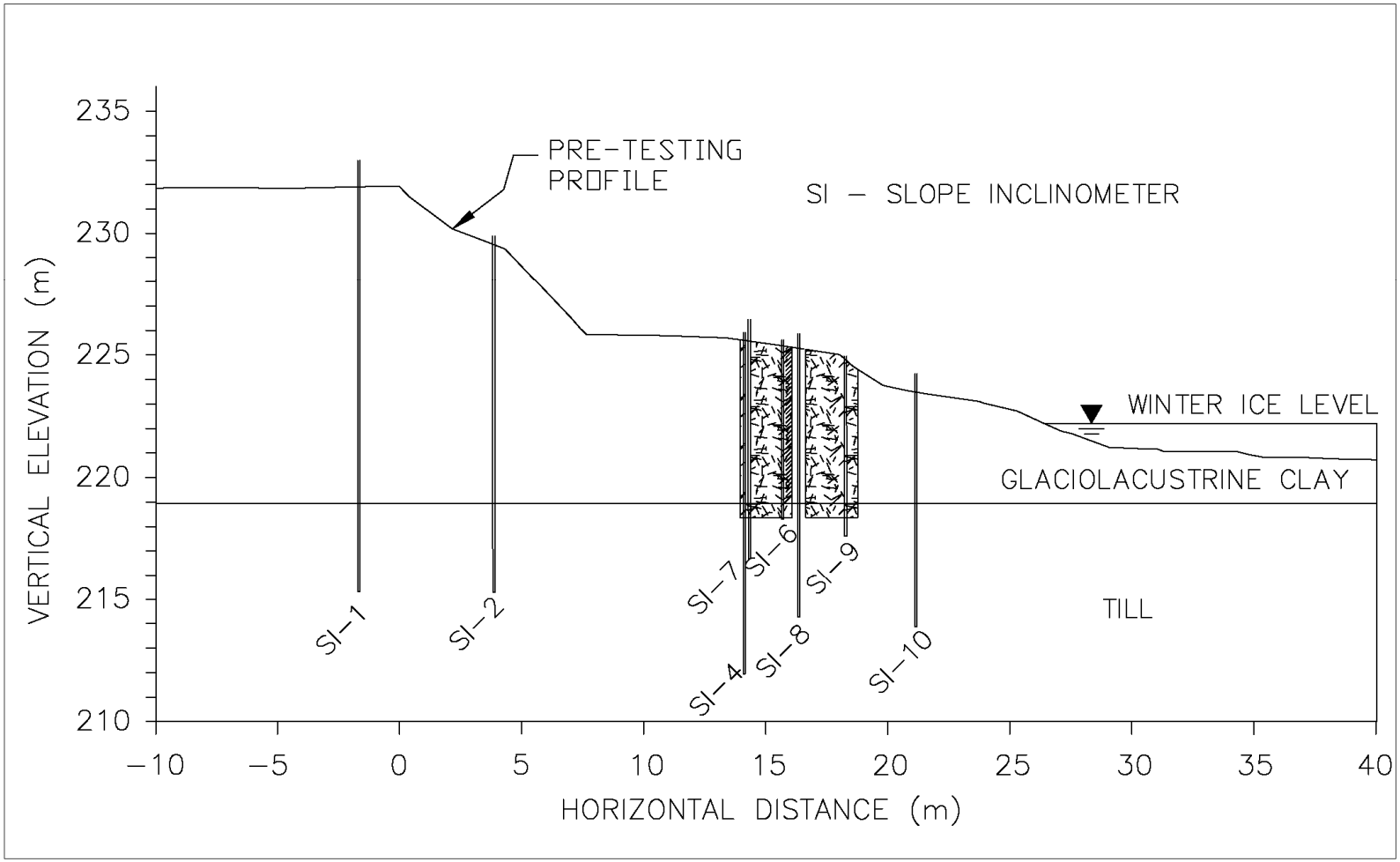


Figure 4.2 Instrumentation cross section with slope inclinometer installations.

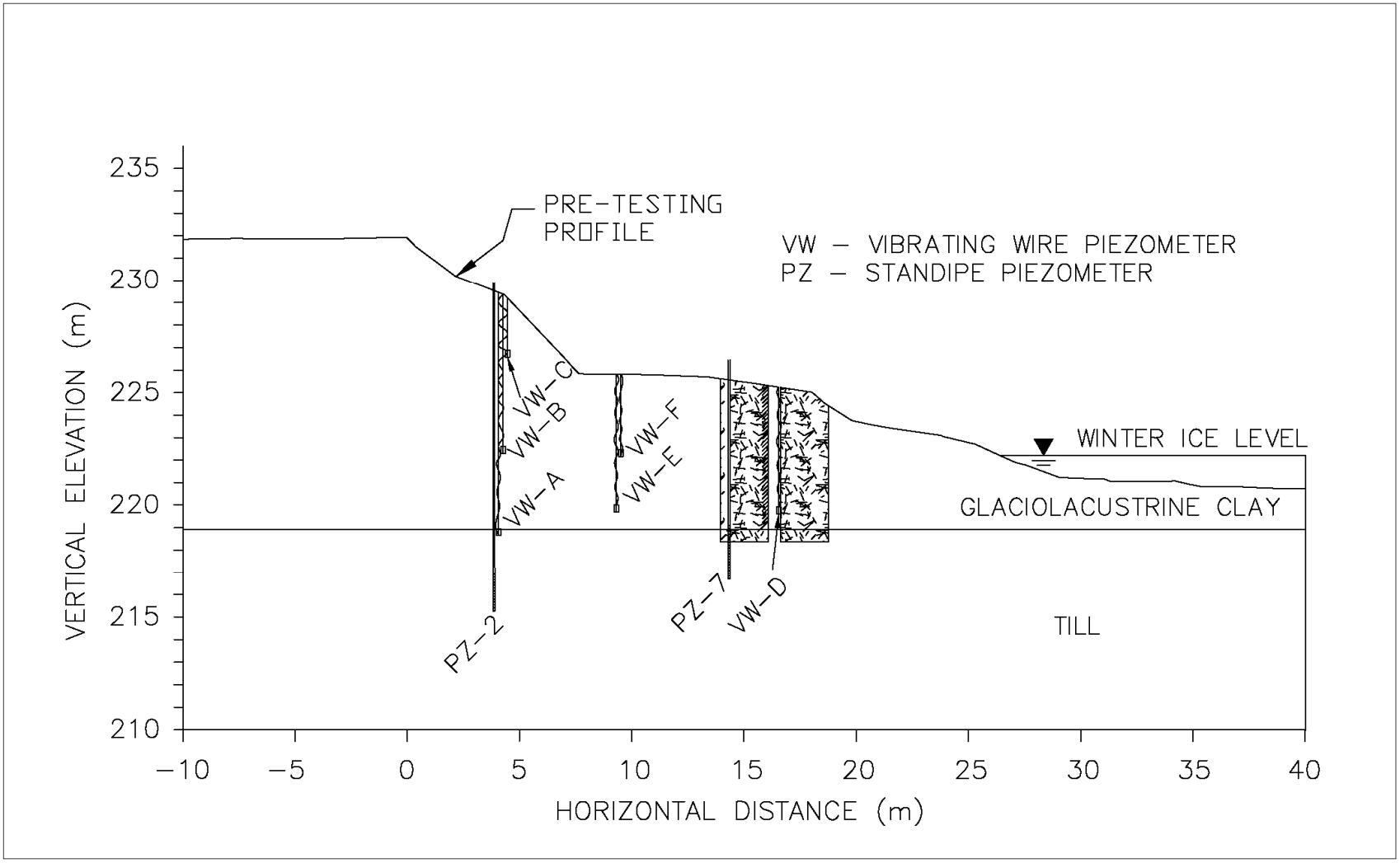


Figure 4.3. Instrumentation cross section with piezometer installations.

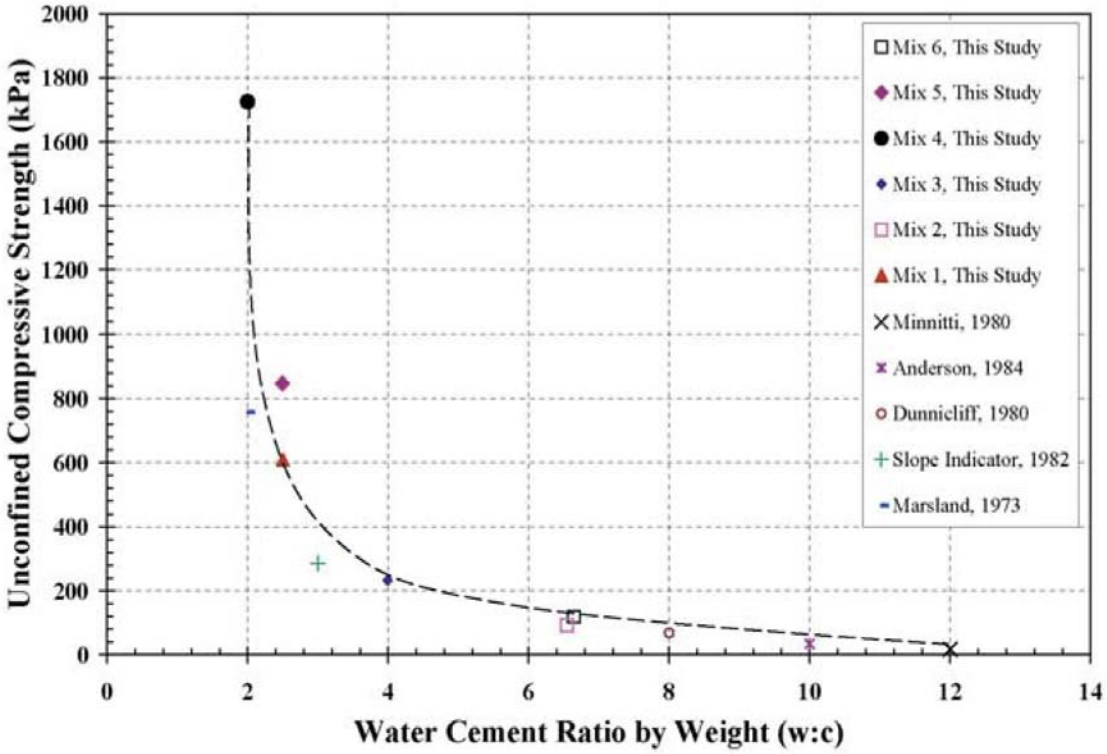


Figure 4.4. Required water:cement ratio to achieve a desired unconfined compresseive strength for cement-bentonie grout. After Contreras et al. (2008).

Reproduced with permission from Contreras, January 2010.

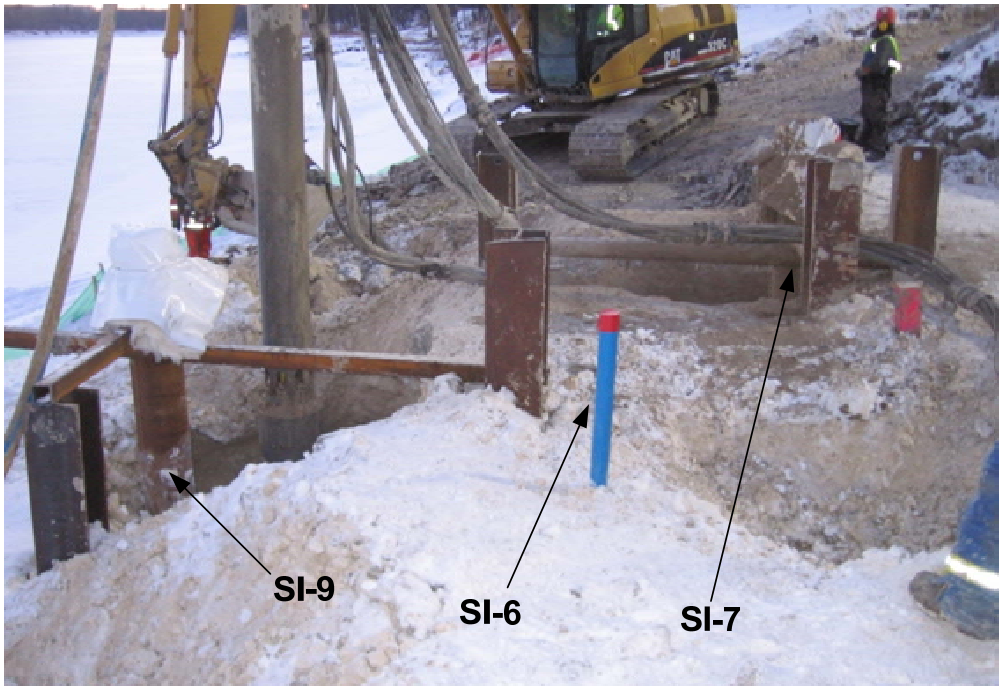


Figure 4.5. Compacting around SI-9, installed directly into a rockfill column

Figure 4.6. Installing a string of in-place inclinometers in SI-9.

Figure 4.7. Late night monitoring of slope inclinometers.

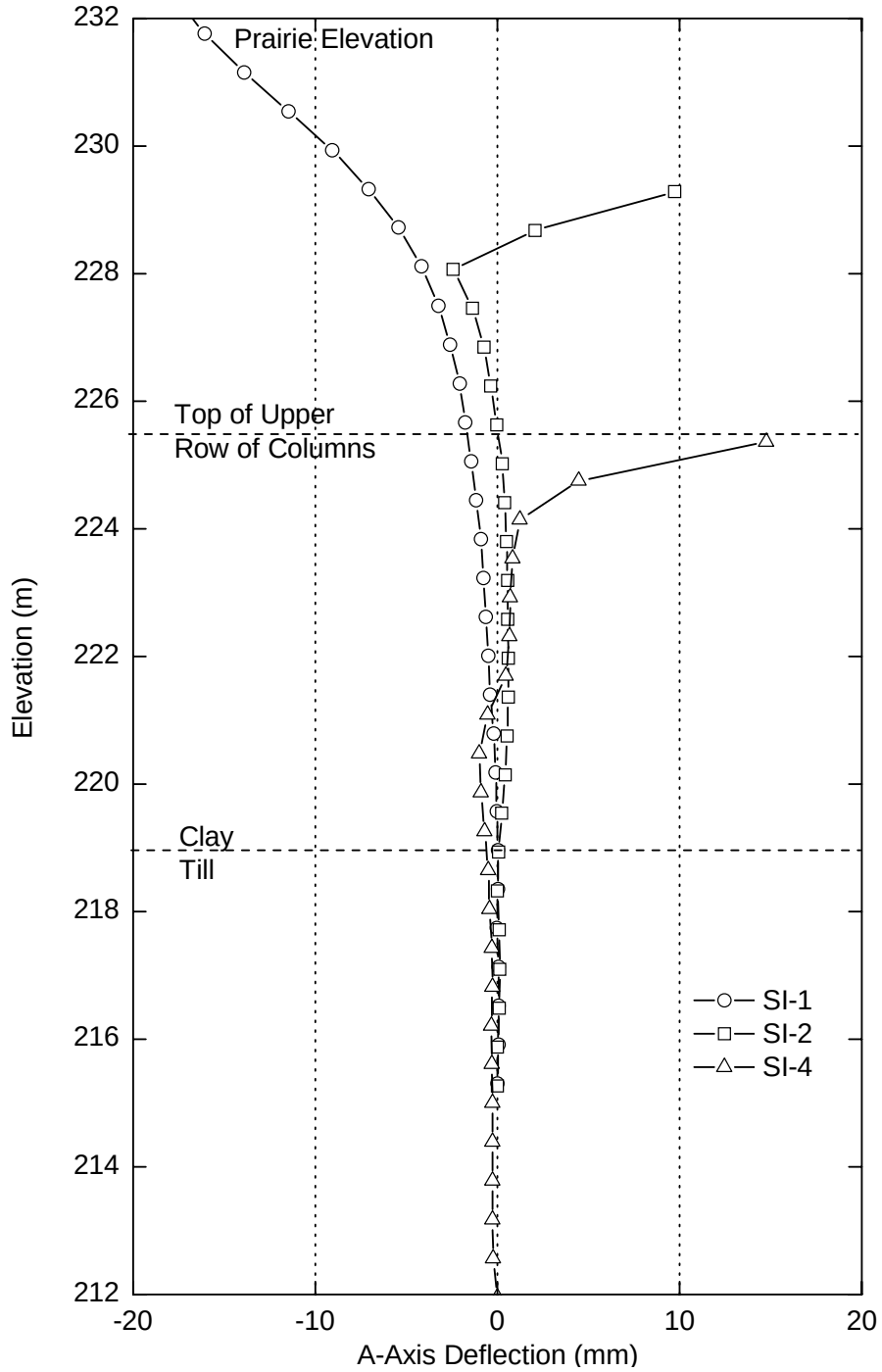


Figure 4.8. Measured Phase I slope deformations in the A-direction prior to column installation. August 2006-November 2007.

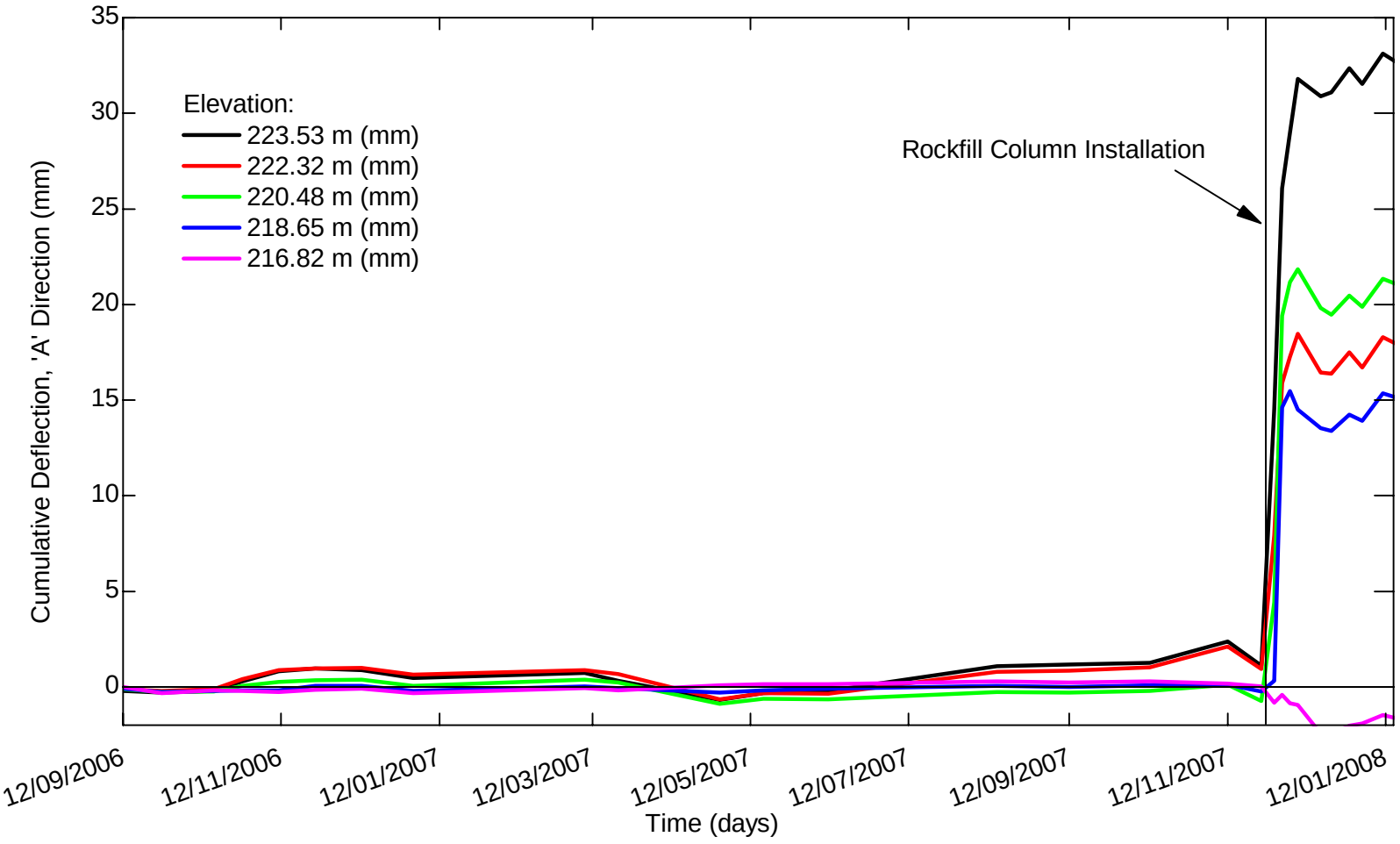


Figure 4.9. Time vs. displacement for SI-4, from the time of installation to the beginning of the test loading.

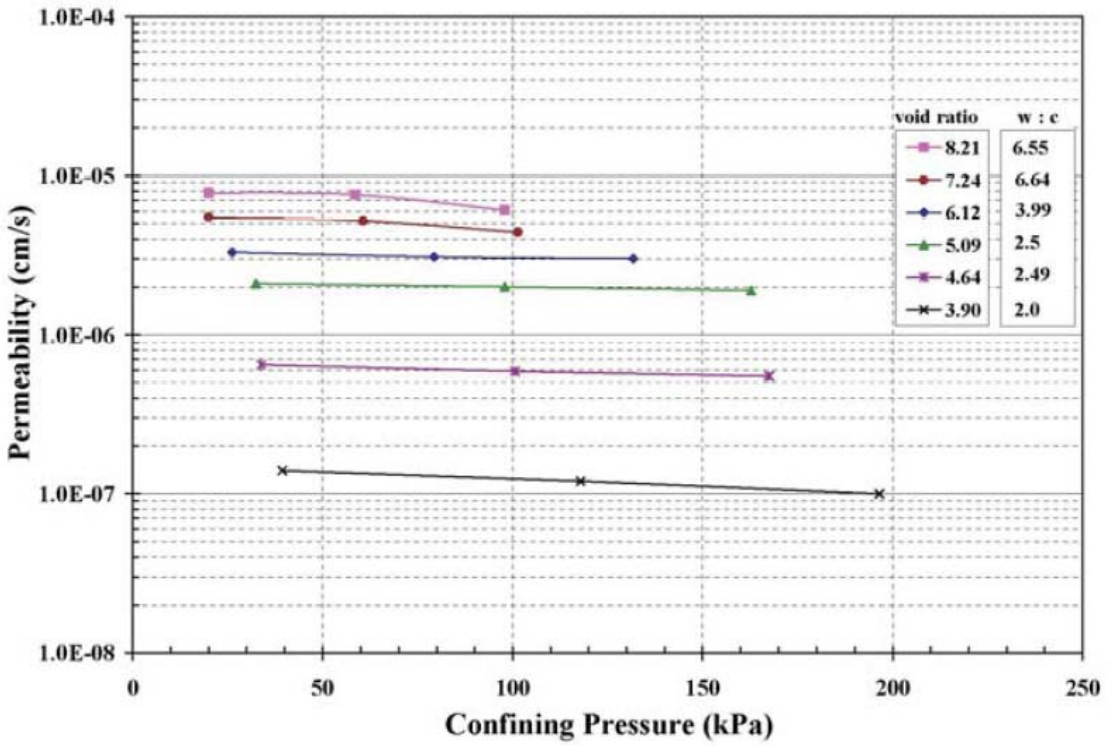


Figure 4.10. Recommended water:cement ratios for grout used for backfillling piezometers. After Contreras et al. (2008). Reproduced with permission from Contreras, January 2010.

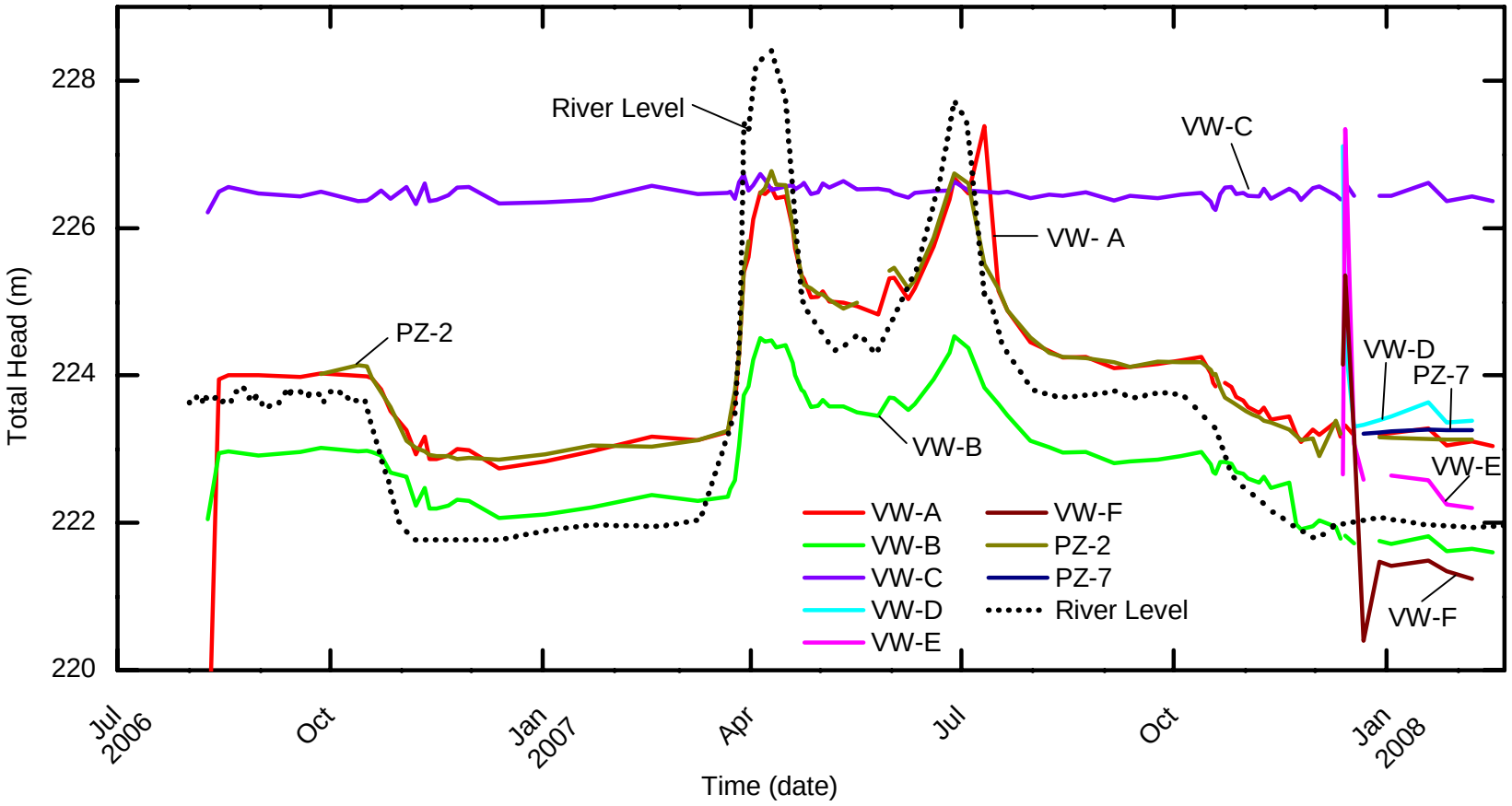


Figure 4.11 River levels and total heads measured at test site prior to field test (Aug 2006 to February 2008)

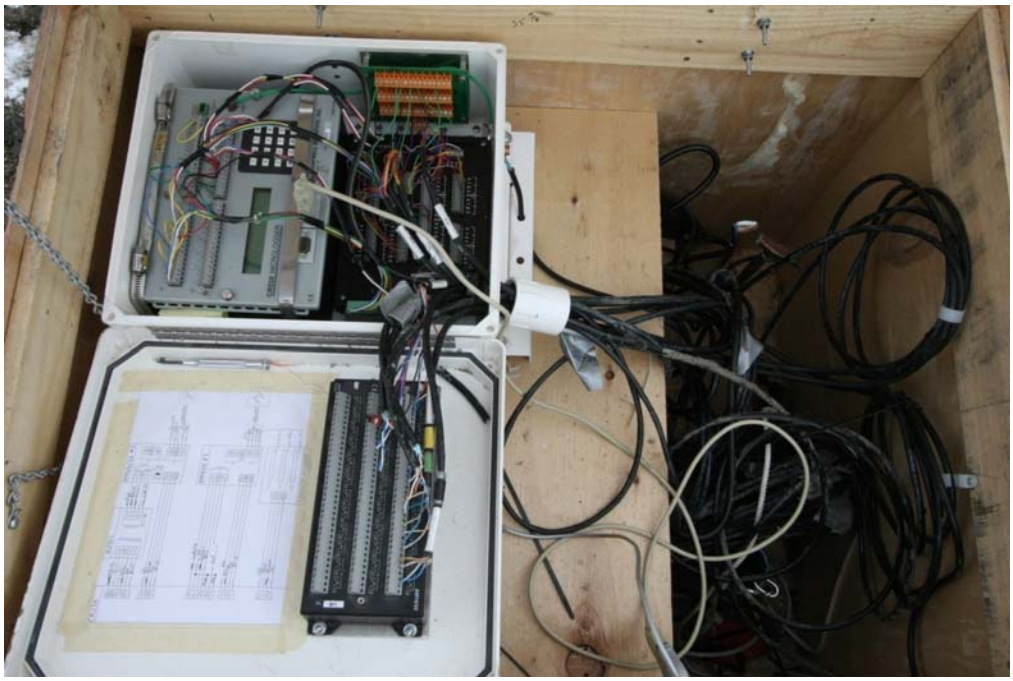

Figure 4.12. Data logger and peripherals in protective box

.

Figure 4.13. Protecting instrumentation cables prior to test loading a) PZ-E and F facing the river b) beneath the fill footprint.

Figure 4.14. Tethered aerostat at research site.

# 5. FIELD TESTING PROGRAM

This chapter discusses the execution of a full-scale test of a riverbank section stabilized with rockfill columns, including the design, construction and test loading. The highlight of this research project was the eleven days when the riverbank was being loaded, but the preparations for this event were critical to ensuring that the experiment would provide the data needed to advance the research.

The field test was designed and managed by the author, with guidance from academic advisors and the project steering committee. The author was involved in all aspects of the project even though the construction activities were carried out by a project sponsor and contractor, Subterranean (Manitoba) Ltd..

## 5.1 Design

The design objective for the field test was to produce an experiment that would load a “typically” reinforced riverbank, causing measurable stress and deformation responses to be measured. Analysis of the measured responses would lead to an improved understanding of the underlying physical mechanisms developed in the reinforcement materials. The design for the field test balanced the need for controlled test conditions, while ensuring that the test reflected conditions of a typical rockfill column application. The constraints of the test site, the budget and the schedule all influenced the design and implementation of the test loading. The purpose of the field test was to study the deformation

behaviour of a reinforced riverbank. Nonetheless, the possibility of catastrophic failure during the testing process was considered.

The test conditions differed somewhat from many commercial rockfill column applications in a number of ways. Most rockfill column applications in Manitoba are on sites where slow moving slide masses exist, and no major additional surcharge load is applied following construction; after construction, porewater pressure fluctuations and toe erosion lead to stress changes in the reinforced slope. The slope that was reinforced for this research project was not showing evidence of global instability. The testing then involved loading it rapidly with a large surcharge weight.

The riverbank at the research site was reinforced with two rows of columns spaced at 3.1 m center to center, using a triangular spacing as shown in Figure 5.1. The columns were 2.13 m (7') in diameter, thus resulting in an edge-to-edge spacing of 0.97 m. These rockfill column dimensions are similar to those commonly used on riverbank stabilization projects in Winnipeg. This layout is equivalent to a 2.3 m equivalent shear key (as defined in Chapter 2) or two 1.15 m shear keys.

The column layout at the test site is shown in Figure 3.9. A total of 17 columns were installed, although the central 11 columns were the focus of the test. The three columns installed upstream and downstream of the void columns (discussed in Section 5.13) provide additional stabilization for the slope outside of the test section by passively restricting deformations to the area between the

rows of void columns. These additional columns also contribute to the long term stability of this portion of the riverbank.

Table 5.1 shows some of the results from the stability analysis, which investigated the expected improvement provided by the rockfill columns. The cross-section used for stability modeling is shown in Figure 5.2. Reinforcement of the slope increased the factor of safety by 0.43 assuming a rockfill friction angle of 64° (as measured by Abdul Razaq (2007)). For the same analysis with a rockfill friction angle of 50° a factor of safety increase of 0.23 was predicted. This stability analysis was done using the finite element method with Slope/W from GeoSlope International Ltd. Slope stability analysis methods and results will be discussed in more detail in Chapter 7.

Existing projects using rockfill columns have used up to 6 or more rows of columns. The number of required rows depends on the site geometry, in-situ soil strength, porewater pressure conditions, desired factor of safety increase, and assumed rockfill properties.

### 5.1.1 Rockfill material

The specified material for backfilling the columns was a crushed limestone with a 150 mm maximum grain size. This material is available locally and is similar to the rockfill typically specified for projects in the Winnipeg area. The rockfill was supplied by Inland Aggregates Limited. (2494 Ferrier St. Winnipeg, MB.)

Rockfill material was delivered by end-dump semi-trailers to site where it was temporarily stockpiled until it was used to backfill the columns. The stockpile never exceeded the volume required for backfilling two columns. Delivery tickets were collected for each load as an accounting measure to record the total mass of delivered material.

### 5.1.2 Column layout

The rockfill columns were installed upslope of the regulated normal summer river level. This decision was made to help satisfy the requirements of the Department of Fisheries and Oceans. The rows of columns were set to be parallel to a line tangential to the critical points of the regulated summer shoreline. Rockfill columns on commercial projects have often been installed between the regulated summer water level and the winter ice level.

The location of the columns was established prior to drilling and again before the compaction process was started. Most layout work was done by chain, but was also aided by a total station.

### 5.1.3 Void columns

A concern in designing the full-scale field test was how to best conduct an experiment that could be reasonably modeled as a 2-dimensional plane-strain problem. The available width for the test section was 19 m, which was similar to the distance from the crest to the base of the columns. Ideally, the test would have been carried out over a much longer length of riverbank, but this was not

possible, given the site conditions. A larger test section would also have had proportionally larger costs associated with the construction and test loading.

A way of minimizing the edge effects, and improving the plane-strain assumptions was to reduce the resistance to shearing of the lateral edges of the test section. The option that was finally implemented involved drilling relatively closely spaced "void columns" along the lateral edges of the test section. Sixteen, 483 mm diameter void columns were drilled along each edge of the test section as shown in Figure 3.9 and Figure 5.3.

The center to center spacing between borings was 900 mm. The columns create "perforations" along the edges of the test section, providing a preferential path for shearing, by reducing the net shear resistance. The theory is that deformations will concentrate along this zone, because of the low resistance. Ideally the test section could have been bounded by frictionless surfaces, which would still have proved full confining pressures parallel to the riverbank. It is estimated that the void columns reduced the total edge shear resistance by 25% for the slide mass discussed in Section 5.1:

- The modified portion of the total slide mass cross section was 47% (that is 82 $m^2$ ÷ 175 $m^2$)
- The cross-sectional surface area reduction is 54% (that is 483 mm ÷ 900 mm) in the modified zone, where the void column diameter is 483 mm and the centre to centre spacing is 900 mm.
- The total reduction in shear resistance is 0.54 * 0.47 = 0.25 (or 25%)

Even though the void columns did not completely resolve the issue of shear resistance along the edge of the test section, they did help to improve the assumptions of plane-strain analysis.

In addition to being a safety concern, the void columns did have other drawbacks. By removing soil along the edge of the test section, it did allow for some relatively minor deformations perpendicular to the axis of the test section (parallel to the riverbank). Figure 5.4 shows the B-direction (parallel to the riverbank) displacements measured in SI-11 and SI-12 along the downstream and upstream edges of the test section. Both inclinometers showed movement outward from the centerline of the test section, with the largest strains occurring near the base of the void columns, near the clay till interface.

## 5.2 Logistics

Undertaking this large field test in a public, urban and environmentally sensitive area required some regulatory approvals and added care and consideration when doing site work. An information package was submitted to the Department of Fisheries and Oceans Canada (DFO) in October, 2007, and a Letter of Advice was issued by DFO in November, 2007, prior to the start of the site works.

A Waterways Permit was obtained from the City of Winnipeg's Waterways Engineer. A Use of Streets Permit was also required. The City of Winnipeg Public Works Department, and specifically the Parks Services provided the site

to do the test, and they were also involved in the final rehabilitation and restoration.

The author arranged and supervised the geotechnical site investigation, including the test hole drilling and sampling. Paddock Drilling Ltd. was contracted to provide the drilling services, and Glenat Enterprises Inc. did a small amount of re-grading work to provide access to the lower slope for the geotechnical drill rig.

The main construction activities were managed by Subterranean (Manitoba) Ltd. They provided the equipment, materials and labour required for preparing the site, constructing the columns, test loading the bank and doing the rough re-grading after the completion of the testing.

The University of Manitoba contracted McEwen Bros. Ltd. to do the final restoration work. This work included doing final landscaping, soil amendments and establishing riparian vegetation.

Members of the media and community had a number of opportunities to learn about the project. An open house was hosted in the community in July 2006, prior to the initial site investigation. A media and public information session and site tour was held during the field testing in February 2008. A final media event involving some local students was held in September 2009, highlighting the site restoration work.

## 5.3 Scheduling

The on-site components of this project can be divided into four major phases as illustrated by Figure 1.4 in Chapter 1. The construction of the rockfill columns and installation of the Phase 2 instrumentation took place between November 19 and December 13, 2007. The Phase 3 test loading started on February 21, 2008 with the final load being placed on February 29, 2008. The unloading of the slope began on March 3, and was completed on March 5, 2008. The re-grading started on March 5, 2008 and was complete on March 20, 2008.

Scheduling activities for this project presented a number of challenges, and required some compromises. Some of the scheduling constraints included weather, river levels, permitting, funding availability, and contractor availability.

Column installation was scheduled for the latter part of November 2007 in anticipation of some frost penetration to help with equipment movement on the soft soils of the lower bank area. This timing also followed the annual drawdown of the water level in the Red River to the winter ice level. The low water level provided a larger work area, and reduced concerns of negatively impacting water quality and fish habitat by accidentally damaging the river bottom or introducing deleterious materials.

The field test was scheduled to maximize the monitoring period between installation and test loading, while still allowing for the field test and subsequent site clean-up to be completed before the expected spring freshet which typically arrives in the latter part of March.

The adopted schedule had some drawbacks. Firstly, the monitoring period between installation and testing was limited. Results that will be discussed in the following pages show that rate of post construction movements did slow significantly, but did not stop completely. There would have been some benefit to monitoring the reinforced slope through the annual fluctuations in groundwater conditions, before starting the test loading, but this was not possible.

Secondly, the ground conditions during the winter test loading were not optimal. There was potential for the frozen ground and river to influence the deformations, but mitigating measures are believed to have been effective. The test loading was also done while porewater pressures were at their annual low. Higher porewater pressure conditions would have resulted in a more pronounced response to loading, assuming that the soil would behave in a non-linear manner.

## 5.4 Construction

### 5.4.1 Installation of rockfill columns

The process of installing the rockfill columns involved:

- Site preparation
    - Build an access ramp to the lower slope.
    - Cut/fill a working bench on the lower slope.
- Construct columns
    - Drill the column 1(+) m into till or until practical refusal.

    - Backfill the column with crushed rockfill to the surface.

- Compaction
    - Charge the column with water.
    - Advance the vibrolance to base of column, driven by self weight and aided by jetted air.
    - Retract vibrolance in 0.6 m increments from base to surface, pausing at each depth for 2 minutes while continuing vibration.
    - Add additional loose rockfill in measured amounts during compaction
- Top off the column with rockfill to the level of the construction bench

The drill rig used for this project, pictured in Figure 5.5, was a crawler mounted SoilMec R516-HD with a telescopic Kelly bar. The rig was outfitted with a 84" (2.13 m) diameter auger. The R516-HD has a maximum torque of 180 kN·m, a maximum drilling speed of 30 rpm and 230 kW of engine power. The nominal weight of the machine is 54 tonnes.

Installation of the rockfill columns took place between November 27 and December 3, 2007. Three to five columns were installed each day. The supply of rockfill material was the critical limitation with respect to productivity. In total, 45 end-dump, dual axle, semi-trailer loads of limestone rockfill were delivered to site for the backfilling of the columns. Backfilling was done with a Caterpillar 320CL excavator outfitted with a $1m^3$ swivelling bucket.

Each column was backfilled before the drilling began for the next column because the limited work area restricted the movement of the large equipment. Having multiple holes open also increases the possibility of slope instability, and local instability between columns. There was some concern that the intact soil remaining between columns could fail at depth, allowing rockfill material from one column to displace into a neighbouring column that had not yet been backfilled. This was not observed during the project.

Drilling progress was monitored and observations of till contact depth, and final depth were recorded for each column. These measurements were done by hand with a tape, and were later tied-in with a survey to determine elevations.

When drilling through the loose till, sloughing can occur, thus increasing the column volume. Sloughing of soft or loose soils can lead to “blowout” of rockfill material from a backfilled rockfill column into an open column, before backfill has been completed. This presents a safety risk and also compromises the independent nature of the columns.

Six of the columns were terminated upon refusal on a large boulder or when significant sloughing began to occur at depth. The rest of the columns were terminated after penetrating 1 m into the loose till (as characterized in Chapter 3). It would have been preferable to extend the rockfill columns into the dense till layer, but that would have been more expensive and time consuming, while increasing the risk of sloughing.

### 5.4.2 Compaction

Compaction or the rockfill columns was accomplished using a 9.4 m long vibratory lance suspended by a crane. Figure 5.6 shows the lance and crane setup. A Manitowoc model 222 crawler crane was employed for this project. It has a 91 tonne (100ton) capacity and a 45.7m boom.

A Vibrolance 400 HL, manufactured by PTC was used for compaction. It was powered by a model V-400 hydraulic power pack, also from PTC. The power pack had an engine rating of 246 kW, produced 400 l/min of flow, and had a maximum hydraulic working pressure of 350bars. The maximum power of the Vibrolance was 235 kW, at a maximum frequency of 30 Hz.

The crane was set up on a pad built on the access ramp from where it could reach all 17 columns. The rockfill columns were charged with water prior to compaction to improve the densification of the crushed limestone. The vibrolance also advances more easily through saturated rockfill. Air was jetted through the tip of the lance at a high rate while dropping the lance through the backfilled column; however the air flow was decreased while incrementally retracting the lance. (per. comm. White 2007)[1]

The rockfill columns at the research site were compacted using the standard procedure used locally. Compaction was done in 0.6 m lifts, with the lance pausing for 2 minutes at each depth while maintaining the vibration. The

[1] Personal communication with Don White, Subterranean (Manitoba) Ltd.. Winnipeg Manitoba. November 2007.

compaction effort was monitored by watching the hydraulic pressure. Figure 5.7 is sample printout from the vibrolance controller. The figure plots the hydraulic pressure and depth versus time.

The compaction effort increased the in-situ bulk unit weight from an estimated 18.5 kN/$m^3$ to 22.5 kN/$m^3$. The dry unit weight, assuming a moisture content of 4.3% (Section 3.5.7.2) would be 21.6 kN/$m^3$. The unit weight calculations are based on the known weight of delivered rock, and loose placed volume (the volume of the remaining unused rockfill was estimated). The drop of the top of the rockfill in the drilled hole, due to compaction, was measured. The compacted unit weight could then be calculated, knowing the initial (loose) density of the rockfill. Based on local experience and the testing and literature cited in Chapter 2, it is assumed that there is negligible displacement of rockfill into the surrounding clay and till.

During the compaction of the columns, loose silt till material “blew up” into the two temporary steel pipes used for installing the inclinometer for SI-7 and SI-9 casings (Section 4.3.1), with 2.3 m of till at SI-7 and 1.28 m at SI-9. Presumably, the vibration during compaction liquefied the saturated loose till causing it to flow upwards into the steel pipes. The till materials that blew up into steel pipes were drilled out with augers to permit installation of the inclinometers. The re-drilling provided the additional benefit of allowing the inclinometer casings to extend below the base of the rockfill column by continuing the hollow stem auger boring below the depth of the steel pipes.

### 5.4.3 Post-construction monitoring

The site was monitored after the construction of the columns, with a special interest in deformations associated with the installation of the rockfill columns. The deflection profiles in Figure 5.8 show the slope movement between October 2007 and February 2008. Positive (+) A-axis displacements are in the downslope direction. These profiles include the cumulative displacements which occurred during construction and in the 70 days following the construction of the columns. The deflections of SI-4 were greater than for SI-1 and SI-2 because of its close proximity to the rockfill columns (and drilling and compacting).

Slope inclinometers SI-6 to SI-12 were installed during or immediately after the column installation and were monitored a number of times prior to the start of the test loading. The deformations versus time at select elevations for SI-4, 7, 8 and 10 are plotted in Figure 5.9.

These results show that the construction related deformations had not ceased, but they do show a slight tendency towards a decreasing rate of deformation at some points, with SI-7 being the exception. Monitoring data from during and after the field test will be discussed in the following chapters.

## 5.5 Test Loading

The procedure for test loading the slope consisted of placing a series of lifts of fill material upslope of the rockfill columns. A total of 1930 tonnes of 50 mm clean limestone gravel was placed as the fill material. The material was delivered over

a period of nine days, and the final load was left in place for an additional three days. Each daily lift had a mass ranging from 240 to 430 tonnes. A detailed discussion of the monitoring program was discussed in Chapter 4 and testing results are presented in Chapter 6.

The impact of frozen ground was a concern because the engineering properties of clay change greatly when the soil is near saturation and frozen. The depth of the frost was measured at various locations prior to the test loading. Along the rows of void columns, the frost depth varied from 0.3 to 0.75 m, with an average thickness of 0.4 m. Along the top of the slope, the frost depth varied from 0.3 to 0.9 m. The frozen layer was ripped in a continuous line about 3 m back from the crest before the test loading. Numerical models suggested that this was one of the places where it had the most potential to influence the test. The void columns also reduced the influence of frozen ground along the lateral edges of the test section. The frozen ground was not expected to have much of an influence because of the high area replacement ratio of the columns in the area of the rockfill columns. Freezing conditions had little effect on the performance of the rockfill columns themselves because the rockfill was not saturated near the surface. A south facing slope and significant snow cover both helped limit the depth of the frost.

### 5.5.1 Schedule

Through the rest of the document, “time” during the test loading will be referenced to the placement of the first load of fill material. The first load of fill

was delivered at 08:00, February 21, 2008 at time 0.0 d (days). The final load was placed at 12:34, February 29, 2008 at time 8.19 d. Unloading of the slope began at 11.0 d and was completed at 13.1 d. Figure 5.10 plots the cumulative mass of the placed fill against time.

Loads were placed on days 1, 2, 5, 7, 8 and 9. The two-day break on days 3 and 4 was planned and served two purposes. The break provided a schedule buffer in case the start of the loading was delayed. The break also provided an opportunity to monitor the time dependent responses of deformation and porewater pressure to loading at a stress level that was not expected to be near the peak capacity of the system. Day 6, Tuesday February 26, 2008 was scheduled to be another loading day, but an external circumstance meant that fill could not be delivered for that day.

The daily routine during the field test included the following tasks, (not necessarily in order):

- Monitor slope indicators before 08:00, between rounds of fill and after final round of fill.
- Delivery and placement of loading fill.
    - Truck scale tickets were collected.
    - Time of placement for each load was recorded.
- Photograph site.
- Fly aerostat and take aerial photos if conditions permitted.

- Download and reduce IPI and piezometer data.
- Survey fill and monitoring pins with RTK-GPS.

### 5.5.2 Load placement

Figure 5.11 through Figure 5.18 show the site throughout the test loading program. A number of the photos have equipment or people on them to provide a sense of scale.

The surcharge fill material was purchased from Mulder Construction and Materials Ltd, and delivered and placed by Subterranean (Manitoba) Ltd.. The contractor chose clean 50 mm crushed limestone material instead of clay because it would not require compaction, it would be easy to remove, and it's high frictional properties made the fill pile more stable.

The material was delivered by end-dump tandem axle semi trailers. The material was dumped at the top of the access ramp, and pushed into place with a bulldozer. Final placement was done with a 24 tonne tracked excavator. The load pile was built up with the slope sitting at the natural angle of repose, ranging between 36° and 40°. The final height of the fill embankment was 10.0 m, measured from the working pad and reached 3.5 m above natural prairie elevation to 235.5 m ASL. The natural angle of repose of the limestone fill material is very similar to the transition friction angle of 37°, estimated by Abdul-Razaq (2007).

The fill material was delivered in two rounds per day. The first round arrived at 08:00 and took approximately 2 hours to place. The second round was delivered around 12:00. The break between delivery rounds was used to complete another set of monitoring, providing an interim data point.

The large volume of the fill required the footprint of the fill to extend outside of the 19 m wide test section. Daily surveys were used to create surfaces in a CAD program for each day of loading. Volumes and weight distributions were then calculated from the surface information. It is estimated that 1751 of the 1930 tonnes (that is, 91% of the total load) was concentrated within the test section between the two rows of void columns. The slope also supported the 25 tonne weight of the excavator and 22 tonnes of "Jersey Barriers." In total the slope was loaded with 94.6 tonnes (928 kN) per lineal meter of the 19 m long test section. Table 5.2 lists the weight of the fill materials and dimensions of the fill pile by day.

The concrete Jersey Barrier wall was setup immediately upslope of the upper row of rockfill columns. This barrier acted (unintentionally) as a retaining structure for the fill pile and also protected people working on the instrumentation from small rocks rolling down the surface of the fill pile.

A rough calculation of the as-placed density of the fill was determined to be 16.7 kN/m$^3$. This was calculated using a mechanical scale, and buckets of a known volume. The buckets were shaken to increase density. The density of the load fill was also calculated from the surveyed volume of the pile and the total weight of stone delivered. An average density of 15.3 kN/m$^3$ was calculated from

the volume surveys. The placed density is not critical because the regions of fill in the numerical analysis were sized to accurately model mass of the fill and necessarily the density, and therefore this discrepancy has inconsequential impact on the analysis.

### 5.5.3 Termination of the test

Prior to beginning the field test, a list of conditions for termination was established. On day nine, it was decided, with advice from the steering committee, that it was not safe to place additional material at the top of the pile. The pile reached 3.5 m above prairie elevation, and adding additional material vertically would have required a larger footprint, thus limiting the desired loading effect. Analysis also showed that placing additional fill further back from the crest would provide little additional driving force. In retrospect, the use of a denser fill material would have allowed for more weight to be placed safely.

The full final load, minus the excavator, was left in place for three days of monitoring. At that point, it was necessary to remove the fill material and begin site restoration in order to be prepared for the anticipated spring freshet.

### 5.5.4 Load removal and site re-grading

The removal of the load began on March 3, 2006 at 08:00 (day 11.0). The removal rate of the fill material was not tracked as precisely as during the loading stages. The remaining fill volume was surveyed at the conclusion of the work on day 11 and day 12. During the load removal, the excavating equipment

accidently pulled up the HDPE pipe (shown in Figure 5.11), tearing the cables to vibrating wire sensors VW A, B, C, F, and G.

The void columns were backfilled with some of the 50 mm clean limestone which had been used as the loading fill. Each boring was sealed at the bottom with bentonite chips to inhibit the vertical flow of groundwater. As the void columns did not extend into the till, this was not a great concern. Some of the void columns were checked for groundwater intrusion but no groundwater was noted.

On March 10, 2008 re-grading work began at the site. Clay fill was delivered from other construction sites. The clay fill was placed, shaped and lightly compacted with a tracked excavator. The intent of the clay fill and re-grading was to reduce the average slope of the site and eliminate the over-steepened face. The estimated mass of the clay fill used for re-grading was 510 tonnes.

Figure 5.19 shows the site during and after re-grading. It should be noted that the slope above the elevation of the rockfill columns was not reinforced, and has not been designed for long-term stability. Extensive re-grading or additional stabilization of the slope above the rockfill columns was beyond the scope of the project.

## 5.6 Restoration

Funding was provided by the Province of Manitoba's Water Stewardship Fund for restoration of the site. These funds were used to establish native riparian vegetation in the disturbed test area. The City of Winnipeg's Naturalist Services

Branch was involved in the restoration planning and the work was done by a specialty contractor. The restoration work in the test area included the following:

- the slope was protected with a temporary geosynthetic cover during the 2008 spring freshet
- a soil amendment was added to the clay in the restoration area to support plant growth
- the slope was protected with a coconut erosion control blanket to prevent erosion, and maintain soil moisture while the vegetation established itself.
- native riparian trees and shrubs were planted on the slope
- native wheat grass was planted in the upland area where the plant cover had been disturbed by the site works
- the plants were maintained for one growing season.

Over 140 individual plants from thirteen native shrub and tree species were planted on the slope. The vegetation serves to improve the appearance of the site, increase natural bio-diversity and also provide natural stabilization and surface protection (Barker 1986). The site has since been turned over to The City of Winnipeg's Public Works Department.

Table 5.1. Calculated factors of safety for slope at research site (without loading)

| Case | Finite Element Method | | Morgenstern-Price Method | |
|---|---|---|---|---|
| Rockfill Friction Angle (°) | 50 | 64 | 50 | 64 |
| Critical state only[1] | | | | |
| No stabilization | 1.21 | 1.21 | 1.20 | 1.20 |
| With columns (22 kN/m$^3$)[2] | 1.44 | 1.67 | 1.52 | 1.89 |
| With columns (17 kN/m3)[3] | 1.35 | 1.51 | 1.41 | 1.68 |
| Critical state and residual[4] | | | | |
| No stabilization | 1.05 | 1.05 | 1.03 | 1.03 |
| With columns (22 kN/m$^3$) | 1.28[5] | 1.48[5.] | 1.37 | 1.56 |
| With columns (17 kN/m3) | 1.19 | 1.35 | 1.26 | 1.77 |

1. All clay is assigned critical state strength with $\phi$=18 and c=5 kPa.

2. Rockfill unit weight is assumed to be 22 kN/m$^3$

3. Rockfill unit weight is assumed to be 17 kN/m$^3$ to be the same as the surrounding clay. This is conservative assumption.

4. Clay region above till, downslope of columns is assigned residual strength with $\phi$=8.3 kPa.

5. Values used for calculating factor of safety increase.

Table 5.2. Summary of weights and volumes of delivered fill

| Day | Daily load (tonnes) | Cumulative weight (kN) | Footprint[1] ($m^2$) | Volume[1] ($m^3$) | Unit weight[2] ($kN/m^3$) | Bounded volume[1,3] ($m^3$) | Bounded weight[1,3] (kN) |
|---|---|---|---|---|---|---|---|
| 1 | 434 | 4260 | 210 | 301 | 14.1 | 263 | 3710 |
| 2 | 338 | 7580 | 304 | 540 | 14.0 | 479 | 6720 |
| 5 | 239 | 9920 | 334 | 677 | 14.6 | 598 | 8750 |
| 7 | 336 | 13210 | 380 | 848 | 15.6 | 759 | 11820 |
| 8 | 292 | 16070 | 413 | 1079 | 14.9 | 969 | 14430 |
| 9 | 292 | 18930 | 468 | 1238 | 15.3 | 1123 | 17170 |

Based on daily volume surveys of the fill pile.

Calculated from cumulative weight and volume measurements.

Calculated as the fill volume sitting between the rows of void columns

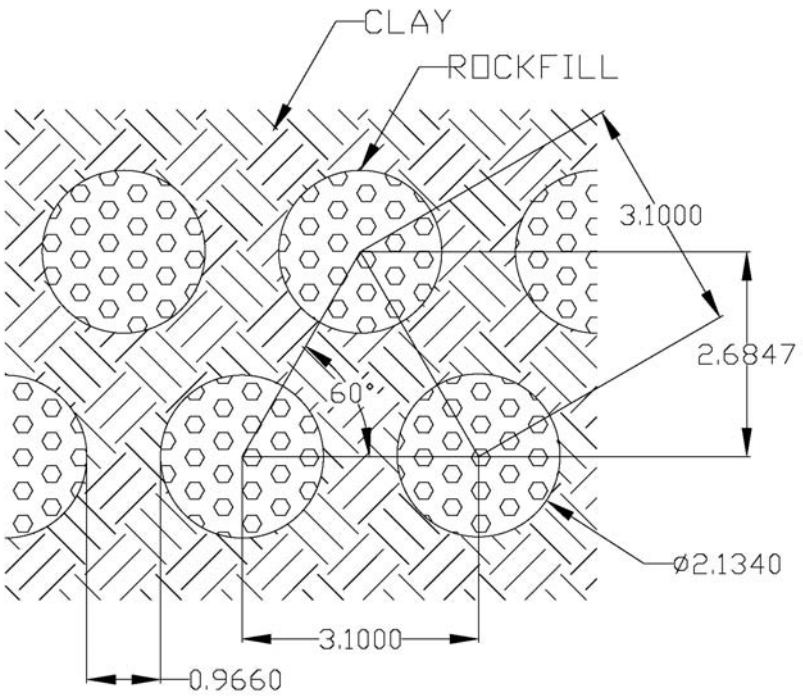


Figure 5.1. Rockfill column layout detail.

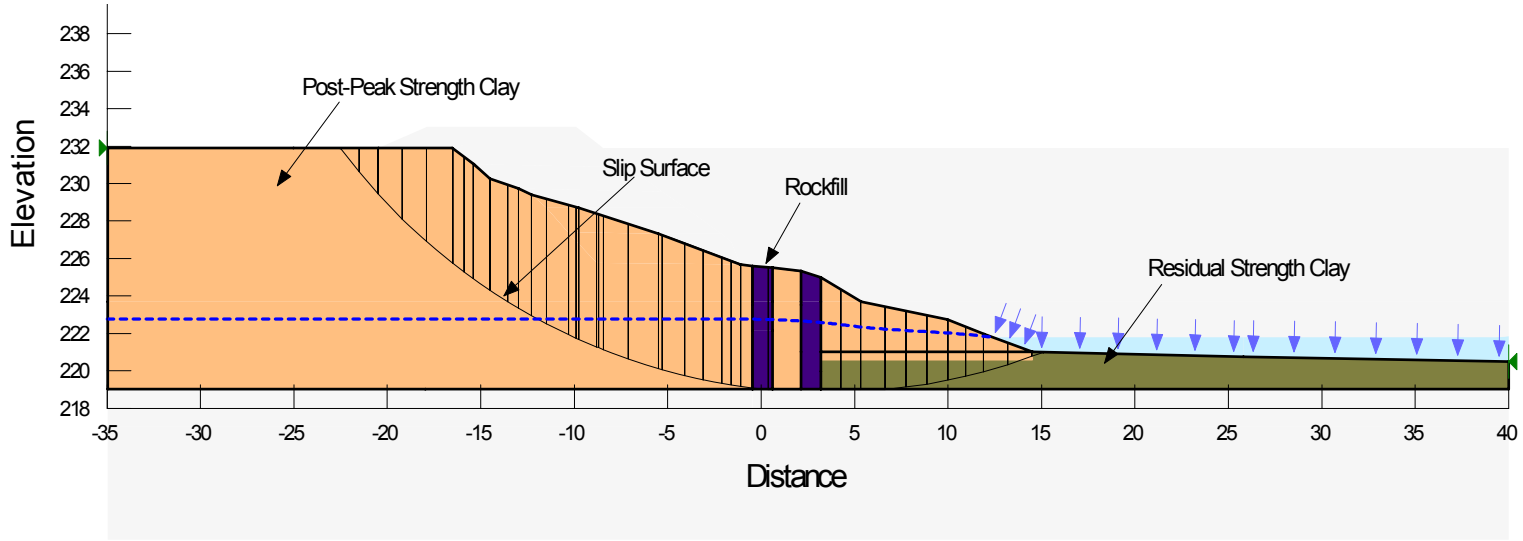


Figure 5.2. Cross-section used for stability analysis, with winter water level.

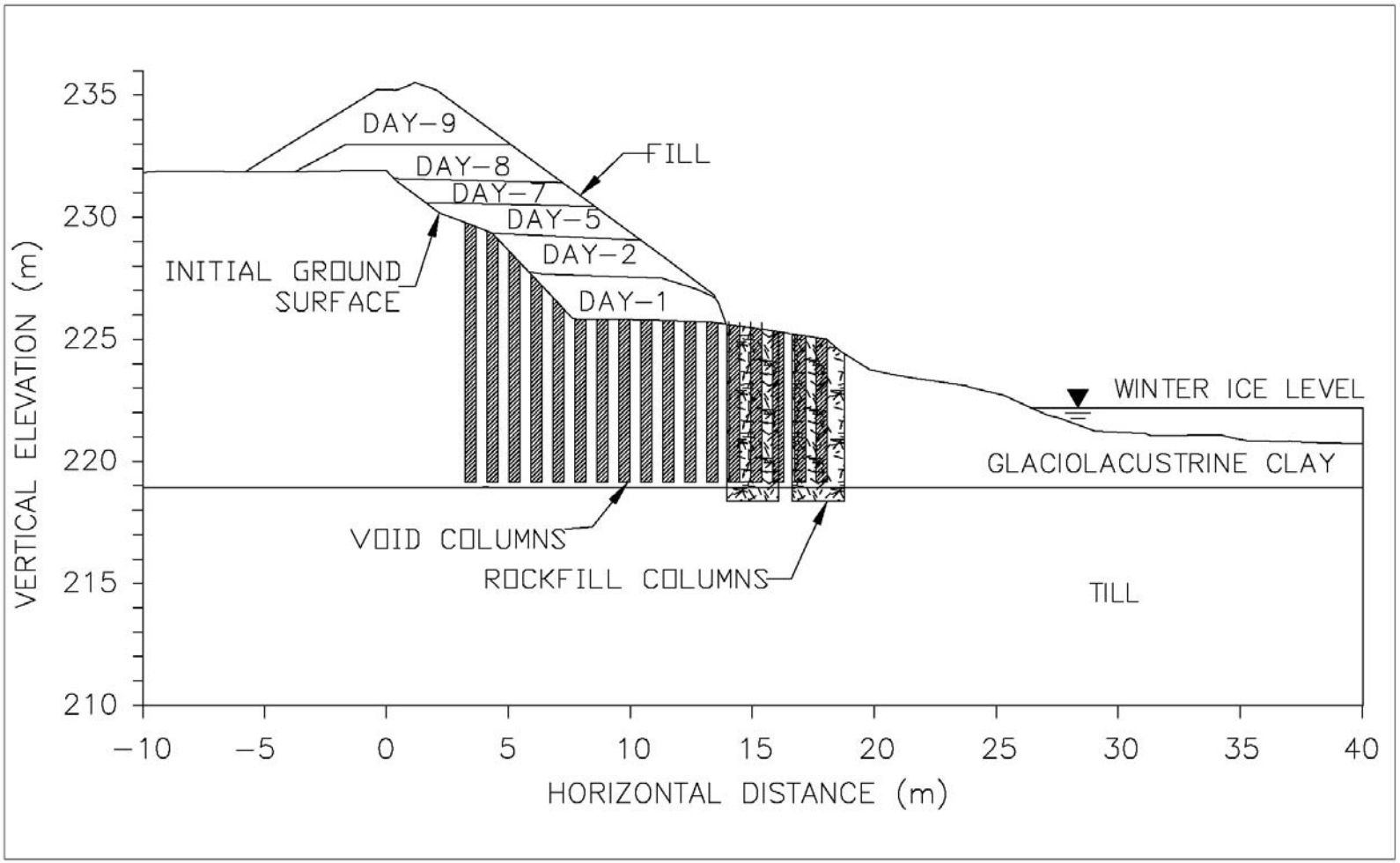


Figure 5.3. Cross section showing void columns and fill pile.

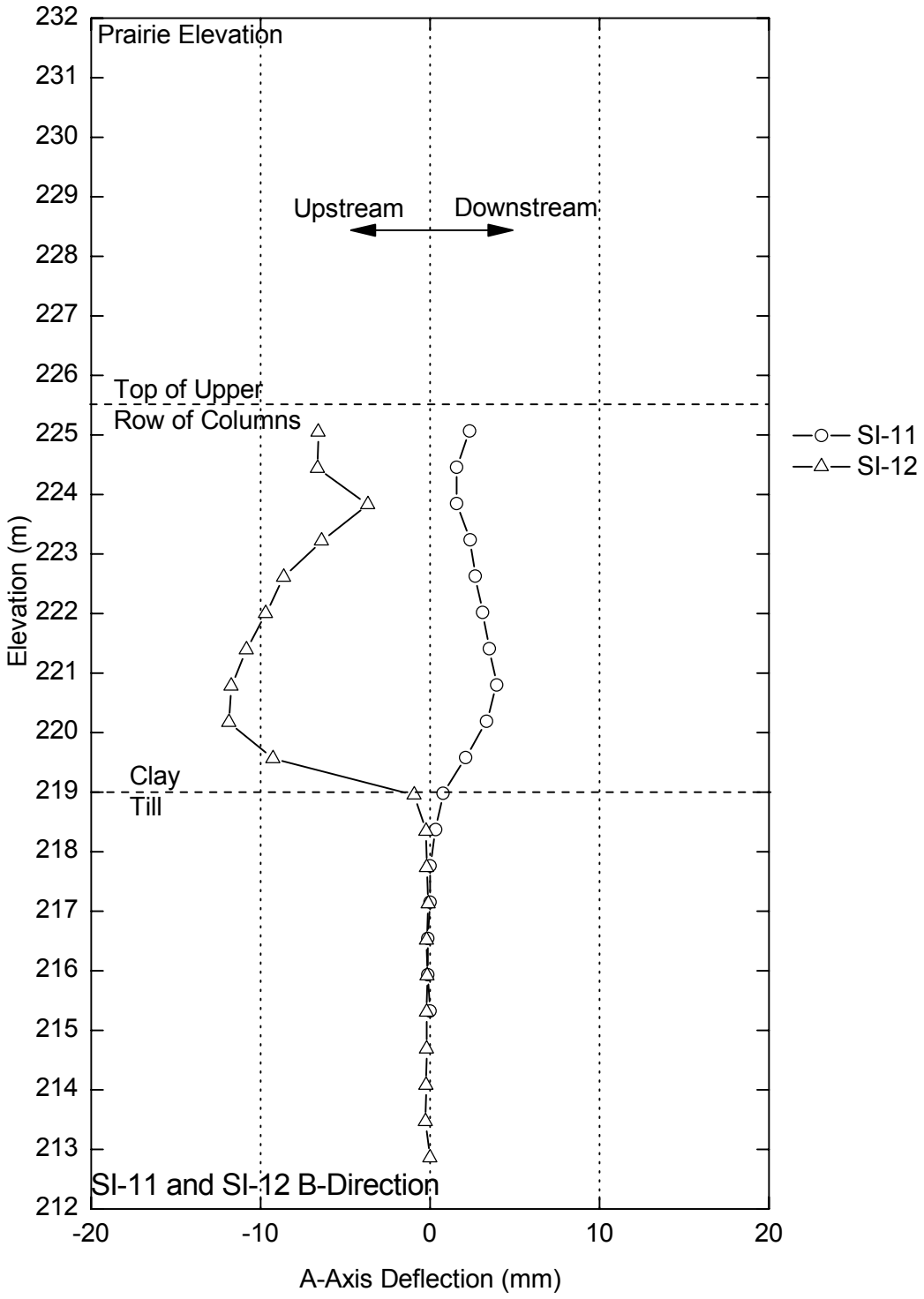


Figure 5.4. B-direction displacements measured in SI-11 and SI-12 over the test loading period to look at the effect of the void columns.


Figure 5.5 Drilling rockfill columns.


Figure 5.6 a) and b) Compacting rockfill with vibrolance

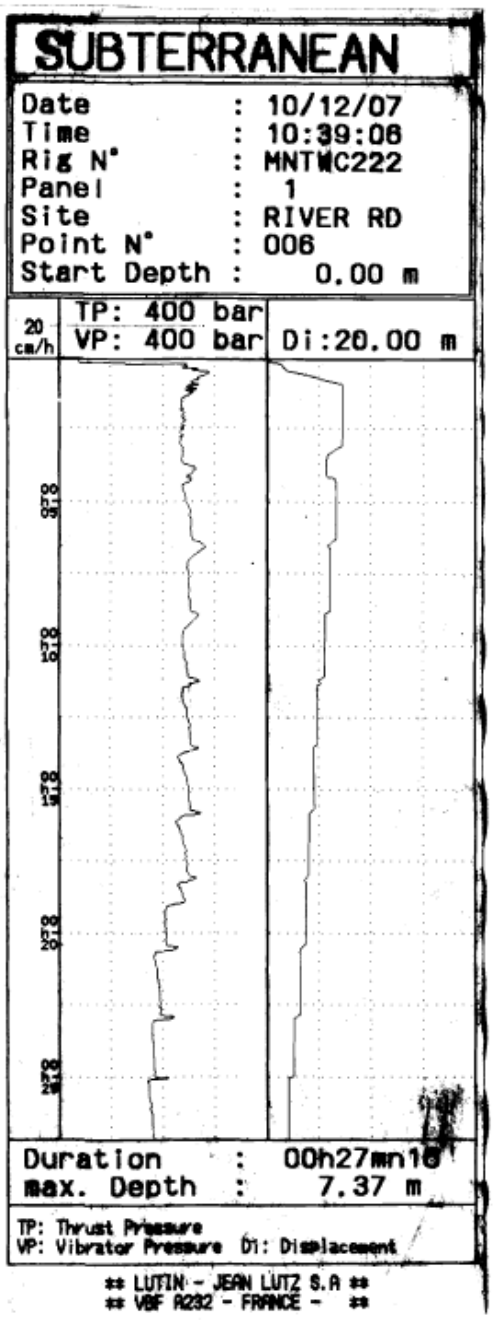


Figure 5.7. Sample printout of compaction effort from vibrolance control module. Hydraulic pressure and depth are plotted versus time.

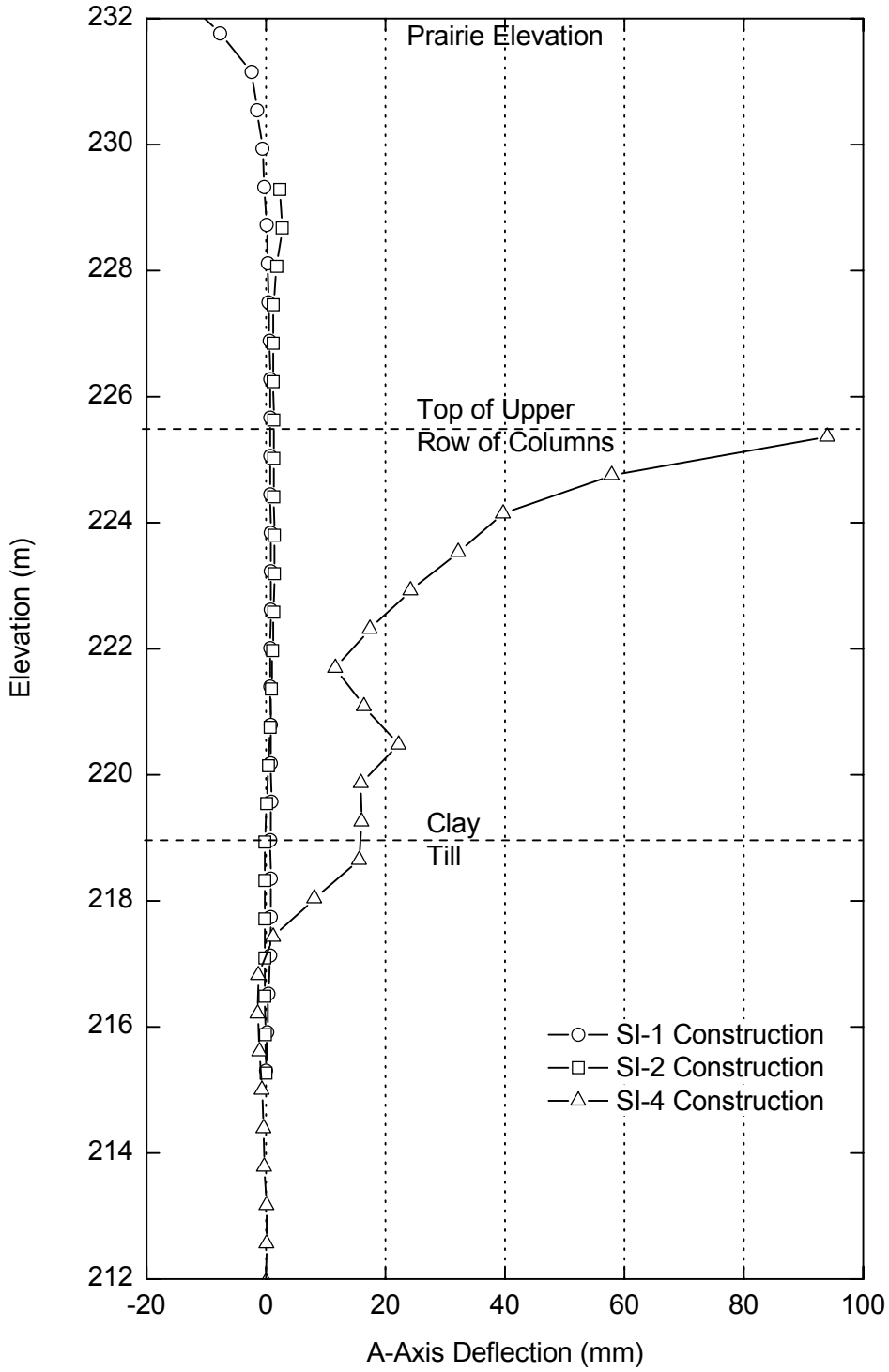


Figure 5.8. Deformations measured in SI-1, 2 and 4 from October 2007 to February 2008. The columns were installed in November 2007.

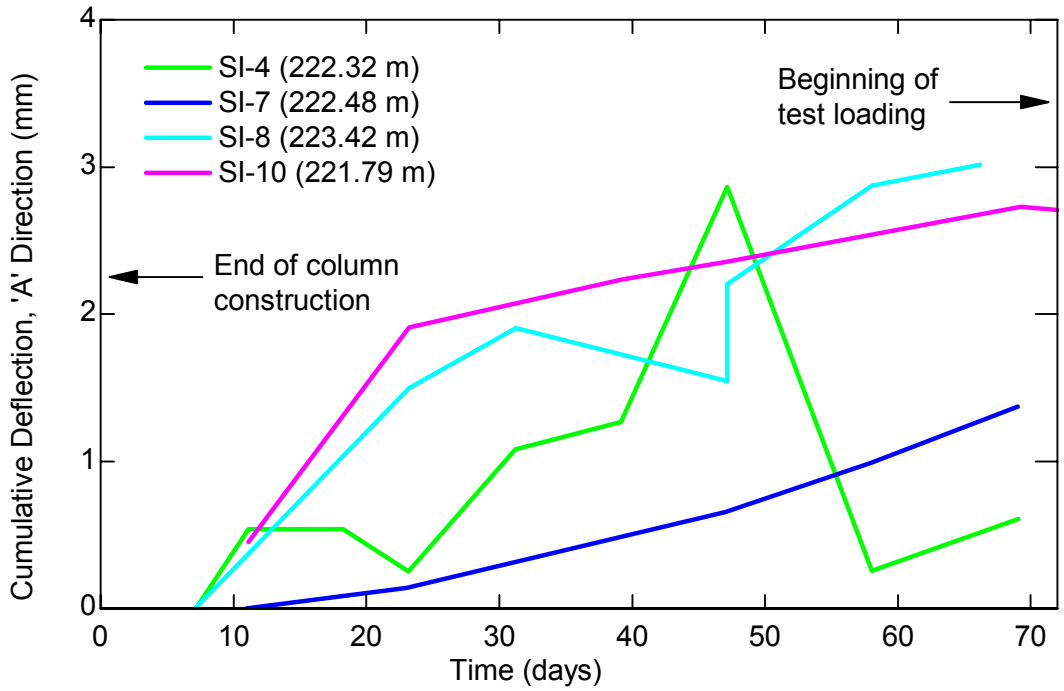


Figure 5.9. Displacement vs. time for SI's 4,7,8 and10 following construction (Dec 14, 2007 to Feb 20, 2008)

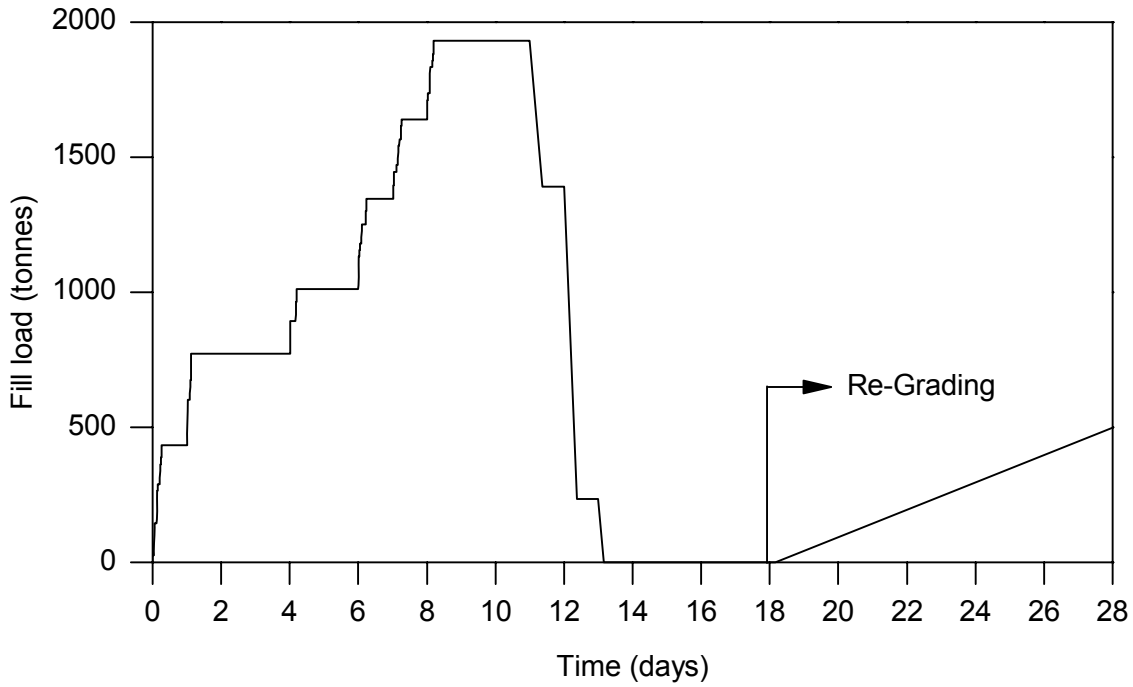


Figure 5.10. Plot of fill load vs time during test loading.

Figure 5.11. Test site one day prior to start of test loading.

Figure 5.12.Test site on Day 1 of loading.

Figure 5.13. a) and b)Day 2 of test loading.

Figure 5.14. a) and b) Day 5 of test loading.

Figure 5.15. a) and b) Day 7 of test loading.

Figure 5.16. a) and b) Day 8 of test loading.

Figure 5.17. a) and b)Test site with final load in place on Day 9.  Photos taken from river.

Figure 5.18. Test site on day 9 at end of loading. Photos taken along crest a) from downstream and b) from upstream


Figure 5.19. Research test section a) during re-grading and b) after the final site remediation work.

# 6. OBSERVATIONS, RESULTS AND COMMENTARY

## 6.1 Introduction

This chapter presents and discusses the results and observations of the full-scale field test of rockfill columns. In contrast to most scientific research projects, a full-scale field test typically provides only one set of data, which cannot be confirmed with additional trials. Interpreting the results of such full-scale field tests, is more akin to interpreting the field performance of geotechnical engineering works than it is to interpreting laboratory test results. The scale of the test, the natural material variability, the challenging logistical constraints of the test procedures and the inevitable poorly controlled boundary conditions introduce uncertainty into the results. The one-off nature of full-scale field tests usually means that results cannot be physically checked for accuracy, sensitivity, repeatability or be tested under modified conditions. It is therefore important to have a well designed experiment and a reliable measurement system to obtain the full benefit of such tests.

The rockfill column test was designed and the results interpreted, with careful consideration of these constraints. This chapter identifies the significant results, and proposes interpretations of some results. Not every aspect of the results can be explained fully because too many phenomena are contributing to the measured results to be able to isolate individual relationships with certainty.

When only one set of data is available, educated discretion is required to decide whether results should be accepted or rejected. Statements which confirm hypotheses or develop theories based on the results of a single trial need to be made with caution.

As discussed in the previous chapters, the current project is a load-deformation test. The load component is calculated by measuring the amount of fill placed as discussed in Chapter 5. The inclinometer monitoring results are the focus of this chapter because they are the primary measure of deformation. The porewater pressures are also important. The porewater pressures responded to the loading, and they are directly related to the effective stresses, and therefore the available shear resistance, of the in-situ soils.

A large amount of data was collected as part of this field test, and it is not possible to reasonably present it in its entirety within the body of this document. The complete set of monitoring results is included in the digital appendix.

## 6.2 Survey results

Daily topographical surveys were useful for tracking the volumes and distribution of the loading fill. The bounded volumes and bounded weights were included in Table 5.1. It was assumed for the purpose of analysis that the loading material sitting outside of the rows of void columns (Figure 3.9) did not contribute to the stress development within the test section, between the rows of columns. This is a necessary simplification of the complex three-dimensional interactions within

and between the fill, the void columns and the in-situ clay. The limited width of the test section did not allow for all of the loading material to be contained between the two rows of void columns.

The surveyed cross sections were used in developing the standard cross sections for computer analysis. The results of the survey pin monitoring are not presented because the deformations were too small to be reliably measured with the available equipment. The slope inclinometers were more suitable for the task of measuring small deformations, using the bases of the inclinometer casings as the reference points.

## 6.3 Inclinometer monitoring results

Inclinometers are most commonly used for identifying zones of shearing within soil or rock. In this field test, the inclinometer results are used to identify and characterize more nuanced behaviours. Gould and Dunnicliff (1971) discuss the use of inclinometers for determining moments in retaining structures, and they comment on the accuracy required to accomplish this.

The definitions of the terms cumulative displacement (H) and incremental displacement (h) are illustrated in Figure 6.1. Unless otherwise noted, all displacements discussed in this chapter are referenced to day 0 (baseline), before the beginning of the test loading.

Deflections parallel to the river (in the B-direction) are not reported for all inclinometers, but are included in the digital appendix. The B-direction

displacements were much smaller, and not correlated with the loading. The monitoring probe is less accurate in the B-direction because of “play” between the wheels and casing, thus reducing the reliability of the B-direction readings, especially if the incremental displacements are small (Green and Mikkelsen 1988).

It is important to note that the inclinometers only measure the horizontal components of the displacement vectors along the length of the casing. Vertical displacements were not measured, and therefore cannot be discussed. As illustrated by Figure 6.2, the deformations measured by an inclinometer underestimate the total displacement if the displacement vector is not horizontal.

Shear strains ($\gamma$) can be roughly calculated from inclinometer data using (Gould and Dunnicliff 1971):

$$\gamma \approx \frac{h}{T\cos^2\theta} \qquad 6.1$$

where:

h = horizontal displacement over a specified increment

T = vertical interval (2 ft or 0.61 m for a standard inclinometer probe)

$\theta$ = angle of shear measured from horizontal

Shear strain calculated by Equation 6.1 is the average shear strain over the increment but localized shear strains may be greater. It should be noted that if a

body of soil “rotates” about some point, the incremental displacements may not be indicative of shear strains over that interval.

In the following sections the results of the inclinometer monitoring are grouped in zones as illustrated in Figure 6.3. Zone 1, Zone 2 and Zone 3 include the upslope area, the column area, and the downslope area respectively.

Figure 6.4 to Figure 6.13 show the displacements measured at select times during the field test for individual inclinometers. The terms ‘deformation’ and ‘displacement’ will refer to ‘horizontal deformation’ and ‘horizontal displacement’ respectively, unless noted otherwise. Plotting all of the inclinometer surveys is impractical because of the large number of data sets. The figures generally show displacement profiles for day 3, day 6 and day 11 corresponding to times with 40, 70 and 100% of the final load in place. Day 18 deflections are included in some figures. The removal of fill was completed on day 13, and the final re-grading work began on day 18. Figure 6.14 shows the cumulative displacements for select elevations from SI-4, SI-7 and SI-10, plotted versus time. The in-place inclinometers installed in SI-8 and SI-9 (Figure 4.1) provide a high resolution measurement of the rate of incremental displacements. The in-place inclinometer results are plotted in Figure 6.15.

The displacements measured during the test loading are minor (less than 20 mm) by most civil engineering standards, but they are still significant to the interpretation of rockfill column behaviour. The accuracy and precision of the inclinometer probe is suitable for measurement of these displacements if used

carefully (Chapter 4 discussed the accuracy and types of errors of slope inclinometer monitoring results). The large number of data points, and the double pass survey method have given confidence that the monitoring results are sufficiently accurate for the analysis presented in the following sections.

An implicit assumption when presenting the results of inclinometer monitoring is that the base of each casing remains fixed with time. This is a reasonable assumption for inclinometer casings anchored deep in the till but the assumption is less sound for inclinometers SI-6, SI-7 and SI-9 which did not have a long anchor length in a stable stratum. Comparison of the displacement profiles of the inclinometers installed in rockfill columns (SI-6, SI-7 and SI-9 in Figure 6.7, Figure 6.8 and Figure 6.10) to those installed between the columns, through the clay and into the till (SI-4 and SI-8 in Figure 6.6 and Figure 6.9) suggests that the base of the casings installed in the rockfill columns only moved a very small amount (probably less than 1 mm). The measured incremental displacements are unaffected by movement of the inclinometer base. The lack of an embedment length in a stable soil layer does not allow for bias corrections for SI-6, SI-7 and SI-9.

In general, incremental displacements near the surface should be interpreted cautiously, as they are more easily influenced by phenomena such as temperature changes, vibrations or other disturbance at or above ground level.

### 6.3.1 Zone 1: SI-1 and SI-2

Slope inclinometer casings SI-1 and SI-2 were installed in the upslope area of the test section. As shown in Figure 6.3, the placement of fill progressed upslope towards SI-1 and SI-2, eventually surrounding the casings (on day 5 for SI-2 and day 8 for SI-1). The casings were extended to accommodate ongoing monitoring during the last days of the test loading. SI-2 could not be read between Day 8 and Day 14 because the fill prevented safe access to the top of the casing.

SI-1 and SI-2 show a slight negative (that is upslope) deflection between elevations 219 m and 226 m during the test loading (Figure 6.4, Figure 6.5). These deflections are less than 2 mm in magnitude, but they were observed in consecutive surveys, confirming that the observations are meaningful. The placement of the fill material applied an increment of normal pressure to the natural slope face. The normal pressure would cause some horizontal compression of the in-situ soil into the slope face, thereby explaining the negative A-axis deflections.

As the fill was removed, a slight relaxation was observed as evidenced by downslope movement above 219 m, after day 11. The relaxation (positive deflection) is greater than the negative deflection initially caused by the loading, suggesting that there was unrecoverable plastic yielding within the slope, or some other release of energy.

The deflections observed in the upper two meters of SI-1 are not considered significant to the interpretation of the test results. They are likely related to the

disturbance caused by the removal of the frost at the crest and/or the heavy equipment traffic along the crest

### 6.3.2 Zone 2 Centerline: SI-4, SI-6, SI-7, SI-8 and SI-9

Slope inclinometers SI-4, SI-6, SI-7, SI-8, and SI-9[1] were installed near the centerline of the test section as shown in Figure 4.1. The inclinometers were concentrated in a small area around the rockfill columns to capture the response of the columns and the column-clay interaction.

The five inclinometers along the centerline of Zone 2 show the following similar traits (Figure 6.6 to Figure 6.10):

- There was insignificant displacement below 217 m (less than 1 mm). The density of the till increases below 217 m, as noted in the testhole logs and the dense till is more resistant to deformations than the loose upper till. Secondly, the columns extended to an elevation between 217.5 to 218 m, and therefore the influence of the columns would decrease rapidly below this elevation.
- The cumulative displacements gradually increase with elevation between ~217.5 m and ~223.5 m. The slope inclinometers installed in the rockfill (SI-6, SI-7 and SI-9) show that the length of the column embedded in the

[1] In-place inclinometers (IPI) were installed in SI-9 for most of the test loading. During the test the IPI suspension system became frozen into the casing. The entire casing shifted while removing the in-place inclinometers on day 9, as a result. The deflection profile of SI-9 is included for completeness, but the author believes that all measurements in SI-9 after day 9, are not accurate because the orientation and elevations are in error. When the orientation or elevation of a casing changes between the baseline and subsequent readings, the measured deflections are influenced by the installed profile of the casing. The IPI results shown in Figure 6.15 are not affected.

till rotates and/or undergoes shear strains as a result of the loading. The displacements appear to rotate about a point at elevation approximately 217.5 m, very near the base of the columns. This type of movement supports the theory that rockfill columns transmit horizontal loads via shear and bending from the clay to a reaction in the till. No deformation can occur without a transfer of force or moment.

- The incremental displacements show an increasing trend with increasing elevation between ~217 m and 223.5 m. This is illustrated in Figure 6.16, and is discussed further in Section 6.7.3.
- There is a noticeable increase in the incremental and cumulative displacement, concentrated over a small zone around elevation 224 m. These displacements become more pronounced as the load increased. The zone of increased deformation approximately coincides with the top of the well compacted rockfill. The effectiveness of the vibrolance at compacting the upper portion of the column is questionable because there was little confining pressure and the vibrolance occupied a large volume in the center of the column. The rockfill also “dropped” as it was being densified. Additional material was added during compaction, but the top of the compacted rockfill in most columns remained approximately 1m below the ground surface when the vibro-lance was removed. The remaining length of drilled shaft was filled with loose rockfill. The increased strains observed near the surface by the Zone II slope

inclinometers may be attributed to the lower stiffness and shear strength of the loose rockfill near the surface.

- There is a small negative incremental displacement near the surface. This observation is not considered specifically in the analysis, as the cause may be the result of some surface effects.

When comparing the deformations observed in SI-4 and SI-8 installed in the in-situ clay, with the deformations observed by SI-6, SI-7 and SI-9 installed in rockfill columns, it can be concluded that the columns and surrounding soil deform as a unit with no noticeable differential movements. Figure 6.14 and Figure 6.15 also show that the time dependant responses of the columns and surrounding clay are very similar.

The in-place inclinometers can only measure the incremental displacement over the span of the sensor, unless they are installed in a series. The incremental displacements were less than 2mm/m at the elevation of the installed IPI's, as shown in Figure 6.15. The IPI's were installed around the clay-till interface because that is where the peak shear stresses (and shear strains) were expected, based on preliminary numerical models.

### 6.3.3 Zone 2 Edges: SI-11 and SI-12

SI-11 and SI-12 were installed in the vicinity of the rockfill columns near the downstream and upstream edges of the test section as shown in Figure 4.1. SI-11 and SI-12 are discussed separately from the inclinometers in Section 6.3.2

because there is a notable displacement component in the direction parallel to the river (B-direction) as shown in Figure 5.4.

The ground is pre-disposed to deforming in the downslope, A-direction, because of the geometry and in-situ shear stresses, but the ground also responded in the B-direction at the edges of the fill. There are a number of inter-related factors that are presumed to have caused the B-direction displacements. The placement of the pile of fill material caused horizontal compressive and shear stresses perpendicular to the face of the pile, in the underlying foundation soil. Secondly, the void columns along the edges of the test section increase the compressibility and reduce the available shear resistance of the soil in the B-direction.

The development of compressive and shear stress, in the B-direction, is analogous to the stress development beneath the edge of an embankment. Poulos and Davis (1991) present elastic solutions for stress development due to embankment loading. The assumptions of Poulos and Davis (1991) do not fully apply, but the deformation profiles in Figure 5.4 are reasonable if the stress distributions in Figure 6.17 and Figure 6.18 are considered along with the weakening and softening effect of the void columns.

SI-12 (Figure 6.13) shows a greater shear strain near the clay-till interface than any other inclinometer during loading. Approximately 7 mm of displacement occurred over a vertical increment of less than 1.2 m. The actual height of the zone of shearing and the angle of shear are unknown. The displacement was

measured over a 1.2 m length of casing, thus the actual peak shear strain must be greater than 0.6%, but could be significantly larger.

### 6.3.4 Zone 3: SI-10

The only inclinometer installed in Zone 3, downslope of the rockfill columns, was SI-10. The deformations measured by SI-10 (Figure 6.11 and Figure 6.14b) are significant to the understanding of the rockfill column behaviour when considered in comparison to the deformations measured by the Zone 2 inclinometers. The following are some observations based on the displacements measured by SI-10:

- The magnitude of displacement near the surface was similar to the deformations measured in Zone 2 (in SI-4, SI-7 and SI-8).
- There were negligible displacements in the till and relatively small (less than 2.6 mm) cumulative displacements below elevation 220.6 m, noting that the clay-till interface is at elevation 219 m.
- The average incremental displacement between elevation 220.6 m and 223.0 m is 4.8 mm/m, and is greater than the incremental displacement measured in any other inclinometer over a similar range of elevations.

Slope inclinometer SI-10 was installed below the summer water level, within the zone of observed lower slope instabilities described in Section 3.4 and shown in Figure 3.11. Therefore, it is probable that much of the soil in this zone was previously sheared beyond the peak strength, and it is likely that there are bands

of soil that were sheared (on prior occasions) to a state of residual strength. It is reasonable to believe that at the start of the test loading, even though the soil was stable, only a small additional stress was required to re-mobilize the full residual shear strength.

### 6.3.5 SI-5

Slope inclinometer SI-5 was installed near the slope crest, downstream of the test section, to monitor for any changes in the behaviour of the adjacent slope due to the site activities. The purpose of the installation was to help identify potential risks rather than to specifically contribute to the research. SI-5 was not monitored with the same regularity as the other inclinometers. There were no displacements observed at SI-5 caused by the loading. The results are not presented here, but are included in the digital appendix.

## 6.4 Piezometer monitoring results

The measured porewater pressures during the loading are not a direct indicator of the performance of the rockfill columns, but they are essential for calibrating the numerical models. Chapter 4 discusses the installation methods, the monitoring program and the monitoring results leading up to the field test. The installed locations of the piezometers are shown in Figure 4.1 and Figure 4.3. Figure 6.19 shows the monitoring results measured during the field test. The datalogger malfunctioned at day 8.5, resulting in the gap in the data to day 10.5,

as discussed in Chapter 4. Table 6.1 summarizes the measured daily porewater pressure response.

The following are some comments regarding the measured porewater pressure responses:

- The character of the porewater pressure response to loading changed for each piezometer as the test progressed. The concept of a $\bar{B}$ response is useful, although it cannot be applied rigorously to the loading scenario in this project. The $\bar{B}$ coefficient is calculated as:

$$\bar{B} \approx \frac{u_{peak} - u_0}{\left(\frac{\text{weight of bounded fill}}{\text{footprint area of bounded fill}}\right)} \qquad 6.2$$

where:

$u_{peak}, u_0$ = maximum and initial porewater pressure

The $\bar{B}$ is not plotted, but visually one can tell the $\bar{B}$ response for VW-E is greatest on day 0 to day 2, and decreases beyond day 2. VW-A and VW-B, installed further upslope, showed an increasing porewater pressure response as the fill was placed directly over the installation after day 4.

As the footprint of the fill grew, the additional weight was spread over a larger area; thus the vertical stress increase ($\Delta\sigma_z$) per unit of fill delivered, decreased as the test progressed. Table 5.2 lists the weight, volume and the footprint area for the end of each day.

- Some of the porewater pressure changes (both positive and negative) may be a result of volumetric strains associated with shearing, and not only due to a change in vertical stress.
- The porewater pressure response measured by VW-D is less than 2 kPa over the course of the test. VW-D was installed between the rows of rockfill columns. The columns provide vertical drainage paths to help dissipate excess porewater pressures more rapidly. VW-D was subjected to a smaller vertical stress increase than the other vibrating wire piezometers because it was situated outside of the fill footprint. Some of the porewater pressure response may be caused by horizontal stress changes.
- It is apparent that there is significant dissipation of excess porewater pressures over the testing period. Table 6.1 shows a summary of the daily maximum and minimum porewater pressures. At the critical point, immediately after the final load was placed on day 8.0, an average of 57% of the excess porewater pressures had already dissipated. The estimated time to 50% consolidation was calculated to be approximately 50 days, based on a general 1-dimensional consolidation solution (not considering the sloping geometry, or additional drainage provided by the rockfill columns). It is interesting to note that VW-B was situated near the middle of the soil layer and had the longest drainage path, but the dissipation of porewater pressures was similar to other measurement locations.

- The porewater pressures responded immediately to the rapid unloading of the slope. The porewater pressures measured by VW-A, VW-B and VW-D immediately after unloading are lower than the initial porewater pressure at day 0. The reduction in porewater pressure caused by unloading is larger than the remaining excess porewater pressure at the end of the loading phase.
- Vibrating wire piezometer VW-E responds gradually to porewater pressure changes. VW-A, VW-B and VW-D respond more rapidly, and the transition from increasing to decreasing porewater pressure trends at the end of each loading phase is almost instantaneous. VW-E and VW-F were push-in style piezometers and these two sensors were previously used by a consultant on a different project. Care was taken during installation to try to maintain saturation of the tip and porous stone, but this is more difficult with push-in piezometers than it is for standard piezometers. A possible air-pocket in the tip may have contributed to the slower response. For the purpose of calibrating the numerical models, it is assumed that the actual porewater pressure response was more rapid than the response measured by VW-E.
- The performance of VW-F is questionable. It appears to be functioning on occasions as it shows an increase in porewater on day 0, and it also reports a rapid drop in porewater pressure on day 12 during unloading. From day 0.5 to day 12, there is an increasing trend in the measured pressure, but it does not respond to the loading as expected.

The monitoring data from VW-C are not included in Figure 6.19 because the piezometer was located above the water table and it did not report any meaningful results.

Calibration of the numerical model to the piezometer monitoring results is discussed in the following chapter.

## 6.5 Ongoing monitoring

Figure 6.20 and Figure 6.21 show the displacements of inclinometer casings for several dates up to 640 days after the completion of the field test. Generally the displacements in the till are negligible, except for SI-4 which shows small displacements below elevation 219 m. The displacements of all inclinometers increase dramatically near the surface with incremental displacements of more than 35 mm, and cumulative displacements of more than 70 mm. The magnitudes of the displacements measured after the restoration of the site are greater than the displacements measured during the test loading.

The maximum displacements measured by SI-4 and SI-8, both installed in the clay, are greater than the displacements measured by nearby SI-6 and SI-7 which were installed directly into rockfill columns, possibly indicating some flow of clay between the rockfill columns at shallow depths. This difference is only obvious in the upper two inclinometer readings, and may be the result of some downslope migration of the previously frozen, re-contouring fill.

As described in Chapter 5, clay fill was placed to re-grade the site. Some of the early displacements may be associated with consolidation, but the author does not believe that the long term displacements are explained by primary consolidation. The fill material placed for re-grading was approximately equal in weight to the soil removed during Phase II and it was about 25% of the weight of the fill placed during the test load (noting also that the during the load test, the fill material was applied to a smaller footprint). Any consolidation should therefore be elastic, with final pressures below the preconsolidation pressure.

Furthermore, when the re-grading fill was placed, the in-situ porewater pressures were probably below the hydrostatic values because of the removal of the test loading fill 5 days earlier. The initially depressed porewater pressures would reduce the potential excess porewater pressure generated by the placement of the re-grading fill.

If the ongoing displacements, mostly at shallow depth, are not due to primary consolidation or immediate elastic-plastic strains, then they must be the result of creep or other stress changes. The spring floods and fall drawdowns (of the Red River water levels) in 2008 and 2009 would have "stressed" the ground at depth, but not as severely as the test loading did.[2]

Conversely, the high river levels in the spring of 2008 and 2009 likely introduced a temporary downward gradient with high porewater pressures near the surface.

[2] The test loading created porewater pressure conditions in the clay which were similar to the porewater pressures measured in the spring of 2007 (for example VW-B measuring a total head of ~224.2 m). The major differences were that during the test loading the bank was subjected to the surcharge load and it did not have the benefit of floodwater pressures stabilizing the toe. Porewater pressures near the surface were not measured.

Noting again that the top 1 m or more of the rockfill columns was not compacted, and that the re-grading work was done in March with partially frozen clay fill that was not compacted, it is reasonable to believe that these near-surface deformations were caused by a high porewater event. Additional shear resistance of the columns is mobilized these events, especially near the ground surface.

As Figure 6.22 demonstrates, the deformations are ongoing, but their rates have slowed significantly, especially when compared to the rate of deformation before day 200. The influence of creep mechanisms both within the clay and the rockfill is an important consideration, but creep analysis is beyond the scope of the current research project.

## 6.6 Other observations

Surficial cracks were observed at two locations, shown in Figure 6.23. The cracks were noticed on day 10 of the test loading, one day after the last fill material was placed. One crack was located near the centerline of the test loading, and it extended from beneath the fill, running perpendicular to the crest of the riverbank. An untested hypothesis is that the crack was caused by lateral spreading due to the loading. The void columns provide a compressible and weak zone enabling B-direction (cross-slope) deformations, as discussed in Section 6.3.3.

The second crack was found extending back from the crest of the slope at the downstream edge of the pile of loading fill. The crack curved from the lip of the crest, in behind the behind the fill and was less than 5 m long. It may have been a tension crack or shear plane forming along the outer edge of the zone of deformation.

The depth of the cracks is unknown. The cracks were monitored closely from day 10 to day 12 but they did not seem to change significantly with time. The cracks were disturbed by equipment during the unloading of the slope, and could not be found later.

## 6.7 Additional Interpretation

### 6.7.1 Load – deformation

Figure 6.24 approximates a load deformation plot for the test loading. The plot shows the cumulative displacements at several points, measured over the 24 hour periods following each additional application of fill, thus ignoring displacement from day 2.0 to day 4.0 and day 5.0 to day 6.0. This serves to highlight (imperfectly) the elastic response, by removing some of the components of displacement that are time dependant.

As additional fill was added with time, the volume of in-situ soil being stressed increased as the footprint of the loading fill increased. This effect cannot be easily or accurately quantified, but it is implicitly accounted for in finite element stress deformation models that will be shown in the following chapter. A more

accurate measure of a load deformation response would require the application of a surface pressure over a constant footprint. Figure 6.25 plots the average normalized ground pressure (that is average pressure/final average ground pressure) against displacement. The differences between Figure 6.24 and Figure 2.5 are due to the increasing footprint of the fill, as the pile became larger, and extended further upslope. It is apparent that the ratio of the displacement increment to pressure increment increased as the test progressed, indicating a non-linear response to loading.

### 6.7.2 Elastic rebound

The partial elastic rebound from unloading can be seen in Figure 6.6 to Figure 6.12, Figure 6.14 and Figure 6.24. The incomplete rebound is evidence that both elastic (recoverable) and plastic (non-recoverable) deformations occurred due to loading. There is noticeably less rebound in the upper 1.5 m. The average rebound was calculated as:

$$\text{Percent rebound} = \frac{(\sum \text{Day 18 cumul. displacement}) - (\sum \text{Day 11 cumul. displacement})}{\sum \text{Day 11 cumul. displacement}} \times 100$$

where:

$\Sigma$ Day ... cumul. displacement = the sum of the cumulative displacements at each inclinometer measurement point.

The average rebound for SI-4, to SI-11 (ignoring SI-9) was 21%. The average rebound for the same inclinometers was 39% if the rebound in the upper 1.5 m of each inclinometer was not included in the calculation. The behaviours observed

by SI-4, SI-7, SI-8 and SI-10 were quite similar with rebound percentages ranging from 17% to 26% if the whole length is considered. Notably, SI-6 (installed in a rockfill column) had the greatest individual average rebound at 39%, while SI-11 had the lowest percentage of rebound at 4%. It is possible that the lower confining pressure along the void columns contributed to yielding of the clay and therefore less recoverability of deformations, in the area around SI-11.

The elastic rebounding effect cannot be attributed solely to the contribution of the rockfill columns as the principal and shear strains in the clay also have an elastic component. SI-1 and SI-2 rebounded/relaxed in the downslope direction upon unloading as discussed in Section 6.3.1.

### 6.7.3 Bending behaviour

Discussion in the following paragraphs focuses on the displacements observed between elevation 219 m (the clay-till interface) and 223 m, that is it ignores the larger deformations in the shallow region where the rockfill was not fully compacted. When the incremental displacements are plotted against elevation, as shown in Figure 6.16, it is apparent that the incremental displacements tend to increase with increasing elevation. This is also very obvious when considering the post-construction displacements shown in Figure 6.20 and Figure 6.21.

The incremental displacement is analogous to the first derivative of cumulative displacements along the length of the casing.

$$\frac{h_{inc}}{z_{inc}} \cong \frac{dH}{dZ} \qquad 6.3$$

The second derivative is the rate of change in the incremental displacement with respect to elevation:

$$\frac{\Delta h_{inc}}{z_{inc}^2} \cong \frac{d^2H}{dZ^2} \qquad 6.4$$

It is useful to compare the rockfill column with a beam placed vertically into the slope. From elastic beam theory, the analogous relationship is:

$$\frac{d^2\upsilon}{dx^2} = \frac{M(x)}{EI} \qquad 6.5$$

where:

$\upsilon$ = deflection

M = moment

I = 2$^{nd}$ moment of area of the cross section

Evaluating Equation 6.5 incrementally along the length of the inclinometers is limited by scatter in the measurements and the large reading increments of the slope inclinometers. The hand drawn trendlines (dash-dot) in Figure 6.16 c) and d) illustrate that generally the relationship ($\Delta h_{inc}/z_{inc}$) is positive and relatively constant.

The curvature caused by shear alone in an elastic beam for comparison is (Przemieniecki 1985)

$$\frac{d^2\upsilon}{dx^2} = \frac{-\alpha_s q(x)}{GA} \qquad 6.6$$

where

$\alpha_s$ = shear coefficient (taken as 4/3 for a circular cross section or 3/2 for a rectangular cross section)

q(x) = distributed load

G = shear modulus

A = cross sectional area

A positive second derivative implies that either:

- Shear strains increase with increased elevation, and bending deformations are insignificant

or

- Deformations of the columns and surrounding soil are partially caused by internal moments in the rockfill columns and the associated bending deformations, in addition to deformations associated with shear strains.

Considering the above comments, it is difficult to explain the characteristics of the deformations observed in Figure 6.14 as the result of simple shearing.

Rockfill columns are understood, as demonstrated by this research, to transmit stress from the unstable clay mass into the stronger and stiffer till. For this to occur there must be a mechanism to transfer the primarily horizontal loads over a vertical distance.

Continuum mechanics requires that an element that is subjected to shear stress in one dimension must have conjugate shear stresses along the perpendicular faces to satisfy moment equilibrium (

Figure 6.26). In the same way, a larger body subjected to shear stresses must also maintain moment equilibrium, though the shear stresses are resolved internally through the development of compressive and extensive stresses acting on opposing sides of the body. In structural mechanics, this behaviour is referred to as bending.

Figure 6.27 pictures a rudimentary laboratory test performed by the author demonstrating that a loose, dry sand column can resist bending stresses if a positive effective stress is maintained for all particles (here via the difference between external atmospheric pressure and a vacuum pressure inside the voids of the specimen). Pre- or post-tensioning of concrete structural members achieves the same objective of maintaining positive (compressive) stress across the cross section of the member, even while subjected to moderate bending and shear stresses. In a rockfill column, the compressive stress is provided in the form of positive effective overburden pressures, which are a function of depth.

The stresses within the column must still be considered within the context of soil mechanics, considering in-situ confining and shear stresses and the non-linear constitutive relationships. As mentioned in Chapter 2, bending resistance in rockfill can only exist while all particles remain in compression: granular materials cannot resist tension stresses.

Bending should be considered as a possible deformation mode in rockfill columns because the rockfill is stronger and stiffer than the surrounding clay and it “attracts” stresses from the softer and weaker clay. A complete understanding of bending behaviour in a rockfill column must address the complex stress interactions between the column and surrounding soil. This research cannot fully explore these interactions, but they will be examined in a preliminary way in the numerical modeling presented in the following chapter.

### 6.7.4 Till anchor

Most designs (in Manitoba) for stabilization of a slope with rockfill columns call for extending the columns into the till. The underlying assumption is that the stronger and stiffer till anchors the base of the column and provides the reaction for the stabilizing forces.

The displacement profiles of SI-6, SI-7 and SI-9 (Figure 6.7, Figure 6.8 and Figure 6.15b) do not show a significant change in the characteristics of deformation of the rockfill column at the clay-till interface. They do show rotation (or leaning) of the inclinometer that extends to the column base, and into the till below. As discussed in Chapter 3, the upper till stratum was looser than the

typical basal till common in the region. The direct shear tests on till specimens discussed in Chapter 3 show that the till has high shear strength, even though it is loose. The fact that there were displacements in the till, coinciding with the base of the columns, indicates that the columns were transmitting stresses into the till. Therefore, there must also be shear straining and accompanying volumetric straining in the till.

### 6.7.5 Impacts of frozen ground

Chapter 4 noted that the ground was frozen at the surface to a depth ranging from 0.3 to 1 m when the test fill was constructed and that steps were taken to minimize the impact of the frozen soil. The monitoring results do not suggest that the frozen ground impacted the test results. Based on the results of numerical analysis, the influence of a very stiff and very strong crust would be to constrain displacements at the surface. The deformations plotted in Figure 6.6 to Figure 6.13 generally show increased deformations in the upper 1.5 m, rather than a decrease. The upper-most measurements in SI-4, 6, 7, 10, 11 and 12 do possibly indicate a slight resistance to downslope movement, but generally the accuracy of very shallow movements are disregarded because they are easily influenced by protective casings and surface activities.

## 6.8 Summary and conclusions

There are a number of significant observations from the full-scale field test that are important to advancing the understanding of rockfill column behaviour:

- The columns and the surrounding clay deformed as a unit, with no noticeable differential movements (flow between columns) during the test loading.
- The maximum magnitude of displacements in the columns and the clay downslope of the columns were similar. No displacements were observed in the till downslope of the rockfill columns.
- The entire length of the columns displaced under loading, including the portion embedded in the till.
- The deformations measured during the field test showed a non-linear response to increases in the ground pressure.
- Approximately 40% of the displacements below 1.5 m depth, caused by the test loading, were recoverable upon unloading.
- The displacements due to loading show a trend of increasing incremental displacement with increased elevation, and this trend is more pronounced in the post construction displacements.
- The long term displacements are greater in magnitude than the displacements caused during the test loading, especially at shallow depths.

These observations are discussed further in the following chapter. The numerical modeling will further clarify the links between the observed behaviour with physical mechanisms at work.

Table 6.1. Summary of total pressure head (m) measured by vibrating wire piezometers.

| | VW-A | | VW-B | | VW-D | | VW-E | | VW-F | |
|---|---|---|---|---|---|---|---|---|---|---|
| | Max | Min | Max | Min | Max | Min | Max | Min | Max | Min[4] |
| Initial | 223.05 | | 221.60 | | 223.39 | | 222.20 | | 221.24 | |
| Day 0-1 | 223.45 | 223.25 | 222.26 | 221.84 | 223.62 | 223.48 | 224.15 | 222.86 | 221.46 | 221.17 |
| Day 1-4 | 223.66 | 223.28 | 222.93 | 222.17 | 223.66 | 223.40 | 225.23 | 224.20 | 221.57 | 221.46 |
| Day 4-6 | 223.69 | 223.43 | 223.39 | 222.69 | 223.59 | 223.46 | 225.35 | 225.03 | 221.65 | 221.54 |
| Day 6-7 | 223.74 | 223.48 | 223.72 | 223.14 | 223.54 | 223.42 | 225.37 | 225.19 | 221.70 | 221.63 |
| Day 7-8 | 223.74 | 223.57 | 223.98 | 223.57 | 223.51 | 223.43 | 225.40 | 225.28 | 221.75 | 221.67 |
| Day 8-11 | 223.98 | 222.79 | 224.40 | 221.44 | 223.67 | 223.05 | 225.66 | 223.18 | 221.97 | 221.52 |
| Gross Excess[1] (kPa) | 21. | | 55.6 | | 9.8 | | 62.7 | | 7.2 | |
| Net Excess[2] (kPa) | 9.1 | | 27.5 | | 2.7 | | 34.0 | | 7.2 | |
| Dissipation[3] (%) | 58 | | 51 | | 72 | | 46 | | 0[4] | |

[1]Gross excess porewater pressure is calculated as the sum of daily increases in porewater pressure due to placement of additional load.
[2]Net excess porewater pressure is equal to the peak porewater pressure from day 8-11 minus the initial porewater pressure.
[3]Dissipation (%) = ((Gross-Net)/Gross)*100
[4] VW-F reported a continuously increasing trend in porwater pressures during the test, and therefore no dissipation. Refer to the discussion in Section 6.4.

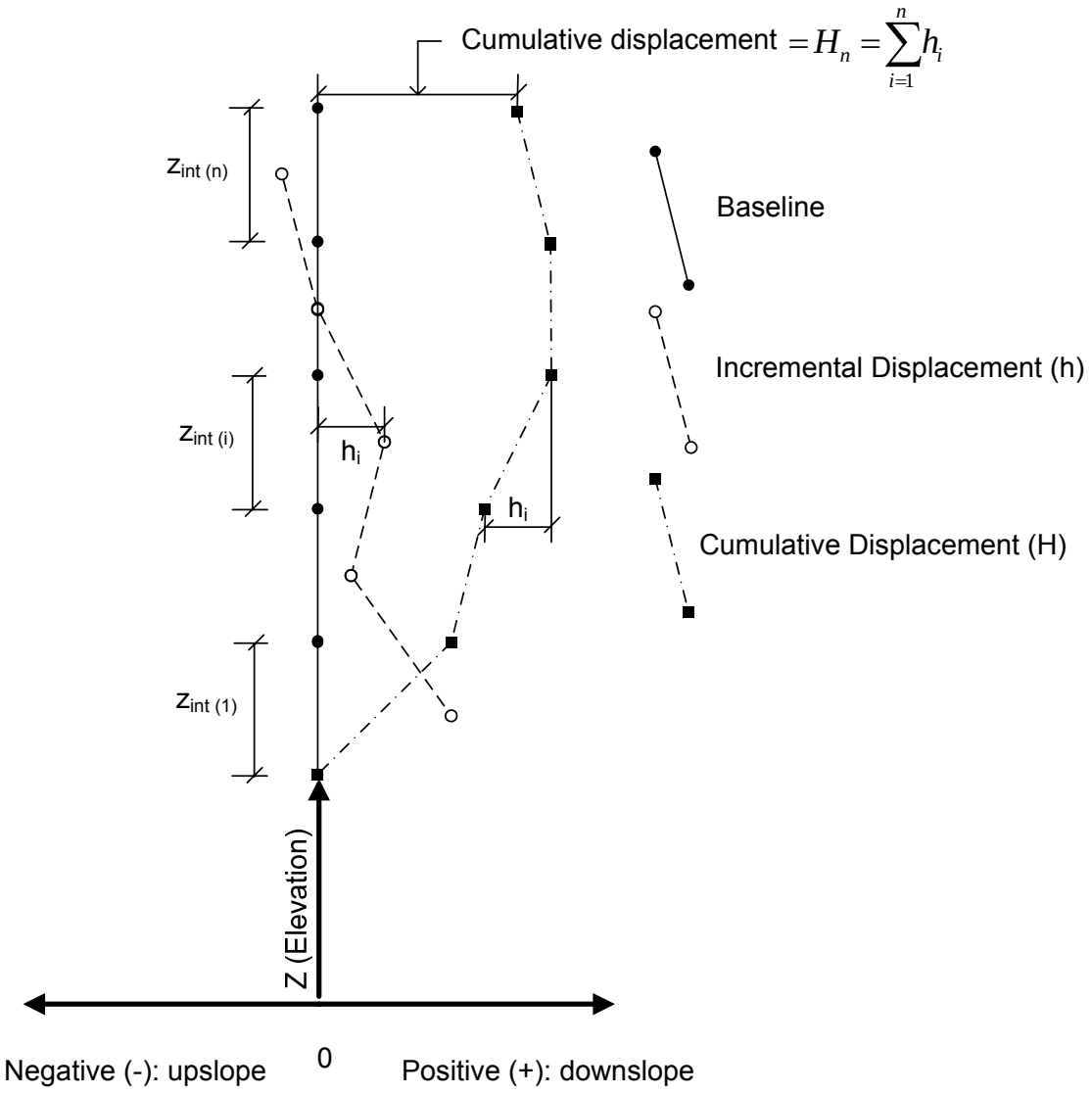


Figure 6.1. Illustration of relationship between baseline readings and incremental and cumulative displacements from slope inclinometer monitoring.

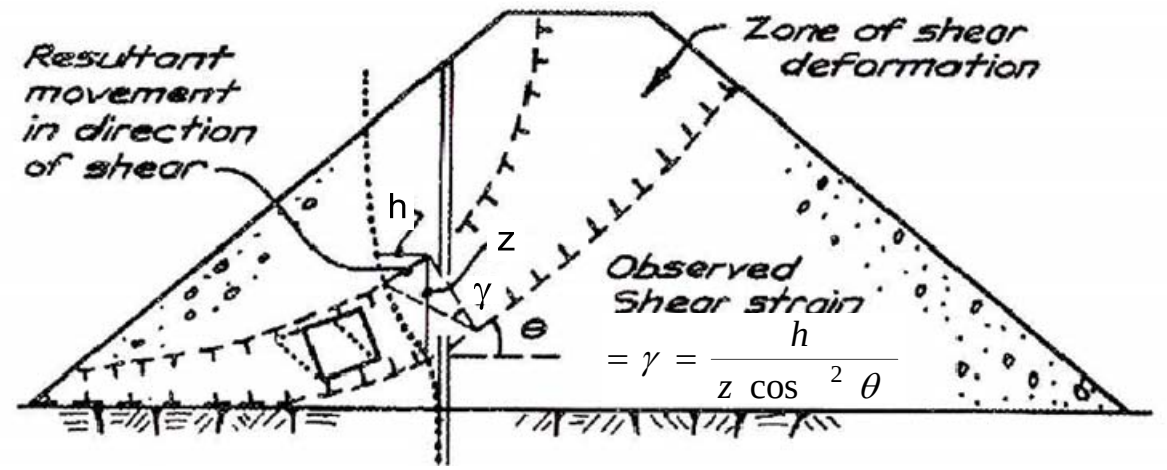


Figure 6.2. Relationship between horizontal displacement and shear strain along sloped shear zones. Modified from Gould and Dunnicliff (1971).
Reproduced with permission from ASCE, November 2009.

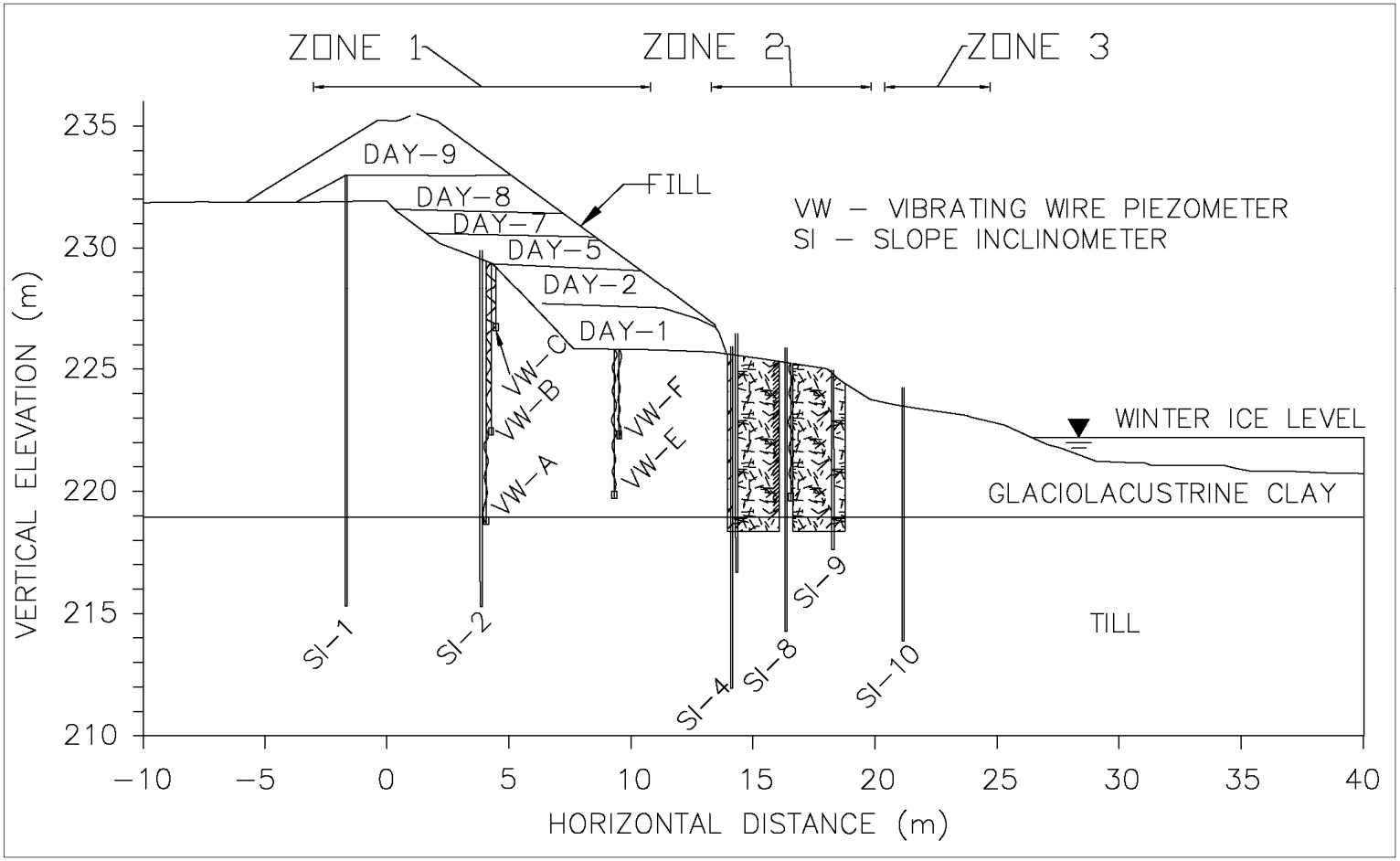


Figure 6.3. Select instrumentation and instrumentation zones at the research test site.

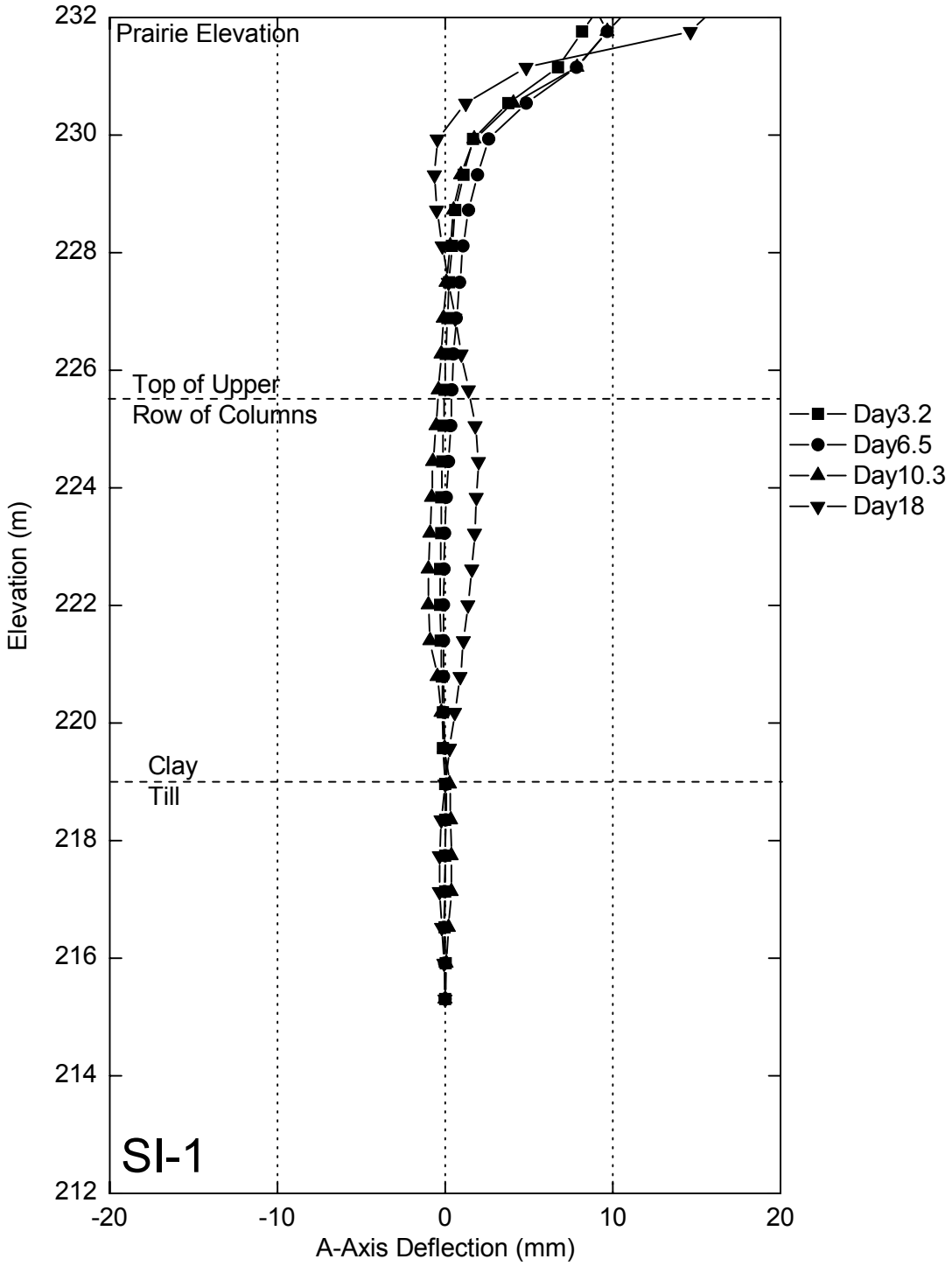


Figure 6.4. SI-1 deflections during the field test. Back from crest of slope.

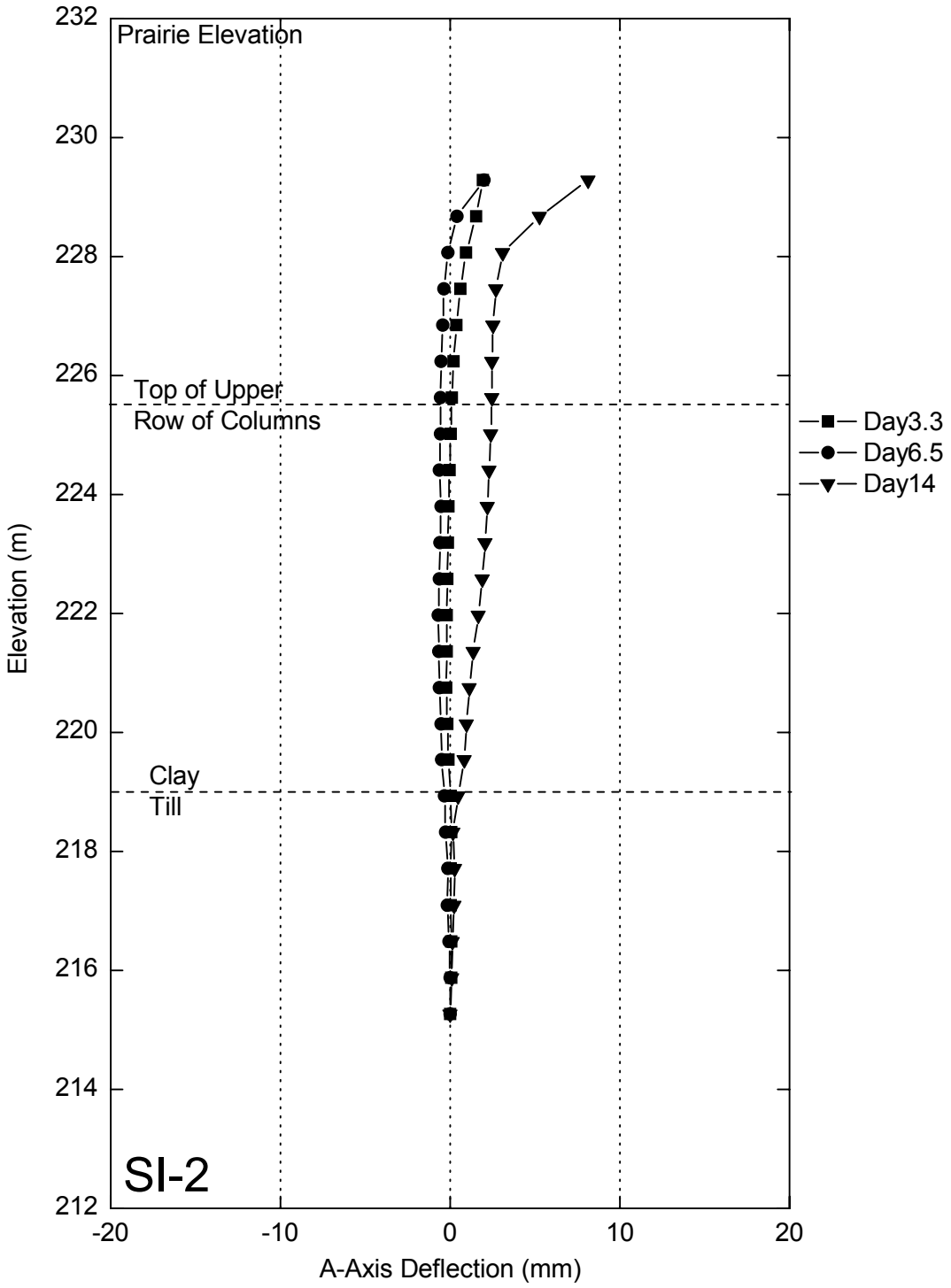


Figure 6.5. SI-2 deflections during field test. Downslope from crest.

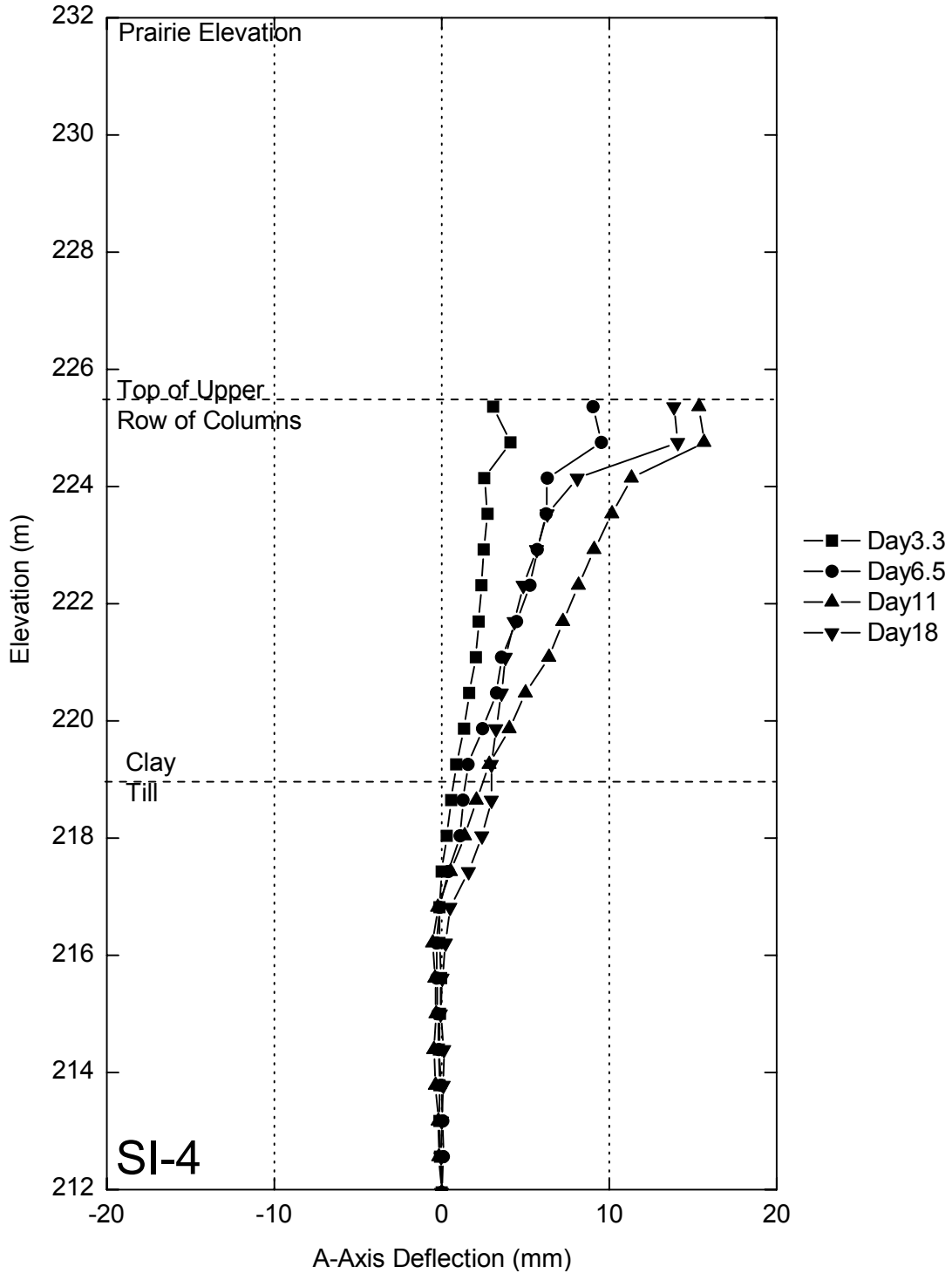


Figure 6.6. SI-4 deflections during field test. Installed between rockfill columns in upper row.

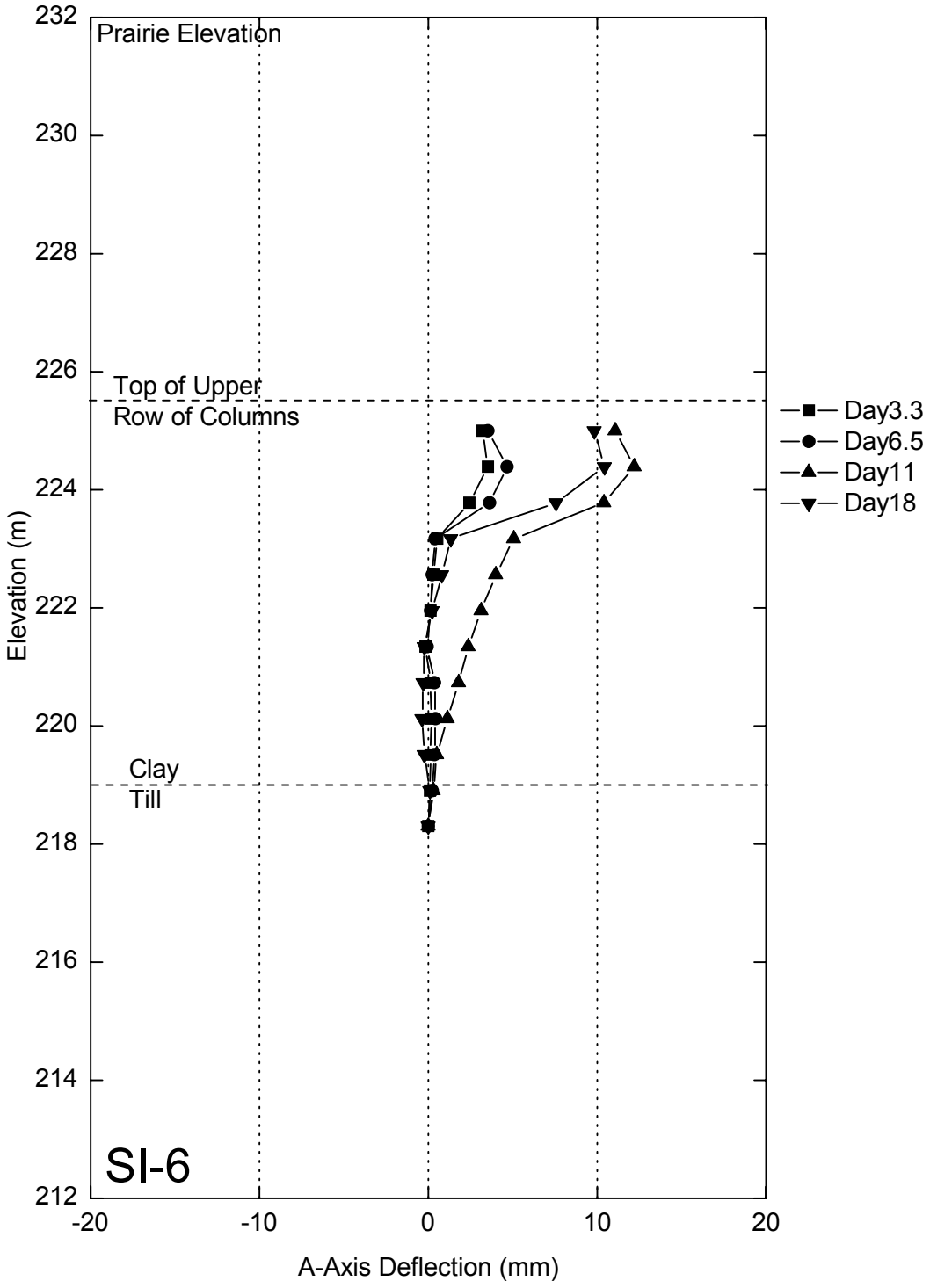


Figure 6.7. SI-6 deflections during field test. Installed in a column in upper row.

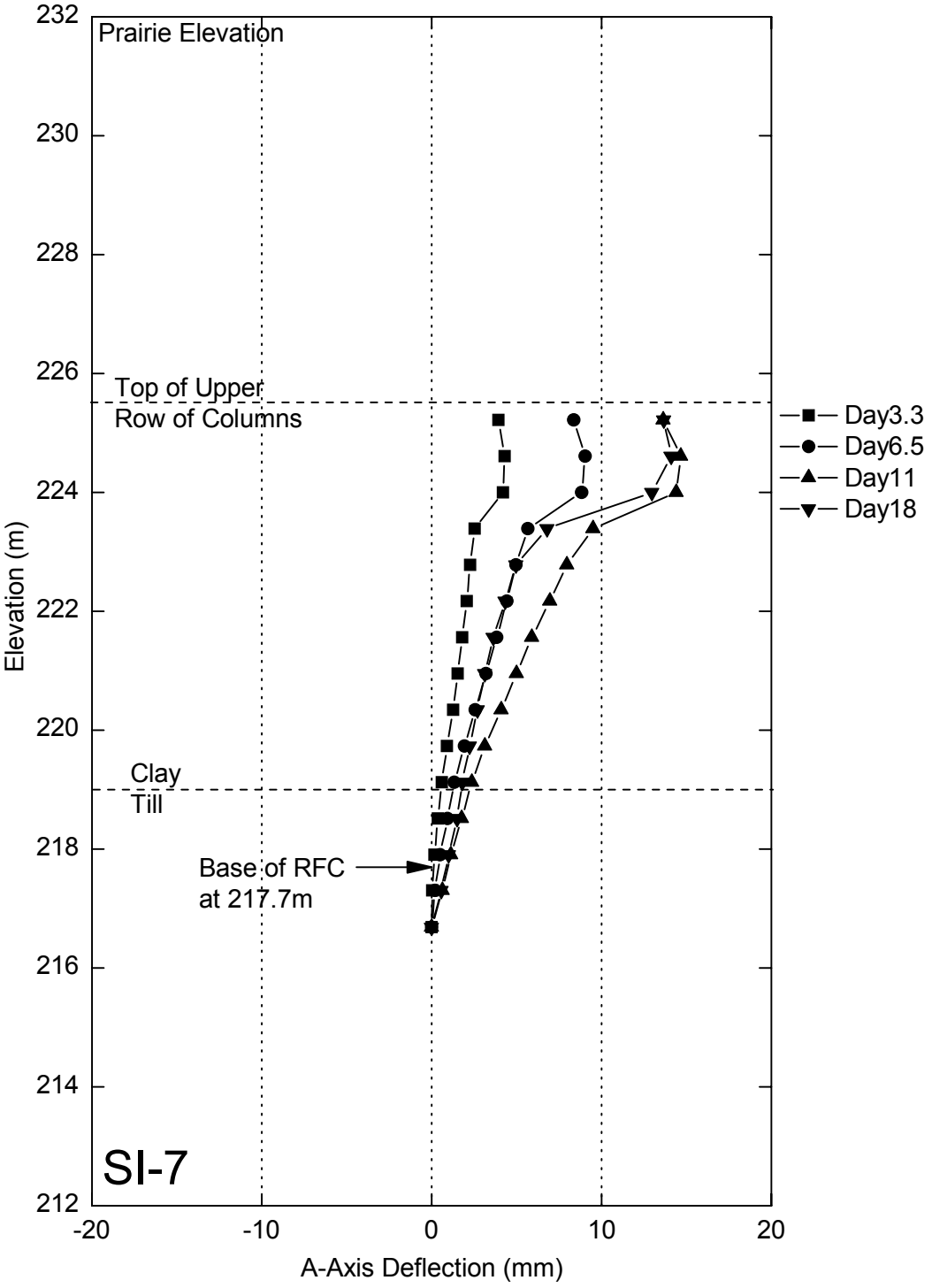


Figure 6.8. SI-7 deflections during field test. Installed directly in a rockfill column in the upper row.

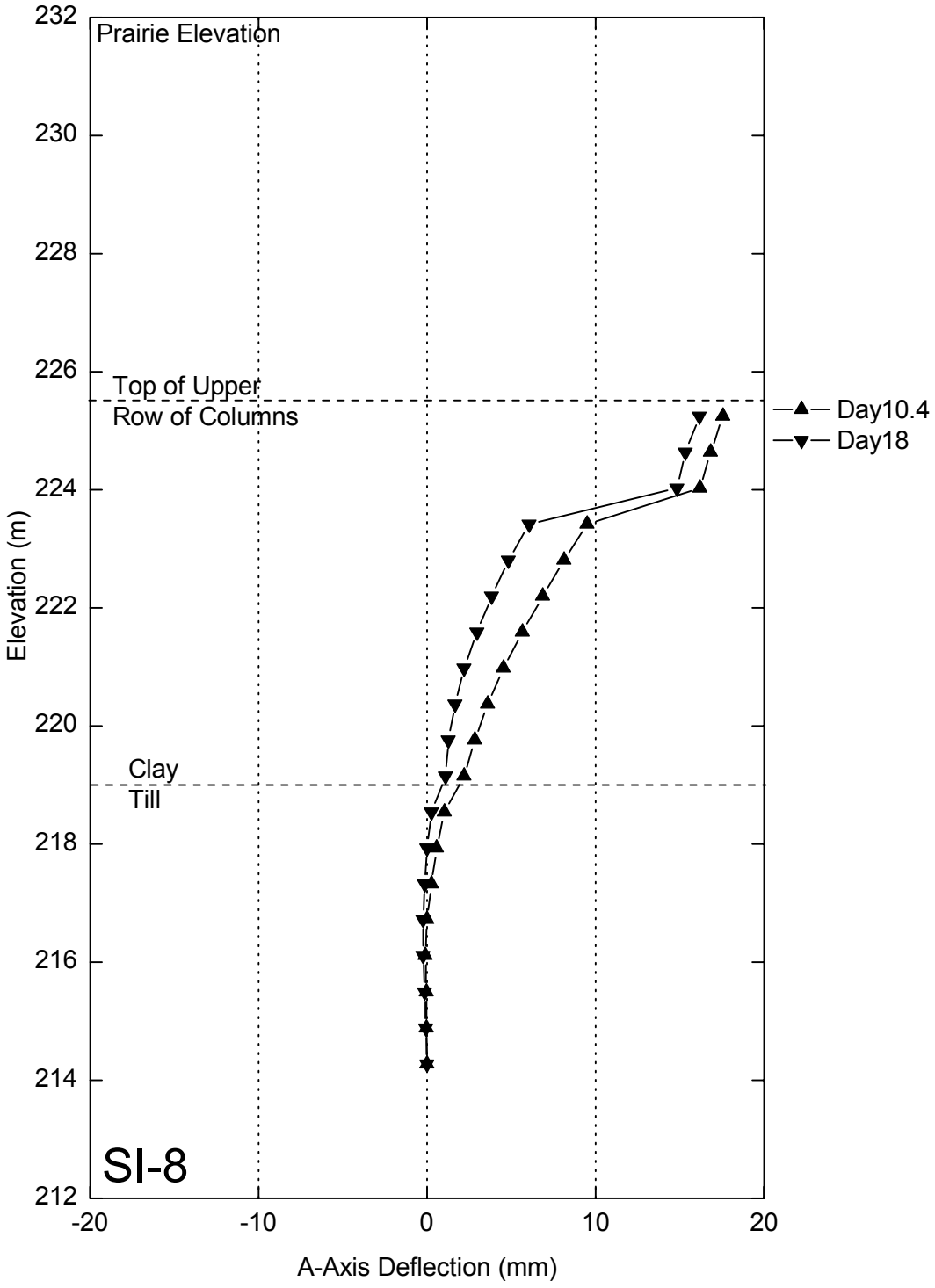


Figure 6.9. SI-8 deflections during the field test. Installed between rows of rockfill columns

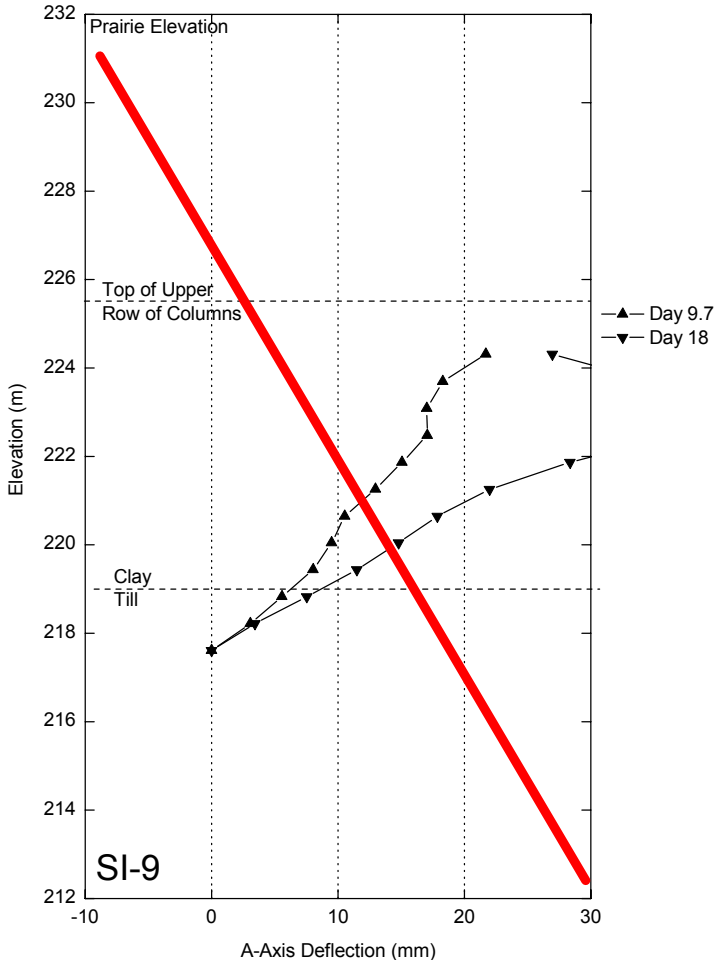


Figure 6.10. SI-9 deflections during the field test. Installed in column in lower row. Readings are erroneous due to shifting of casing during removal of in-place inclinometers.

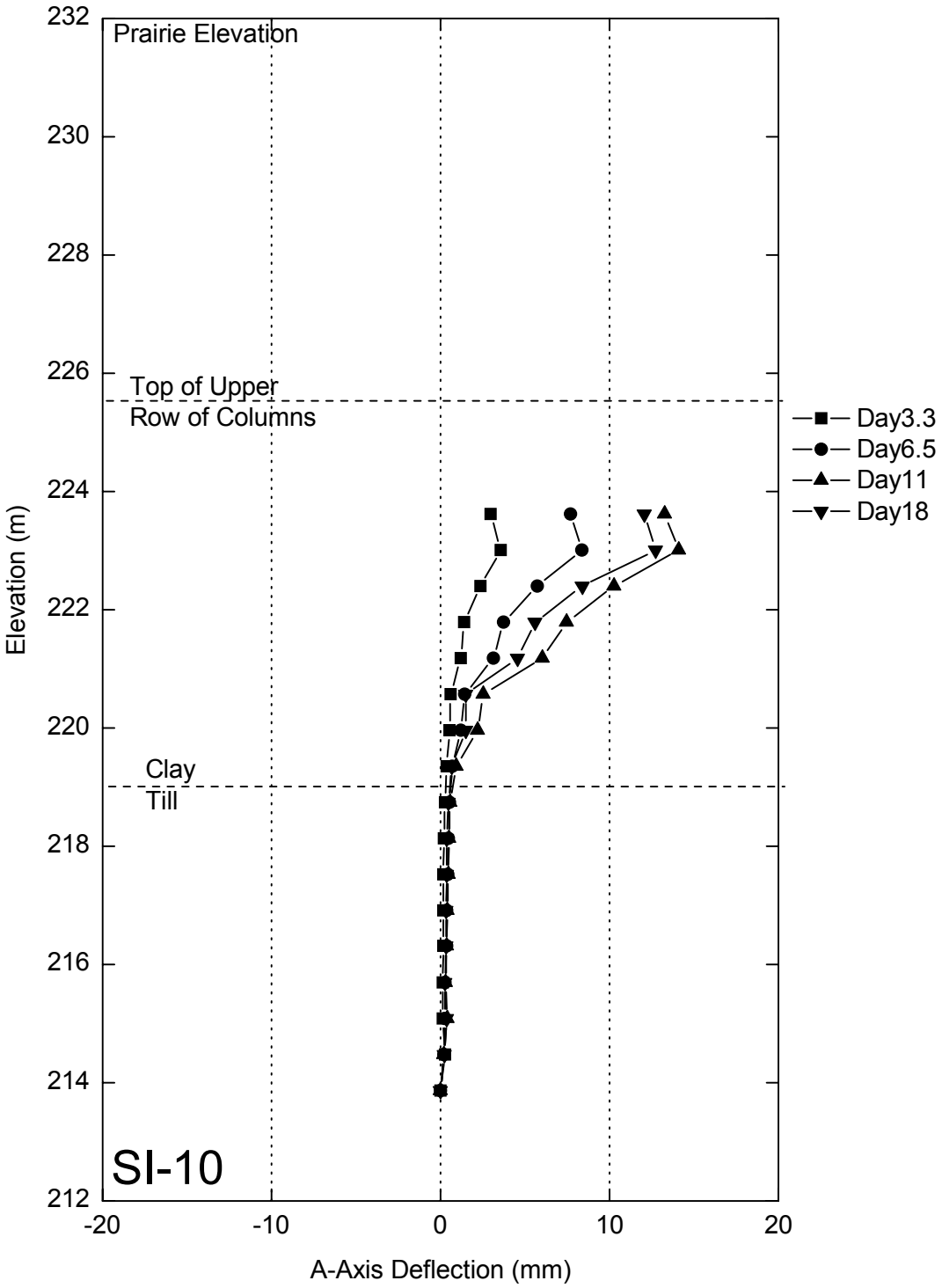


Figure 6.11. SI-10 deflections during the field test. Installed downslope of columns.

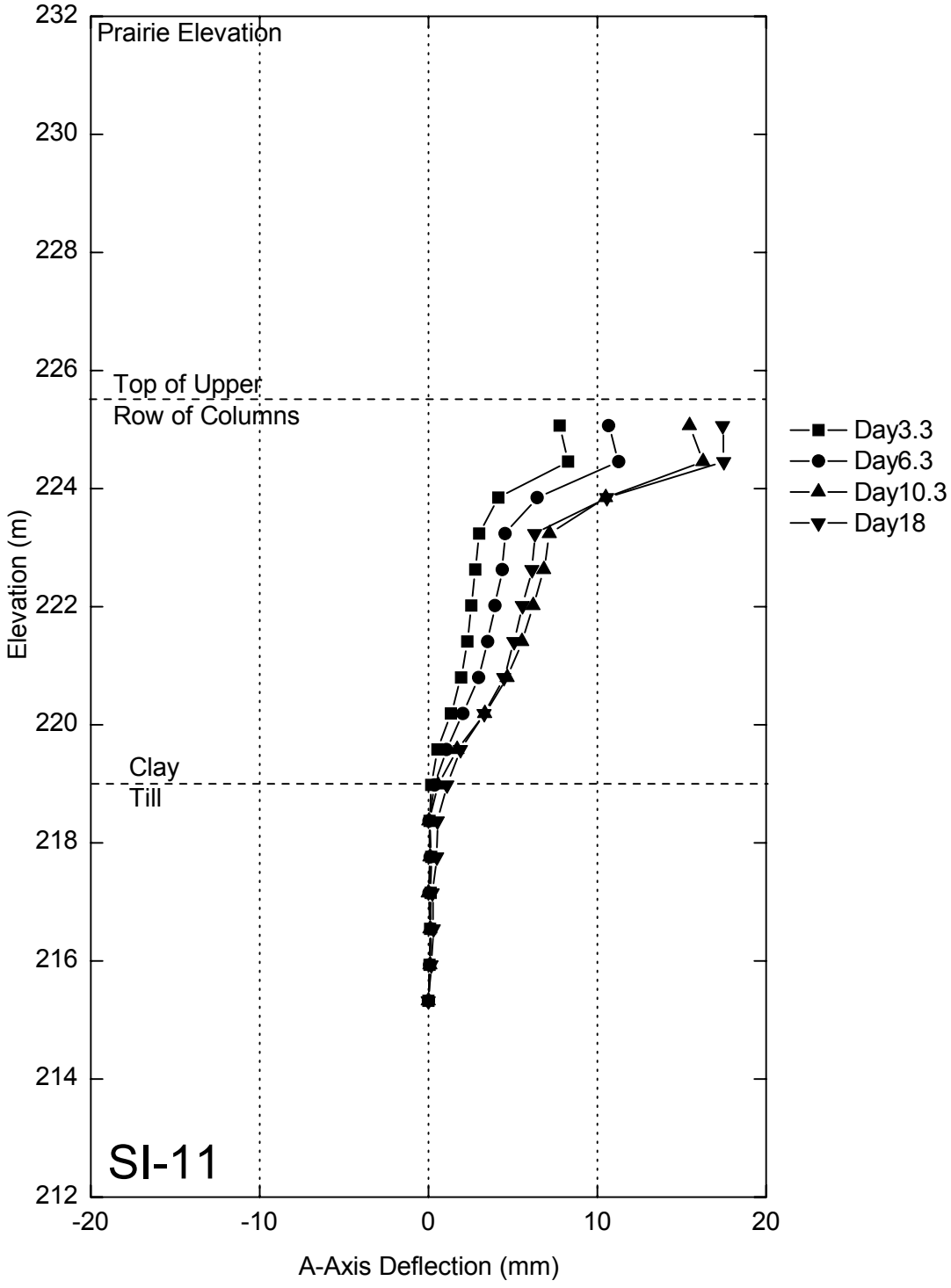


Figure 6.12. SI-11 deflections during the field test. Installed near downstream edge of test site, between rows of columns.

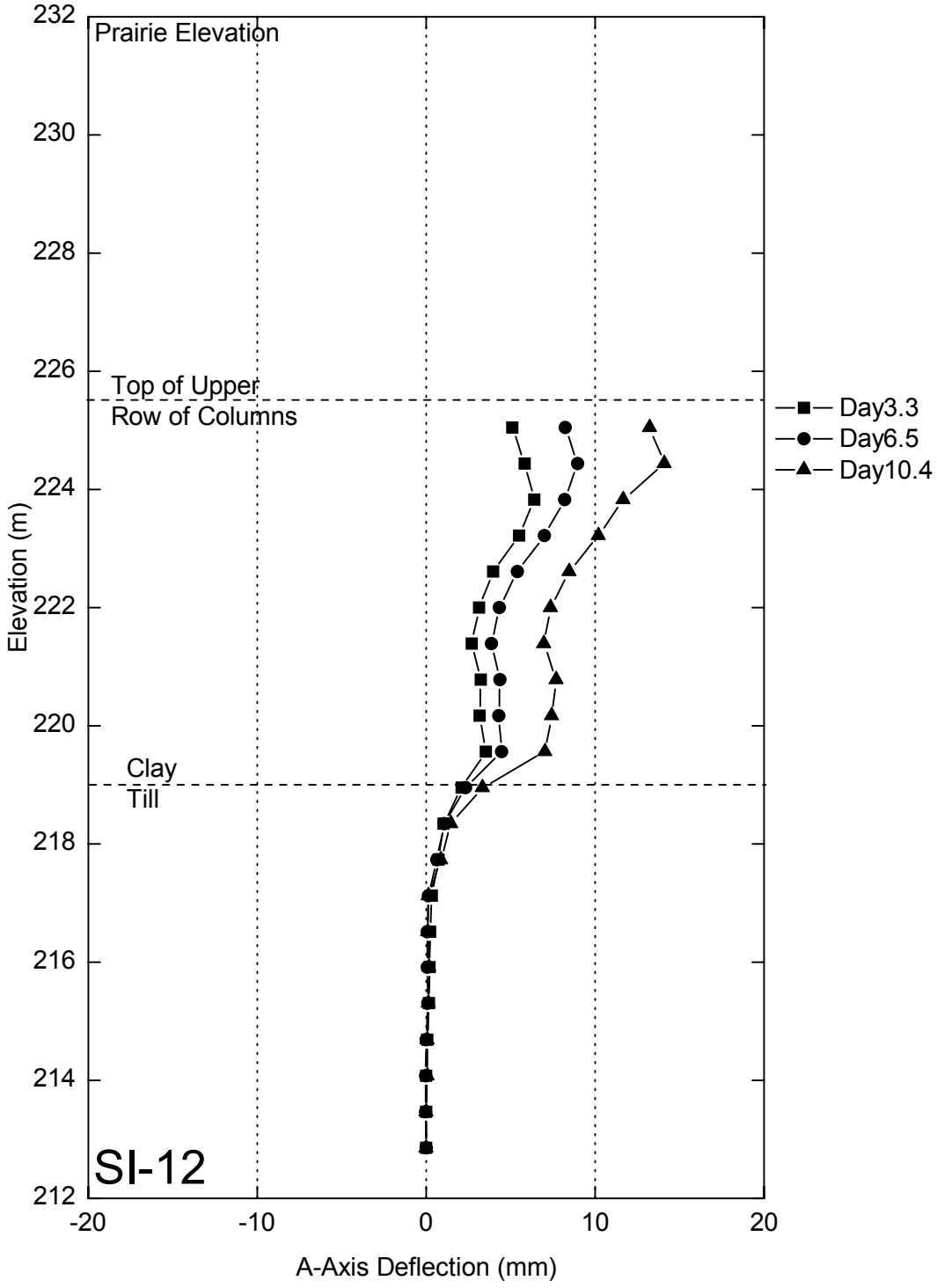


Figure 6.13. SI-12 deflections during the field test. Installed near upstream edge of test section, upslope of columns.

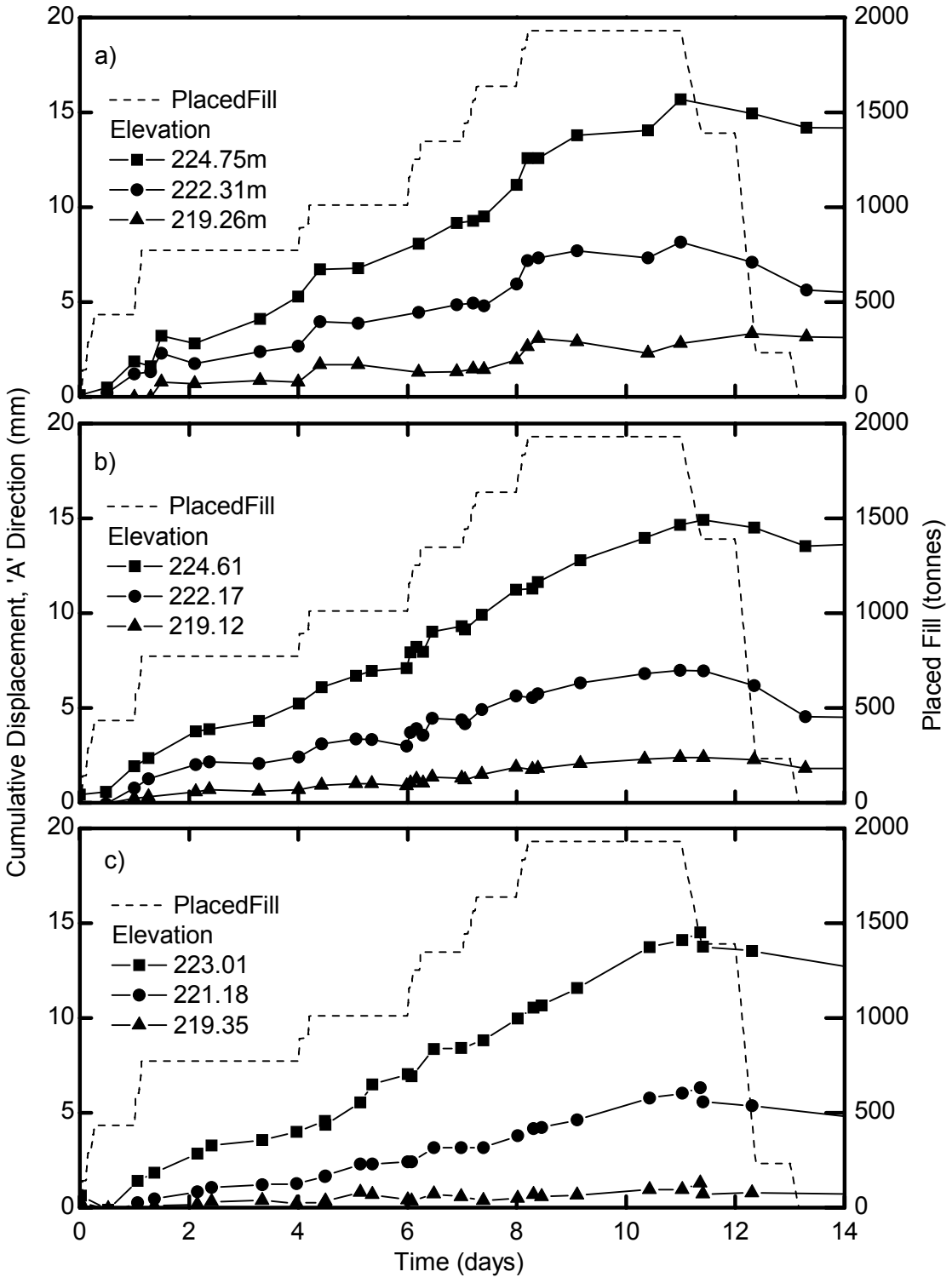


Figure 6.14. Cumulative displacement vs. time at specified elevations for a) SI-4 and b) SI-7 and c) SI-10

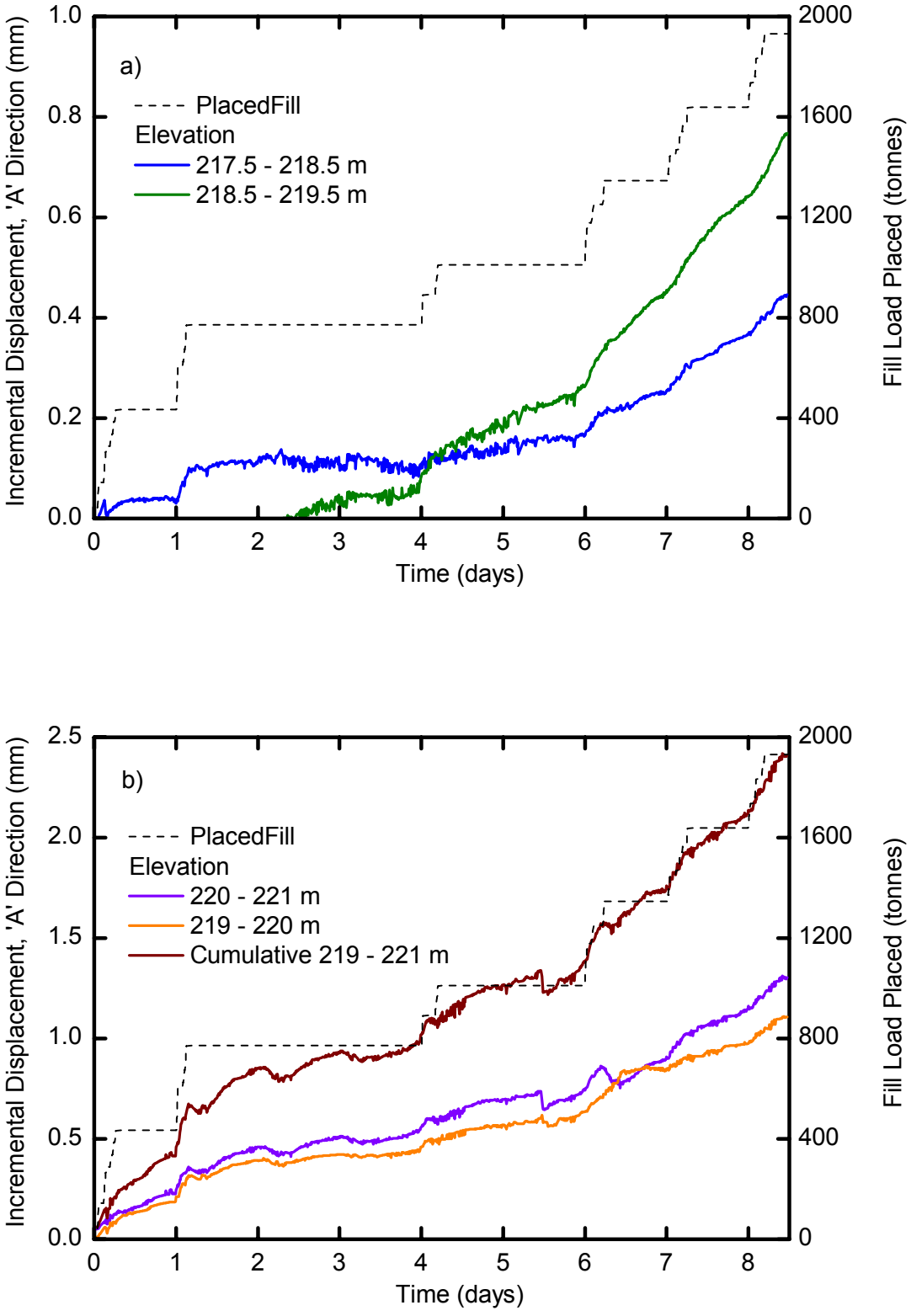


Figure 6.15. Incremental displacement measured by in-place inclinometers in a) SI-8 (note: IPI 218.5-219.5 inoperable before day 2.5) and b) SI-9.

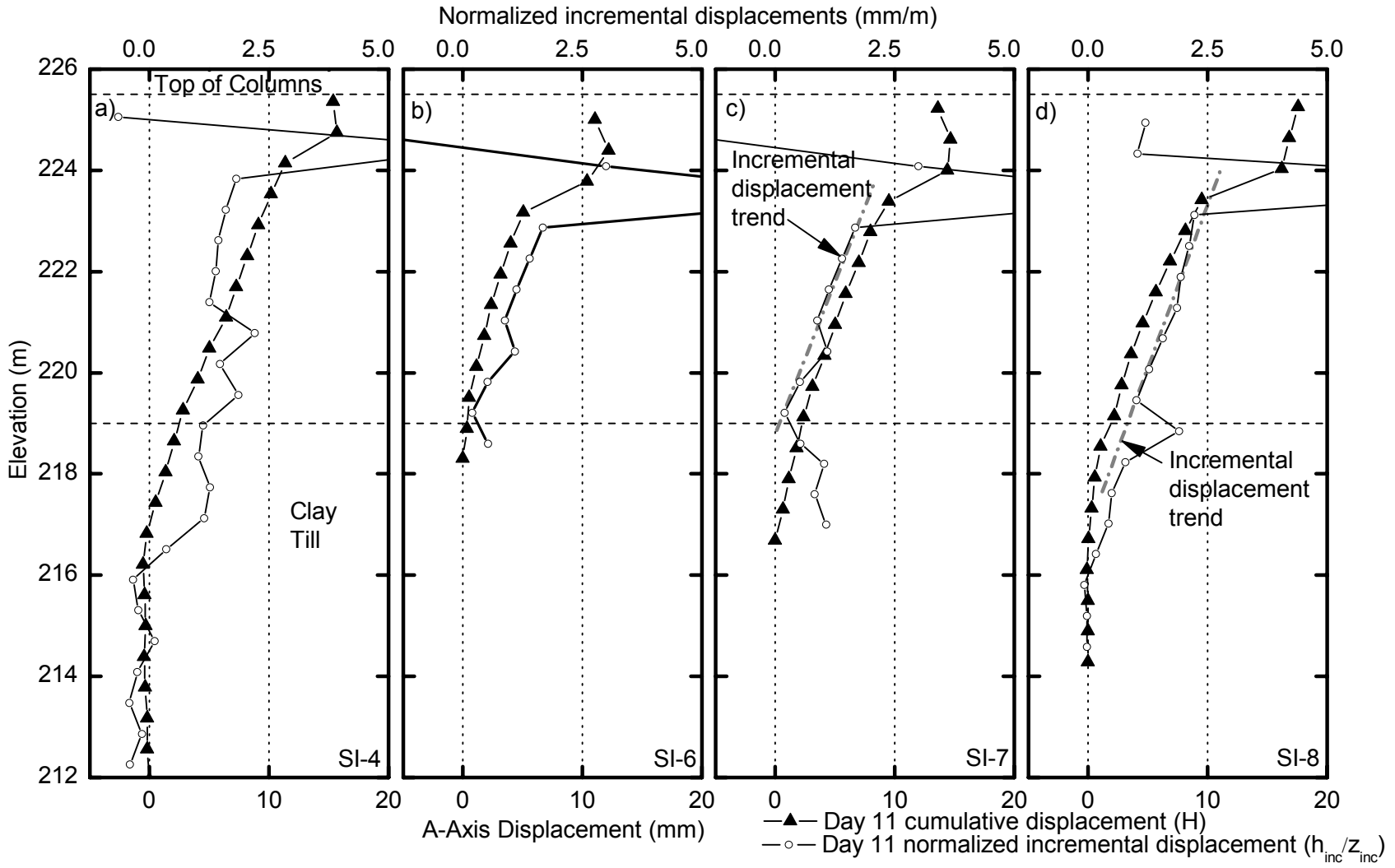


Figure 6.16. Cumulative displacements and normalized incremental displacements for a)SI-4, b)SI-6, c) SI-7, d) SI-8.

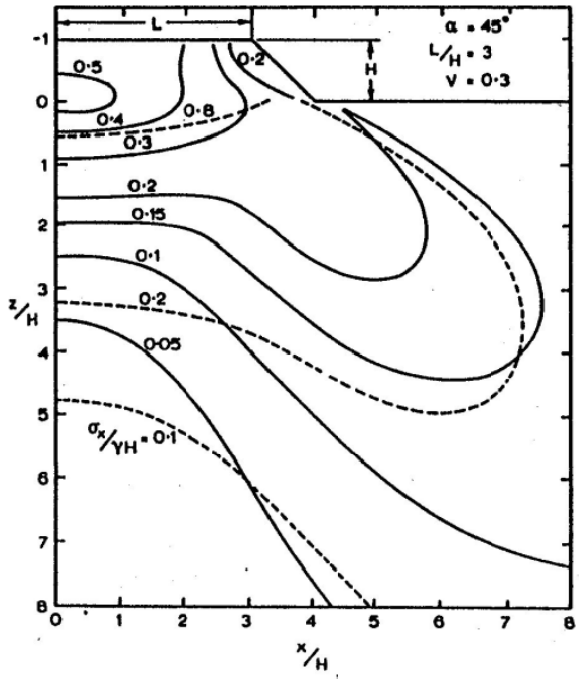


Figure 6.17. Contours of horizontal stress $\sigma_x$ beneath an embankment. After Poulos and Davis (1991). Reproduced with permission from Poulos, April 2010.

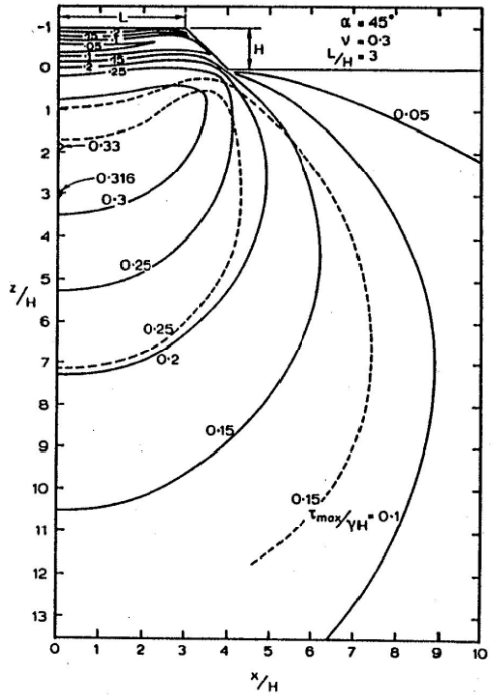


Figure 6.18. Contours of maximum shear $\tau_{max}$ beneath and embankment. After Poulos and Davis (1991). Reproduced with permission from Poulos, April 2010.

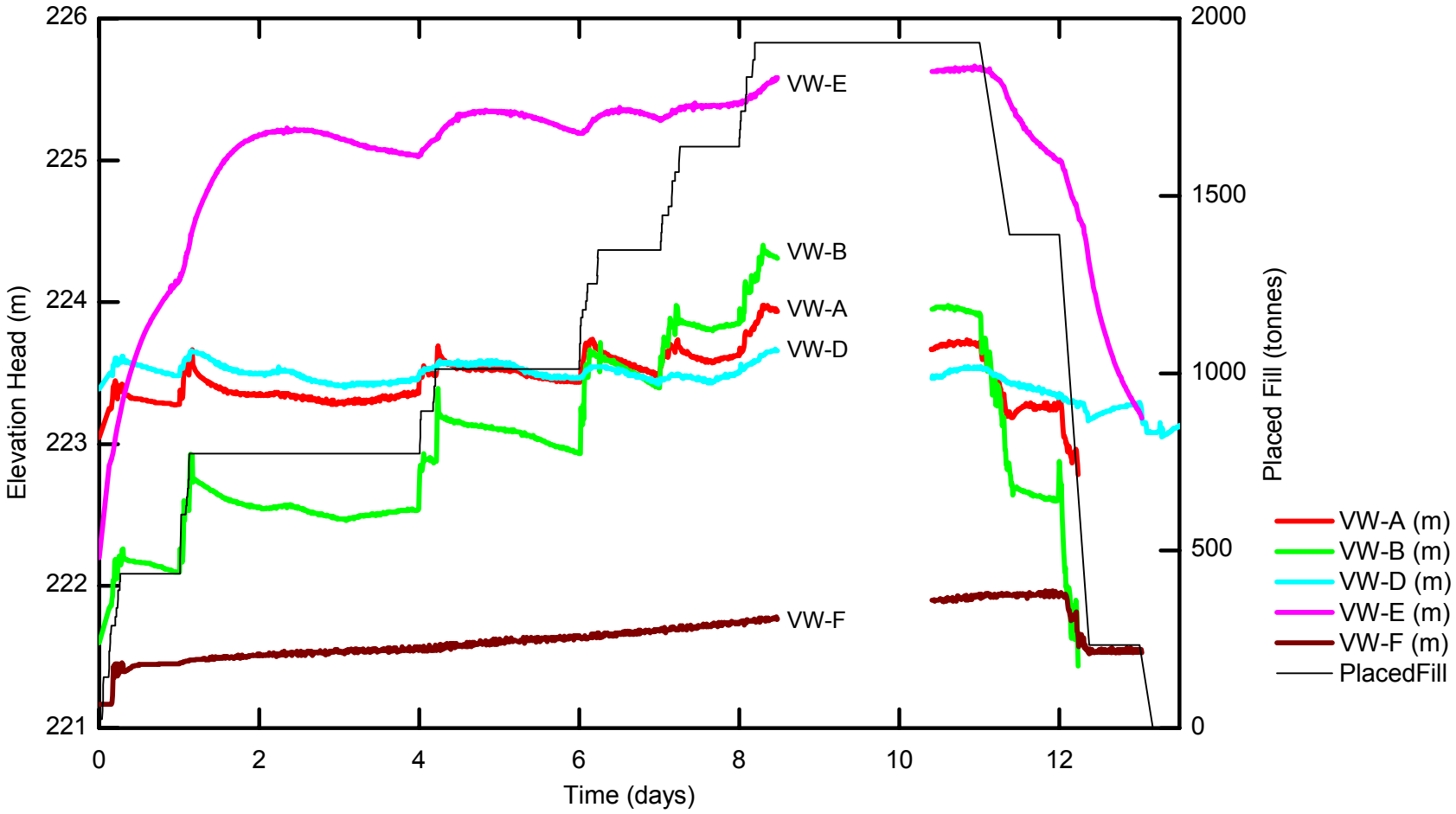


Figure 6.19. Porewater pressure response to loading and unloading

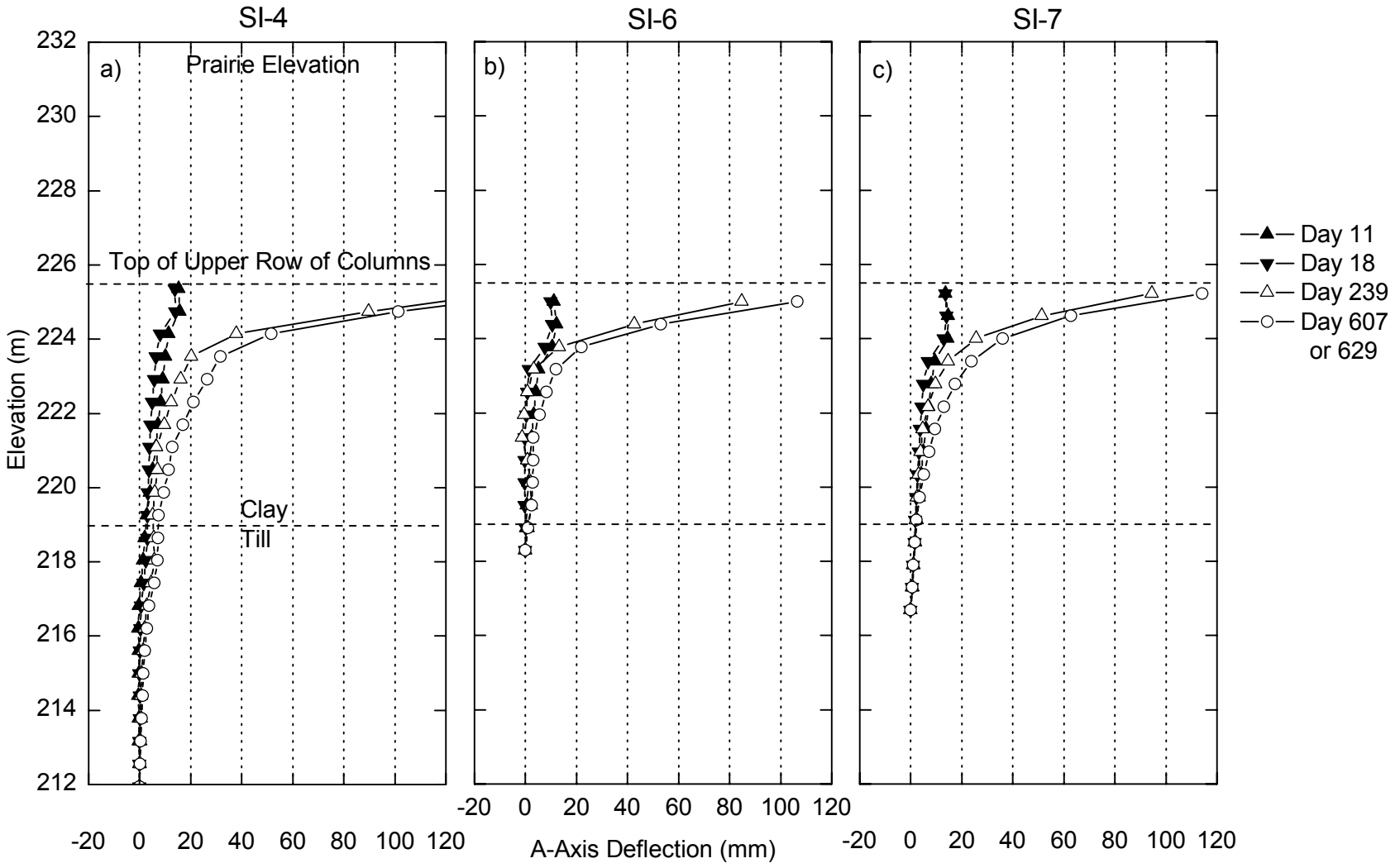


Figure 6.20. Displacements measured after test loading a) SI-4, b) SI-6, c) SI-7

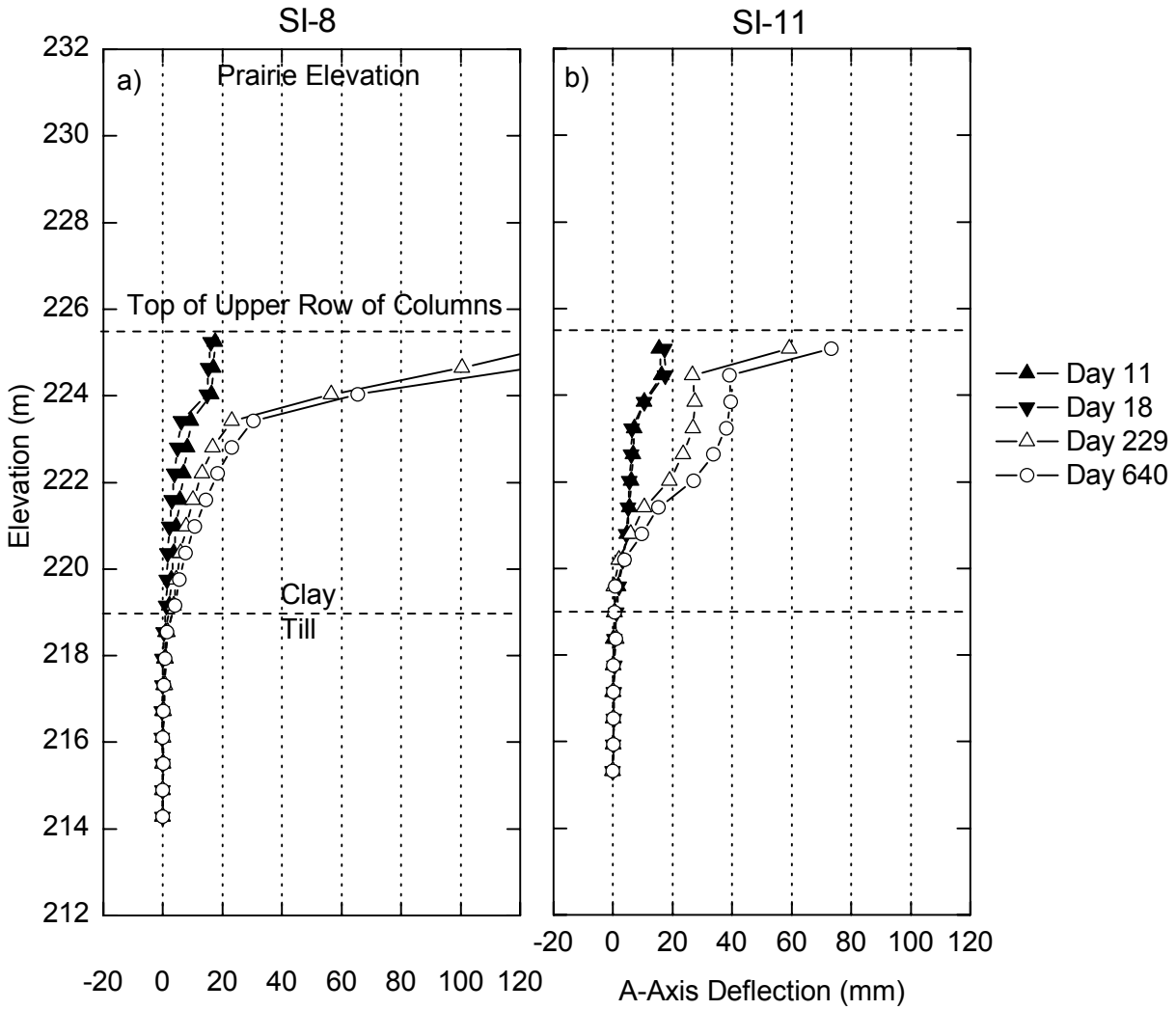


Figure 6.21. Displacements measured after test loading a) SI-8, b) SI-11

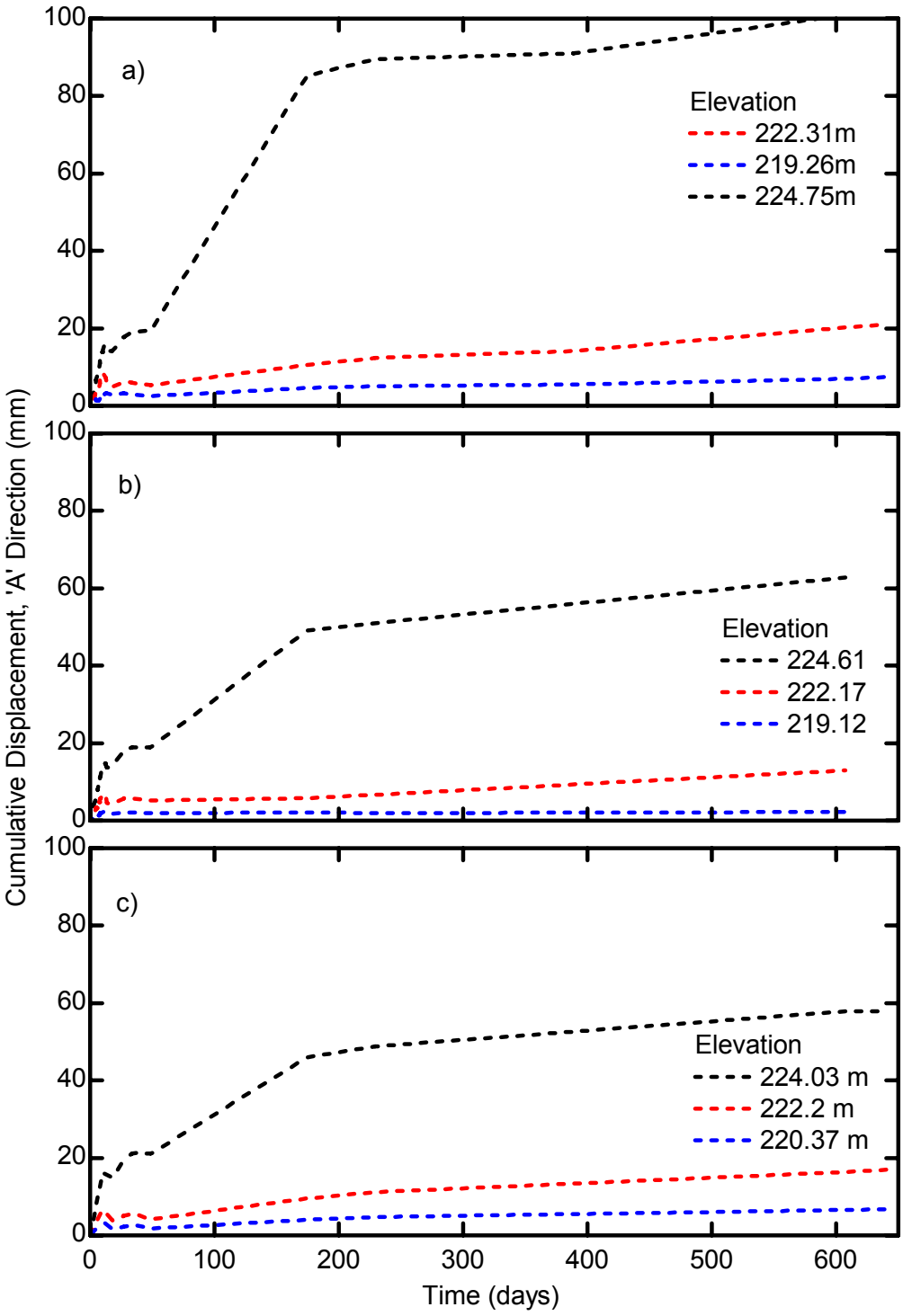


Figure 6.22. Dispacement plotted against time at select elevations for a) SI-4, b) SI-7, and c) SI-8.



Figure 6.23. a) Locations of cracking at test site on day 10 of testing b) crack at crest near centerline of test section

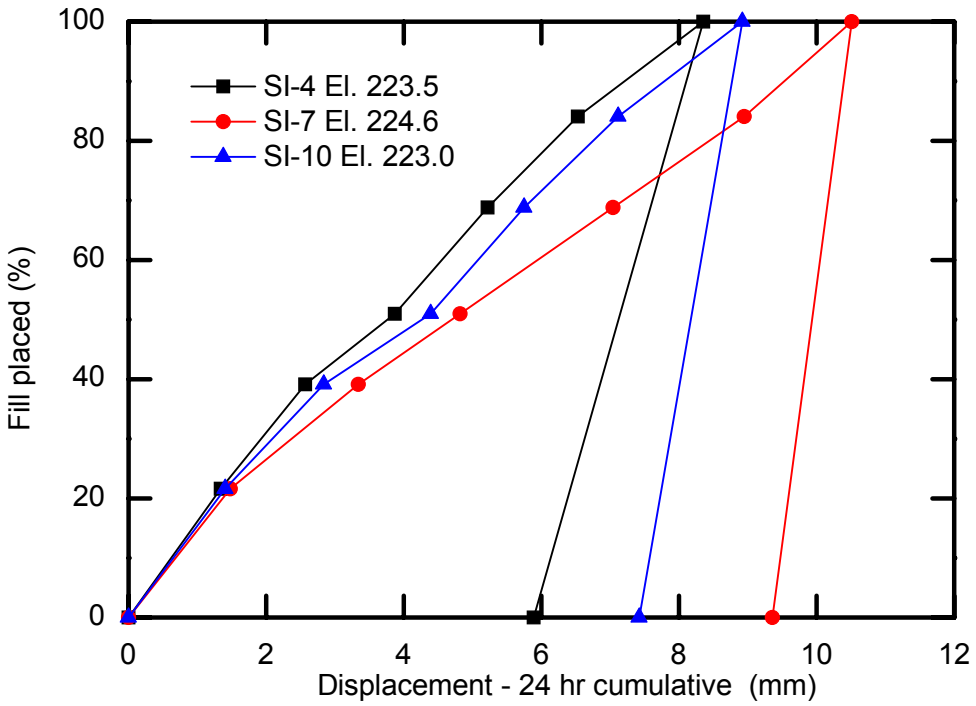


Figure 6.24. Percentage of total fill placed versus cumulative displacement, including unload.

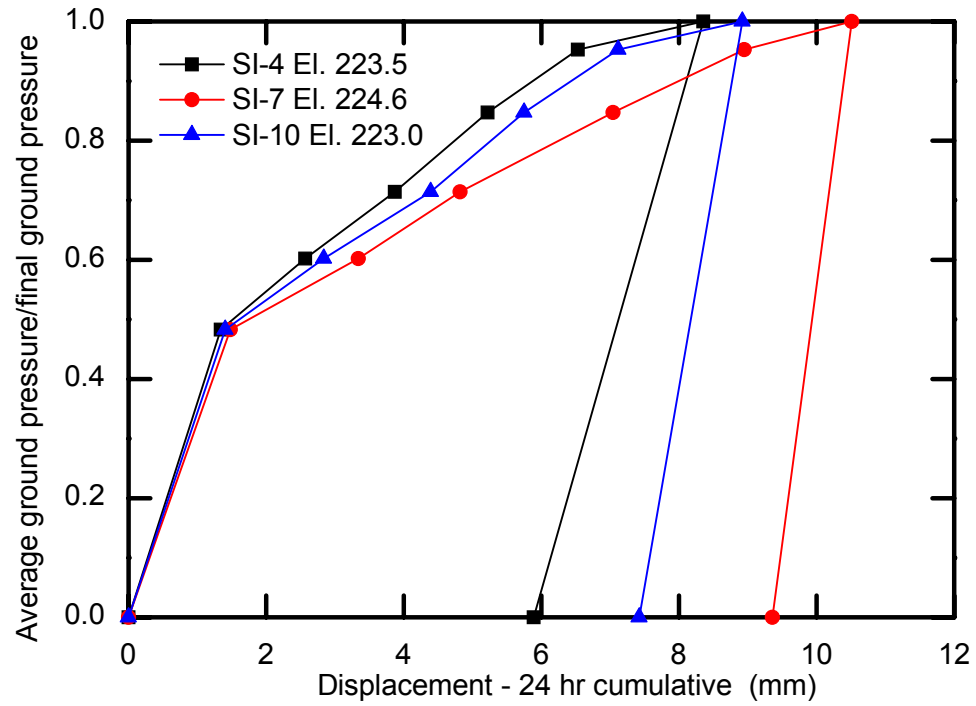


Figure 6.25. Normalized average ground pressure due to fill plotted against displacement

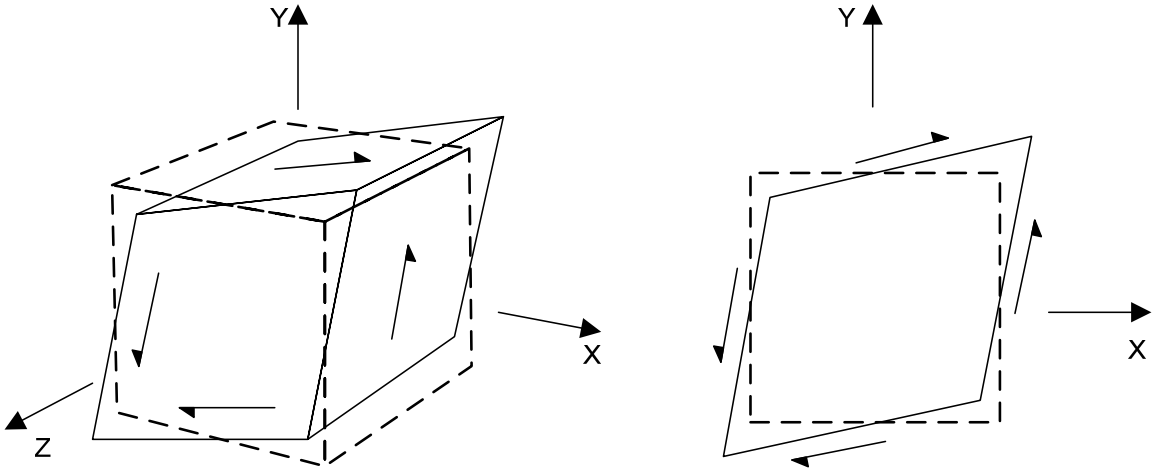


Figure 6.26. Stress deformation of an element.


Figure 6.27. Dry sand sample under vacuum pressure, subjected to approximately 20 N cantilever load.

# 7. ANALYSIS AND NUMERICAL MODELING

## 7.1 Introduction

The objective of the numerical model development was to calibrate the measured response to the test loading in order to identify performance characteristics that contribute to the understanding of rockfill column behaviour. The analysis that is presented in this chapter is considered a type C1 prediction, or more accurately, an autopsy, as defined by Lambe (1973): a prediction of behaviour made after an event, with the knowledge of the results. Lambe (1973) notes that:

> "Autopsies can of course be very helpful in contributing to our knowledge. However, one must be suspicious when an author uses type C1 predictions to 'prove' that any prediction technique is correct."

Keeping this in mind, this chapter presents a number of models and interpretations, with the understanding that none of them are perfect. The strengths and weaknesses of various ideas and methods are discussed as applicable. In this chapter the results of the numerical analysis are used to illustrate behaviours of the stabilized slope that are not apparent by only considering the data presented in the previous chapters. The models are then used for sensitivity analysis to investigate the contributions of various material parameters and boundary conditions.

There are very few "knowns" in geotechnical modeling, even in a type C1 autopsy. In this project, the surface geometry, horizontal displacements at

inclinometer locations, and porewater pressures at piezometer locations are known with reasonable certainty. Material properties, boundary conditions, and in-situ conditions are assigned with some level of uncertainty regarding the actual values.

Over the course of the project, a large number of models were produced using varying methods, conditions and parameters. The following sections focus on four models which are believed to reasonably replicate the full-scale field test, and demonstrate the contribution of rockfill columns to the stability of reinforced slopes. It would be impractical and of limited benefit to report the full breadth of the numerical modeling investigation, some of which was more successful than others. The models presented each have some key differences that highlight the influence of various ground conditions. Table 7.1 summarizes the four models that are discussed in detail.

- Case 1: Linear elastic (LE) analysis with no in-situ stress development, or porewater pressure dissipation.

- Case 2: Coupled consolidation with the clay modeled by an elastic-perfectly plastic (EPP) constitutive relationship, and the rockfill modeled by a hyperbolic (HB) constitutive relationship. The rockfill and clay are both modeled with a unit weight of 17 kN/m$^3$.

- Case 3: Coupled consolidation with the clay modeled by the modified Cam-Clay (MCC) formulation. Advanced $K_0$ analysis was used to develop in-situ stresses. Dense rockfill is modeled with a unit weight of 22 kN/m$^3$.

Interface elements are used to isolate the equivalent strips for in-situ stress development (refer to Chapter 2 for a discussion on modeling rows of columns with equivalent strips).

- Case 4: Based on Case 2, except that interface elements are introduced at elevation 223.7 m (corresponding to the bottom of the loose rockfill) to help simulate the larger shallow displacements reported by inclinometers. A Poisson's ratio of 0.33 is applied to clay, which decreases overall displacements.

The focus of the discussion is on stress-deformation modeling, but some stability analysis results are presented briefly. Slope stability modeling, using limit equilibrium based methods, is an important aspect of the design process for stabilizing slopes with rockfill columns. Some comments and recommendations regarding stability analysis are provided at the end of the chapter.

This document does not comment in a general way on the various constitutive models or modeling techniques except where non-standard methods were used, or where it is specifically relevant to the analysis. All modeling was done with the GeoStudio suite of software from Geo-Slope International Ltd[1]. The Sigma/W, Seep/W and Slope/W components were used for stress-deformation, seepage and slope stability analysis respectively. The three components are integrated; the Sigma/W and Seep/W solvers are used simultaneously for coupled consolidation analysis, and Slope/W can import stresses from Sigma/W and

[1] GeoStudio 2007 (Version 7.16 build 4840) Geo-Slope International Ltd. Calgary, AB, Canada

porewater pressures from either Seep/W or Sigma/W. The reference books included with the suite of software were used extensively throughout the modeling process (Geo-Slope International Ltd. 2010a, 2010b, 2010c).

## 7.2 Model development

### 7.2.1 Cross sections

The ground surfaces used in the numerical modelling were created from the site surveys completed at various stages of the project. Figure 7.1 shows a typical cross section used in the numerical modeling of the test loading.

The daily three-dimensional surveys of the fill were used to develop cross sections representing the appropriate mass of placed fill for each day. Therefore the daily fill regions in the model do not accurately reflect the geometry of the surveyed cross section at a specific time. For this reason, the modeled fill is not as high as the actual placed fill (when comparing Figure 7.1 with Figure 5.3, for example) because the maximum height of the fill did not extend across the entire test section due to the fill slopes.

The stratigraphy used in the numerical models is simplified, using only one layer of clay in deformation analyses, and two layers for seepage analyses and in-situ stress development. The upper complex zone was not modeled because of the relatively small thickness and inconsistency of the layer. The loose upper till was modeled separately from the denser till below for stress-deformation analysis.

### 7.2.2 Clay

This section discusses the development of the material parameters to be assigned to clay units in the model, with the understanding that the focus of the research is on the rockfill columns, and that the properties of Lake Agassiz clay have been extensively studied and used in numerical analysis by others (Chapter 2 and 3). The measured material properties discussed in Chapter 3 are used as the basis for assigning material parameters for use in the analysis. However, as demonstrated in Chapter 2 and Chapter 3, there is significant natural variation of soil properties and one must anticipate that overall site conditions will differ from the results obtained in the laboratory. The elastic-perfectly plastic (EPP) and modified Cam-Clay (MCC) parameters for the clay units are summarized in Table 7.2 and Table 7.3 respectively.

A Poisson's ratio of 0.4 was used for clay regions in Case 1, Case 2 and Case 3 scenarios as an assumption. This value is not based on testing results specific to this project. The calculated ratio from triaxial test results varied from 0.1 to 0.4. A Poisson's ratio of 0.4 for Lake Agassiz clay was used in numerical modeling by several researchers and practitioners including Anderson et al. (2004) Kim (2007) and Skaftfeld et al. (2009).

Based on references presented in Section 2.3, the strength of the in-situ clay upslope of the rockfill columns is assumed to be reasonably defined by the post-peak strength. The zone of clay downslope of the columns was assigned a shear strength envelope corresponding to the measured residual strength. This

can be justified by the significant soil movements observed in 2006 and 2007 in this area.

The brown and grey clay layers were modeled as a single unit for stress-deformation analysis. The brown and grey clay layers have the same origin and composition and the laboratory testing showed that the post-peak strengths are reasonably approximated by a single shear strength envelope, as discussed in Chapter 2. The laboratory test results show conflicting measurements of stiffness; the triaxial results indicate that the upper brown clay is stiffer, while one-dimensional consolidation and direct shear test results indicate that the lower grey clay was stiffer[2]. On balance, it was decided that there was no reason to differentiate the layers based on the elastic modulus.

An elastic modulus (E) of 20,000 kPa was used in the analysis presented in this chapter. This value is close to the initial tangent modulus (Table 3.1) evaluated from triaxial test results, and is significantly larger than the secant modulus (Table 3.1). In the stress deformation scenarios, most elements are strained very little (less than 0.5%) and using the initial tangent modulus is a reasonable assumption. The consequence is that the strains of elements that undergo large stress-increments are underestimated.

[2] The various measures of stiffness are not equivalent. The triaxial tests were undrained (providing $E_u$), while the direct shear and one-dimensional consolidation tests were drained. The direct shear test provides a poorly controlled measure of the shear modulus (G), and the one-dimensional consolidatation test provides the constrained elastic modulus ($E'_c$).

#### 7.2.2.1 Modified Cam Clay

The Modified Cam Clay model, used in the Case 3 analysis, was developed from the laboratory measured clay properties. The constitutive properties used in this project compare well with those developed for other MCC models of Lake Agassiz clay (Anderson et al. 2004, Van Helden et al. 2008).

The compression and unload-reload indices, lambda (λ) and kappa (κ) were calculated from $C_c$ and $C_r$ respectively, measured by the one-dimensional consolidation tests, according to:

$$\lambda = \frac{C_c}{\ln(10)} = 0.434\ C_c \qquad 7.1$$

And

$$\kappa = \frac{C_r}{\ln(10)} = 0.434\ C_r \qquad 7.2$$

The initial void ratio ($e_0$) at p'=1 was calculated as 2.64. The slope of the volumetric water content function in a saturated state, $m_v$, is related to elastic modulus E by:

$$m_v = \frac{1}{E} \qquad 7.3$$

The method proposed by Van Helden et al. (2008) was used to determine the appropriate value of $m_v$ to minimize numerical incompatibility at the depth where the largest strains occurred (immediately above the clay-till interface).

The application of the MCC model to the full-scale field test has limitations. The MCC model was developed for saturated soils without consideration for more advanced techniques of calculating unsaturated soil strength, such as the methodology proposed by Vanapalli et al. (1996). The soil above elevation ±222 m was unsaturated, and as a result had negative porewater pressures at the start of the field test. Establishing a reasonable distribution of in-situ stresses with appropriate preconsolidation pressures is necessary for the effective application of the MCC model; unfortunately, the stress-state of soil in a riverbank is difficult to measure, predict or replicate as it is influenced by a history of deposition, weathering, unloading, shearing and possibly failure.

It was still considered valuable to model the field test using the MCC model for the clay. The clay layers were assigned overconsolidation ratios (OCR) to allow calculation of preconsolidation pressures by the software. The layer of brown clay, above elevation 224 m, was assigned an OCR of eight and the grey layer an OCR of three. The assigned value of OCR for the upper brown clay layer was lowered from the measured value of 13 from consolidation tests. An OCR of 8 was more representative of the expected OCR directly beneath the fill at approximately 225.5 m (Figure 3.12). An OCR of 8 is also more in line with the OCR's used in other numerical analyses of local clays, using the MCC model (for example Van Helden et al. (2009) or Anderson et al. (2004)). In the MCC model, the clay is assigned a critical state (post-peak) friction angle but elements can be stressed beyond this critical state line if the stress state remains within the elliptical failure surface defined by the preconsolidation pressure. The implication

is that, when using the MCC model, yielding in an element initiates at a different stress state than if the EPP formulation were used. The MCC formulation is thought to be a better predictor of actual clay behaviour in this regard, though it is known to underestimate strain softening behaviour.

### 7.2.3 Rockfill

The author has not conducted any testing of rockfill material, but has gathered available data, primarily from Abdul Razaq (2007), Kim (2007) and Alfaro et al. (2009), in order to develop appropriate constitutive and strength relationships for use in numerical analysis. A strength envelope based on Maksimovic (1996), and a hyperbolic constitutive model based on Duncan and Chang (1970) have been developed. Some additional interpretation, including extrapolation of trends, was required to develop these relationships from the available data because there was not an opportunity to conduct supplementary testing.

#### 7.2.3.1 Failure envelopes for rockfill

Abdul-Razaq (2007) (shown in Figure 2.2) and Kim (2002) present alternative interpretations of the peak strength of rockfill. Abdul-Razaq (2007) presented peak strengths estimated from hyperbolic curves fitted to the data. Kim (2007) estimated the peak shear strength from the transition friction angle and dilation angle (ψ) according to (Budhu 2000):

$$\tau = \sigma_n \tan^{-1}(\Phi'_{transition} + \Psi) \qquad 7.4$$

The dilation angle was evaluated by Kim, from the results of the large scale direct shear tests according to (Budhu 2000):

$$\psi = \tan^{-1}\left(\frac{-\Delta z}{\Delta x}\right) \qquad 7.5$$

The shear strengths presented by Kim (2007) are more conservative than those presented by Abdul-Razaq (2007).

It is useful to have a relationship to describe the shear strength as a function of confining pressure, knowing that the peak strength of granular materials is not adequately defined by a single friction angle (Section 2.4). Figure 7.2 shows failure envelopes developed to fit the test results of Abdul Razaq (2007) and UMA Engineering Ltd. (1992) using Equation 2.1 from Maksimovic (1996). A "basic friction angle" ($\phi_B$) of 37°, equal to the transition friction angle from Abdul-Razaq (2007), was used to develop the Maksimovic failure envelopes. A "median angle normal stress" ($p_n$) of 276 kPa was evaluated for the dense envelope and $p_n$ of 75 kPa was evaluated for the loose envelope. The median angle normal stress is the normal stress at which the secant friction angle is the average (or median) of the friction angle at a normal stress of zero and the base friction angle. These values were determined according to the method outlined by Maksimovic (1996). UMA Engineering Ltd. (1992) reported a friction angle of 54° from their tests, but only obtained results at confining pressures greater than 240 kPa (refer to comments in Section 2.4.1). The secant friction angle is the angle (Figure 7.2) from the origin to the failure envelope at some normal stress.

The tests by Abdul-Razaq and Kim were performed at dry densities of 15.1 (loose), 17.3 (medium) and 19.05 kN/m$^3$ (dense) while the dry density of the rockfill compacted at the research site was estimated at 21.6 kN/m$^3$ (void ratio e = 0.23). A modified strength envelope for rockfill at the density achieved in the field has not been proposed. It was considered to be imprudent to further expand the interpreted strength envelopes, since the peak strength was not physically measured by the laboratory tests (Abdul Razaq 2007, Kim 2007). Furthermore, an increased shear strength envelope is not supported by the results in Figure 7.3. Figure 7.3 shows the estimated ultimate strength of loose, medium and dense samples tested by Abdul-Razaq (2007) and Kim (2007). The estimated ultimate strengths are the asymptotes of the hyperbolic curves, which were fitted according to the method outlined by Duncan and Chang (1970). The ultimate strength is not equivalent to the estimated peak strength discussed previously. The relationships illustrated in Figure 7.3 suggest that the ultimate strength does not continue to increase with increased density above a certain density. More advanced methods for interpreting the shear test results of granular materials such as the state parameter method discussed by Been and Jefferies (1985) were not possible because the test results did not reach the peak or critical states of the rockfill.

The secant friction angle, plotted in Figure 7.3, clearly illustrates the importance of understanding the potential stress conditions to which the in-situ rockfill will be subjected. Geo-Studio 2007 does not support non-linear failure envelopes for the hyperbolic model using effective stress parameters, and therefore a

representative friction angle must be chosen. The results from stress-deformation analysis of the field test indicated that the rockfill was subjected to a peak confining stress of approximately 160 kPa: using the relationships shown in Figure 7.2, an appropriate choice of a friction angle is 60°. The objective of this choice was to be accurate, and not to produce a "safe" design. It should be noted that a large part of the peak strength is due to particle interlocking of the large rockfill pieces, which allows for the high friction angles.

#### 7.2.3.2 Poisson's ratio

Poisson's ratio ($\nu$) has not been measured for local crushed limestone. Budhu (2000) suggested that the range of Poisson's ratio for dense granular material was from 0.25 to 0.35 with looser material having a lower ratio. Varadarajan et al. (2003, 2006) did testing on a variety of rockfill materials and reported values of $\nu$ between 0.28 and 0.44 with an average of approximately 0.33 for quarried rockfill. A value of 0.33 for $\nu$ was used as the standard value for the modeling in this thesis project.

It should be noted that Poissons's ratio varies with stress (Duncan 1992), but this is not easily accommodated in commercially available finite element software.

#### 7.2.3.3 Hyperbolic model

Rockfill can be suitably modeled with a linear elastic constitutive model in many cases where the stresses, and therefore strains, remain small relative to the peak

state. A problem with doing stress deformation modeling with linear elastic constitutive relationships is that any one element can resist unlimited stresses. A general principle in continuum mechanics is that stiff regions attract stresses when the continuum is deformed. In the case of rockfill, like other geo-materials, the tangent stiffness decreases as it undergoes straining as shown in Figure 2.3. It is therefore important to at least consider this when conducting numerical analysis.

The hyperbolic model, presented by Duncan and Chang (1970) was fitted to the stress-strain curves for rockfill, presented in Abdul Razaq (2007). Table 7.4 lists the parameters used in the development of the hyperbolic model for rockfill. Figure 7.4 shows the stress-shear strain plots for compacted test specimens, and fitted hyperbolic curves for three confining pressures. The stress-strain curves in Figure 7.4 are from direct shear tests and plot shear stress versus shear strain. The hyperbolic formulation was initially fitted to the direct shear test results and therefore shear modulus (G) replaced the elastic modulus (E) in Equation 2.5. For use in the modeling the $E_i$ was calculated from $G_i$ according to Equation 3.10. Equation 2.4 was fitted to the measured data points (Figure 7.5) with the parameters k (modulus number) and n (exponent for curve fitting). The scatter in the measured initial modulus values was large, and the parameters were fitted manually. The fitting parameters listed in Table 7.4 are comparable to those measured by Varadarajan et al. (2006) for a variety of rockfill materials.

The density of the rockfill achieved by compaction of the constructed rockfill columns was greater than the density of the tested samples, and so the modeling

parameters were adjusted to reflect the increased density. The curve in Figure 7.5 for e = 0.23 was developed by choosing k from the extrapolated best fit line in Figure 7.6. The void ratio was evaluated as 0.23 for the compacted rockfill in the columns at the test site. The exponent n was kept as 0.45 and was not varied with density. The relationships illustrated in Figure 7.5 should pass through the origin, based on Equation 2.4, but maintaining a positive elastic modulus at all stresses is necessary to maintain numerical stability.

Figure 7.7 illustrates the relationship between the mobilized friction angle and shear strain, based on a hyperbolic constitutive relationship. It is important to understand that to achieve the peak strength, the rockfill must undergo large strains. The engineering practitioner should be aware that the magnitude of potential deformation increases drastically as less conservative design values are chosen and as higher shear resistances are mobilized.

### 7.2.4 Till

A minimal amount of testing was done on the till (Chapter 3), and there were no test results suitable for developing constitutive relationships with confidence. The till was modeled both as a linear-elastic soil and an elastic-perfectly plastic material with a friction angle of 42°. Generally, linear elastic relationships were adequate because the peak strength of the till was not fully mobilized. If the till is modeled as an elastic material, its unit weight does not matter (because it is on the bottom of the model), and it is best matched to the weight of the rockfill, so as

to minimize unrealistic stress concentrations around the perimeter of the equivalent strips.

### 7.2.5 Loading fill

The loading fill was a clean 50 mm limestone, and it was not compacted. There were no laboratory tests completed on the fill to characterize its properties as its primary purpose was to act as a surcharge material. The density was estimated from 3-D volume surveys, but as discussed in Section 7.2.1, accounting for the total mass is more important than knowing the exact density. The angle of repose was measured as 37°, and this value is used as the friction angle in the analysis (although the models did not indicate that it was yielding). A stiffness of 20,000 kPa was assumed to be consistent with the adjacent clay as there was no better information or test results.

## 7.3 Porewater pressure modelling

Soil water characteristic curves and hydraulic conductivity functions were developed to accommodate the modeling of the unsaturated soil conditions in the slope. Figure 7.8 shows the curves used for this project. The volumetric water content function was estimated based on the grain size distribution using modified Kovacs method. The hydraulic conductivity curve was estimated using the Van Genuchten method. Tools for developing these curves are included in Seep/W (Geo-Slope International Ltd. 2010c). These curves are broadly similar to those measured by Garinger (2002) for Lake Agassiz clay if the differences in

the measured hydraulic conductivity and grain size distributions are taken into account.

Sensitivity analysis was used to determine a hydraulic conductivity that gave reasonably accurate porewater pressure responses to loading. The hydraulic conductivities used in the analysis are listed in Table 7.1. Arbitrarily adjusting the hydraulic conductivity in the numerical models was considered reasonable because there was a large scatter in the laboratory test results, and the laboratory testing does not capture the effects of secondary permeability (such as fissures or silt seams). Adjusting the hydraulic conductivity was necessary for calibration, but it does not directly affect the interpretation of rockfill behaviour.

The clay was assigned a hydraulic conductivity two times greater in the horizontal direction than in the vertical direction to address the anisotropy of the hydraulic conductivity, as recommended by Render (1970).

### 7.3.1 In-Situ porewater pressure development

The objective of developing the in-situ porewater pressure conditions for the modelling of the field test was to arrive at conditions that reflected the observed in-situ porewater pressure conditions at the start of the field test. The in-situ porewater pressures at the start of the test loading were calibrated based on observations from the VW-A, VW-B, VW-D, and VW-E and standpipes PZ-2 and PZ-7.

Developing the in-situ porewater pressure regime was complicated by the partial unloading of the bank during construction (to build the working pad). The swelling due to unloading was modeled, resulting in the depressed porewater pressure conditions shown in Figure 7.9 (compared to assumed typical winter water table shown in Figure 7.1). The drop in porewater pressure during column construction was evident in the monitoring of VW-B, Figure 4.11. The initial porewater pressure condition for the test loading was chosen so that the average porewater pressures at the piezometer locations in the model were equal the average of the measured porewater pressures. The modeled piezometer locations are shown on Figure 7.9.

The test loading took place over a short duration in late winter. From local experience it is reasonable to assume that groundwater conditions were in a steady-state condition, not considering the influence of the field test.

The columns are modeled as a drained material that maintains the piezometric head of the underlying till. This was confirmed at the base of the column with a standpipe piezometer (PZ-7). It is assumed, based on the monitoring of PZ-2 and 7, that the porewater pressure conditions in the till and rockfill were unaffected by the unloading and loading of the bank.

## 7.4 Stress deformation modeling

### 7.4.1 Model development

The following principle was used as guidance in the development of the in-situ stresses and stress states for the purposes of modeling:

> "There is no fully rational way of analyzing a natural slope unless the processes involved in its formation are known and can be modelled." (Duncan 1992)

The Red River valley was carved by erosion into the lakebed of glacial Lake Agassiz. Since the end of the glacial period, the valley has expanded (on the outside bends) due to the ongoing processes of erosion and slope failure (James 2009). Developing in-situ stresses by "turning on gravity" does not accurately produce the in-situ stresses, and stress histories of a natural slope. To develop historically reasonable horizontal stress distributions and preconsolidation pressures, the modeling process started with a horizontal ground surface. Once the horizontal stress distribution was developed, and the preconsolidation pressures were assigned, the valley was 'cut out' numerically, resulting in a re-distribution of stresses.

The methods used for developing the in-situ stresses varied with the kind of constitutive model used. Linear elastic models require no in-situ stress development if the load-deformation response is the only interest; linear elasticity is stress-path indipendent. The EPP, hyperbolic, and MCC material models all

require in-situ stresses to determine limit states and stress-deformation characteristics.

Two different processes were used to develop in-situ stresses; one that used a $K_0$ term to develop horizontal stresses (Cases 2 and 4), and a second method which used surcharge loads to create a more complex $K_0$ distribution (Case 3). As previously mentioned, the preconsolidation pressures for MCC analysis of the clay regions were defined by assigning overconsolidation ratios based on the stress distributions under a horizontal ground surface.

#### 7.4.1.1 Coefficient of earth pressure at rest ($K_0$)

The coefficient of earth pressure at rest, $K_0$, is used to describe the relationship of horizontal to vertical in-situ effective stresses according to:

$$K_0 = \frac{\sigma'_h}{\sigma'_v} \qquad 7.6$$

The horizontal effective earth pressure depends on many factors including soil type and stress history. This matter is complicated further because both vertical and horizontal in-situ stresses are difficult to measure, and were not measured as part of this project. It was assumed that there are no “locked-in” vertical stresses and therefore the relationship, $\sigma_z' = \gamma z - u$, is applicable.

Numerous empirical relationships were developed to estimate $K_0$ under various conditions. Jaky (1948), Brooker and Ireland (1965) and Mayne and Kulhawy

(1982) developed $K_0$ equations for normally consolidated soils based on the internal friction angle. The latter two also presented relationships for overconsolidated soils. Brooker and Ireland (1965) include curves relating $K_0$ to the plasticity index $I_p$.

Using the relationship presented by Mayne and Kulhawy (1982) for overconsolidated soils, it was determined that $K_0$ would be approximately 1.5 at 229 m, decreasing to 0.9 at 222 m, based on the measured overconsolidation ratios. For Case 3 the $K_0$ distribution shown in Figure 7.10 was developed by applying the following steps:

1. Develop vertical and horizontal stresses by “turning on gravity” with a Poisson’s ratio of 0.49.

2. Apply a 50 kPa downward pressure at the surface with a Poisson’s ratio of 0.49, thus increasing the vertical and horizontal pressures by approximately 50 kPa.

3. Apply a 50 kPa upward pressure at the surface with Poisson’s ratio of 0.01 applied to the clay regions to lock in the increased horizontal stresses (created in the previous step).

This modeling technique is described in the manual for the modeling software PISA (reference unknown). The model developed negative porewater pressures above elevation 224.5 m, the approximate elevation of the water table. Suction

pressures were not measured at the site, but it is reasonable to assume that there would be negative porewater pressures above the water table.

For Case 2 and Case 4, $K_0$ was assigned as 0.8, which is the upper bound reported by Baracos (1983a) for the Winnipeg region.

The $K_0$ value of 0.5 for the till was adopted based on the charts in Brooker and Ireland (1965) which relate $K_0$ to the plasticity index ($I_p$) (the plasticity index of till is shown on Figure 3.12). It was assumed that the till was normally consolidated, which is reasonable considering that at the clay interface it was characterized as an ablation till.

#### 7.4.1.2 Creating the valley

After developing a reasonable distribution of initial stresses, as described in the previous section, the river valley was numerically "carved" out from the flat prairie. This process is thought to most accurately reflect the stress history of the in-situ soil. The modeling step of carving out the valley was done for the benefit of the horizontal stresses, which were developed as described in the previous section. The importance of preserving the effects of $K_o$ in the stability analysis of natural slopes is discussed by Chowdhury (1976).

#### 7.4.1.3 Column stresses

Accurately modeling the in-situ stresses in the rockfill has a number of challenges. The actual vertical or horizontal stress distributions have not been

measured in a compacted rockfill column. A general assumption is that $\sigma_{zrockfill} = z \cdot \gamma_{rockfill}$ and that $\sigma_x = \sigma_z$ (that is $K_0 = 1$). However, it is unknown how the placement and compaction of the rockfill within a long cylindrical cavity affects the stress distribution, and whether this assumption is valid. Figure 7.11 shows typical total vertical stress distributions for clay and rockfill, and illustrates a plausible distribution of stresses within a rockfill column. It is possible that some of the weight of the rockfill is transferred via shear into the surrounding clay as is the case for vibro-replacement columns (Priebe 2005). This would introduce shear stresses along the clay-rockfill interface and increase the vertical stress in the surrounding clay, while reducing the vertical stress in the rockfill to some value less than $z \cdot \gamma_{rockfill}$.

In engineering practice the choice of vertical stress distribution should be considered carefully and applied cautiously. The effective stresses at depth affect all aspects of rockfill's constitutive behaviour including strength and deformation properties.

A challenge in the finite element modeling of columns (modeled as equivalent strips) is to numerically develop the in-situ stresses within the dense rockfill without introducing unreasonable stress conditions, especially along the interface between materials. Geo-Studio develops in-situ stresses by "turning on" gravity. This works well for primarily horizontal layers, but the columns are modeled as vertical inclusions which are denser than the surrounding soils. Various techniques were tried with limited success, including modifying boundary conditions, adjusting modulus values, and applying surcharge loads.

A method that produced a reasonable initial stress distribution in the rockfill involved partially isolating the rockfill by adding slip surface elements along the vertical edges of the equivalent strips. The following steps were used to develop the in-situ stresses for Case 3 (Figure 7.12):

1. Develop in-situ stresses for the whole domain, with clay properties assigned to rockfill regions.

2. Assign interface elements with a low strength to the vertical edges of the rockfill region. Increase the stiffness of the rockfill region, and apply a downward pressure over the regions, to compensate for the difference between the rockfill unit weight and the clay unit weight. Shear strains concentrate along the interface, and the adjacent regions are relatively unaffected by the application of stress to the rockfill region

3. Apply the appropriate rockfill constitutive model and continue stress-deformation modeling, using the in-situ stresses developed in the above step.

The above method, although it provides more realistic in-situ stress distributions, does not necessarily give improved results. If interface elements are introduced in a model, they must remain in the model for subsequent modeling stages. It was found that stresses and strains tended to concentrate along the interface elements in the following stages of analysis, even if the interface elements were assigned the same properties as the surrounding regions.

An accurate vertical stress distribution in the rockfill zones is only important if a non-linear constitutive relationship is being used, and even then the difference may not be significant if the strain increments are small. The initial modulus used with the hyperbolic model varies with the confining pressure to the power of 0.45 (Equation 2.4). For example, a 30% error in in-situ density will only result in a 13% error in the initial modulus.

Proper determination of in-situ stresses in rockfill regions is more important when considering the shear strength of the rockfill, such as in stability analysis. The above concerns about stress-development in the model are not relevant to limit equilibrium stability analysis using the method-of-slices because the base-normal pressure is calculated for each slice individually, based on the overlying soil layers. The analyst must still choose an appropriate unit weight.

For Case 2 and Case 4, the rockfill was modeled at the same unit weight as the surrounding clay, thus avoiding the need for interface elements, and the associated strain concentrations. The consequences of this are a slightly lower stiffness in the rockfill (see above discussion) and a lower strength, which is only a concern if calculating a factor of safety, or if yielding is initiated in the rockfill.

#### 7.4.1.4 Modeling of test loading

The test loading was modeled as a series of steps utilizing coupled consolidation analysis to predict the immediate and time-dependent deformations, along with the porewater pressure response. The coupled-consolidation analysis allowed

the porewater pressure response to be reasonably modeled. The load was applied at time zero for each day of loading, and the domain was allowed to consolidate for the time interval until the next load was applied. The stresses, porewater pressures and deformations were carried forward with each step in a cumulative manner.

The porewater pressures and stress conditions from the coupled consolidation analysis of the test loading are used as inputs for slope stability analysis.

## 7.5 Stress-deformation analysis: Results and commentary

The results of the four modeling cases, introduced in Section 7.1 are presented and discussed with the purpose of highlighting the performance of the rockfill columns. There are occasional references to other analyses conducted as part of this research, but not every scenario can be presented in detail. For the following discussion the positive X-direction is horizontal out of the slope surface and the Z-direction is vertical in the plane of the model.

Figure 7.13 and Figure 7.14 show the modeled displacements and porewater pressures from the four cases, plotted alongside the measured values. Case 1, which uses linear-elastic constitutive relationships for all soil units, is used for sensitivity analysis, and to illustrate the incremental stress changes caused by the test loading.

The results from Case 2 are used to highlight specific characteristics of the rockfill behaviour. Case 2 over-predicts the displacements caused by the test

loading; however, the slightly larger deformations accentuate the development of stresses and strains in the equivalent strips.

Case 3, in theory, should be the most accurate replication of the behaviour of both the clay and the rockfill. The magnitudes of the deflections, and the responses of porewater pressures were modeled well, but the interface elements along the edges of the equivalent strips make it more difficult to identify the characteristics of the rockfill column behaviour.

Case 4 is a variation of Case 2 that was developed to demonstrate a possible mechanism which caused the increased displacements that were observed approximately 1.5 m below the ground surface in the area of the columns. The poisson's ratio and stiffness parameters were also varied to improve the correlation with the observed deformations.

### 7.5.1 Case 1: Linear-elastic analysis

Linear elastic analysis of stress deformation problems is the least 'accurate' analysis method, in terms of the quality of the constitutive model, but it may be the most useful. It is often of interest to know how a change in boundary or loading conditions contributes to the stress regime. Incremental changes in stress between modeling stages cannot be contoured in Geo-Studio 2007, and the impact of incremental loading is visually 'obstructed' by the in-situ stress distribution. Linear elastic analysis does not require the development of an in-situ stress regime, and therefore the influence of loading can be graphically

illustrated more easily. Linear elastic analysis is also the most numerically stable constitutive model.

Figure 7.15 and Figure 7.16 show contours of some of the incremental stress changes and displacement distributions from the linear-elastic analysis. Figure 7.17 shows the results of the sensitivity analysis of elastic parameters. The baseline parameters listed in Figure 7.17 were used to develop the results shown in Figure 7.15 and Figure 7.16. Linear elastic analysis under-estimates deformations if 'initial' modulus values are used, and therefore secant modulus values are used in the analysis shown in these figures. Note that the values shown in Figure 7.15 and Figure 7.16 are incremental stresses due to the placement of the fill, and are in addition to the in-situ stresses, which were not modeled for Case 1.

There are a number of things to note from these results:

- The shear strains in the clay are higher than in the rockfill, while the shear stresses concentrate in the stiffer rockfill (Figure 7.16).

- Subsurface deformations upslope of the pile of loading fill are in the negative X-direction (upslope) (Figure 7.15). Displacements downslope of the fill are in the positive X-direction (downslope) and are greater in magnitude than the negative displacements. This is in agreement with the observations made in Chapter 6.

- Near the clay till interface the upslope edge of the equivalent strips (which represent individual rows of columns) show a vertical (Y) effective stress decrease, while at the downslope edge of the column, there is a large stress increase.

#### 7.5.1.1 Sensitivity analysis

Figure 7.17 shows the sensitivity of displacements in the model to the elastic modulus and Poisson's ratio ($\nu$) for select materials. The displacements were taken from point 4, shown on Figure 7.16a (at the upper edge of the rockfill columns at an elevation of 223.5 m). The parameters are normalized to reasonable upper and lower bounds for each parameter for illustrative purposes. The upper and lower bounds, as well as the baseline values, are listed in the table included in Figure 7.17.

It is apparent that the elastic modulus (E) and Poisson's ratio ($\nu$) assigned to the clay regions have a greater influence on displacements than do the rockfill properties. Notably, the stiffness of the rockfill has a relatively minor influence on the total displacements. The results shown in Figure 7.17 are determined from linear elastic analyses, but they are still indicative of the significance of the individual parameters when using more advanced constitutive models.

### 7.5.2 Case 2: Analysis using the elastic-perfectly plastic model for clay and the hyperbolic model for rockfill

The elastic-perfectly plastic (EPP) soil model is an effective, but unsophisticated way of incorporating the potential for plastic yielding into a stress deformation model. The EPP model treats the soil as a linear elastic material until the shear stresses in an element reach the failure envelope, which is defined by a friction angle and cohesion intercept. The material properties used in the analysis are summarized in Table 7.2. Figure 7.18, Figure 7.19 and Figure 7.20 show contours of the ground conditions at the modeled day 11 of the test loading (the final day).

The rockfill and till were modeled at the same unit weight as clay (17 $kN/m^3$) in Case 2, to avoid some of the numerical difficulties associated with accurately developing in-situ stresses in a relatively small vertical inclusion of dense soils.

The rockfill was been modeled with the hyperbolic formulation in Case 2. Other simulations, not presented here, have also investigated modeling the loading fill and rockfill as an EPP material, with very similar results. This is because at small strains, the stress-strain relationships are almost identical and as demonstrated by Figure 7.17, the model is not very sensitive to the stiffness of the rockfill. The upper till was assigned a relatively low stiffness (30,000 kPa) to reflect its loose condition. Stiffer till produced more pronounced stress concentrations along the clay-till-column interface

Figure 7.14 generally shows good agreement between the modeled and measured porewater pressure responses, but notably VW-B shows more excess

porewater pressure dissipation than the model predicts. The rapid dissipation of excess porewater pressures observed by VW-B (long drainage path), compared to VW-E (shorter drainage path) is contradictory to the expected behaviour based on consolidation theory. This effect is possibly the result of preferential drainage near VW-B in the form of a silt zone or a discontinuity in the clay. The discrepancies between the measured and modeled results average out to be similar, and of course, this was the goal of the calibration.

The zone of clay downslope of the rockfill, which was assigned the residual shear strength, showed extensive yielding. Yielding also occurred upslope of the columns, generally in the zone of the shear strain ($\gamma$) = 0.006 contour shown on Figure 7.19 b). The zone of failure can also be approximated from Figure 7.20 knowing that M (the slope of the failure envelope in q-p' space) is 0.69. Figure 7.20 shows that the clay in the slope is highly stressed, with a large region at a q/p ratio of over 0.6.

Figure 7.21 shows the stress paths of modeled elements, at the approximate location of VW-E and VW-F, as well as in the rockfill strips. Neither of the clay elements ruptured, but both were approaching the failure envelope with the increased loading. At VW-F the response is undrained, while at VW-E, which is closer to the clay-till, interface, the dissipation of excess porewater pressure is evident.

It is also significant that the rockfill responds differently to loading at different points across the width of the equivalent strip (Figure 7.21). In q-p space, the

element near the upslope edge of the column approaches the failure envelope because the mean effective stress decreased with the placement of the simulated load. This is discussed in more detail in Section 7.5.6.

### 7.5.3 Case 3: Analysis using the modified Cam-Clay model for clay and the hyperbolic model for rockfill

Case 3 improves on Case 2 by modeling the clay with the modified Cam-Clay (MCC) formulation. The development of the MCC parameters is discussed in Section 7.2.2.1. The modeled deformations and measured porewater pressure responses are comparable to the measured values (Figure 7.13, Figure 7.14), and are generally an improvement over Case 2. Figure 7.22 shows the modeled contours of Y-effective stress and maximum shear strain at day 11 of the simulated test loading. Note that the vertical stress distribution in the equivalent strips reflects the full overburden weight of the rockfill. The shear stresses in the rockfill were lower in the Case 3 analysis than in Case 2, because the shear strains in the upslope clay were lower (Figure 7.22b versus Figure 7.19b). The clay upslope of the columns was assigned the post-peak shear strength, similar to Case 2, but because the clay was assigned a preconsolidation pressure (based on the OCR), the yield surface is expanded. Figure 7.21 shows that at VW-E, the in-situ stress state calculated for Case 3 differed slightly from Case 2, due to the higher initial $K_0$ used in Case 3. The yield envelope can be estimated at VW-E, knowing that an OCR of 3 was assigned; this is not illustrated.

Kappa (κ) was chosen to be 0.012 to obtain better agreement between the modeled and measured displacements. Using a value of $\kappa = 0.077$, determined

from one-dimensional consolidation, resulted in modeled displacements approximately four times greater than shown in Figure 7.13 for Case 3 (based on an average of displacements at the points 4 to 8, shown in Figure 7.16).

Generally the MCC constitutive model is considered to be an improvement over EPP models especially for consolidation problems or when limit state behaviour is relevant. For these reasons, the use of MCC is reasonable for this project. Conversely, it has been assumed, based on the reviewed literature, that even though the ground is overconsolidated, the strength envelope is best approximated by the post-peak (critical state) strength at this riverbank location (Rivard and Lu 1978, Baracos and Graham 1981).

### 7.5.4 Case 4: Case 2 with interface

Case 4 was developed to demonstrate a possible mechanism that caused increased deformations observed near the surface, though this mechanism has not been confirmed by other observations. The upper 1-1.5 m of the columns were not compacted effectively with the vibrolance, and therefore have less shear resistance and are less stiff than the compacted rockfill. To encourage concentrated displacements at elevation 223.7 m, as reported by the inclinometer monitoring, a horizontal line of interface elements was introduced with an assigned friction angle of $\Phi = 8°$ and a cohesion of c = 2 kPa. The location of this interface is shown in Figure 7.1

The deformation profiles from Case 3 in Figure 7.13 do show this increased shear zone. The reduction of $\nu$ to 0.33, compared to 0.4 used in Case 2, further

reduced the total displacements to be more in-line with the observed deformations.

Another theory is that a 'raft' of frozen soil was mobilized, and caused concentrated shearing along the base of the frozen soil. The frost at the test section varied from 0.3 to 0.9 m thick. This effect has not been proven or reasonably demonstrated. Numerical analysis has shown that a frozen crust would generally work to resist movement, rather than cause a zone of increased displacement.

### 7.5.5 Shear in columns

In the following paragraphs, the discussion focuses on the upslope (left in the figures) equivalent strip, centered at X-coordinate 0 (Figure 7.22), unless otherwise noted. The behaviour and stress changes of the downslope equivalent strip (centered at X-coordinate 2.7) were generally similar to the upslope strip.

The change in horizontal stresses due to loading along vertical lines corresponding to the upslope and downslope edges of the equivalent strip, are plotted in Figure 7.23. The stress change is calculated as $\sigma'_{x\text{-}Day11} - \sigma'_{x\text{-}Day0}$. The increase in horizontal stresses is obviously reduced across the width of the equivalent strip. At the clay-till interface, the positive spike in the downslope horizontal stress demonstrates the anchoring effect of the in-situ till.

The stress change was also calculated in-between the equivalent strips, in the clay. This distribution (the green line in Figure 7.23) is very similar to the

distribution along the downslope edge of the columns above 219 m, indicating that the intervening zone of clay is providing very minimal additional resistance to slope deformations; it is merely conveying horizontal, downslope stresses. The discontinuities around 223.5 correspond with the interface between the loose and dense rockfill regions.

Figure 7.24 shows the modeled maximum shear stress along the centerline of the equivalent strip and into the underlying till. The solid line in Figure 7.24 is the integral of the downslope horizontal stress change minus the upslope horizontal stress changes (Figure 7.23), integrated from the ground surface downward which is analogous to the shear stress of an independent structural member:

$$Shear\ stress \approx \int_{\text{ground (225.5 m)}}^{\text{base(211 m)}} \frac{(\sigma_{\text{x-day 11}}-\sigma_{\text{x-day0}})_{\text{downslope}} - (\sigma_{\text{x-day11}}-\sigma_{\text{x-day0}})_{\text{upslope}}}{\text{width of strip}} dy \qquad 7.7$$

This function was numerically integrated from the model results assuming a condition of shear stress equal to zero at the ground surface. This plotted integration is very similar to the maximum shear stress profile in the columns. This implies that the columns transfer the horizontal stresses that are applied over the length of the column, to a reaction in the till via shear in the column. It is interesting to note that between the strips, there is spike in shear stress in the till, as the till resolves the horizontal stress applied by the strips.

### 7.5.6 Bending behaviour in columns

The present analysis was not able to completely reproduce the observed effect of increasing incremental displacement with increased elevation throughout the column profile that was identified in Chapter 6 (Figure 6.16). In the numerical analysis, this trend was concentrated closer to the clay-till interface, but the numerical models indicate some parallels between the behaviour of the equivalent strip and a structural member.

A common result from all the stress-deformation modeling is the re-distribution of the vertical (z) stresses within the equivalent strips upon loading near the clay-till interface. This is illustrated in Figure 7.15, Figure 7.18 and Figure 7.25. There is a decrease in vertical effective stresses ($\sigma'_z$) in the up-slope half of the strip below elevation 220.5 m, while showing an increase of $\sigma'_z$ in the downslope half of the strip. This is illustrated clearly in Figure 7.25. This stress distribution is very similar to that of a structural member subjected to a combination of bending and axial compressive stresses. This implies that an internal moment couple is developing within the rockfill column cross section. There is little evidence from the numerical models, of internal moments in the equivalent strips above elevation 220.5 m.

The internal moment within the left equivalent strip was evaluated as approximately 13 kNm, considering only the vertical stresses shown in Figure 7.25. A baseline compression of 105 kPa was assumed. This estimate of moment, and the stress distribution in Figure 7.25, are also in agreement with the

stress distribution described by the following equation which is commonly used in structural analysis:

$$\sigma = -\frac{My}{I_{strip}} \qquad 7.8$$

where:

$\sigma$ = internal stress parallel to the longitudinal axis at a point

M = moment

y = distance from centroid

$I_{strip}$ = 2$^{nd}$ moment of area

Equation 7.8 can theoretically be used to estimate the moment capacity of column at a specified depth. Bending failure in a vertical rockfill column will occur when $\sigma_z$ approaches zero. By setting $\sigma$, in Equation 7.8**Error! Reference source not found.** equal to $\sigma_{zo}$, and calculating y and I for a column, a failure bending moment can be estimated, assuming elastic behaviour. As discussed in Chapter 2 the assumption of linear elastic behaviour is not valid for rockfill subjected to medium to large strains.

Considering Figure 7.23, the moment at the clay-till interface should be approximately 83 kN·m, if only the horizontal stress increase is considered (the difference between the upslope and downslope stress changes). This can be calculated according to:

$$M(z_2) = M(z_1) - \int_{z_1}^{z_2} V(z)dz \quad 7.9$$

Where

z = vertical coordinate

V(z) = Shear force as a function of z.

This discrepancy with the moment calculated from Figure 7.25 (13 kN·m) demonstrates that simple beam mechanics cannot consider all of the complex stress interactions between the columns and the surrounding clay. For example, the shear stresses acting on the edges of the columns (Figure 7.19) also contribute to the internal moment: in this case decreasing the moment.

It is considered that finite element analysis adequately models the internal stress distributions in columns with respect to apparent bending behaviour and internal moments. As an engineering designer, the point of concern is whether the material models are adequate, considering the internal stress distribution in the rockfill. To reiterate earlier comments, rockfill cannot resist negative stresses, and because rockfill is a frictional material, its ability to resist shear stresses depends on the confining pressure. The significance of the stress redistribution is shown in Figure 7.21 and Figure 7.26: as the mean effective stress (p') along the upslope edge of the column decreases, the capacity to resist the additional shear stress also decreases. Near the downslope edge of the strip, both the

mean effective stress and deviatoric stress (q) increase, resulting in little change to the q-p' ratio.

#### 7.5.6.1 Equivalent stiffness and second moment of area

It is readily demonstrated that the 2nd moment of area (I) per unit width of a row of cylindrical rockfill columns is not equivalent to the I of an equivalent strip. If bending is a significant mode of deformation, then it follows that $(EI)_{column}$ should be equal to $(EI)_{equivalent\ strip}$ to ensure equality of bending behaviour (Equation 6.5). The elastic modulus could be arbitrarily modified to create this equality; this is not recommended because the parameter E is related to the shear modulus G. Modifying E will then alter the shear strain characteristics. Furthermore, the effect of increasing the modulus of the rockfill on the overall displacements is relatively minor, as demonstrated by the sensitivity analysis. The equivalent modulus, calculated using the method above, is 44% greater than the modulus estimated in Section 7.2.3.3. Applying an equivalent stiffness to the rockfill in the Case 2 analysis decreased the total deflections by 5% (using an average of 5 points).

For these reasons, the author does not recommend pursuing equivalent stiffness methods in 2-D finite element models. 3-D models inherently address this issue.

#### 7.5.6.2 Rockfill columns as a structural element

To address the inequalities between an equivalent strip and the cylindrical columns, it may seem reasonable to model the columns as structural elements rather than as a soil. The one significant benefit of modeling rows of rockfill columns with a structural beam element is that the stiffness (E), and 2$^{nd}$ moment of area (I) are assigned to be equivalent to that of rows of cylindrical columns. In the author's investigation, it was found that using a structural beam element gave similar stress deformation results for small strain problems. However, using structural members to represent a granular column is not recommended for the following reasons:

- The large volume of the rockfill material is replaced by an element with no volume.
- A structural element behaves as a linear elastic beam, with unlimited capacity.
- The non-linear stress-deformation behaviour of rockfill is not accounted for.
- The properties of a structural member are independent of stress conditions.
- Stress and strain concentrations along the material interfaces (such as shown in Figure 7.19) will be misrepresented.

- Structural elements in Geo-Studio, deform in bending only, without consideration for shear deformations (such as described by Equation 6.6).

- A structural beam element can accept unlimited shear stresses. Stresses are not properly re-distributed into the surrounding continuum elements because deformations due to shear are not considered. This can cause unreasonably large concentrations of shear stresses in the structural members.

- Structural members are not compatible with stability analysis.

In summary, there are a number of shortcomings in modeling rows of rockfill columns as equivalent strips, but these issues are not compensated for by replacing the strips with structural members.

### 7.5.7 Elastic rebound

Figure 7.27 shows the elastic rebound for SI-8, comparing the modeled and measured rebounds. It was found that the component of elastic re-bound was generally overestimated in the numerical model results. This implies that the elastic component of the modeled deformation is too large relative to the plastic component. If the strength of the soils (rockfill or clay) is decreased so that the plastic increment increases, the modeled displacements become much larger than the displacement measured at the test site.

It is believed that this is a limitation of the elastic-plastic and MCC constitutive models because the soil behaves as a true linear-elastic material up to the point

of yielding. Davis and Selvadurai (1996) suggest that fine grained soils only behave linearly to approximately one third (stress) of the peak strength, after which there is a plastic component to the deformations. The measured initial tangent modulus of the clay is approximately three times greater than the secant modulus (to the peak) as shown in Table 3.1. The non-linearity before yielding is illustrated clearly in Figure 3.18. As shown in Figure 7.20, much of the clay was stressed to a stress ratio (M) very near the post-peak stress ratio of 0.69 (noting that the soil was also assigned 5 kPa of cohesive strength). It is apparent why the elastic rebound is over-estimated, considering the limitations of the model at reproducing true elastic-plastic soil behaviour as yielding is approached.

### 7.5.8 Other Comments

- The averaged parameters method presented in Section 2.5.1 is not compatible with stress-deformation analysis because it does not account for any deformation parameters (such as E, $\nu$, or other variables used in the definition of individual constitutive relationships). Finite element modeling packages are designed to handle multiple materials in a single model, and therefore it is an unnecessary oversimplification to try to represent multiple rows of columns and intervening native soil with a single equivalent hypothetical soil material. Such a hypothetical soil model will not succeed in capturing the complex stresses and deformations occurring in and around the rows of columns.

- Conducting sensitivity analysis on the peak strength of the rockfill in stress-deformation analysis is not beneficial unless the clay surrounding the columns has been stressed to a limit state. The strains required to mobilize the full shear strength of the rockfill are greater than for the in-situ clay, especially if the clay is being sheared in an undrained condition (Abdul Razaq 2007). The shear deformations induced by the field test were not large enough to 'fail' the entire slope, although some local yielding is assumed to have occurred in the clay, as discussed in Chapter 6, and demonstrated in the numerical analysis.

- Combining the two equivalent strips into a single strip (2.2 wide) produced very similar stress deformation results, to modeling the rows of columns independently.

## 7.6 Post-construction deformations

There are two potential mechanisms that contribute to post-construction deformations: time dependent deformations (such as creep or consolidation), or changing stress conditions. As discussed in Chapter 6, long term consolidation is not a reasonable explanation for the post-construction deformations at the research site. Consolidation is not a relevant concern for most commercial slope stabilization projects either, unless there is a significant change in bank geometry or some other long term loading that coincides with construction.

Stress changes will occur after construction in the form of changing porewater pressures. It is difficult to model this effect because the 'driving' force is a change in the in-situ stress conditions. In Geo-Studio 2007, this is best modeled with the stress redistribution analysis. The specifics of natural porewater pressure fluctuations caused by a flood event are unpredictable. They are a function of:

- initial porewater pressure distribution
- flood conditions (magnitude, duration, rate of increase and decrease)
- porewater pressure conditions in the till
- precipitation and infiltration
- other ground conditions including hydraulic conductivity, degree of saturation, fissures and so on.

To illustrate the mechanisms that may have caused the deformations after construction (Figure 6.20 and 6.21), a flood event was simulated. A simple transient boundary condition shown in Figure 7.28 was applied to the ground surface, the base of the till, and the vertical edges of the rockfill columns (Figure 7.29). The flood boundary condition was applied to the base of the till because there is a fairly close correlation between the river level and the till piezometric conditions as shown in Figure 4.11. The columns at the research site are also hydraulically connected to the till, and to the surface, and therefore they report water levels very similar to river level along their length. Figure 7.30 shows the

stress distributions from the flood modeling (at X-coordinate 5 m from Figure 7.29). Note that there is a slight error in the stress distributions near the ground surface due to interpolation of stresses in between nodes.

Figure 7.31 shows the deformations that result from the simulated flood at the research site along with the measured displacements 608 days after the start of the field test. The bank had experienced two spring freshets and two fall river draw-downs (2008 and 2009) between column construction and day 608. The flood conditions increase the porewater pressures near the ground surface, and at the clay till interface thus causing some elements to yield and re-distribute excess stresses. As shown in Figure 7.31, the model produced a very similar deformation profile up to elevation 223.5 m, and showed a similar trend near the surface, but was not able to fully replicate the large displacements measured at shallow depths. Sigma-W uses a small strain formulation, and does not handle large strains properly (Geo-Slope International Ltd. 2010a).

Replicating the shallow deformations by a numerical model is further complicated by the complex soil conditions near the surface, including: alluvial veneers, relic landslide material, sporadic rip-rap, soils at a residual strength, tension cracks, and eroding surfaces. These model results are for the purpose of illustration and are not necessarily applicable at other sites. Analysis using the techniques described above, have shown that similar conditions may have contributed to the deformations described by Yarechewski and Tallin (2003) observed at a site along the Seine River (in Winnipeg).

The condition of marginal stability in the lower slope was demonstrated by the movements observed in 2006 and 2007 (Figure 3.11). The implications of marginally stable soils downslope of a rockfill column installation should not be overlooked. Rockfill, being a granular material which derives its strength through inter-particle friction and interlocking, requires confining pressure to be able to contribute strength and stiffness to a soil mass. Slope failure (even shallow movements) or erosion of soil downslope of a row of rockfill columns can reduce the confining pressure on the rockfill columns. In addition to providing confining pressure, the soil downslope of the columns is integral to the stability of overall slope. If instabilities or erosion remove soil from the toe region, the overall stability of the slope is negatively impacted as the result of the loss of mass and shear resistance.

### 7.6.1 Test loading with surcharge compared to piezometric loading

The full-scale test loading, does not exactly replicate the critical conditions (extreme porewater pressure events) experienced by a typical slope reinforced by rockfill columns. There are a number of significant differences between the test loading, and natural porewater pressure events, with respect to in-situ stresses:

- The test loading was driven from loading up-slope of the columns which generally increased mean effective stresses.
    - Mean effective stresses in the columns remained neutral on average or increased (Figure 7.15a, Figure 7.25), with the

exceptions noted in Section 7.5.6. This supports the theory of Enoki et al. (1991) discussed in Chapter 2.

- Mean effective stresses in the in-situ clay remained neutral under initial loading (assuming undrained conditions) and increased with consolidation (Figure 7.21)

- In-situ soils that are the most stressed (in the upslope area as shown in Figure 7.15) were generally over-consolidated, experiencing suction pressures, and un-failed.

- Flood events and the subsequent drawdown drive deformations in the lower slope by decreasing mean effective stresses:

  - Mean effective stresses in the columns remain neutral, or decrease due to higher porewater pressures.

  - Confining pressure around the rockfill may decrease as failures in the lower bank reduce horizontal pressure.

  - Mean effective stresses in the in-situ clay near the surface and at the clay-till interface decrease due to increased porewater pressure (Figure 7.30).

  - In-situ soils that were the most stressed by the infiltration of floodwater (near the surface along the lower portion of the slope)

were probably saturated, at or near a post-peak or residual state, and not overconsolidated (alluvial, or slumped lacustrine clay).

The differences between the test loading scenario and the post-flood scenario are analogous in some ways to the differences between passive (increasing $\sigma'_1$) and active pressures (decreasing $\sigma'_3$) respectively.

## 7.7 Slope stability analysis

The focus of this research project was on the deformations associated with the mobilization of shear and bending resistance within rockfill columns. However, slope stability analysis remains the most important consideration when designing riverbank stabilization works using rockfill columns. Stability analysis of the natural slope was discussed in Chapter 5.

The modeling cross-section and a critical slip surface (#1719) are shown in Figure 7.32. The parameters used in the stability analysis are listed in Table 7.5, and the results of the stability analysis are summarized in Table 7.6, and plotted in Figure 7.33. The factors of safety based on the Case 3 analysis are larger than for Case 2, due in part to the higher density of the modeled rockfill, but it is important to note that this is not the only difference. The mean effective stress was also higher for most elements in the Case 3 analysis because of the $K_0$ distribution. The stability of the slope was considered with post-peak strengths applied to all clay regions, and also with residual strength assigned to the region downslope of the toe, in separate calculations (Table 7.6).

The results in Figure 7.33 suggest that the slope was very near the failure point at the end of the test loading. The factors of safety versus load curves show that this relationship is not linear. As porewater pressures dissipated during the test, the strength of the in-situ soil was increasing due to the increased effective stresses.

Figure 7.34 shows the shear strength and mobilized shear resistance along the slip surface 1719. The X-coordinates on the graph correspond to the coordinates shown in Figure 7.32. The 'spikes' are the contributions of the rockfill columns. Figure 7.35 shows the distribution of pressures along the slip surface. The suction pressures contribute to the shear strength according to the method proposed by Vanapalli et al. (1996).

### 7.7.1 Comments on slope stability

The finite element method (FEM) used by Geo-Slope in their Slope/W module for stability analysis, is different than the strength reduction or gravity increase methods of FEM stability analysis. Geo-Slope uses stresses from the finite element stress-analysis (Sigma/W) within the framework of limit equilibrium analysis. Instead of calculating the base normal stresses from overburden pressure, they are taken from the stress-distribution already developed by the FEM module. The details of this method are discussed in Krahn (2003) and the product manual (Geo-Slope International Ltd. 2010b). For the stability analysis of the test loading, the FEM stability method is appropriate because of the non-uniform stress and porewater pressure distributions.

For most stability analysis scenarios, the till was assumed to be much stronger than the clay and therefore it was not modeled as a soil unit. This forces the potential failure surfaces to follow the clay-till interface where the slip surface radius would otherwise extend into the till. This method does not mobilize any resistance within the till layer. For most sites this is a reasonable assumption but the potential for a failure developing through the till and beneath the rockfill columns should also be considered, by introducing a till layer of appropriate strength. It is good practice to then also use a slip surface optimization technique to find potential non-circular failure surfaces with a lower factor of safety.

There is no fundamental difference between modeling of multiple rows of rockfill columns with a single equivalent strip or multiple individual strips, for the purpose of stability analysis. The differences in the results are reflections of the geometry of the slip surface, and the overburden pressure. In that way it is more reasonable to model each row of columns with a strip so that overall impact of the geometry is captured. Both methods have been tried, and they have produced very similar results.

## 7.8 Summary and conclusions from numerical analysis

The modeling work discussed in the chapter has shown that the field test results can be modeled with reasonable accuracy. The numerical model is useful because once it is calibrated, various parameters and conditions can be varied to determine the model's sensitivity to individual variables.

This chapter has demonstrated a number of important concepts:

- The Maksimovic (1996) strength envelope fits the measured shear strength of dense rockfill very well (Figure 7.2). It provides a tool for determining an appropriate friction angle for stress-deformation or stability analysis.

- The hyperbolic model (Duncan and Chang 1970) fits the stress-deformation characteristics of rockfill, and is an improvement over a linear elastic constitutive relationship (Figure 7.4).

- The non-linear constitutive behaviour of rockfill means that if strength parameters are chosen with little conservatism, large strains will be required to mobilize the required resistance (Figure 7.7).

- The benefit of the stiffness of the rockfill is limited by the relatively small overall area replacement (Figure 7.17).

- The columns ‘collect’ horizontal stress from the clay upslope of the columns, and transfer this stress to a reaction in the till, through both shear and bending mechanisms (Figure 7.23,Figure 7.24).

- There is a redistribution of stress within rockfill columns upon loading, especially at the clay till interface. The stress distributions are analogous to the distribution of bending stresses in structural members (Figure 7.25).

- Methods of improving the modeling of bending characteristics in 2-D analysis are unnecessary, and negatively affect other modes of deformation.

- Structural analysis techniques do not adequately consider the complex stress interactions between the columns and surrounding clay and till.

- Post-construction deformations are reasonably explained by extreme porewater pressure conditions, potentially caused by flood events.

- The results of stability analysis are sensitive to the density and assigned shear strength of rockfill. (Table 7.6)

Table 7.1. Summary of analysis cases presented.

| | Constitutive Model | | Rockfill | $K_0$ –clay | v – clay | E-clay | k | Interface |
|---|---|---|---|---|---|---|---|---|
| | Clay | Rockfill | kN/m3 | | | kPa | m/s | |
| Case 1 | LE | LE | - | - | 0.33 | 8000 | - | No |
| Case 2 | EPP | HB | $\gamma$ = 17 | 0.8 | 0.4 | 20,000 | $1 \cdot 10^{-9}$ | No |
| Case 3 | MCC | HB | $\gamma \approx 22$ | Varies | 0.4 | - | $8 \bullet 10^{-10}$ | Columns |
| Case 4 | EPP | HB | $\gamma$ = 17 | 0.8 | 0.33 | 15,000 | $1 \bullet 10^{-9}$ | el. 224 m |

Abbreviations:
LE = Linear elastic
EPP = Elastic perfectly-plastic
HB = Hyperbolic
MCC = Modified Cam-Clay

Table 7.2. Summary of parameters used for modified elastic-perfectly plastic clay materials.

| | Intact Clay | Residual Clay | Limestone Fill | Rockfill | Till |
|---|---|---|---|---|---|
| Φ (°) | 18 | 8 | 37 | 60 | 42 |
| c (kPa) | 5 | 2 | 0 | 0 | 0 |
| E (kPa) | 20,000 | 20,000 | 20,000 | 32,000[1] | 30,000 |
| ν | 0.4 | 0.4 | 0.33 | 0.33 | 0.33 |
| γ (kN/m$^3$) | 17 | 17 | 15.6 | 17 | 23 |

[1] At 100 kPa confining pressure. Calculated according to Equation 2.4.

Table 7.3. Summary of parameters used for modified Cam-Clay materials.

| | Intact | Residual |
|---|---|---|
| Φ (°) | 19 | 8.3 |
| λ | 0.277 | 0.277 |
| κ | 0.012[1] | 0.012[1] |
| $e_o$ | 2.64 | 2.64 |
| ν | 0.4 | 0.4 |
| γ (kN/m$^3$) | 17 | 17 |

[1]Assigned based on sensitivity analysis. Measured values of κ ranged from 0.062 to 0.085

Table 7.4 Summary of parameters used for the numerical modeling of rockfill using the Duncan and Chang (1970) constitutive model for nonlinear analysis.

| | Loose<br>e = 0.80 | Dense<br>e = 0.42 | Field Density<br>e = 0.23 |
|---|---|---|---|
| $\nu$ | 0.33 | 0.33 | 0.33 |
| n | 0.45 | 0.45 | 0.45 |
| k | 100 | 240 | 316 |
| Rf | 0.9 | 0.9 | 0.9 |
| $\Phi_{peak}$ (°) | 46 | 60 | 60 |
| c (kPa) | 0 | 0 | 0 |

Table 7.5 Summary of parameters used for the slope stability analysis

| | Clay: Post-Peak | Clay: Residual | Rockfill | Limestone Fill | Till |
|---|---|---|---|---|---|
| $\gamma$ (kN/m$^3$) | 17 | 17 | 22/17 | 15.6 | 23 |
| $\Phi$ (°) | 18 | 8 | 60 | 37 | 42/$\infty$ |
| c (kpa) | 5 | 2 | 0 | 0.5 | 0 |

Table 7.6. Summary of stability analysis.

| | Case 2 | | | | Case 3 | | | | Limit Equilibrium | |
|---|---|---|---|---|---|---|---|---|---|---|
| | With Residual | | No Residual | $\Phi_{RFC}$ = 50° | With Residual | | No Residual | $\Phi_{RFC}$ = 50° | With Residual | |
| | Critical[1] | Slip 1719 | Critical[1] | Critical[1] | Critical | Slip 1719 | Critical[1,2] | Critical[1] | Critical[1] | Slip 1719 |
| Initial | 1.48 | 1.95 | 1.98 | 1.36 | 1.68 | 2.23 | 1.82 | 1.57 | 1.52 | 2.16 |
| Day 1 | 1.33 | 1.48 | 1.61 | 1.16 | 1.53 | 1.64 | 1.817 | 1.32 | 1.26 | 1.62 |
| Day 2 | 1.21 | 1.26 | 1.45 | 1.06 | 1.36 | 1.38 | 1.648 | 1.19 | 1.20 | 1.39 |
| Day 5 | 1.17 | 1.18 | 1.36 | 1.04 | 1.28 | 1.28 | 1.518 | 1.13 | 1.18 | 1.30 |
| Day 7 | 1.09 | 1.09 | 1.25 | 0.98 | 1.17 | 1.17 | 1.38 | 1.04 | 1.15 | 1.22 |
| Day 8 | 1.04 | 1.04 | 1.19 | 0.95 | 1.11 | 1.11 | 1.30 | 0.99 | 1.13 | 1.18 |
| Day 9 | 1.01 | 1.01 | 1.18 | 0.95 | 1.07 | 1.07 | 1.29 | 0.99 | 1.12 | 1.16 |

[1]Critical slip surface was considered to be a one which passed through the columns at least 3 m below the surface. Lower slope failure surfaces were only critical up to day 2.

[2]Slip 1719 was critical from day 5 to day 9

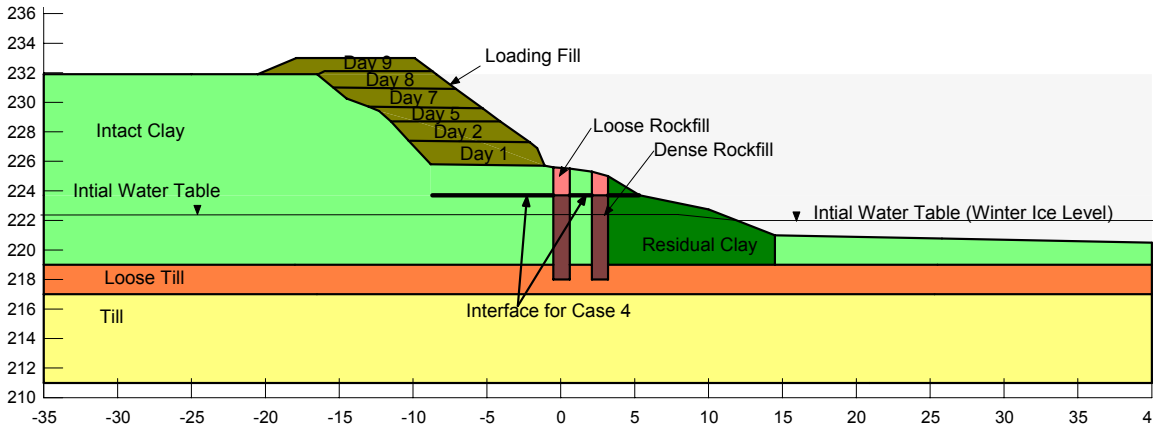


Figure 7.1. Typical section of test loading used in numerical analysis.

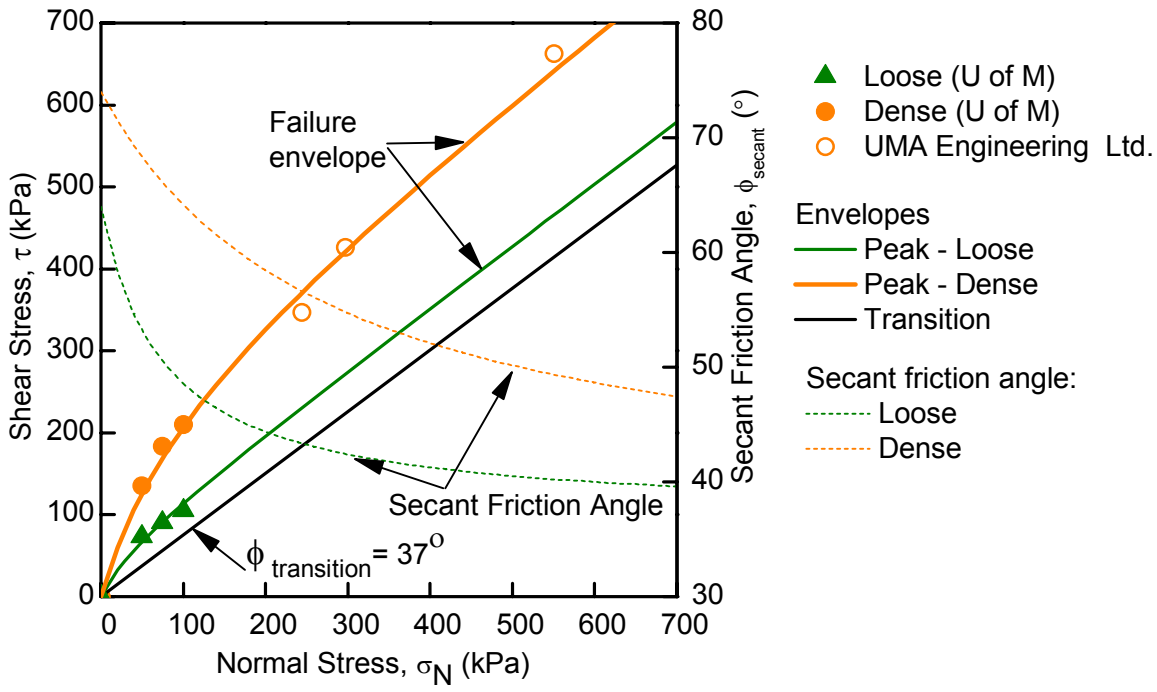


Figure 7.2. Interpreted failure envelopes for rockfill using method presented in Maksimovic (Maksimovic 1996).

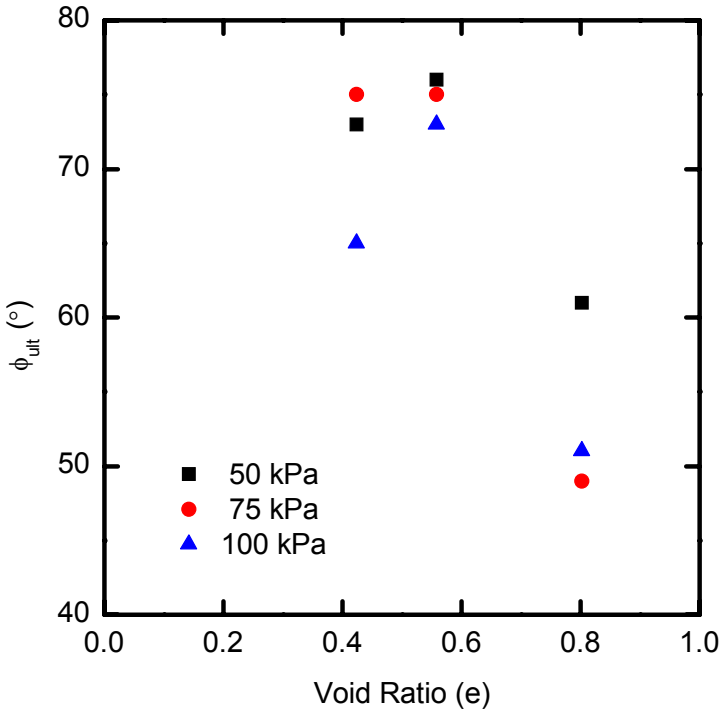


Figure 7.3. Friction angle corresponding to the estimated ultimate strength (asymptote to a fitted hyperbolic stress-strain curve) versus void ratio for crushed rockfill.

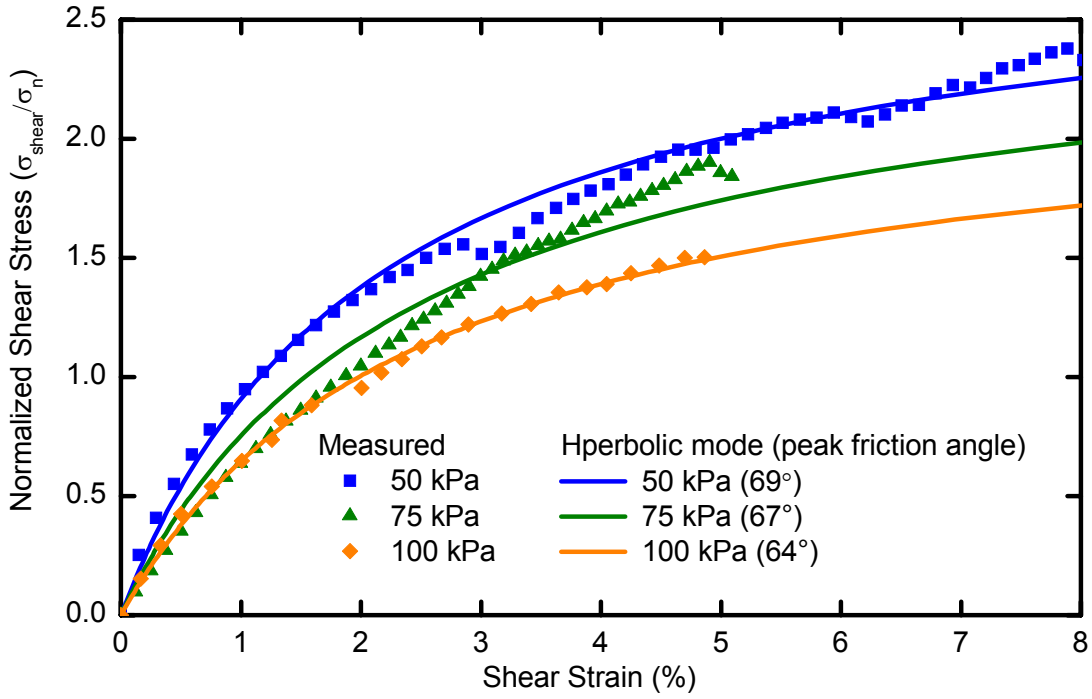


Figure 7.4. Stress-strain curves for direct shear tests of dense limestone rockfill fitted with the hyperbolic model.

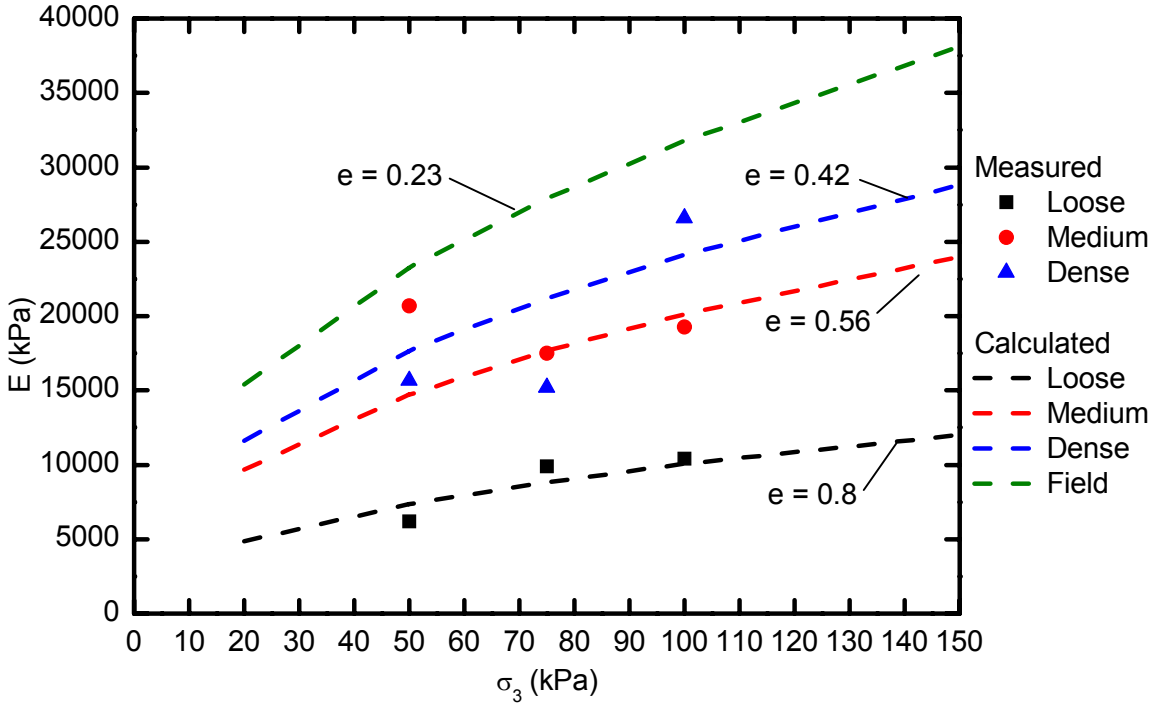


Figure 7.5. Modulus of elasticity of rockfill (initial) versus confining pressure at various densities.

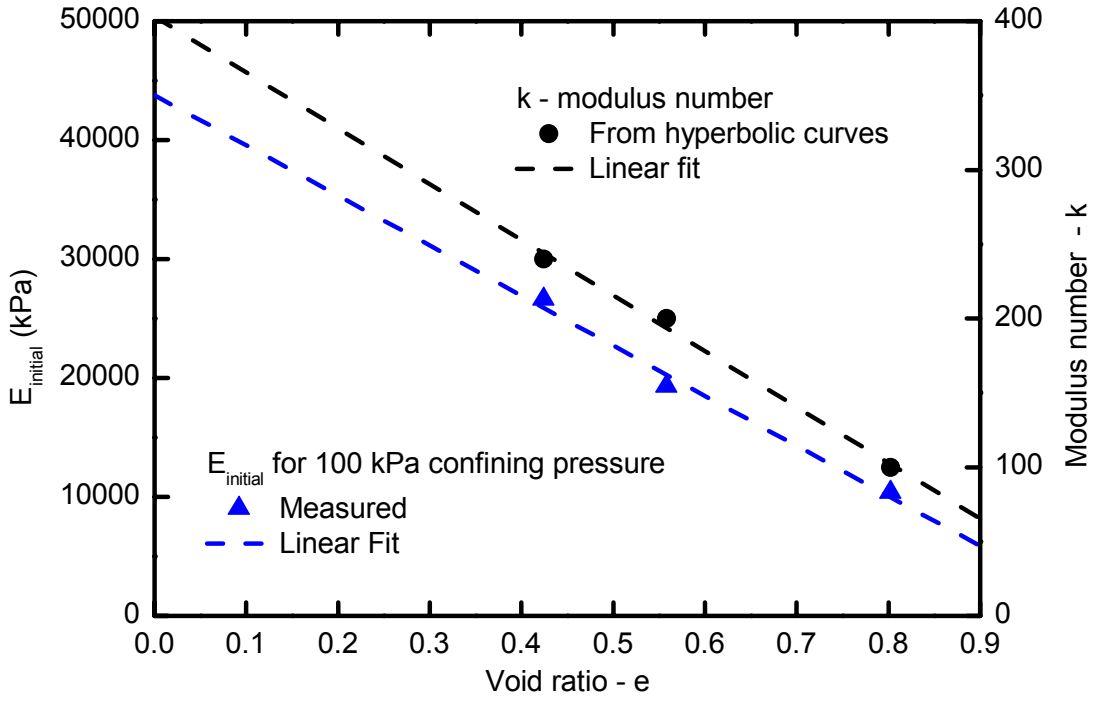


Figure 7.6. Modulus of elasticity of rockfill (initial) and modulus number plotted versus initial void ratio.

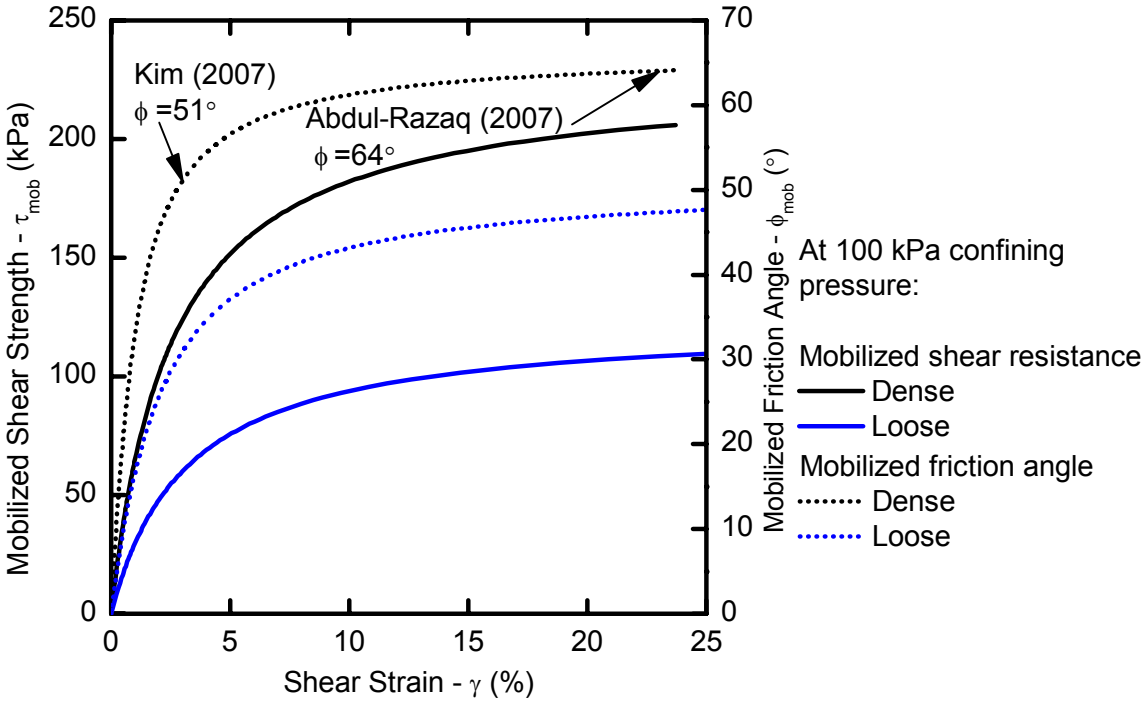


Figure 7.7. Mobilized shear strength and friction angle for dense specimen at 100 kPa confining pressure. Based on hyperbolic constitutive model fit to large scale direct shear test results.

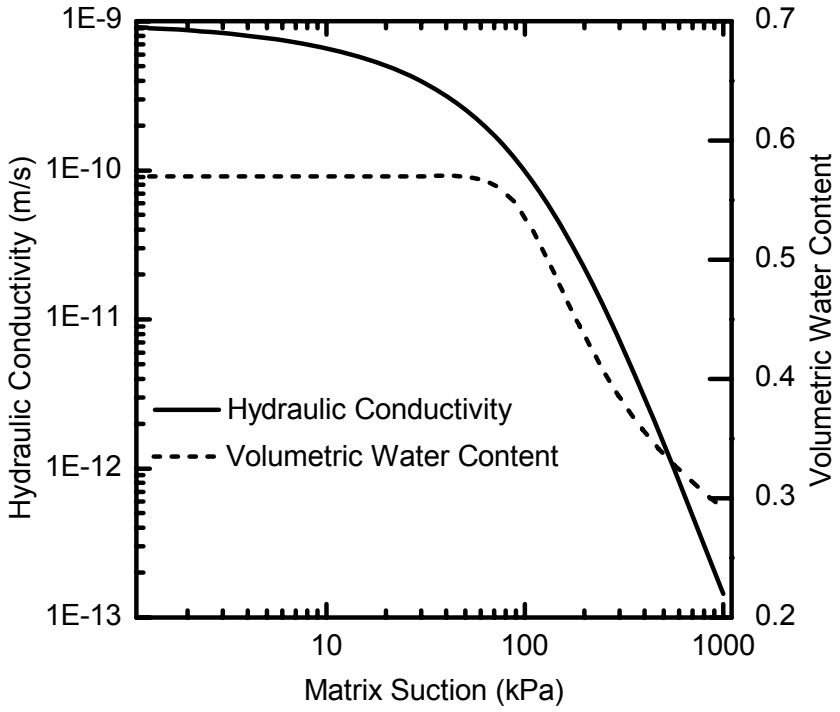


Figure 7.8. Hydraulic conductivity and volumetric water content curves for clay, used in the numerical modeling.

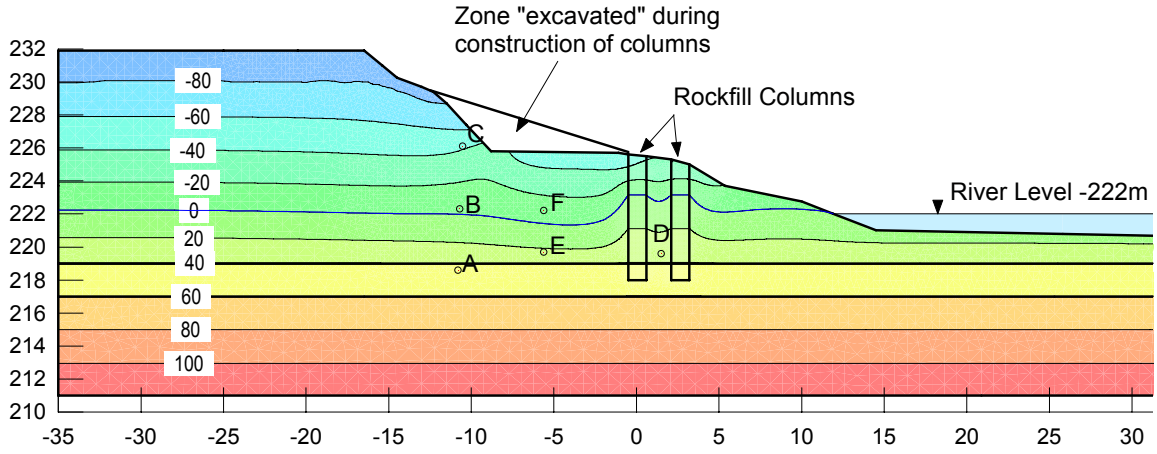


Figure 7.9. Initial porewater pressure distribution, after simulating unloading during construction.

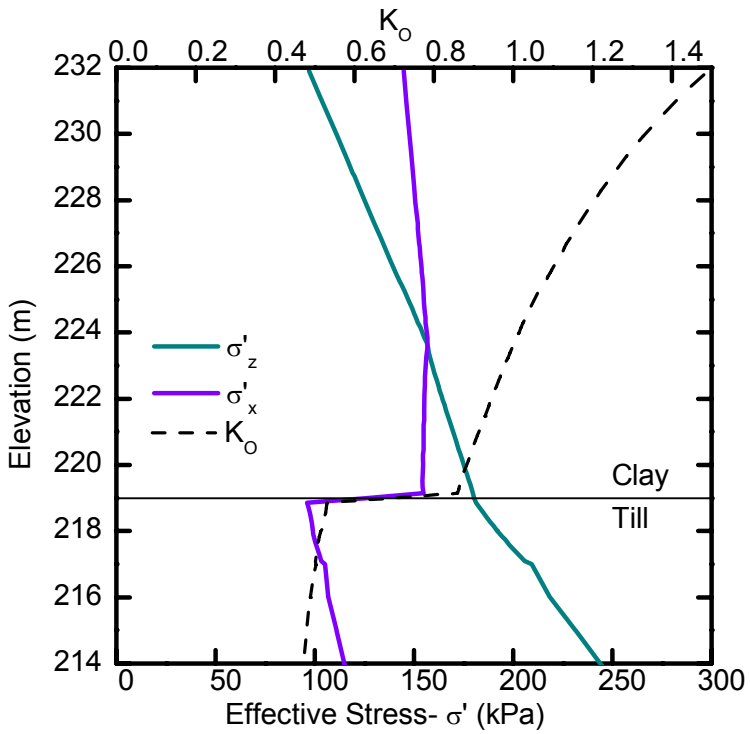


Figure 7.10. Vertical and horizontal effective stresses and Ko distribution for Case 3.

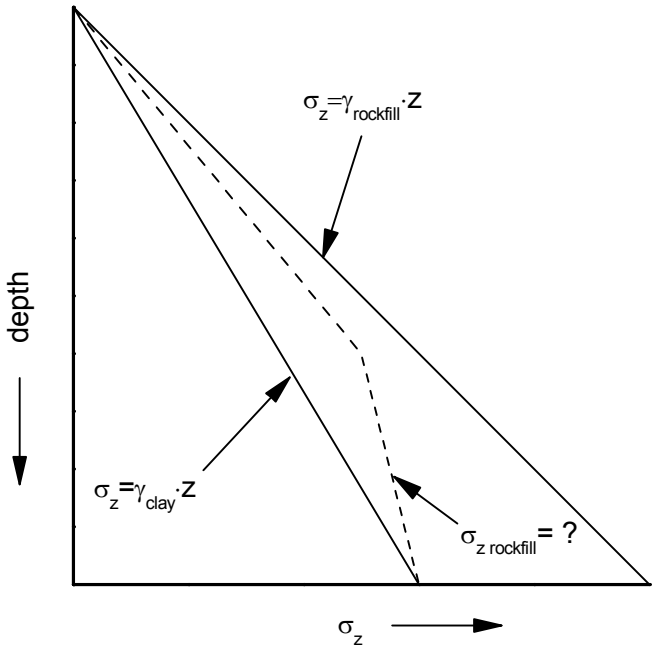


Figure 7.11 Illustration of plausible in-situ vertical stress profiles in a compacted rockfill column.

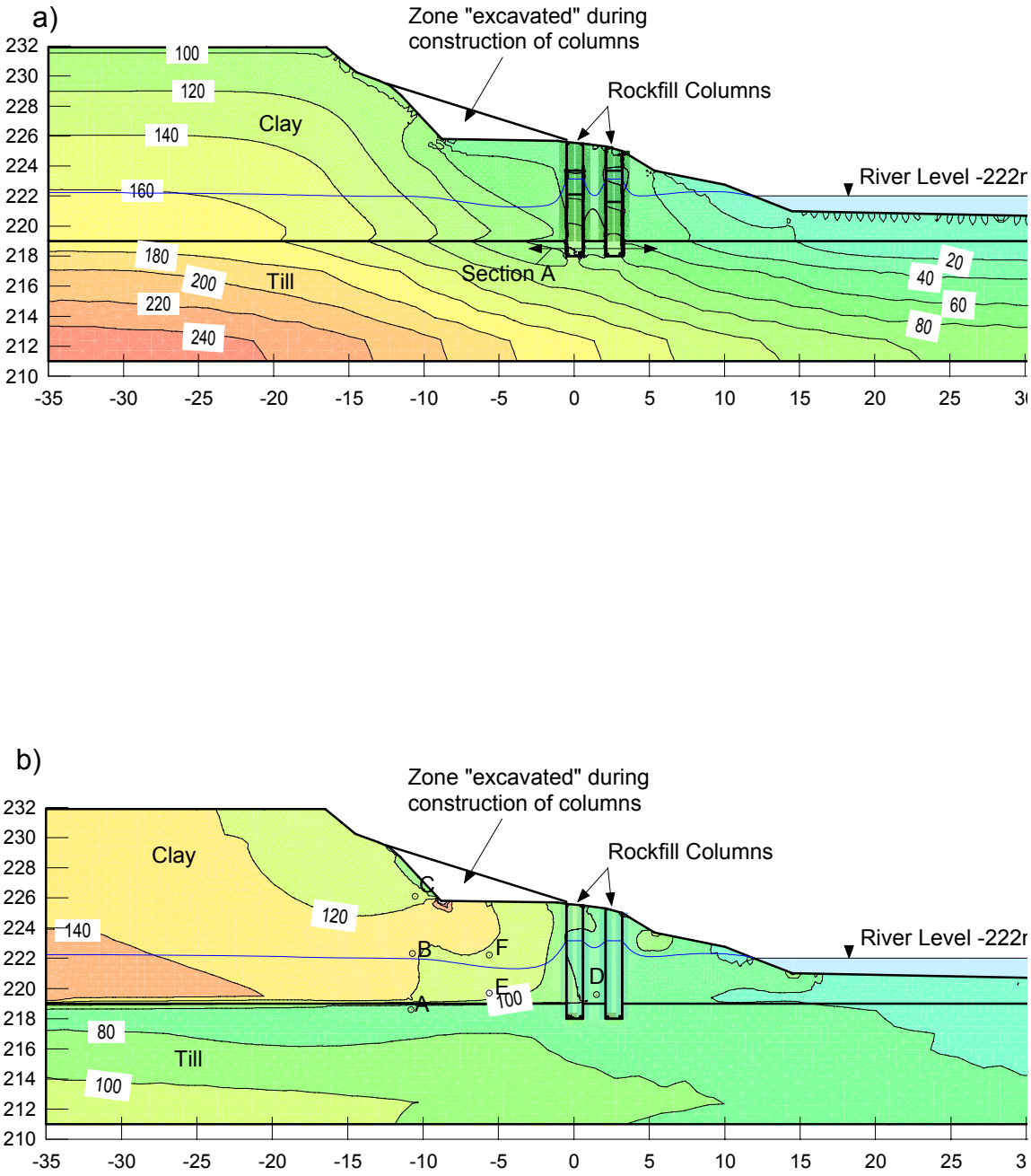


Figure 7.12. In-situ stresses used for day 0 for MCC stress-deformation modeling (Case 3). a) Vertical effective stress and b) horizontal effective stress.

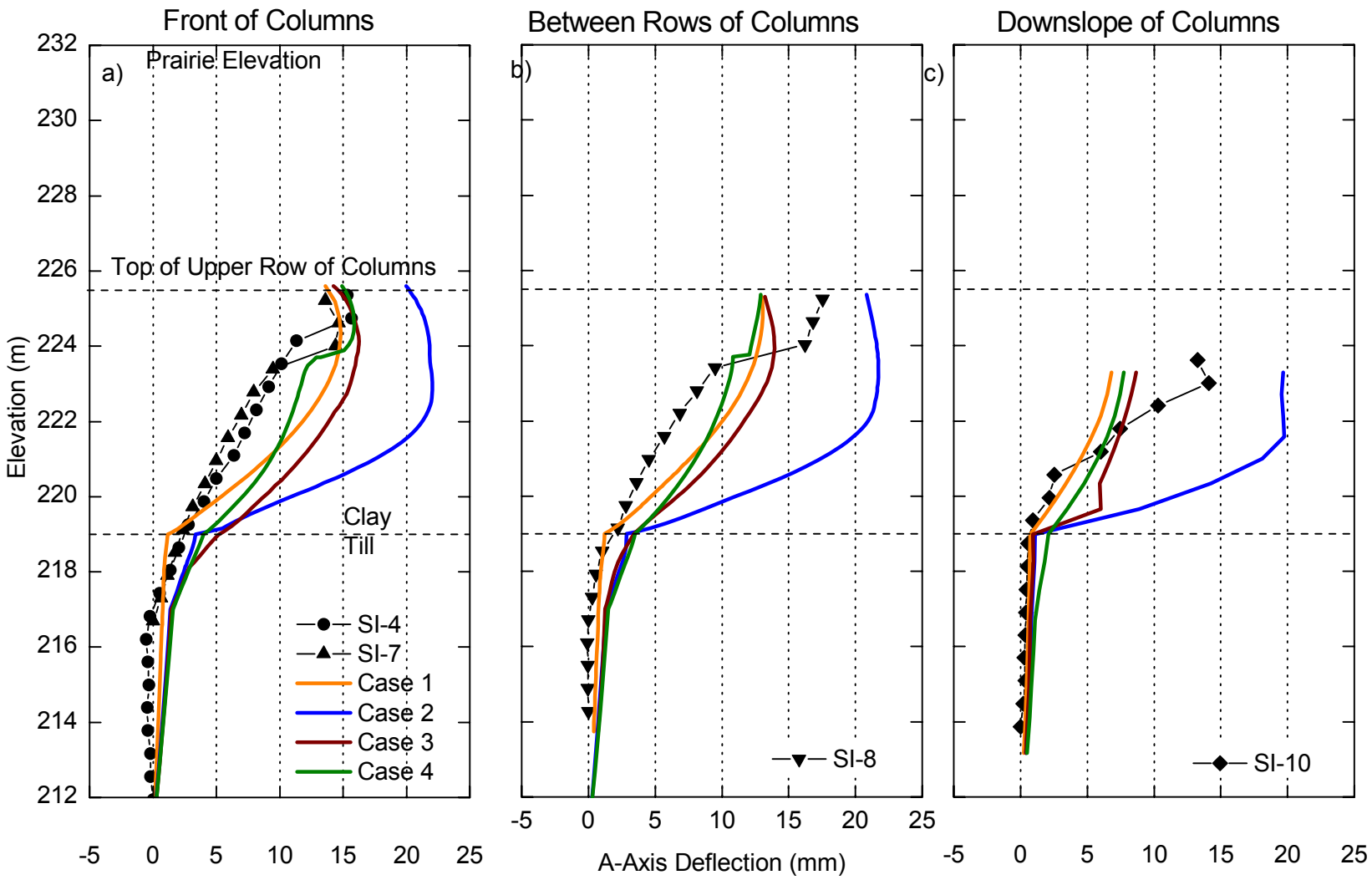


Figure 7.13. Measured displacements compared to modeled displacements from the four modeling cases.

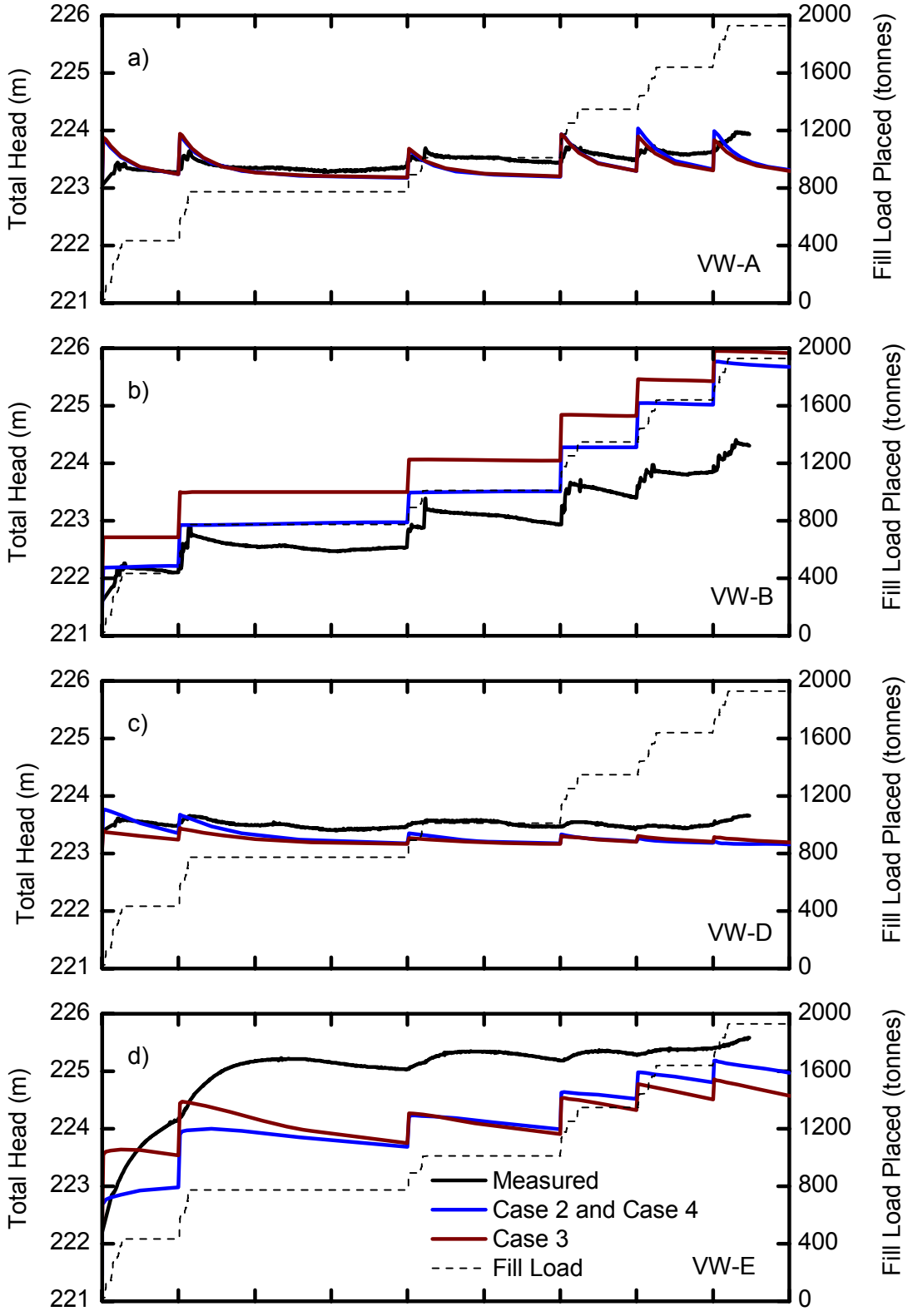


Figure 7.14. Modeled versus measured porewater pressures for a) VW-A, b) VW-B, c) VW-D and d) VW-E.

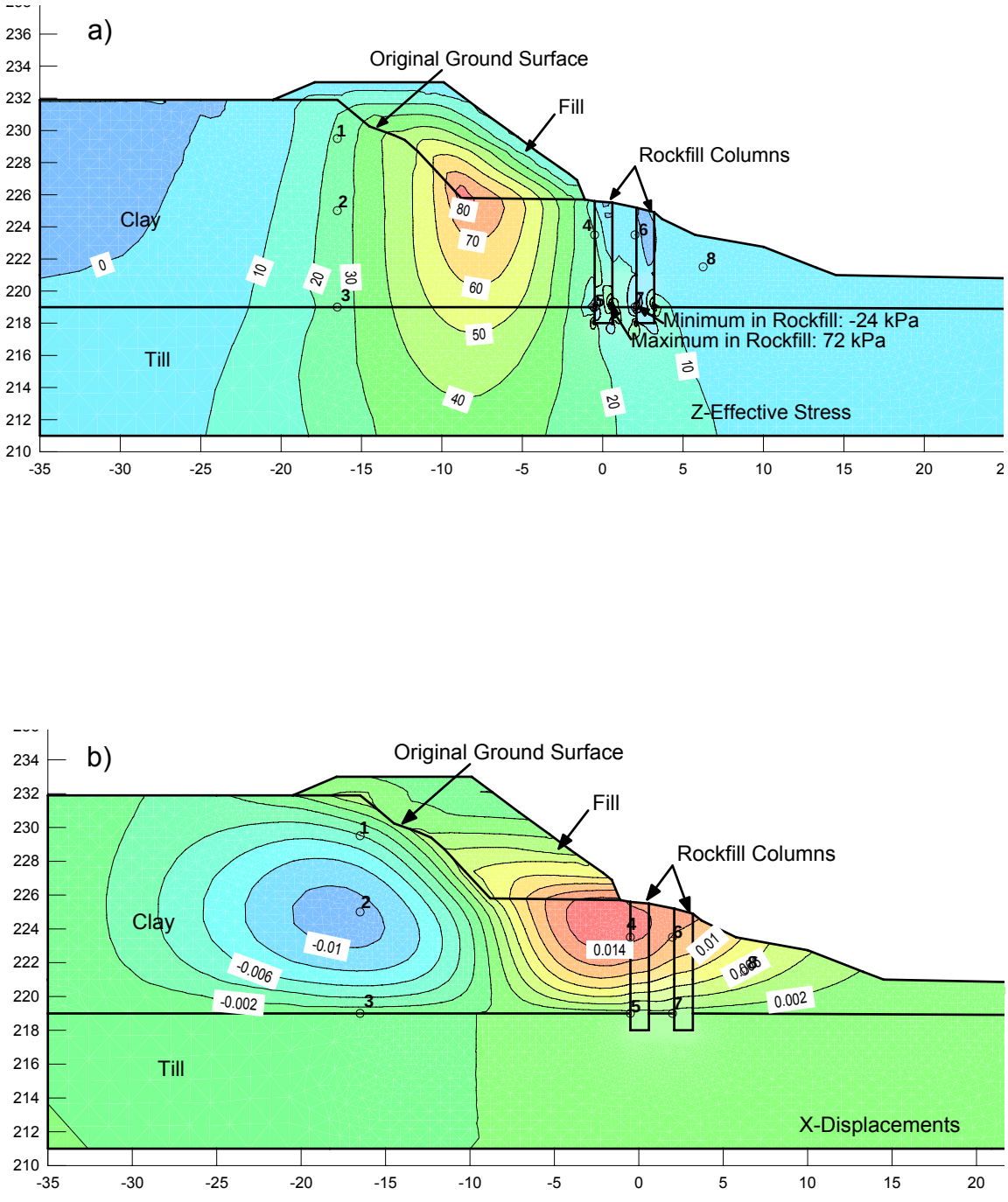


Figure 7.15. Linear-elastic analysis (Case 1) of test loading showing a) Y-effective stress increase and b) X-direction displacement due to loading.

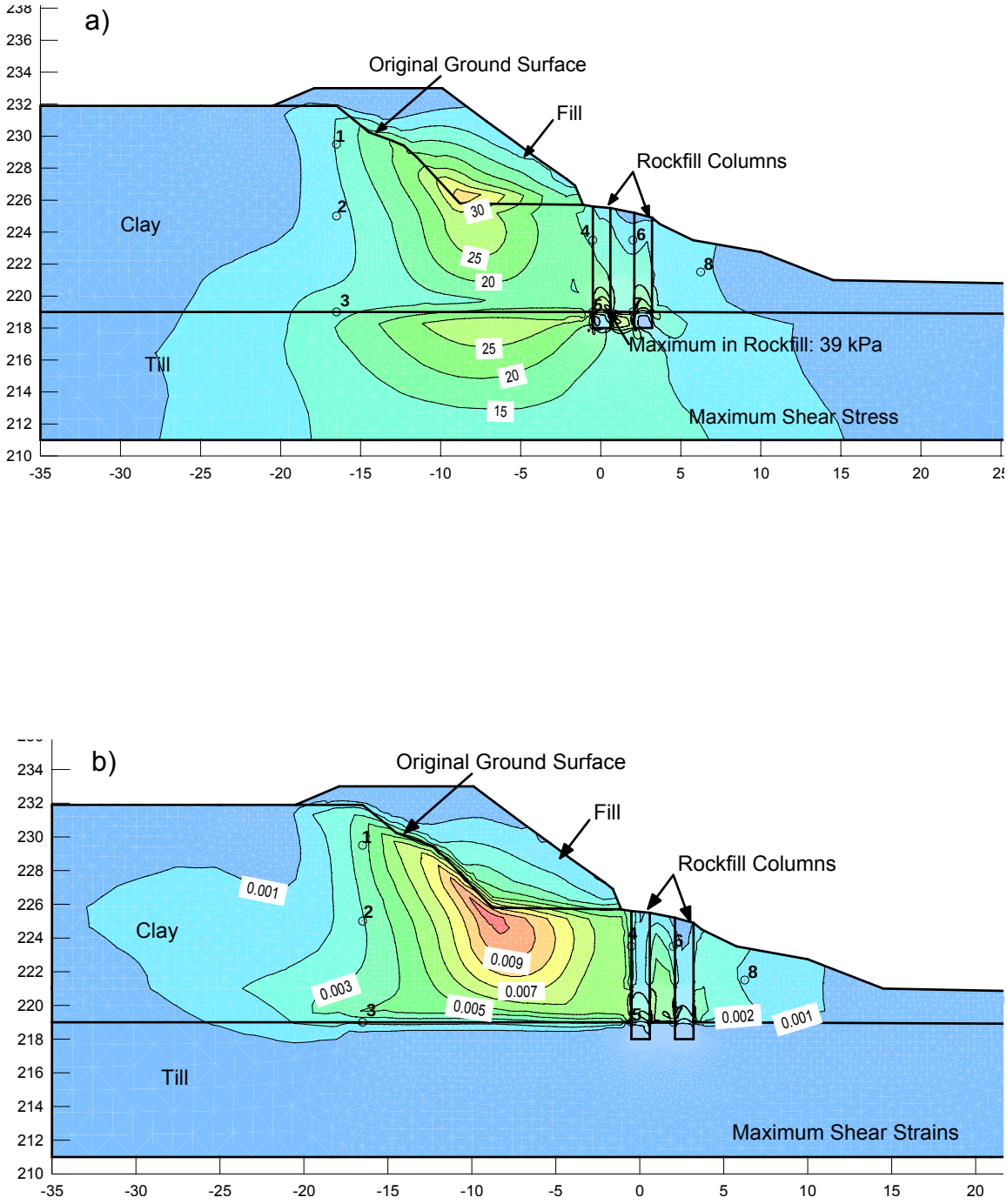


Figure 7.16. Linear-elastic analysis (Case 1) of test loading showing a) maximum shear stress and b) maximum shear strains at day 11 of the test loading.

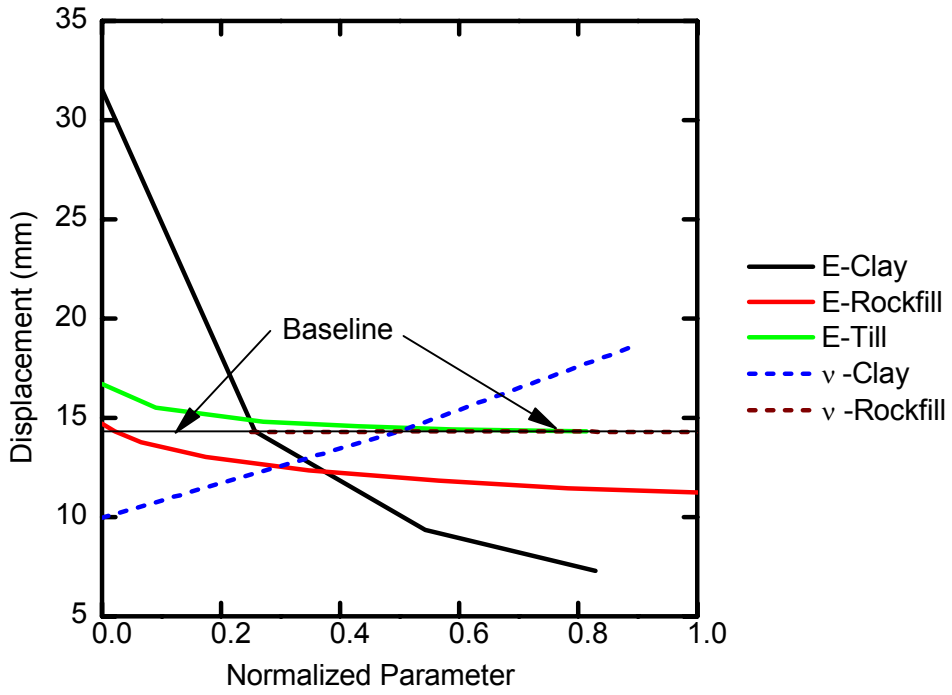


| | Minimum (Normalized = 0) | Maximum (Normalized = 1) | Baseline |
|---|---|---|---|
| E – Clay (kPa) | 3,500 | 21,000 | 8000 |
| E – Rockfill (kPa) | 20,000 | 250,000 | 25000 |
| E – Till (kPa) | 20,000 | 240,000 | 200000 |
| ν – Clay | 0.3 | 0.5 | 0.4 |
| ν - Rockfill | 0.2 | 0.4 | 0.33 |

Figure 7.17. Sensitivity of displacement to normalized parameters. Maximum and minimum values (normalized to 0 and 1 respectively) are typical or reasonable bounds for the specific parameter. Displacements were recorded at elevation 223.5 (Point '4' in Figure 7.16)

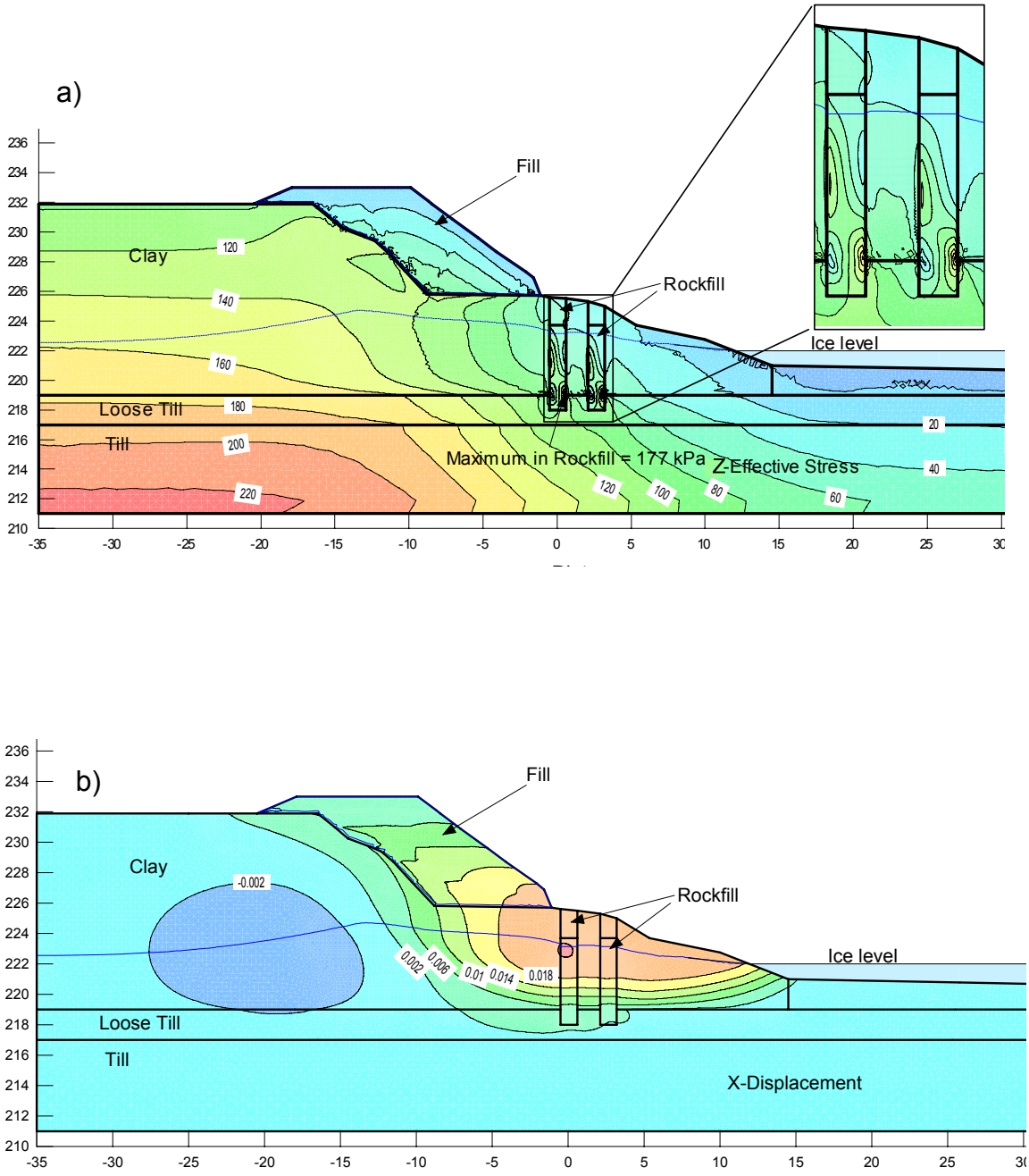


Figure 7.18. Case 2 stress-deformation analysis of test loading showing a) Z-effective stresses and b) X-direction displacement at day 11 of the test loading.

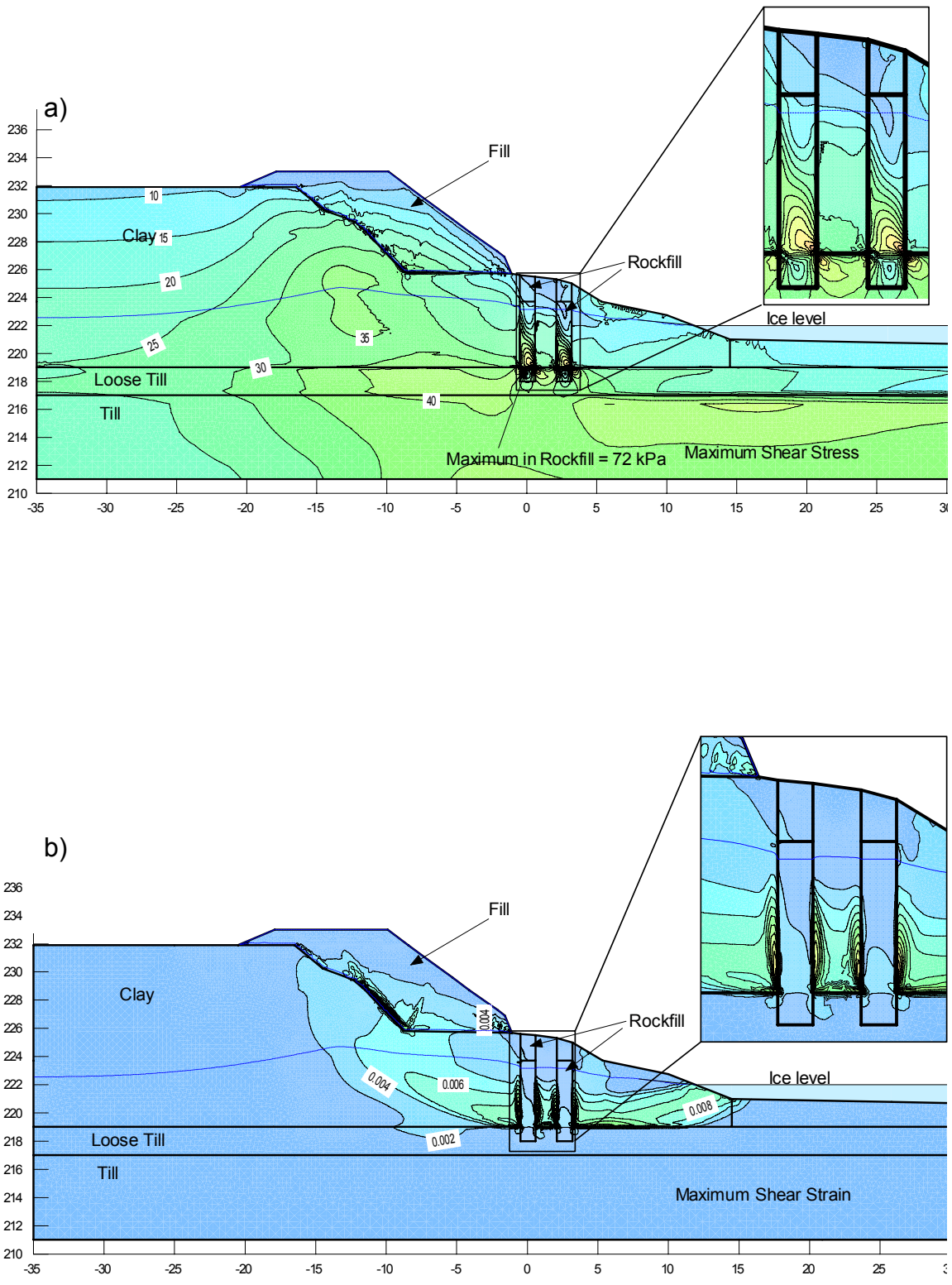


Figure 7.19.Case 2: Stress-deformation analysis of test loading showing a) maximum shear stress and b) maximum shear strains, at day 11 of the test loading

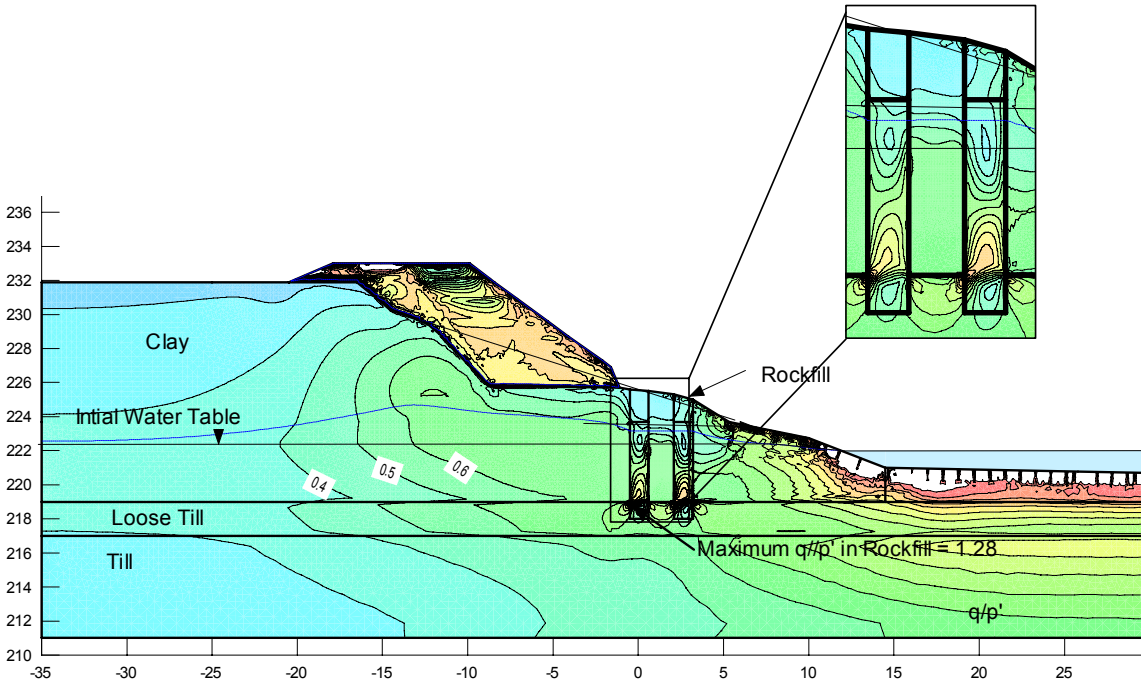


Figure 7.20. Case 2 q/p'.

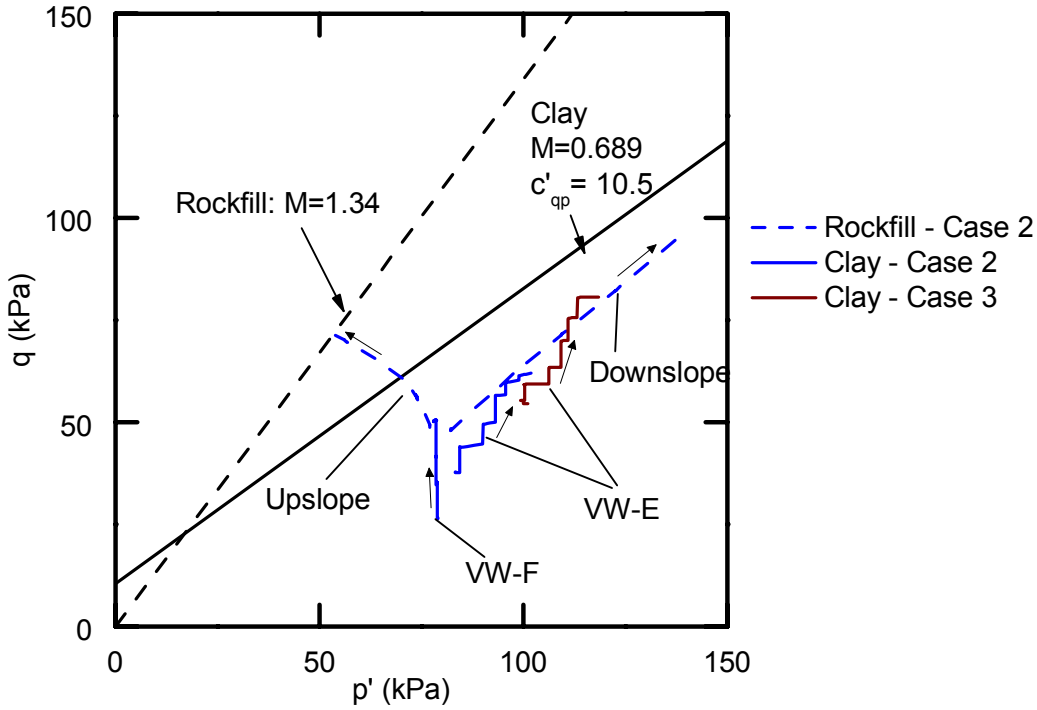


Figure 7.21. Stress-paths in q-p' space for select points. Rockfill points are taken at the clay-till interface, ~0.1m from the upslope and downslope edges of the upper equivalent strip.

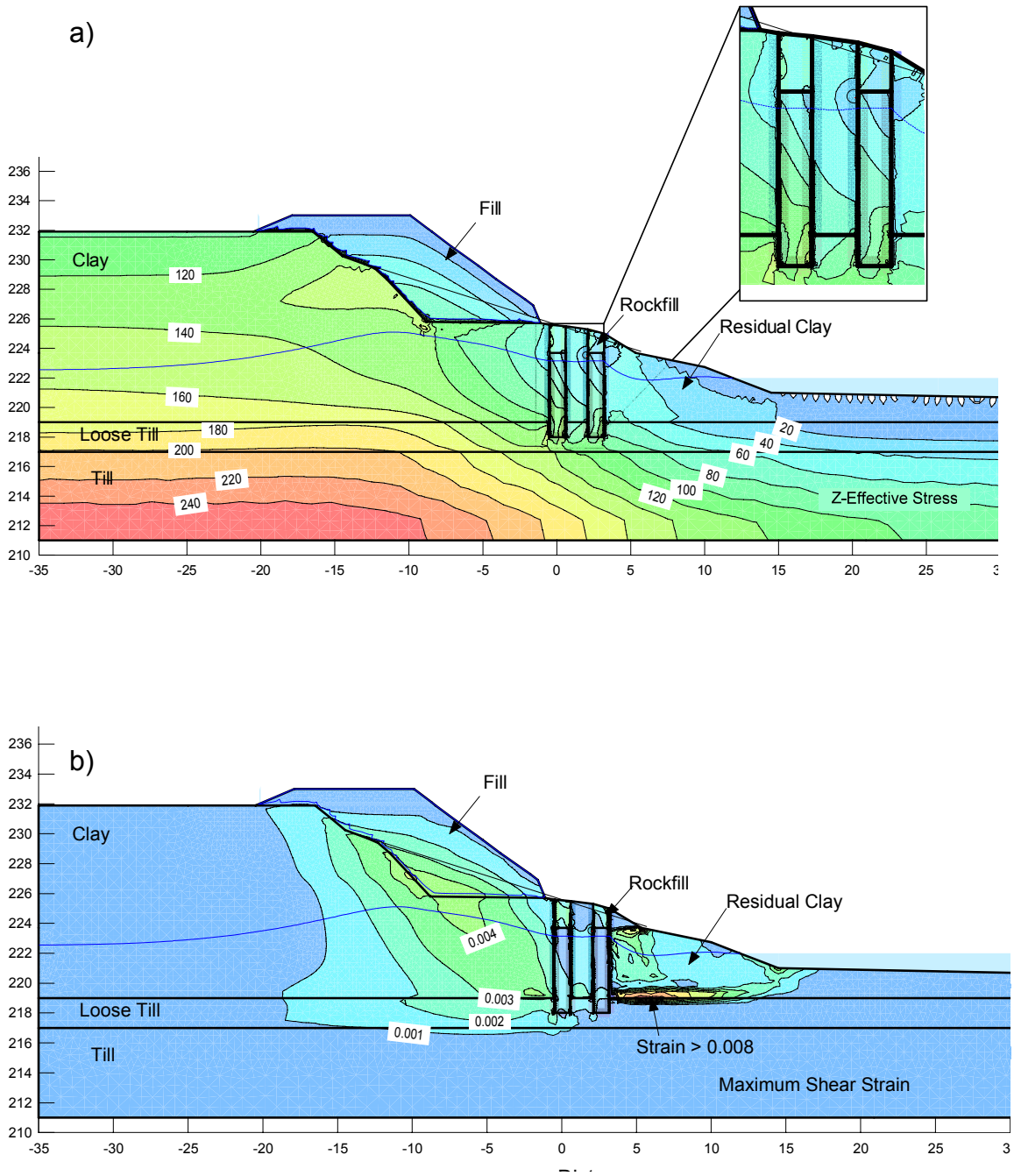


Figure 7.22. Case 3: a) Contours of Z-effective stress, and b) maximum shear strain.

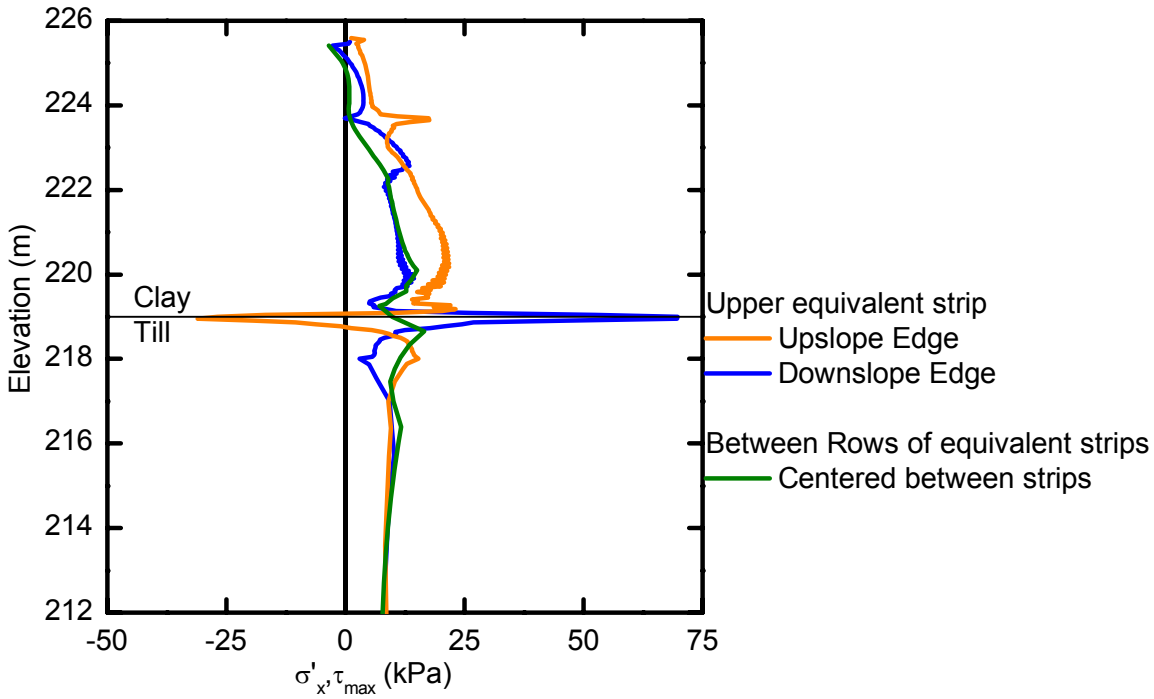


Figure 7.23. Horizontal stress change distributed along vertical edges of the upslope row of columns (equivalent strips) and in-between rows. Max shear stress along centerline of upper row column.

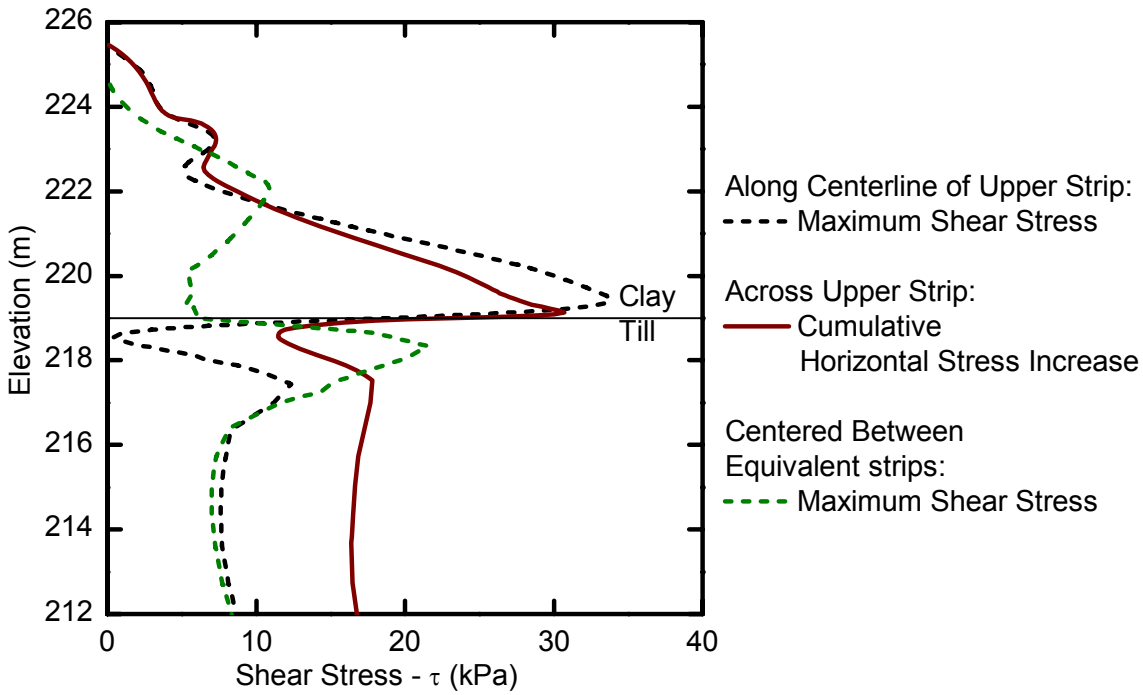


Figure 7.24. Incremental shear stresses (day 11 –day 0) in modeled equivalent strip, and between equivalent strips, also showing cumulative (integrated from surface downward) incremental stress increase across equivalent strip.

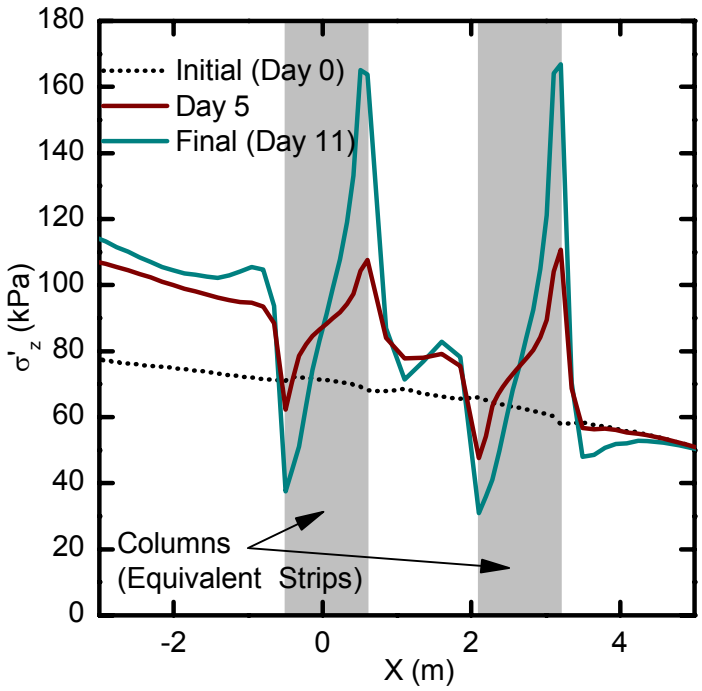


Figure 7.25. Vertical effective stress distribution across the equivalent strips at elevation 219 m. Section (A-A) shown in Figure 7.12 a).

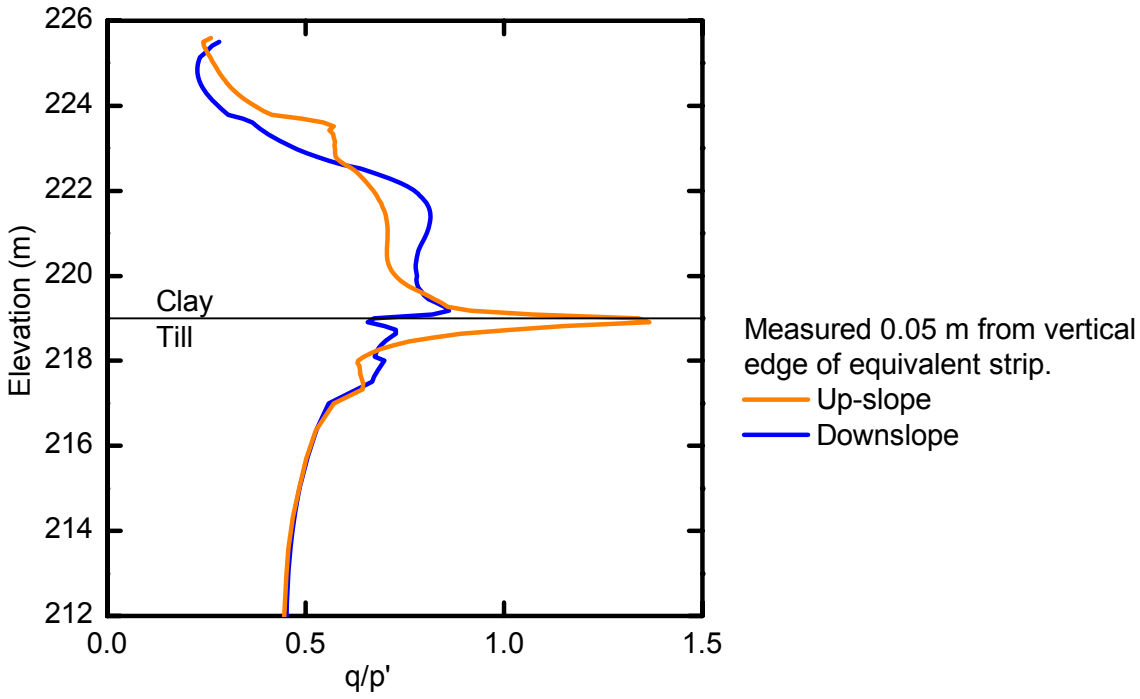


Figure 7.26. Deviatoric stress (q) and mean effective stress (p') near the edges of the upslope equivalent strip.

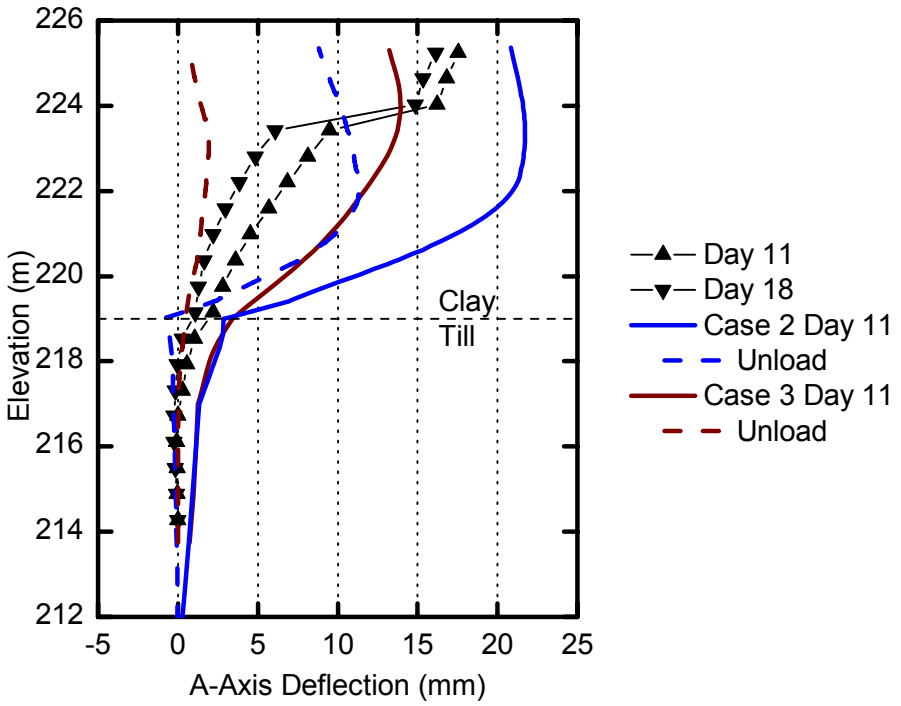


Figure 7.27. Elastic rebound, measured and modeled for SI-8, in-between rows of columns.

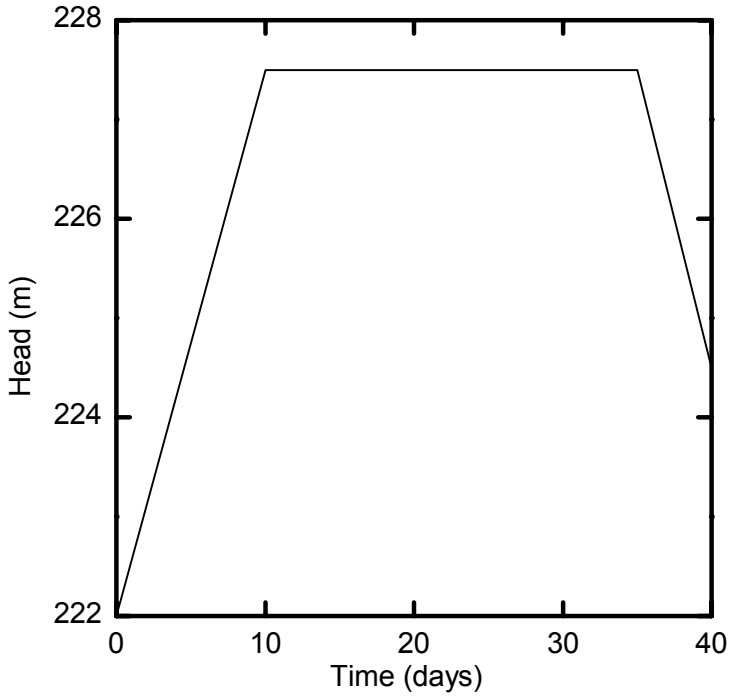


Figure 7.28. Total head boundary condition for simulated flood event.

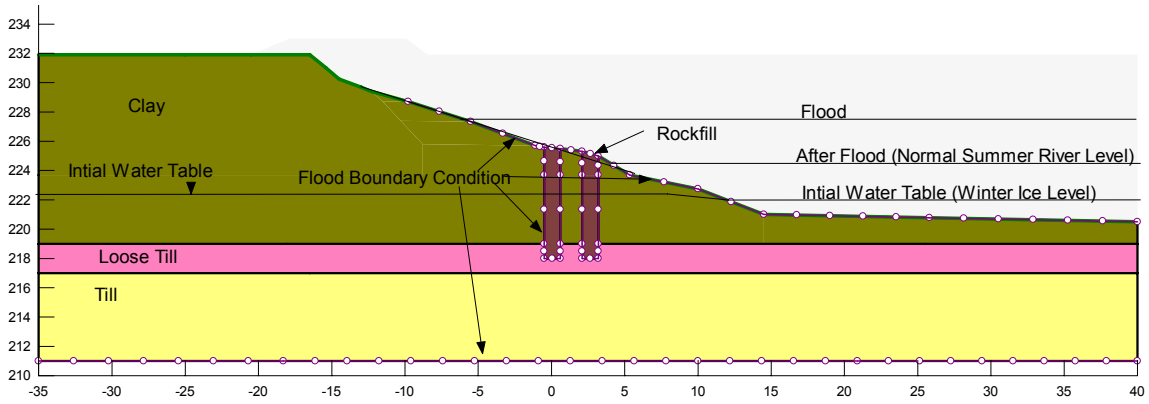


Figure 7.29. Boundary conditions for flood event analysis.

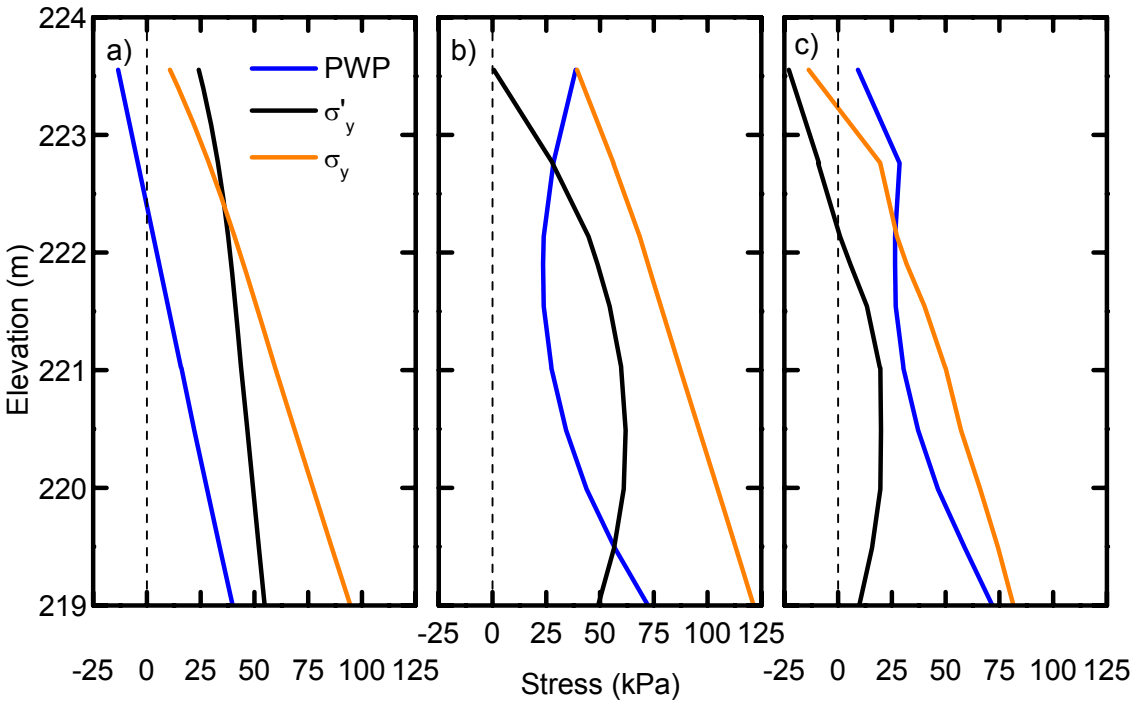


Figure 7.30 Porewater pressure, vertical effective and vertical total stress distributions in clay for a) initial condition b) day 35 of flood stage c) immediately after drawdown.

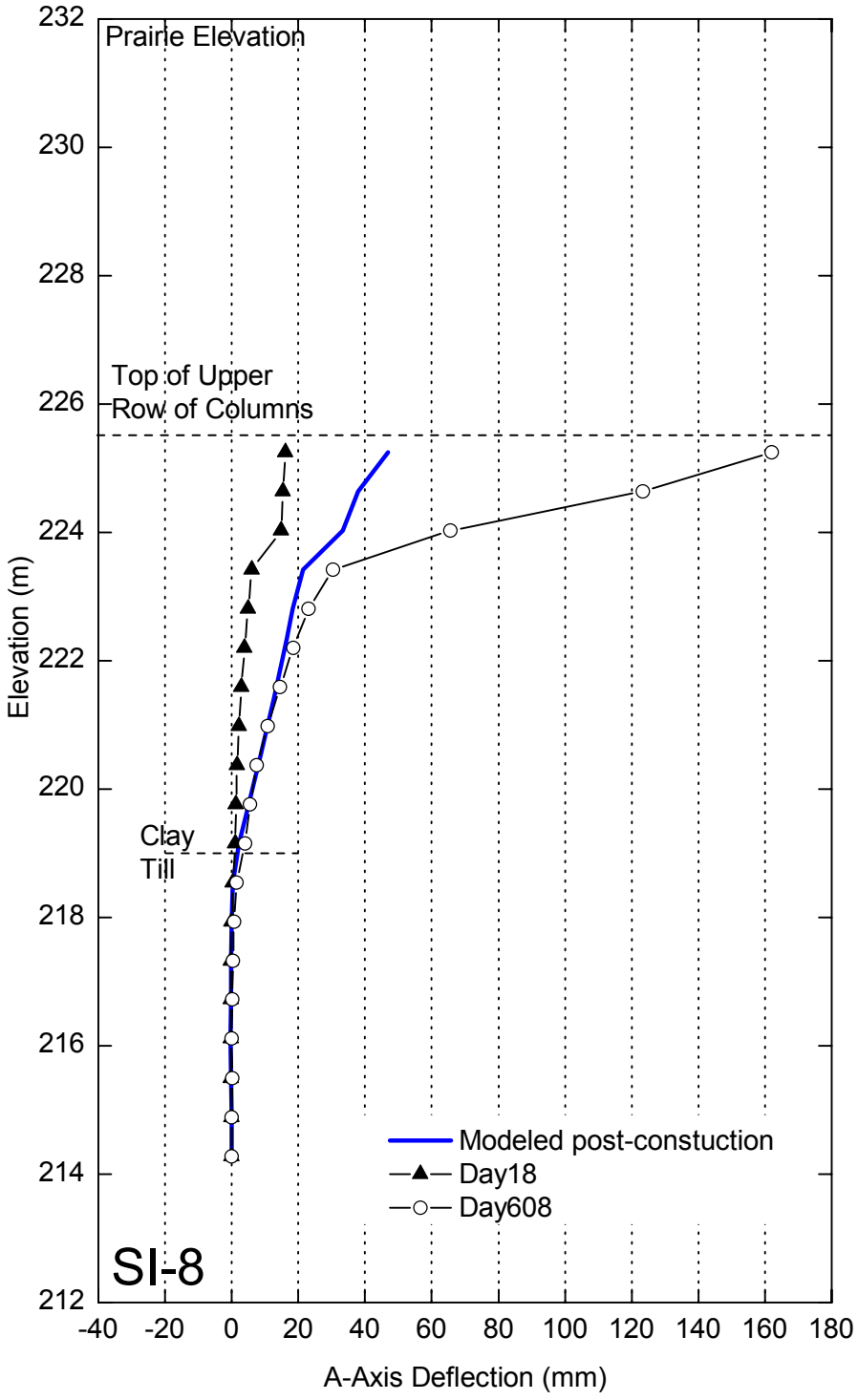


Figure 7.31 Post-test displacements from the research site, both measured and modeled.

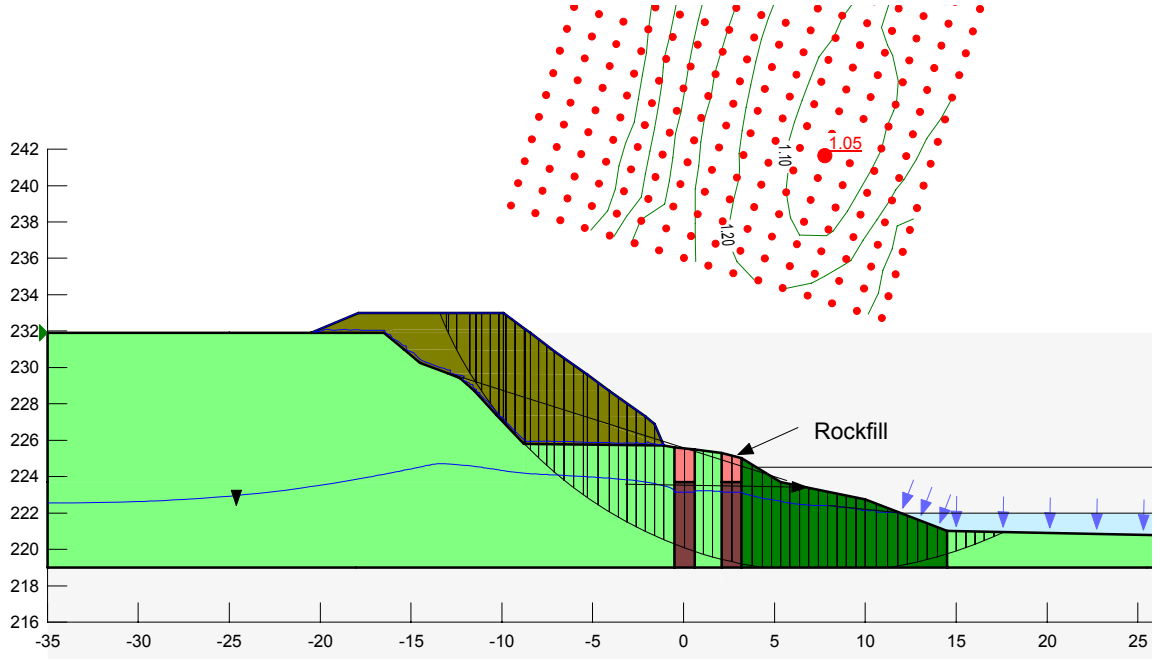


Figure 7.32.Cross section from stability analysis, showing slip surface 1719.

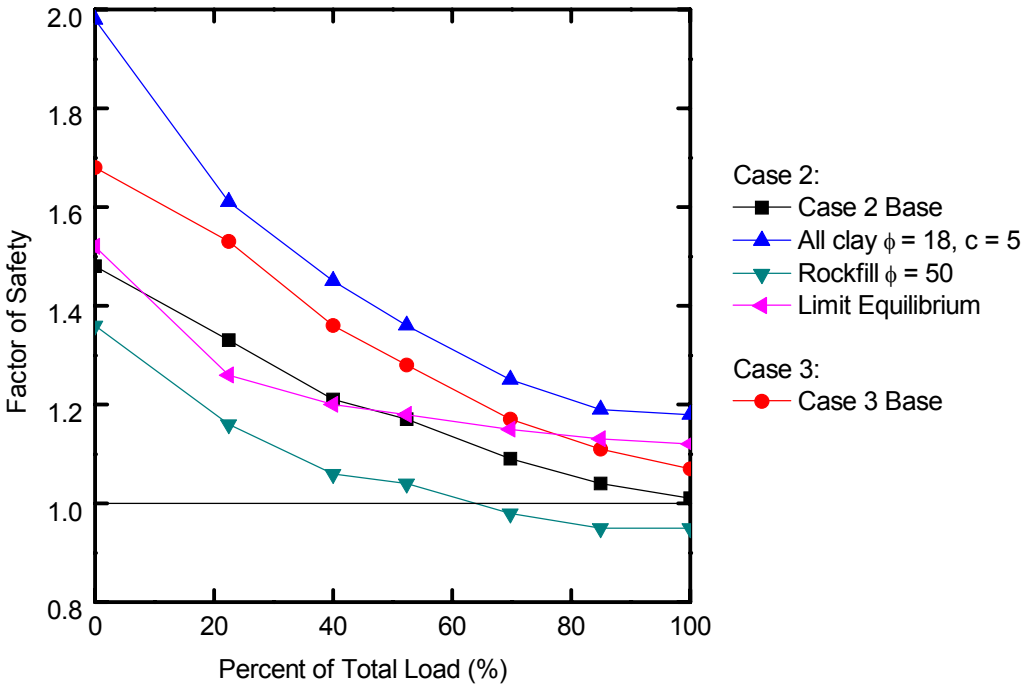


Figure 7.33. Summary of stability analysis results for test loading. The base cases have a zone of soil at residual strength at the toe.

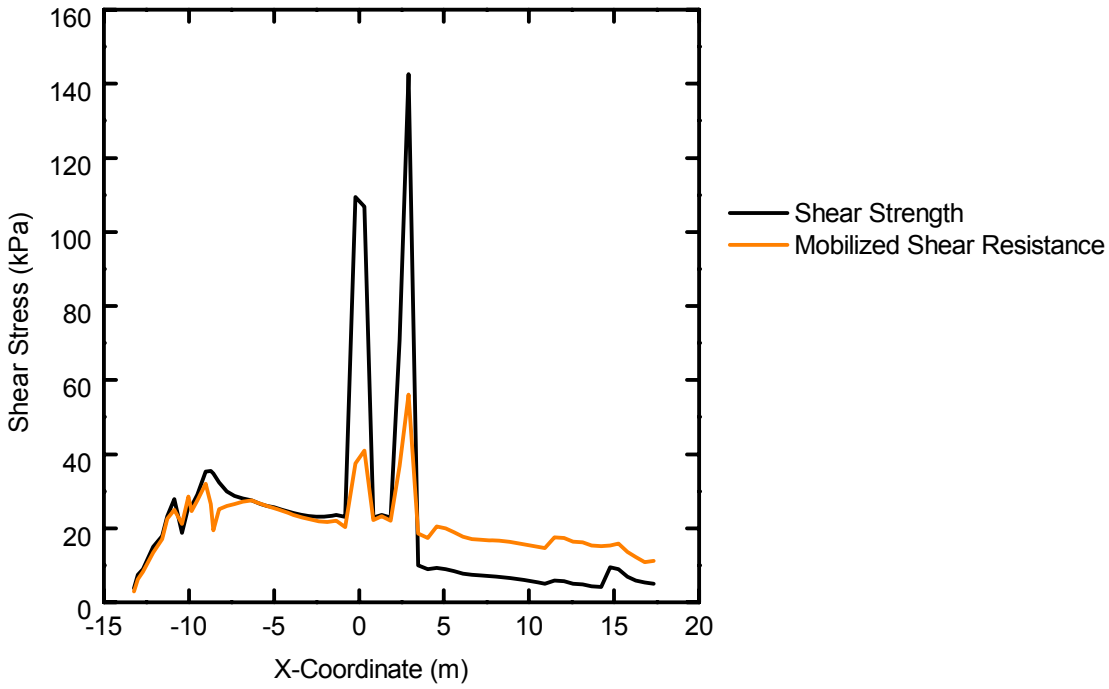


Figure 7.34. Mobilized shear strength and shear resistance along slip surface 1719 (day 9)

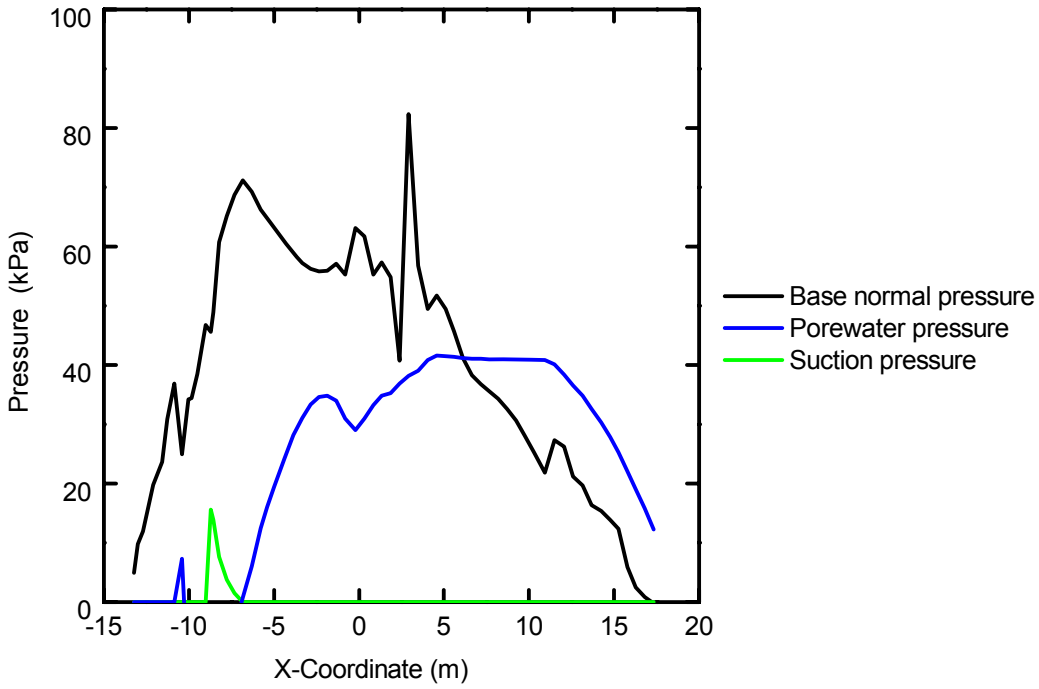


Figure 7.35. Distribution of normal, porewater and suction pressures along slip surface 1719 (day 9)

# 8. SUMMARY, CONCLUSIONS AND RECOMMENDATIONS

## 8.1 Summary

This research project investigated the performance of rockfill columns for the stabilization of a riverbank in natural clay. A full-scale field test was conducted over a period of 11 days in February-March 2008. The test section was located along the Red River in the City of Winnipeg. A 19 m test section was loaded with a surcharge of over 1900 tonnes of fill material that was placed on the bank, upslope of the rockfill columns, and caused deformations of the slope.

The porewater pressure response to loading was monitored by standpipes and vibrating wire piezometers. Deformations were measured by nine slope inclinometers. Two strings of in-place inclinometers and the vibrating wire piezometers were continuously monitored with a data acquisition system during the test loading. Displacements of up to 18 mm were measured during the test loading. The slope demonstrated partial rebound upon unloading, which shows that both elastic and plastic deformations had occurred during the test loading. Ongoing monitoring of the site has identified additional deformations that are understood to have been caused by high porewater pressure events since the completion of the test loading. The site investigation, instrumentation, design, construction, testing and results are discussed in detail in Chapters 3 to 6.

The mechanisms of the performance of rockfill columns were further investigated with the development of numerical models that were calibrated to the results of the test. The hyperbolic constitutive model (Duncan and Chang 1970) was used to fit the test results of Abdul-Razaq (2007) and Kim (2007). A non-linear strength envelope was also used to fit the laboratory testing data, using the method proposed by Maksimovic (1996). These constitutive models were used to develop a coupled consolidation model using the finite element method. The numerical analysis was able to replicate most aspects of the observed behaviour during the test loading. The modeling verified the re-distribution of stresses within the rockfill columns as a result of loading. Sensitivity analysis illustrated the relative influence of various rockfill and clay parameters on the overall slope behaviour.

## 8.2 Major Conclusions

1. Rockfill columns undergo shear strains in the process of resisting slope movements.

   *Supporting Comments:*

   a. Displacements were measured along the full length of the rockfill columns during the test loading, including in the till.

   b. The modeling results have shown a reduction in horizontal stresses across the equivalent strips ($\sigma_{x\ upslope} - \sigma_{x\ downslope}$). The integral of the horizontal stress change is very similar to the maximum shear

stress distribution, multiplied by the strip width, indicating that the shear stresses in the rockfill are associated with horizontal stabilizing forces. Numerical analysis also demonstrates the development of reaction stresses in the till.

2. Rockfill columns undergo bending deformations in the process of resisting slope movements.

   *Supporting Comments:*

   a. The characteristics of bending behaviour were identified in the displacements measured in the test loading.

   b. The numerical modeling further confirmed these observations by demonstrating that internal moments develop within modeled equivalent strips.

3. Rockfill columns are an effective method of slope stabilization provided attention is given to details that need to be considered. Deformations are required to mobilize the shear resistance of the columns. A relatively low initial modulus and high peak strength require large strains to mobilize the full capacity of the rockfill. The length of the columns, and the distribution of horizontal stresses on the column will also influence the total displacements. Compacted rockfill has both high stiffness and higher strength characteristics compared to un-compacted rockfill.

4. The deformations of rockfill columns subjected to loading can be modeled approximately.

   *Supporting comments:*

   a. Stress-deformation and coupled-consolidation models of a slope stabilized with rockfill columns are more sensitive to assigned material parameters for the clay than to those of the rockfill.

   b. The hyperbolic constitutive model provides a good fit to the stress-deformation characteristics of rockfill: linear elastic or elastic-perfectly plastic constitutive models are adequate if strains are relatively small.

5. High porewater pressure events caused by flooding or extended wet periods are the likely cause of displacements after construction.

   *Supporting Comments:*

   These events mobilize the shear resistance of the columns. The displacements measured after the test loading have been greater than the displacements initiated by the test loading. High porewater pressures cause displacements by reducing the effective stresses in the in-situ clay and rockfill and therefore their strengths.

### 8.2.1 Minor Conclusions

1. Inclinometer casings can be installed in a rockfill column, and these installations provide a valuable measure of column performance.

   *Supporting Comments:*

   a. Inclinometer casings installed directly into the column, before backfilling and compaction, have a reasonable probability of surviving the compaction process without being critically damaged. This is an economical way of providing an opportunity for long term deformation modeling.

2. The rockfill columns and the surrounding in-situ clay displaced as a continuum during the test loading.

3. The magnitude of the maximum displacement measured downslope of the columns was similar to the maximum displacement in the area of columns.

4. Flow of clay around the rockfill columns was not observed during the test loading.[1]

5. The non-linear strength envelopes developed using the method proposed by Maksimovic (1996) fit the measured strengths of local crushed limestone rockfill quite well. The secant friction angle is useful for

[1] Post-construction monitoring has measured shallow displacements that are greater in the clay adjacent to the columns than in the columns themselves. The Author has not come to a conclusion regarding whether these differential movements are the result of a mechanism related to the columns, or are caused by some other unrelated phenomenon.

determining an appropriate design strength provided the correct range of stresses is used.

6. Plotting the mobilized friction angle versus shear strain (using the hyperbolic constitutive model) is a useful tool for determining the magnitude of straining to be expected under design conditions.

7. Some conclusions from the numerical analysis:

    a. Rockfill columns increase the 'stiffness' of a soil mass, but the benefit is limited because

        i. Rockfill is only 2-4 times stiffer than the in-situ clay.

        ii. The area replacement ratio is typically quite small considering the entire soil mass being stabilized.

    b. It is difficult to develop an appropriate stress distribution within the equivalent strips, if the full unit weight of the rockfill is to be modeled. This has a limited impact on the load deformation characteristics of a modeled domain, but it has larger consequences for stability modeling (see point a.ii above).

## 8.3 Design and construction considerations

The following comments highlight some design considerations that have come out the current work, and are not meant to be a comprehensive design guide.

Abdul-Razaq (2007) provided an extensive list of design and construction guidelines.

### 8.3.1 Rockfill Properties

Choosing design values for rockfill properties should be done on a case-by-case basis, unless numerical design tools can incorporate a non-linear strength envelope. It is common practice to use a friction angle in design that is greater than the critical state friction angle, with the understanding that the dilitant nature of compacted rockfill will reliably provide shear resistance up to some peak strength. A suitable friction angle for a specific design should be chosen based on the expected range of effective stresses, the allowable deformations, the consequences of failure, and engineering judgement. Although the non-linear strength envelopes presented in this thesis do not incorporate critical state theories, they are still an improvement over linear strength envelopes. A case has also been made in this thesis for choosing design strength parameters based on allowable strains in the design of rockfill column for riverbank stabilization.

### 8.3.2 Compaction

It has been demonstrated in this thesis and previous work (for example Abdul Razaq 2007 and Alfaro et al. 2009 ) that effective compaction greatly increases the shear strength and stiffness of limestone rockfill. For example, at 100 kPa confining pressure, the peak friction angle of dense rockfill is 15.5° higher than for loose rockfill (at the densities tested by Abdul Razaq (2007)). Loose rockfill, in comparison to dense rockfill, requires shear strains 4.3 times greater to

mobilize 80 kPa of shear resistance ($\phi$ = 38.6°) at 100 kPa confining pressure and 6.9 times more shear strain to mobilize 100 kPa ($\phi$ = 45°). For the reasons of improved performance, compaction of the rockfill is recommended for all applications. A compacted unit weight of greater than 21 kN/m$^3$ is achievable with the available equipment, would provide a significant improvement in performance over loosely placed rockfill, as demonstrated by this research.

### 8.3.3 Overall stability

The stability and durability of the lower slope (downslope of the rockfill columns) should be considered in a rockfill column design. Loss of soil downslope of the rockfill columns will reduce confining pressure on the rockfill columns, thus reducing the stiffness and available shear strength. Appropriate protection of the lower bank should be a consideration for any rockfill column installations along a riverbank. Stability of the slope above the rockfill columns should also be considered.

### 8.3.4 Limiting shallow deformations

It is recommended that designers and contractors consider carefully how to minimize potential near-surface deformations. At some sites shallow movements in the order of 25-250 mm may be acceptable, but in other circumstances, they may be a fatal flaw in the design.

The following recommendations should help to limit shallow deformations if they are a major concern:

- Compact the top of the rockfill column and any final “top-off” lifts with hoe-pack or similar device. The vibro-lance does not compact the very shallow depths very effectively.

- Compact the clay cap, and other fill materials, if they are required.

- In cases of extra concern, physically connecting the tops of the columns with a thick granular mat will provide additional rigidity. The mat could be incorporated with a rip-rap blanket if required. Options for landscaping will be limited by this design.

Construction of rockfill columns is typically done in the winter months when low river levels and frozen ground improve working conditions. Winter construction makes working with fine-grained soils very difficult. Clay fill is likely to be frozen, as is the upper-crust of the in-situ clay. Effective compaction of frozen fine-grained soil is usually not possible. It is difficult to prevent shallow movements when the slope is subjected to high porewater pressures combined with the low strength of the loose clay and rockfill.

UMA Engineering Ltd. (2001a) also noted that the compactability of frozen rockfill decreased with increased water contents. The concern of frozen rockfill can be mitigated at greater depths by charging the column with water before compaction, but this may not be possible or effective at shallow depths.

## 8.4 Recommendations for future research

1. It has been demonstrated through a simple qualitative test that granular materials can support bending if positive (compressive) effective stresses are maintained through the entire cross section. Testing of crushed limestone in bending would be useful to confirm and characterize this mechanism of load resistance and the associated deformations. Further investigation is also required to determine the relative contributions of bending and shear deformations to the overall deformation of a column and reinforced slope.

2. Research was cited in Chapter 2 that both supported and refuted the idea that vibro-compaction of rockfill columns will improve the engineering properties of the surrounding in-situ high plasticity clay. A comparison of measured properties from before and after column installation would indicate whether the in-situ Winnipeg clay benefits from the vibro-compaction. A CPT investigation may be well suited to this. The same investigation could also determine whether the till properties (especially loose till) are improved.

3. It was illustrated in Chapter 6 that slope movements are ongoing at the research site, and future extreme stress conditions can be expected to cause additional displacements. Long term monitoring of the research site or other stabilized sites may provide observations that can be used to

further develop the ideas presented in Chapter 7 regarding post-construction deformations.

Creep has not been considered as a mode of deformation for either rockfill or in-situ clay. Some of the long term (weeks, months, years) post-construction deformations observed at the research site and other sites stabilized with rockfill columns, may be due to creep.

4. Chapter 7 demonstrated that there is some uncertainty regarding the in-situ stress distribution in a rockfill column after compaction. The increased density, in theory, should lead to increased in-situ stresses at depth, but this has not been measured, and no relevant research was found in the literature addressing the vertical stress distribution in columns installed by similar methods. Soil pressure measurements at depth would reduce this uncertainty. Stress measurements in the rockfill would also be able to confirm the re-distribution of horizontal and vertical stresses at depth, due to loading.

5. 3-D analysis of slopes stabilized by rockfill columns would be more appropriate than the 2-D analysis presented in this document, for investigating the questions of equivalent stiffness, flow between columns, and clay-column interactions.

6. Large scale triaxial testing of rockfill would be useful for more advanced and accurate characterization of rockfill. As demonstrated in this thesis, the rockfill in columns is subjected to compressive and extensive strains in

addition to shear strains. These loading conditions are more accurately replicated by triaxial testing than by direct shear testing. An actual measure (versus an extrapolation) of the peak state would be useful for further refining the strength envelopes of rockfill. Triaxial testing would also provide a better measure of modulus parameters.

7. This thesis has demonstrated the application of the Duncan and Chang (1970) hyperbolic model and the Maksimovic (1996) strength envelope to locally sourced crushed limestone rockfill. The development of a more rigorous material model for local crushed limestone, such as the one proposed by Varadarajan et al. (2006) would be beneficial. A more advanced model would explicitly account for variables such as hardness, grain size, volume change and stress-strain behaviour in one formulation.

## References


Abdul Razaq, W.F. 2007. Evaluation of riverbank stabilization using rockfill and soil-cement columns. Ph.D. University of Manitoba, Winnipeg, Manitoba.

Aboshi, H., Ichimoto, E., Enoki, M., and Harada, K. 1979. The "compozer" - a method to improve characteristics of soft clays by inclusion of large diameter sand columns. *In* Colloque International Sur Le Renforcement des Sols: Terre Armee Et Autres Techniques, Vol. 1: 211-216.

Abramson, L.W., Lee, T.S., Sharma, S., and Boyce, G.M. 1996. Slope stability and stabilization methods. John Wiley & Sons, Inc., Toronto.

Alfaro, M.C., Blatz, J.A., Abdulrazaq, W.F., and Kim, C. 2009. Evaluating shear mobilization in rockfill columns used for riverbank stabilization, Canadian Geotechnical Journal, 46(8): 976-986.

Anderson, D., Kenyon, R., Blatz, J., and Smith, J. 2004. Numerical modelling of the 1962 Red River Floodway test pit excavation. *In* Proceedings of the Canadian Geotechnical Conference, Quebec: 40-46.

ASTM Standard D2435-04. 2004. Standard test method for one-dimensional consolidation properties of soils using incremental loading. ASTM, West Conshohocken, PA.

ASTM Standard D3080-04. 2004. Standard test method for direct shear test of soils under consolidated drained conditions. ASTM, West Conshohocken, PA.

ASTM Standard D422-63. 2002. Standard test method for particle-size analysis of soils. ASTM, West Conshohocken, PA.

ASTM Standard D4318-05. 2005. Standard test methods for liquid limit, plastic limit and plasticity index of soils. ASTM, West Conshohocken, PA.

ASTM Standard D4767. 2004. Standard test method for consolidated undrained triaxial compression test for cohesive soils. ASTM, West Conshohocken, PA.

ASTM Standard D5084-03. 2003. Standard test methods for measurement of hydraulic conductivity of saturated porous materials using a flexible wall permeameter. ASTM, West Conshohocken, PA.

Bachus, R. and Barksdale, R. 1984. Vertical and lateral behavior of model stone columns. *In* Proceedings of International Conference on In-Situ Soil and Rock Reinforcement, Paris: 99-104.

Bachus, R.C. and Barksdale, R.D. 1989. Design methodology for foundations on stone columns. *In* Foundation Engineering: Current Principles and Practices: 244-257.

Baracos, A. 1978. The effects of river levels, groundwater, and other seasonal changes on river banks in Winnipeg. *In* Proceedings of 31st Canadian Geotechnical Conference, Winnipeg MB: 7.2.1-7.2.19.

Baracos, A. 1977. Compositional and structural anisotropy of Winnipeg soils - a study based on scanning electron microscopy and X-ray diffraction analyses, Canadian Geotechnical Journal, 14: 125-137.

Baracos, A. 1957. The foundation failure of the Transcona Grain Elevator, The Engineering Journal, 40(7): 6.

Baracos, A. and Graham, J. 1981. Landslide problems in Winnipeg, Canadian Geotechnical Journal, 18: 390-401.

Baracos, A., Kingerski, D., and Leung, K. 1989. Riverbank stability analyses with uncertain soil properties. *In* 42nd Canadian Geotechnical Conference: 184-195.

Baracos, A., Shields, D.H., and Kjartanson, B. 1983. Geological engineering report for urban development of Winnipeg. University of Manitoba, .

Baracos, A., Graham, J., and Domaschuk, L. 1980. Yielding and rupture in a lacustrine clay, Canadian Geotechnical Journal, 17: 559-573.

Baracos, A., Graham, J., Kjartanson, B., and Shields, D.H. 1983. Geology and soil properties of Winnipeg. *In* ASCE Conference on Geologic Environment and Soil Properties, Houston Tx: 39-56.

Barker, D.H. 1986. Enhancement of slope stability by vegitation, Ground Engineering, 19: 11-15.

Barksdale, R.D. and Takefumi, T. 1991. Design, construction and testing of sand compaction piles. *In* Symposium on Deep Foundation Improvements: Design, Construction, and Testing: 4-18.

Barksdale, R.D. and Bachus, R.C. 1983. Design and construction of stone columns. FHWA/RD-83/026, Federal Highway Administration, Atlanta.

Barksdale, R.D. 1987. State of the art for design and construction of sand compaction piles. U.S. Army Engineer Waterways Experiment Station, Vicksburg, Miss.

Bauer, E. and Zhu, Y. 2004. Constitutive modeling of the influence of pressure, density and moisture content on the mechanical behavior of rockfill. *In* Proceedings of the 4th International Conference on Dam Engineering - New Developments in Dam Engineering: 139-146.

Been, K. and Jefferies, M.G. 1985. State parameter for sands, Geotechnique, 35(2): 99-112.

Bergado, D.T. 1996. Granular piles. *In* Soft ground improvement in lowland and other environments *Edited by* D.T. Bergado, L.R. Anderson, N. Miura and A.S. Balasubramaniam. ASCE Press, Atlanta GA: 186-233.

Blatz, J. and Skaftfeld, K. 2003. Transcona Grain Elevator failure: A modern perspective 90 years later. *In* 56th Canadian Geotechnical Conference.

Bowles, J.E. 1997. Foundation analysis and design. The McGraw-Hill Companies, Inc., Toronto.

Brandshaug, T., Solseng, P., and Schiller, P. 2001. A 2D approach to the evaluation of the 3D effects of landslide stabilization using piles. *In* Geotechnical Special Publication, Virginia Polytechnic University: 130-144.

Broms, B.B. and Anttikoski, U. 1984. Soil stabilization. *In* Proceedings of the Eighth European Conference on Soil Mechanics and Foundation Engineering: Improvement of Ground., Vol. 3: 1289-1315.

Brooker, E.W. and Ireland, H.O. 1965. Earth pressures at rest related to stress history, Canadian Geotechnical Journal, 2: 1-15.

Budhu, M. 2000. Soil mechanics and foundations. John Wiley & Sons, Inc., Toronto.

Byrum, C. 2008. Modeling the effect of stone columns on lateral squeeze of weak soils. *In* TRB 87th Annual Meeting Compendium of Papers, Washington D.C.

CFEM. 2006. Canadian foundation engineering manual: 4th edition. The Canadian Geotechnical Society, Richmond B.C.

Chen , L. and Poulos, H. 1994. A method of pile-soil interaction analysis for piles subjected to lateral soil movement. *In* Computer methods and advances in geomechanics, Vol 3, Morgantown, WV: 2311-2316.

Chen, B.S. and Bailey, M.J. 2004. Lessons learned from a stone column test program in glacial deposits. *In* GeoSupport 2004 - Drilled Shafts, Micropiling, Deep Mixing: 508-519.

Chen, L.T. and Poulos, H.G. 1997. Piles subjected to lateral soil movements, Journal of Geotechnical & Geoenvironmental Engineering, 123(9): 802.

Chowdhury, R.N. 1976. Initial stresses in natural slope analysis. *In* Rock engineering for foundations & Slope: 404-414.

Christoulas, S., Giannaros, C., and Tsiambaos, G. 1997. Stabilization of embankment foundations by using stone columns, Geotechnical and Geological Engineering, 15: 247-258.

City of Winnipeg. 2004. Riverbank stability characterization study for city owned riverbanks. City of Winnipeg Planning, Property & Development Department: Waterways Section, Winnipeg, Manitoba.

City of Winnipeg. 2000. Riverbank stability characterization study for city owned riverbanks. City of Winnipeg Planning, Property & Development Department: Waterways Section, Winnipeg, Manitoba.

Contreras, I.A., Grosser, A.,T., and Ver Strate, R.H. 2008. The use of the fully-grouted method for piezometer installation: Part 2. Geotechnical News: 33-37.

Datye, K.R. 1981. Design approach and field control for stone columns, Proceedings of the International Conference on Soil Mechanics and Foundation Engineering: 637-640.

Davis, R. and Selvadurai, A. 1996. Elasticity and geomechanics. Cambridge University Press, New York, USA.

Deluzarche, R. and Cambou, B. 2006. Discrete numerical modelling of rockfill dams, International Journal for Numerical and Analytical Methods in Geomechanics, 30: 1075-1096.

Deng, Y., Liu, S., and Hong, Z. 2006. Optimal column modulus of deep mixed column foundations under embankments. *In* Ground Modification and Seismic Mitigation - GeoShanghai Conference: 9-16.

Diyaljee, V.A. and Pariti, M. 1990. Stone column use in highway construction, Proceedings of the 43rd Canadian Geotechnical Conference.Part 2, Oct 10-12 1990 Canadian Geotechnical Conference : 711-718.

Duncan, J.M. 1996. State of the art: Limit equilibrium and finite-element analysis of slopes, Journal of Geotechnical Engineering, 122(7): 577-596.

Duncan, J.M. 1992. State of the art: Static stability and deformation analysis. In Stability and performance of slopes and embankments II: Proceedings of a specialty conference: 222-266.

Duncan, J.M. and Chang, C. 1970. Nonlinear analysis of stress and strain in soils, Journal of the Soil Mechanics and Foundations Division, 96(5): 1629-1653.

Dunnicliff, J. 1988. Geotechnical instrumentation for monitoring field performance. Wiley, New York.

Emeriault, F. and Chang, C.S. 1997. Interparticle forces and displacements in granular materials, Computers and Geotechnics, 20(3-4): 223-244.

Enoki, M., Yagi, N., Yatabe, R., and Ichimoto, E. 1991. Shearing characteristic of composite ground and its application to stability analysis. *In* Symposium on Deep Foundation Improvements: Design:19-31.

Fannin, R.J., Eliadorani, A., and Wilkinson, J.M.T. 2005. Shear strength of cohesionless soils at low stress, Geotechnique, 55(6): 467-478.

Filz, G.M. and Navin, M.P. 2006. Stability of column-supported embankments. VTRC 06-CR13, Virginia Transportation Research Council, Charlottesville Virginia.

Freeman, W.S. 1970. Shear strength of Winnipeg clays. Ph.D., University of Glasgow, Glasgow, Scotland.

Freeman, W.S. and Sutherland, H.B. 1973. Slope stability analysis in anisotropic Winnipeg clays. *In* 26th Canadian Geotechnical Conference.

Froiio, F., Tomassetti, G., and Vardoulakis, I. 2006. Mechanics of granular materials: The discrete and the continuum descriptions juxtaposed, International Journal of Solids and Structures, 43(25-26): 7684-7720.

Gajo, A. and Wood, D.M. 1999. Severn-Trent sand: A kinematic-hardening constitutive model: The q-p formulation, Geotechnique, 49: 595-614.

Garinger, B. 2002. Instability of dykes at seven sisters generating station. M.Sc. University of Manitoba. Winnipeg, Manitoba.

Geo-Slope International Ltd. 2010a. Stress-deformation modeling with Sigma/W 2007: An engineering methodology. Geo-Slope International Ltd., Canada.

Geo-Slope International Ltd. 2010b. Stability modeling with Slope/W 2007 version: An enineering methodology. Geo-Slope International Ltd., Canada.

Geo-Slope International Ltd. 2010c. Seepage modeling with Seep/W 2007 version: An enineering methodology. Geo-Slope International Ltd., Canada.

Ghazavi, M. and Shahmandi, A. 2008. Static analysis of slopes reinforced with stone columns. *In* New horizons in earth reinforcement: Proceedings and Monographs in Engineering, Water and Earth Sciences: 451-455.

Goughnour, R.R., Sung, J.T., and Ramsey, J.S. 1991. Slide correction by stone columns. *In* Symposium on Deep Foundation Improvements: Design, Construction, and Testing: 131-147.

Gould, J. and Dunnicliff, J. 1971. Accuracy of field deformation measurements. *In* 4th PanAmerican Conference on Soil Mechanics: 313-366.

Graham, J. 2006. 'The 2003 R.M. Hardy lecture: Soil parameters for numerical analysis in clay, Canadian Geotechnical Journal, 43(2): 187-209.

Graham, J. 1986. Slope stability analysis: Applications in plastic clays. *In* Proceedings 34th Annual Soil Mechanics and Foundation Engineering Conference, Minneapolis MN, 13-48.

Graham, J. 1979. Embankment stability on anisotropic soft clays, Canadian Geotechnical Journal, 16(2): 295-308.

Graham, J., Alfaro, M.C., and Blatz, J. 2009. Natural processes and strength degradation, in review for "Bifurcations, Instabilities and Degradations in Geomaterials" to be published by Springer Publishers.

Graham, J., Alfaro, M., and Ferris, G. 2004. Compression and strength of dense sand at high pressures and elevated temperatures, Canadian Geotechnical Journal, 41: 1206-1212.

Graham, J. and Au, V.C.S. 1985. Effects of freeze-thaw and softening on a natural clay at low stresses, Canadian Geotechnical Journal, 22(1): 69-78.

Graham, J. and Houlsby, G.T. 1983. Anisotropic elasticity of a natural clay, Geotechnique, 33(2): 165-180.

Graham, J., Noonan, M.L., and Lew, K.V. 1983. Yield states and stress-strain relationships in a natural plastic clay, Canadian Geotechnical Journal, 20: 502-516.

Green, G.E. and Mikkelsen, P.E. 1988. Deformation measurements with inclinometers, Transportation Research Record, 1169: 1-15.

Greenwood, D.A. 1991. Load tests on stone columns. *In* Symposium on Deep Foundation Improvements: Design, Construction, and Testing: 148-171.

Guetif, Z., Bouassida, M., and Debats, J.M. 2007. Improved soft clay characteristics due to stone column installation, Computers and Geotechnics, 34(2): 104-111.

I. D. Engineering Company. 1984. 1983-84 engineering study on 6-land drainage outfalls and riverbank stabilization in district #5, .

Independent Test-Lab Ltd. 1993. Monitoring results and slope stability investigation: Minnetonka outfall, Winnipeg Manitoba. City of Winnipeg, Winnipeg, MB.

Jaky, J. 1948. Pressure in silos. In proceedings of 2nd International Conference on Soil Mechanics and Foundation Engineering, Rotterdam, Vol. 1: 103-107.

James, A. 2009. Development of a riverbank asset management system for the City of Winnipeg. M.Sc., University of Manitoba.

KGS Group Ltd. 2002. Rockfill column test compaction program. 02-300-01, Manitoba Transportation and Government Services .

Kim, C.S. 2007. Evaluating shear mobilization in rockfill columns used for riverbank stabilization. M.Sc., University of Manitoba, Winnipeg.

Kitazume, M. and Maruyama, K. 2007. Centrifuge model tests on failure pattern of group column type deep mixing improved ground. *In* 17th 2007

International Offshore and Polar Engineering Conference, ISOPE 2007: 1293-1300.

Kitazume, M., Okano, K., and Miyajima, S. 2000. Centrifuge model tests on failure envelope of column type deep mixing method improved ground, Soils and Foundations, 40(4): 43-55.

Kivelo, M. 1998. Stabilization of embankments on soft soil with lime/cement columns. Ph.D., Royal Institute of Technology, Stockholm Sweeden.

Kivelo, M. and Broms, B. 1999. Mechanical behaviour and shear resistance of lime/cement columns. *In* Dry mix methods for deep soil stabilization: Proceedings of DJM 99, Stockholm Sweden: 193-200.

Krahn, J. 2003. The 2001 R.M. hardy lecture: The limits of limit equilibrium analyses, Canadian Geotechnical Journal, 40: 643-660.

Lambe, T.W. 1973. Predictions in soil engineering, Geotechnique, 23(2): 149-202.

Lefebvre, G. 1986. Slope instability and valley formation in Canadian soft clay deposits, Canadian Geotechnical Journal, 23(3): 261-270.

Leps, T.M. 1970. Review of shearing strength of rockfill, Journal of the Soil Mechanics and Foundations Division, 96: 1159-1170.

Lew, K.V. and Graham, J. 1988. Riverbank stabilization by drains in plastic clay. *In* International Symposium on Landslides, Lausanne Switzerland: 939-944.

MacLeod, I.A. 2005. Structural analysis: Modelling process and guidance. Thomas Telford Publishing, London.

Maksimovic, M. 1996. A family of nonlinear failure envelopes for non-cemented soils and rock discontinuities, Electronic Journal of Geotechnical Engineering.

Maksimovic, M. 1989. Nonlinear failure envelope for soils, Journal of Geotechnical Engineering, 115(4): 581-586.

Manitoba Floodway Authority. 2010. Red River Floodway expansion project [online]. Available from http://www.floodwayauthority.mb.ca [cited February 20, 2010 2010].

Marsal, R.J. 1967. Large scale testing of rockfill materials, American Society of Civil Engineers - Proceedings American Society of Civil Engineers Proceedings, Journal of the Soil Mechanics and Foundations Division, 93: 27-43.

Marsal, R.J. 1973. Mechanical properties of rockfill. *In* Embankment Dam Engineering: Casagrande Volume *Edited by*John Wiley & Sons, Inc, New York: 109-200.

Martin, G.R. and Chen, C.Y. 2005. Response of piles due to lateral slope movement, Computers & Structures, 83(8-9): 588-598.

Mayne, P.W. and Kulhawy, F.H. 1982. Ko-OCR Relationships in soil, Journal of the Geotechnical Engineering Division, 108: 851-872.

McKenna, G.T. 1995. Grouted-in installation of piezometers in boreholes, Canadian Geotechnical Journal, 32: 355-363.

Mikkelsen, P.E. 2003. Advances in inclinometer data analysis. *In* Symposium on Field Measurement in Geomechanics: 13.

Mikkelsen, P.E. 2002. Cement-bentonite grout backfill for borehole instruments, Geotechnical News, 20: 38-42.

Mikkelsen, P.E. and Green, G.E. 2003. Piezometers in fully grouted boreholes. *In* Symposium on Field Measurement in Geomechanics: 10.

Mishtak, J. 1964. Soil mechanics aspects of Red River Floodway, Canadian Geotechnical Journal, 1(3): 133-146.

Morley, J. 1996. 'Acts of god': The symbolic and technical significance of foundation failures, Journal of Performance of Constructed Facilities, 10(1): 23-31.

Munfakh, G.A., Sarkar, S.K., and Castelli, R.J. 1984. Performance of a test embankment founded on stone columns. *In* Piling and Ground Treatment, London England: 259-265.

Murugesan, S. and Rajagopal, K. 2009. Shear load tests on stone columns with and without geosynthetic encasement, Geotechnical Testing Journal, 32(1): 76-85.

Navin, M.P. 2005. Stability of embankments founded on soft soil improved with deep-mixing-method columns. Ph. D., Virginia Polytechnic Institute and State University, Blacksburg VA.

Navin, M.P. and Filz, G.M. 2006. Numerical stability analyses of embankments supported on deep mixed columns. *In* Ground Modification and Seismic Mitigation - GeoShanghai Conference, Shanghai, China: 1-8.

Negussey, D., Wijewickreme, W.K.D., and Vaid, Y.P. 1988. Constant-volume friction angle of granular materials, Canadian Geotechnical Journal, 25: 50-55.

Peck, R. 1967. Stability of natural slopes, ASCE Journal of Soil Mechanics and Foundations Division, 93(SM4): 403-417.

Potts, D.M., Kovacevic, N., and Vaughan, P.R. 1997. Delayed collapse of cut slopes in stiff clay, Geotechnique, 47: 953-982.

Poulos, H.G. 1973. Analysis of piles in soil undergoing lateral movement, American Society of Civil Engineers, Journal of the Soil Mechanics and Foundations Division, 99: 391-406.

Poulos, H. G. 1995. Design of reinforcing piles to increase slope stability, Canadian Geotechnical Journal, 32: 808-818.

Poulos, H. and Davis, E. 1991. Elastic solutions for soil and rock mechanics. Centre for Geotechnical Research, University of Sydney, Sydney.

Prairie Farm Rehabilitation Administration. 1962. Preliminary draft of first progress report on soil mechanics investigation for red river floodway. P.F.R.A., Saskatoon, Saskatchewan.

Priebe, H.J. 2005. Design of vibro replacement, Ground Engineering, 38: 25-27.

Priebe, H.J. and Grundbau, K. 1995. Design of vibro replacement, Ground Engineering, 28: 31-37.

Przemieniecki, J.S. 1985. Theory of matrix structural analysis. Dover Publications, New York.

Reese, L., Wang, S., and Fouse, J. 1992. Use of drilled shafts in stabilizing a slope. *In* Stability and performance of slopes and embankments-II, Vols 1 and 2 *Edited by* R. Seed and R. Boulanger. American Society of Civil Engineers, New York: 1318-1332.

Render, F.W. 1970. Geohyrdology of the metropolitan Winnipeg area as related to groundwater supply and construction, Canadian Geotechnical Journal, 7(3): 243-274.

Rivard, P.J. and Lu, Y. 1978. Shear strength of soft fissured clays, Canadian Geotechnical Journal, 15(3): 382-390.

Saada, A.S. 2000. Laboratory testing for the validation of constitutive models. *In* Modelling in Geomechanics *Edited by* M. Zaman, G. Gioda and J. Booker. John Wiley and Sons Ltd, Chiichester, New York: 247-265.

Sharma, R.S., Kumar, B.R.P., and Nagendra, G. 2004. Compressive load response of granular piles reinforced with geogrids, Canadian Geotechnical Journal, 41: 187-192.

Silvestri, V. and Tabib, C. 1983. Exact determination of gravity stresses in finite elastic slopes: Part 1. theoretical considerations, Canadian Geotechnical Journal, 20: 41-54.

Sitharam, T.G. and Nimbkar, M.S. 2000. Micromechanical modelling of granular materials: Effect of particle size and gradation, Geotechnical and Geological Engineering, 18: 91-117.

Skaftfeld, K. 1998. Failure and righting of the Transcona Grain Elevator, Geotechnical News, 16(2): 61-61.

Skaftfeld, K.M., Kenyon, R.M., and Van Helden, M.J. 2009. The design, construction and expansion of the Red River Floodway. In Proceedings of the 57th Annual Geotechnical Engineering Conference, University of Minnesota: 63-91.

Skempton, A.W. 1985. Residual strength of clays in landslides, folded strata and the laboratory, Geotechnique, 35: 3-18.

Slocombe, B.C. and Moseley, M.P. 1991. Testing and instrumentation of stone columns. *In* Symposium on Deep Foundation Improvements: Design, Construction, and Testing: 85-100.

Slope Indicator. 2007. VW piezometer: Manual. Slope Indicator.

Slope Indicator. 2001. Data reduction and error correction for inclinometers. Slope Indicator.

Stark, T.D. and Yacyshyn, B.M. 1991. Specifications for constructing and load testing stone columns in clays. *In* Symposium on Deep Foundation Improvements: Design, Construction, and Testing: 73-84.

Stewart, M.E., Navin, M.P., and Filz, G.M. 2004. Analysis of a column-supported test embankment at the I-95/Route 1 interchange. *In* Geotechnical Engineering for Transportation Projects: Proceedings of Geo-Trans 2004: 1337-1346.

Sutherland, H.B. 1966. The stability of the river banks in the Winnipeg areaq. River and Streams Authority No. 1., Winnipeg Manitoba.

Tallin, J.E. and Thiessen, K.J. 2009. Riverbank stabilization by rock columns in Winnipeg, Manitoba. *In* University of Minnesota 57th Annual Geotechnical Engineering Conference: 157-165.

Tavenas, F. and Leroueil, S. 1981. Creep and failure of slopes in clays, Canadian Geotechnical Journal, 18(1): 106-120.

Teller, J.T. 1976. Lake Agassiz deposits in the main offshore basin of southern Manitoba, Canadian Journal of Earth Sciences, 13: 27-43.

Thiessen, K.J., Alfaro, M.C., and Blatz, J.A. 2008. Monitoring results from a full-scale field test of rockfill columns. *In* Canadian Geotechnical Conference. Edmonton AB.

Turner, A.K. and Schuster, R.L. 1996. Landslides: Investigation and mitigation. Washington D.C.

Tutkaluk, J.M. 2000. The effect of seasonal variations in the Red River and upper carbonate aquifer on riverbank stability in Winnipeg. University of Manitoba, Winnipeg, Manitoba.

Tweedie, R., Clementino, R., Papanicolas, D., Skirrow, R., and Moser, G. 2004. Stabilization of a highway embankment fill over an arch culvert using stone columns. *In* 57th Canadian Geotechnical Conference: 24-31.

UMA Engineering Ltd. 2001a. Shoal Lake Aquaduct rehabilition: Compaction testing program. The City of Winnipeg, Winnipeg.

UMA Engineering Ltd. 1992. Mager Drive slope stabilization aggregate direct shear testing program. Winnipeg, Manitoba.

Van Helden, M.J., Blatz, J.A., Ferreira, N.J., and Skaftfeld, K. 2008. Numerical modeling of sand drain performance - A case study of the Salter Street Bridge construction, Canadian Geotechnical Journal, 45(6): 751-767.

Vanapalli, S.K., Fredlund, D.G., Pufahl, D.E., and Clifton, A.W. 1996. Model for the prediction of shear strength with respect to soil suction, Canadian Geotechnical Journal, 33(3): 379-392.

Varadarajan, A., Sharma, K.G., Abbas, S.M., and Dhawan, A.K. 2006. Constitutive model for rockfill materials and determination of material constants, International Journal of Geomechanics, 6: 226-237.

Varadarajan, A., Sharma, K.G., Venkatachalam, K., and Gupta, A.K. 2003. Testing and modeling two rockfill materials, Journal of Geotechnical and Geoenvironmental Engineering, 129: 206-218.

Viggiani, C. 1981. Ultimate lateral load on piles used to stabilize landslides. *In* Soil Mechanics and Foundation Engineering 10th Annual Conference, Stockholm, Vol. 3: 555-560.

Wiebe, L. 2009. Riverfront property protection could cost $23M. Winnipeg Free Press,16 May, 2009 .

Yarechewski, D. and Tallin, J. 2003. Riverbank stabilization performance with rock-filled ribs/shear key and columns. *In* 56th Canadian Geotechnical Conference 2003 NAGS.

Young, W. and Budynas, R. 2002. Roark's formulas for stress and stain. McGraw Hill, New York. NY.

Yuen, K., Graham, J., and Janzen, P. 1998. Weathering-induced fissuring and hydraulic conductivity in a natural plastic clay, Canadian Geotechnical Journal, 35: 1101-1108.

# APPENDIX A

Test-hole logs

| | | |
|---|---|---|
| PROJECT: Rockfill Column Test Site | CLIENT: University of Manitoba | TESTHOLE NO: **TH-1** |
| LOCATION: Top of Bank N 5,520,043.6 E 635,005.0 | | PROJECT NO.: |
| CONTRACTOR: Paddock Drilling Ltd. | METHOD: 125mm dia. Solid Stem Auger | ELEVATION (m): 232.006 |

SAMPLE TYPE: GRAB | SHELBY TUBE | SPLIT SPOON | BULK | NO RECOVERY | CORE

BACKFILL TYPE: BENTONITE | GRAVEL | SLOUGH | GROUT | CUTTINGS | SAND

| DEPTH (m) | SLOPE INCLINOMETER | USC | SOIL SYMBOL | SOIL DESCRIPTION | SAMPLE TYPE | SAMPLE # | SPT (N) | Total Unit Wt (kN/m³) 17 19 21 23 / SPT (Standard Pen Test) (Blows/300mm) 20 40 60 80 / PLASTIC M.C. LIQUID 20 40 60 80 | COMMENTS | ELEVATION (m) |
|---|---|---|---|---|---|---|---|---|---|---|
| 0 | | OL | | ORGANIC CLAY - silty, black, stiff, dry to moist, low plasticity | | G1 | | | | 232 |
| 1 | | ML | | SILT - trace organics, light grey, loose to compact , dry, low plasticity | | G2 | | | | 231 |
| | | | | CLAY - silty | | G3 | | | | |
| 2 | | | | - brown mottled grey | | | | | | 230 |
| | | | | - stiff, moist | | G4 | | | | |
| | | | | - medium plasticity | | | | | | |
| 3 | | | | - trace silt inclusions <5mm dia | | G5 | | | | 229 |
| | | | | - 25 mm silt lense at 2.3m | | T6 | | | | |
| | | | | - grey, mottled brown below 2.4m | | G7 | | | | |
| 4 | | | | - trace white sulphite inclusions below 3.2m <10mm dia. | | T8 | | 106.92 | | 228 |
| 5 | | | | | | G9 | | | | 227 |
| 6 | | | | | | T10 | | | | 226 |
| 7 | | CH | | | | | | | | 225 |
| | | | | | | G11 | | | | |
| 8 | | | | - grey below 7.9m | | | | | | 224 |
| | | | | - trace gravel below 8.2m | | G12 | | | | |
| 9 | | | | | | T13 | | | | 223 |
| 10 | | | | | | T14 | | | | 222 |
| 11 | | | | - firm below 10.7m | | G15 | | | | 221 |
| | | | | | | G16 | | | | |
| 12 | | | | - trace sand, soft to firm, medium plasticity below 11.6m | | | | | | 220 |
| | | | | | | T17 | | | | |
| 13 | | | | SILT (Till) - some clay to clayey, trace to some sand, trace gravel | | T18 | | | | 219 |
| | | | | - light grey | | | | | | |
| 14 | | | | - loose, moist | | G19 | | | | 218 |
| | | | | - low to non plastic | | G20 | | | | |
| 15 | | TILL | | | | T21 | | | | 217 |
| 16 | | | | - compact below 15.8m | | | | | | 216 |
| | | | | - wet below 16m | | G22 | | | | |
| 17 | | SW TILL | | SAND - fine to medium grained, dense, wet | | G23 | 50/ 2mm | | >> bouncing at 150mm | 215 |
| | | | | SILT (Till)- sandy, trace gravel, light grey, dense, moist, non-plastic | | S23 | | | | |
| | | | | | | S24 | | | | |
| 18 | | | | END TEST HOLE AT 17.28m IN SILT TILL | | | | | | 214 |
| | | | | Notes: | | | | | | |
| 19 | | | | 1. Auger refusal at 17.28m. | | | | | | 213 |
| | | | | 2. Seepage from till and sand layers. | | | | | | |
| | | | | 3. No sloughing. | | | | | | |
| 20 | | | | 4. Install SI-1 at 17.28m. Backfill with cement grout. | | | | | | 212 |
| | | | | 5. Water level at 10.7m depth. | | | | | | |
| 21 | | | | | | | | | | 211 |
| 22 | | | | | | | | | | 210 |
| 23 | | | | | | | | | | |

| | |
|---|---|
| LOGGED BY: KT | COMPLETION DEPTH: 17.27 m |
| REVIEWED BY: KT | COMPLETION DATE: 8/8/06 |
| PROJECT ENGINEER: Kendall Thiessen, EIT | Page 1 of 1 |

LOG OF TESTHOLE KENDALL'S LOGS.GPJ UMA.GDT 9/8/10

| | | |
|---|---|---|
| PROJECT: Rockfill Column Test Site | CLIENT: University of Manitoba | TESTHOLE NO: **TH-2** |
| LOCATION: Below Crest N 5,520,038.1 E 635,006.7 | | PROJECT NO.: |
| CONTRACTOR: Paddock Drilling Ltd. | METHOD: 125mm dia. Solid Stem Auger | ELEVATION (m): 229.462 |

SAMPLE TYPE: GRAB | SHELBY TUBE | SPLIT SPOON | BULK | NO RECOVERY | CORE

BACKFILL TYPE: BENTONITE | GRAVEL | SLOUGH | GROUT | CUTTINGS | SAND

| DEPTH (m) | USC | SOIL DESCRIPTION | SAMPLE # | COMMENTS | ELEVATION (m) |
|---|---|---|---|---|---|
| 0 | CH | CLAY - silty<br>- brown, mottled grey<br>- stiff, moist<br>- high plasticity<br>- trace silt inclusions <10mm dia. below 0.45m | C25, C27m, C26, C27, C28, C29, C30, C30m, C31, C31m, C32, C32m, C33, C33m, C34, C35, C36, C36m, C37, C38, C39, C39m, C40, C41, C42, C42m, C43, C44, C45m1, C45, C45m2, C46, C47, C48, C48m, C49, C49m, C50, C51, C52, C52m, C53 | PLASTIC M.C. LIQUID<br>20 40 60 80<br>101.34 | 229 |
| 1 | | | | | 228 |
| 2 | | | | | |
| 3 | | | | | 227 |
| 4 | | | | | 226 |
| 5 | | | | | 225 |
| 6 | | - trace gravel below 5.6m<br>- grey below 5.8m<br>- trace sand below 6.1m<br>- firm to stiff below 6.4m | | | 224 |
| 7 | | | | | 223 |
| 8 | | | | | 222 |
| 9 | | - firm below 8.2m | | | 221 |
| 10 | | - firm to soft below 9.4m | | | 220 |
| 11 | TILL | SILT (Till) - some clay to clayey, trace sand, trace gravel<br>- light grey<br>- loose, moist<br>- low plasiticty<br>- some sand, compact below 11.7m | | | 219 |
| 12 | | | | | 218 |
| 13 | | | | | 217 |
| 14 | | - 100mm sand seam at 14m<br>- dense to very dense below 14.1m | | | 216 |
| 15 | | END TEST HOLE AT 14.72m IN SILT TILL | | | 215 |
| 16 | | Notes:<br>1. Sand lock between sampler and augers prevents further progress at 14.72m.<br>2. Seepage from sand and till layers<br>3. No sloughing.<br>4. Install SI-2 at 14.72m, backfill with cement grout.<br>5. Test hole was continuously sampled with wireline sampler. | | | 214 |
| 17 | | | | | 213 |
| 18 | | | | | 212 |
| 19 | | | | | 211 |
| 20 | | | | | 210 |
| 21 | | | | | 209 |
| 22 | | | | | 208 |
| 23 | | | | | 207 |

| | |
|---|---|
| LOGGED BY: KT | COMPLETION DEPTH: 14.73 m |
| REVIEWED BY: KT | COMPLETION DATE: 8/8/06 |
| PROJECT ENGINEER: Kendall Thiessen, EIT | Page 1 of 1 |

LOG OF TESTHOLE KENDALL'S LOGS.GPJ UMA.GDT 9/8/10

| | | |
|---|---|---|
| PROJECT: Rockfill Column Test Site | CLIENT: University of Manitoba | TESTHOLE NO: **TH-3** |
| LOCATION: Below Crest N 5,520,037.8 E 635,004.9 | | PROJECT NO.: |
| CONTRACTOR: Paddock Drilling Ltd. | METHOD: Hollow Stem Augers | ELEVATION (m): 229.618 |

SAMPLE TYPE: GRAB | SHELBY TUBE | SPLIT SPOON | BULK | NO RECOVERY | CORE

| DEPTH (m) | USC | SOIL SYMBOL | SOIL DESCRIPTION | SAMPLE TYPE | SAMPLE # | PLASTIC / M.C. / LIQUID (20 40 60 80) | COMMENTS | ELEVATION (m) |
|---|---|---|---|---|---|---|---|---|
| 0 | | | CLAY - silty | | | | | 229 |
| 1 | | | - brown<br>- stiff, moist<br>- high plasticity | | | | | |
| 2 | | | - trace sulphite inclusions <5mm dia. | | T54 | | | 228 |
| 3 | | | - mottled grey below 2.4m | | G55 | | | 227 |
| 4 | | | | | SV56 | | | 226 |
| 5 | CH | | - grey below 5m | | T57 | | | 225 |
| 6 | | | | | G58 | | | 224 |
| 7 | | | - trace sand, trace gravel below 6.1m | | SV59a | | | 223 |
| 8 | | | - firm below 7.6m | | G59 | | | 222 |
| 9 | | | | | G60 | | | 221 |
| 10 | | | | | G61 | | | 220 |
| 11 | TILL | | SILT (Till) - trace sand, trace gravel, trace cobbles, light grey, moist, loose | | | | | 219 |
| 12 | | | END TEST HOLE AT 11.58m IN SILT TILL<br>Notes:<br>1. Auger refusal on bolder at 11.6m.<br>2. No seepage.<br>3. No sloughing.<br>4. Install nested string of piezometers. VW-A at 10.97m, VW-B at 7.32m and VW-C at 3.05m below ground level. 5. Backfilled with cement grout mix. | | | | | 218 |
| 13 | | | | | | | | 217 |
| 14 | | | | | | | | 216 |
| 15 | | | | | | | | 215 |
| 16 | | | | | | | | 214 |
| 17 | | | | | | | | 213 |
| 18 | | | | | | | | 212 |
| 19 | | | | | | | | 211 |
| 20 | | | | | | | | 210 |
| 21 | | | | | | | | 209 |
| 22 | | | | | | | | 208 |
| 23 | | | | | | | | 207 |

| | |
|---|---|
| LOGGED BY: KT | COMPLETION DEPTH: 11.58 m |
| REVIEWED BY: KT | COMPLETION DATE: 8/9/06 |
| PROJECT ENGINEER: Kendall Thiessen, EIT | Page 1 of 1 |

LOG OF TESTHOLE KENDALL'S LOGS.GPJ UMA.GDT 9/8/10

| | | |
|---|---|---|
| PROJECT: Rockfill Column Test Site | CLIENT: University of Manitoba | TESTHOLE NO: **TH-4** |
| LOCATION: Above Summer River Level N 5,520,028.1 E 635,008.6 | | PROJECT NO.: |
| CONTRACTOR: Paddock Drilling Ltd. | METHOD: 125mm dia. Solid Stem Auger | ELEVATION (m): 225.645 |

SAMPLE TYPE: GRAB | SHELBY TUBE | SPLIT SPOON | BULK | NO RECOVERY | CORE

BACKFILL TYPE: BENTONITE | GRAVEL | SLOUGH | GROUT | CUTTINGS | SAND

| DEPTH (m) | USC | SOIL DESCRIPTION | SAMPLE TYPE | SAMPLE # | SPT (N) | COMMENTS | ELEVATION (m) |
|---|---|---|---|---|---|---|---|
| 0 | FILL | CLAY (Fill) - silty, brown, soft, moist | | | | | 225 |
| | | CLAY - silty<br>- brown<br>- stiff, moist<br>- high plasticity<br>- trace silt inclusions, trace oxidation | | G79 | | | 224 |
| 3 | | - trace sand, trace gravel, mottled grey below 3m | | T80 | | | 223 |
| 4 | CH | - grey below 3.7m | | | | | 222 |
| 5 | | | | T81 | | | 221 |
| 6 | | - firm below 6.1m | | G82 | | | 220 |
| | | - till transition below 6.6m, grey, soft to firm, medium to low plasticity | | G83 | | | 219 |
| 7 | | SILT (Till) - trace sand, trace gravel, trace cobbles<br>- light grey<br>- moist, loose<br>- some sand, trace gravel<br>- low plasticity | | T84 | | | 218 |
| 8 | | | | G85 | | | 217 |
| 9 | | | | T86 | | | 216 |
| 10 | | | | G87 | | | 215 |
| | TILL | - 150mm sand layer at 10.7m<br>- very dense below 10.7m | | S88 | 64/<br>63mm | >> blows over 200mm | 214 |
| 12 | | | | | | | 213 |
| 13 | | | | | | | 212 |
| 14 | | | | G89 | | | 211 |
| 15 | | END TEST HOLE AT 14.33m IN SILT TILL<br>Notes:<br>1. Auger refusal at 9.7 m on boulder. Re-drilled test hole 1 m away.<br>2. Seepage from sand and till layers.<br>3. No sloughing.<br>4. Install SI-4 at 14.33m depth. Backfill with cement grout mixture. | | | | | 210 |
| 16 | | | | | | | 209 |
| 17 | | | | | | | 208 |
| 18 | | | | | | | 207 |
| 19 | | | | | | | 206 |
| 20 | | | | | | | 205 |
| 21 | | | | | | | 204 |
| 22 | | | | | | | 203 |
| 23 | | | | | | | |

SPT (Standard Pen Test) (Blows/300mm) 20 40 60 80

PLASTIC M.C. LIQUID 20 40 60 80

| | |
|---|---|
| LOGGED BY: KT | COMPLETION DEPTH: 14.33 m |
| REVIEWED BY: KT | COMPLETION DATE: 8/10/06 |
| PROJECT ENGINEER: Kendall Thiessen, EIT | Page 1 of 1 |

LOG OF TESTHOLE KENDALL'S LOGS.GPJ UMA.GDT 9/8/10

| | | |
|---|---|---|
| PROJECT: Rockfill Column Test Site | CLIENT: University of Manitoba | TESTHOLE NO: **TH-5** |
| LOCATION: Top of Bank, West of test site N 5,520,034.5 E 634,974.7 | | PROJECT NO.: |
| CONTRACTOR: Paddock Drilling Ltd. | METHOD: 125mm dia. Solid Stem Auger | ELEVATION (m): 231.86 |

SAMPLE TYPE: GRAB | SHELBY TUBE | SPLIT SPOON | BULK | NO RECOVERY | CORE

BACKFILL TYPE: BENTONITE | GRAVEL | SLOUGH | GROUT | CUTTINGS | SAND

| DEPTH (m) | USC | SOIL DESCRIPTION | SAMPLE TYPE | SAMPLE # | PLASTIC / M.C. / LIQUID (20 40 60 80) | COMMENTS | ELEVATION (m) |
|---|---|---|---|---|---|---|---|
| 0 | OL | ORGANIC CLAY - silty, black | | | | | |
| | CH | - very stiff, moist, medium plasticity | | G62 | | | |
| 1 | ML | CLAY - silty, trace organics, brownish grey, moist, very stiff, high plasticity | | G63 | | | 231 |
| | | SILT - light greyish brown, loose, dry, low plasticity | | | | | |
| 2 | | CLAY - silty | | G64 | | | 230 |
| | | - brown, mottled grey | | G65 | | | |
| 3 | | - stiff, moist | | | | | 229 |
| | | - high plasticity | | | | | |
| | | - trace silt and sulphite inclusions < 5mm dia. | | T66 | | | |
| 4 | | - 150mm clayey silt seam, light brown, low plasticity at 2.1m | | | | | 228 |
| | | - brown below 2.1m | | | | | |
| | | | | G67 | | | |
| 5 | | | | | | | 227 |
| | | - increased sulphites between 5.2 and 7.6m | | T68 | | | |
| 6 | | | | | | | 226 |
| | | | | G69 | | | |
| 7 | CH | | | | | | 225 |
| | | | | T70 | | | |
| 8 | | | | | | | 224 |
| | | - trace gravel below 8.2m | | | | | |
| 9 | | | | | | | 223 |
| | | - trace sand below 9.1m | | G71 | | | |
| 10 | | | | | | | 222 |
| | | | | G72 | | | |
| 11 | | - 100 mm silt till inclusion at 10.7m | | | | | 221 |
| | | | | | | | |
| 12 | | - firm below 11.6m | | | | | 220 |
| | | | | T73 | | | |
| 13 | | | | | | | 219 |
| | | | | G74 | | | |
| 14 | | SILT (Till) - trace clay, trace to some sand, trace gravel, trace cobbles | | T75 | | | 218 |
| | | - light grey | | | | | |
| 15 | | - loose, moist | | G76 | | | 217 |
| | | - low plasticity | | | | | |
| 16 | | | | | | | 216 |
| | | - light brown, dense below 16m | | | | | |
| | | - sandy below 16.5m | | G77 | | | |
| 17 | TILL | | | | | | 215 |
| 18 | | | | | | | 214 |
| 19 | | | | | | | 213 |
| 20 | | | | G78 | | | 212 |
| 21 | | END TEST HOLE AT 20.22m IN SILT TILL | | | | | 211 |
| | | Notes: | | | | | |
| 22 | | 1. Auger refusal at 20.22m. | | | | | 210 |
| | | 2. Seepage from till. | | | | | |
| | | 3. No sloughing. | | | | | |
| 23 | | 4. Install SI-5 at 20.22m. Backfill with cement grout mixture. | | | | | 209 |

| | |
|---|---|
| LOGGED BY: KT | COMPLETION DEPTH: 20.22 m |
| REVIEWED BY: KT | COMPLETION DATE: 8/10/06 |
| PROJECT ENGINEER: Kendall Thiessen, EIT | Page 1 of 1 |

LOG OF TESTHOLE KENDALL'S LOGS.GPJ UMA.GDT 9/8/10

# APPENDIX B

Raw monitoring data from test loading – On DVD

Microsoft Excel Files:

Appendix B-KT2010-In-lace inclinometers and piezometer monitoring from data-logger.xlsx

Appendix B-KT2010-manual piezometer monitoring.xlsx

In-Place Inclinometers and Piezometer data from data-logger KT-2010.xlsx

Database File:

File can be opened with Digi-Pro for Windows (Slope Indicator

12123 Harbour Reach Dr, Mukilteo, WA, USA) available at:

http://www.slopeindicator.com/downloads/download-software.html

# APPENDIX C

Modeling files – On DVD

Geo-Slope Files:

Files can be viewed and solved with Geo-Studio 2007 Version 7.16, Build 4840, (Geo-Slope International Ltd.,1400, 633 - 6th Avenue S.W. Calgary, Alberta, Canada):

Case 1-excluding solution.gsz

Case 2-excluding solution.gsz

Case 3-excluding solution.gsz

Case 4-excluding solution.gsz